CIVIL, CONSTRUCTION & ENVIRONMENTAL ENGINEERING

Albuquerque, NM

October 29th, 2023

Search Committee Chair
Lyles School of Civil Engineering
Delon and Elizabeth Hampton Hall of Civil Engineering
550 Stadium Mall Drive
West Lafayette, IN 47907-2051

Dear Search Committee Chair:

I am writing to apply for the advertised tenure-track faculty position in the Lyles School of Civil Engineering at Purdue University, at the level of Associate Professor. I am currently an Associate Professor in Structural Engineering in the Department of Civil, Construction & Environmental Engineering at the University of New Mexico. My research goal is to contribute to engineering with the discovery, development, and dissemination of innovative solutions towards sustainable and resilient communities, to improve the well-being and safety of society as well as its natural and built environments. My application domain interests include infrastructure design, performance assessment, and safety of operations. My fundamental research advances structural dynamics and controls in smart structures and novel human-infrastructure interactions with human-centered new theories and experiments. I want to enhance efficient, sustainable, and resilient structures and systems design with a combination of innovative, out-of-the-box approaches to satisfy the needs of stakeholders of today and the future. My ten and a half years of industry experience informs my infrastructure research methods and practices from cradle (design and construction) to grave (maintenance, repair, and eventually replacement.) My research background, professional experiences, and extensive involvement and commitment to teaching and service as scholar have created a firm foundation to become a successful faculty member at Purdue University.

I want to collaborate with Purdue's College of Engineering and contribute to the Pinnacle of Excellence at Scale. I believe that our common ground would allow us to develop a strong, comprehensive educational and research program. I will develop a research program at the Lyles School of Civil Engineering at Purdue University that is funded both by industry and government agencies (national and international) to respond to infrastructure urgent priorities to achieve resilient and sustainable communities. I have additionally gained significant experience during my

eight years at the University of New Mexico in collaborating with the National Laboratories in experimental dynamics and critical infrastructure design, evaluation, and safety. I recently won the international competition in Structural Health Monitoring (SHM) SHM in Action hosted at the International Workshop in SHM at Palo Alto, CA. Last year I completed a Fulbright fellowship abroad and plan to build and expand my national research program internationally with my international connections. I worked for six months at the National Center for Research and Earthquake Engineering (NCREE) with the National Taiwan University (NTU). I am very interested to contributing to a world-class engineering program and to participate and support the leadership of the Lyles School of Civil Engineering. I visited Purdue earlier on October and became familiar firsthand with some of the outstanding facilities of Purdue University including but not limited to the Bowen Laboratory and the NASA Resilient Extra-Terrestrial Habitats (RETH) Institute. The faculty of the Lyles School of Civil Engineering are worldwide leaders in their discipline, and I will look for collaborations and synergies, planning to contribute to the initiatives in College Engineering. At Purdue University I look forward to both teaching traditional courses and developing my own courses based on my research experience in academia to date and my professional experience acquired throughout the years and my diverse experiences. I am very interested in the opportunity to have a joint appointment with the Division of Construction Engineering and Management. I look forward to participate in the many initiatives at Purdue College of Engineering as scholar, educator, and engineer.

I have enclosed my curriculum vitae, research plan, teaching plan, three representative publications, as well as contact information for five professional references. Please let me know if you need any additional information. Thank you very much for your consideration, and I look forward to hearing from you soon. If you have any questions, please feel free to contact me at fmoreu@unm.edu or you could also call my cellphone (217) 417-1204.

Sincerely,

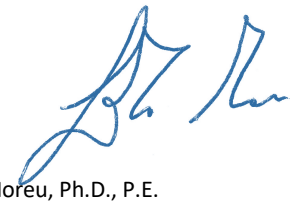

Fernando Moreu, Ph.D., P.E.
Associate Professor, Department of Civil, Construction and Environmental Engineering
Courtesy Appointment, Department of Electrical & Computer Engineering
Courtesy Appointment, Department of Mechanical Engineering
Courtesy Appointment, Department of Computer Science
Centennial Engineering Center 3056
University of New Mexico MSC01 1070
210 University Blvd NE Albuquerque, NM 87131
fmoreu@unm.edu
Office (505) 277-1784
Cell (217) 417-1204
Web http://smilab.unm.edu/

Fernando Moreu, PhD, PE

Associate Professor in the Department of Civil, Construction and Environmental Engineering
Electrical and Computer Engineering Department (cross-appointed)
Mechanical Engineering Department (cross-appointed)
Computer Science Department (cross-appointed)
Director, Smart Management of Infrastructure Laboratory (SMILab)
University of New Mexico
CENT 3056 MSC01 1070 210 University Avenue, Albuquerque, NM 87131-0001
fmoreu@unm.edu • office: (505) 277-1784 • cell: (217) 417-1204 http://smilab.unm.edu/

RESEARCH INTERESTS

Experimental dynamics, large-scale testing, cyber-physical systems, field monitoring and testing, railroad engineering, infrastructure performance and management, structural health monitoring, wireless smart sensor networks, unmanned aerial vehicles, machine learning, human-infrastructure interfaces.

EDUCATION

Ph.D. Civil and Environmental Engineering May 2015
University of Illinois at Urbana-Champaign
Dissertation: *"Framework for Risk-based Management of Railroad Bridge Infrastructure; an Application of Structural Health Monitoring (SHM) using Wireless Smart Sensor Networks (WSSNs)"*
Adviser: Professor B. F. Spencer, Jr.

M. S. Civil and Environmental Engineering May 2005
University of Illinois at Urbana-Champaign
Sponsored by ESCA Consultants, Inc. (Urbana, IL)
Adviser: Professor Doug A. Foutch

B. S. Civil and Environmental Engineering August 1999
University of Granada (Spain)
Senior Project: "Pedestrian Bridge over C/Méndez Núñez at Granada, Spain"
With excellence award from the University of Granada for outstanding students

PROFESSIONAL EXPERIENCE

Los Alamos National Laboratory June 2018-August 2018
May 2016-August 2016

Los Alamos, New Mexico
Research Scientist

- Collaborated with the Los Alamos Dynamics Summer School (LADSS) mentoring and advising of students for 10 weeks
- Developed experiments and validation in remote sensing technologies
- Prepared research grants and journal and conference publications summarizing this research

ESCA Consultants, Inc. November 2000-April 2011
Urbana, Illinois
Structural engineer

- Designed, checked, and constructed diverse structural systems
- Expert in highway and railroad bridges, University laboratories, diverse industry buildings, cooling towers and special foundations
- Diverse specialized services such as concrete ready-mix plant management and mix design, and design, fabrication, and evaluation of pre-stressed concrete beams.

REFEREED JOURNAL PUBLICATIONS

(62 journal papers published to date)

Total Google Scholar Citations: 1240, h-index=19, i10-index=39

1. Malek, K., Ortiz, E., Lee, Y., Murillo, J., Mohammadkhorasani, A., Vigil, L., Zhang & **Moreu, F.** (2023). Design and implementation of sustainable solar energy harvesting for low-cost remote sensors equipped with real-time monitoring systems. *Journal of Infrastructure Intelligence and Resilience*, 2(3), 100051. https://doi.org/10.1016/j.iintel.2023.100051
2. Mohammadkhorasani, A., Malek, K., Mojidra, R., Li, J., Bennett, C., Collins, W., & **Moreu, F.** (2023). Augmented reality-computer vision combination for automatic fatigue crack detection and localization. *Computers in Industry*, 149, 103936. https://doi.org/10.1016/j.compind.2023.103936
3. **Moreu, F.**, Rakoczy, A. M., & Sanei, M. (2023). Lateral Loads and Displacements of Railroad Bridges from Field Investigations. *Journal of Bridge Engineering*, 28(9), 04023059.
4. **Moreu, F.**, Chen, L., Zhu, C., Wu, Z., & Yuan, X. (2023). Measuring Total Transverse Reference-Free Displacements of Railroad Bridges Using Two Degrees of Freedom: Experimental Validation. *Journal of Infrastructure Systems*, *29*(2), 04023009. https://doi.org/10.1061/JITSE4.ISENG-2132
5. Laflamme, Simon, Filippo Ubertini, Alberto Di Matteo, Antonina Pirrotta, Marcus Perry, Yuguang Fu, Jian Li, **Fernando Moreu** et al. "Roadmap on measurement technologies for next generation structural health monitoring systems." *Measurement Science and Technology* (2023). https://doi.org/10.1088/1361-6501/acd135
6. Woodall, J., Maji, A., & **Moreu, F.** (2023). Effective sensor location for detection of change in structural dynamic response. *Journal of Low Frequency Noise, Vibration and Active Control*, 14613484231160151. https://doi.org/10.1177/14613484231160151
7. Robbins, E., Kuether, R. J., Paccini, B. & **Moreu, F.** (2023). Stabilizing a strongly nonlinear structure through shaker dynamics in fixed frequency voltage control tests. *Mechanical Systems and Signal Processing* Volume 190, May, Pg. 110–118. https://doi.org/10.1016/j.ymssp.2023.110118
8. Aguero, M., Doyle, D., Mascarenas, D., & **Moreu**, F. (2023). Visualization of real-time displacement time history superimposed with dynamic experiments using wireless smart sensors and augmented reality. *Earthquake Engineering and Engineering Vibration*, 1-16. https://doi.org/10.3390/robotics9010003
9. Yuan, Xinxing, Alan Smith, **Fernando Moreu**, Rodrigo Sarlo, Christopher D. Lippitt, Maryam Hojati, Sreenivas Alampalli, and Su Zhang. "Automatic evaluation of rebar spacing and quality using LiDAR data: Field application for bridge structural assessment." *Automation in Construction* 146 (2023): 104708. https://doi.org/10.1016/j.autcon.2022.104708
10. Mojidra, R., Li, J., Mohammadkhorasani, A., **Moreu, F.**, Bennett, C., & Collins, W. (2023). Vision-based fatigue crack detection using global motion compensation and video feature tracking. *Earthquake Engineering and Engineering Vibration*, 1-21. https://doi.org/10.1007/s11803-023-2156-1
11. Sanei, M., Yuan, X., **Moreu**, F., & Alampalli, S. (2023). Automated Geometric Quality Inspection of Rebar Layout Using RGBD Data. *MATERIALS EVALUATION*, *81*(1), 46-55. https://doi.org/10.32548/2023.me-04307
12. Nasimi, R., **Moreu, F.**, & Fricke, G. M. (2023). Sensor equipped UAS for non-contact bridge inspections: field application. *Sensors*, *23*(1), 470. https://doi.org/10.3390/s23010470
13. Sadhu, A., Peplinski, J. E., Mohammadkhorasani, A., & **Moreu, F.** (2023). A Review of Data Management and Visualization Techniques for Structural Health Monitoring Using BIM and Virtual or Augmented Reality. *Journal of Structural Engineering*, *149*(1), 03122006. https://orcid.org/0000-0001-5685-7087
14. Xu, J., Wyckoff, E., Hanson, J., Doyle, D., **Moreu, F.** (2022). "Dynamic deformation measurement in

structural inspections by Augmented Reality technology." Smart Structures and Systems, Volume 30, Number 6, December, pages 649-659 DOI: https://doi.org/10.12989/sss.2022.30.6.649

15. Malek, K., Mohammadkhorasani, A., & **Moreu, F.** (2022). Methodology to integrate augmented reality and pattern recognition for crack detection. *Computer-Aided Civil and Infrastructure Engineering*. https://doi.org/10.1111/mice.12932
16. Xu, J., Doyle, D., & **Moreu, F.** (2023). State of the art of augmented reality capabilities for civil infrastructure applications. *Engineering Reports*, e12602.
17. Malek, K. & **Moreu, F.** (2022). Realtime conversion of cracks from pixel to engineering scale using Augmented Reality. *Automation in Construction*, *143*, 104542. https://doi.org/10.1016/j.autcon.2022.104542
18. Robbins, E., Kuether, R. J., & **Moreu, F.** (2022). Measuring nonlinearities of a cantilever beam using a low-cost efficient wireless intelligent sensor for strain (LEWIS-S). *Engineering Research Express*, *4*(3), 035015. https://doi.org/10.1088/2631-8695/ac8337
19. Montoya, A., Habtour, E., & **Moreu, F.** (2022). Detecting hidden transient events in noisy nonlinear time-series. *Chaos: An Interdisciplinary Journal of Nonlinear Science*, *32*(7), 073131. https://doi.org/10.1063/5.0097973
20. Woodall, J., Hossain, M., Maji, A., **Moreu, F.**; Transforming a Simple Structure Model to Represent a Complex Dynamic System with Unknown Boundary Restraints. *Exp Tech* (2022). https://doi.org/10.1007/s40799-021-00494-w
21. Nasimi, R., Atcitty, S., Thompson, D., Murillo, J., Ball, M., Stormont, J., & **Moreu, F.** (2022). Use of remote structural tap testing devices deployed via ground vehicle for health monitoring of transportation infrastructure. Sensors, 22(4), 1458. https://doi.org/10.3390/s22041458
22. Xu, D., Yuan, X., Ozdagli, A. I., Agüero, M., Nasimi, R., Wang, T., & **Moreu, F.** (2022). Over-height truck collisions with railway bridges: attenuation of damage using crash beams. Earthquake engineering and engineering vibration, 21(1), 237-252. https://doi.org/10.1007/s11803-022-2081-8
23. Nasimi, R., **Moreu**, **F.**, & Stormont, J. (2021). Crack detection using tap-testing and machine learning techniques to prevent potential rockfall incidents. *Engineering Research Express*, 3(4), 045050. https://doi.org/10.1088/2631-8695/ac3fa0
24. Yuan, X., **Moreu, F.**, & Hojati, M. (2021). Cost-Effective Inspection of Rebar Spacing and Clearance Using RGB-D Sensors. *Sustainability*, *13*(22), 12509. https://doi.org/10.3390/su132212509
25. Wyckoff, E., Ball, M., & **Moreu, F.** (2021). Reducing gaze distraction for real‐time vibration monitoring using augmented reality. Structural Control and Health Monitoring, e3013. https://doi.org/10.1002/stc.3013
26. Yuan, X., Smith, A., Sarlo, R., Lippitt, C. D., & **Moreu, F.** (2021). Automatic evaluation of rebar spacing using LiDAR data. *Automation in Construction*, *131*, 103890. https://doi.org/10.1016/j.autcon.2021.103890
27. Nasimi, R., & **Moreu, F**. (2021). Development and implementation of a laser–camera–UAV System to measure total dynamic transverse displacement. *Journal of Engineering Mechanics*, *147*(8), 04021045. https://doi.org/10.1061/(ASCE)EM.1943-7889.0001939
28. Maji A, **Moreu F**, Woodall J, Hossain M. Error analyses of a Multi-Input-Multi-Output cantilever beam test. *Journal of Vibration and Control*. July 2021. https://doi.org/10.1177/10775463211033733
29. Reda Taha, M.; Ayyub, B. M.; Soga, K.; Daghash, S.; Heras Murcia, D.; **Moreu, F.**; and Soliman, E. (2021). "Emerging Technologies for Resilient Infrastructure: Conspectus and Roadmap" *ASCE-ASME Journal of Risk and Uncertainty in Engineering Systems, Part A: Civil Engineering* Vol 7, No 2 https://doi.org/10.1061/AJRUA6.0001134

30. Nasimi, R., and **Moreu, F.** "A methodology for measuring the total displacements of structures using a laser–camera system." *Computer-Aided Civil and Infrastructure Engineering* 36, no. 4 (2021): 421-437. https://doi.org/10.1111/mice.12652
31. Robbins, E., Cobo, N,, Diaz J. and **Moreu, F.** (2021) "Development of a low-cost efficient wireless intelligent sensor for strain measurements (LEWIS-S)" *Measurement Science and Technology*, February 5th, 2021 https://doi.org/10.1088/1361-6501/abe339
32. Cardona Huerta, R., **Moreu, F.**, & Lozano Galant, J. A. (2021). Aerial Tramway Sustainable Monitoring with an Outdoor Low-Cost Efficient Wireless Intelligent Sensor. *Sustainability*, *13*(11), 6340. https://doi.org/10.3390/su13116340
33. Chen L-K, Liu P, Zhu L-M, Ding J-B, Feng Y-L, **Moreu F.** (2021) "A simplified iterative approach for testing the pulse derailment of light rail vehicles across a viaduct to near-fault earthquake scenarios". *Proceedings of the Institution of Mechanical Engineers, Part F: Journal of Rail and Rapid Transit.* February 2021. https://doi.org/10.1177%2F0954409720987410
34. Jiaqi, X. and **Moreu, F.** (2021). "A Review of Augmented Reality Applications in Civil Infrastructure during the 4th Industrial Revolution." *Frontiers in Built Environment* 7 (2021): 28. https://doi.org/10.3389/fbuil.2021.640732
35. Maharjan, D., Agüero, M., Mascarenas, D., Fierro, R., & **Moreu, F.** (2020). Enabling human–infrastructure interfaces for inspection using augmented reality. *Structural Health Monitoring*, 1475921720977017. https://doi.org/10.1177/1475921720977017
36. Montoya, A., Habtour, E., & **Moreu, F.** (2020). Quantifying Information without Entropy: Identifying Intermittent Disturbances in Dynamical Systems. *Entropy*, 22(11), 1199. https://doi.org/10.3390/e22111199
37. Garg, P., Nasimi, R., Ozdagli, A., Zhang, S., Mascarenas, D. D. L., Reda Taha, M., & **Moreu, F.** (2020). Measuring Transverse Displacements Using Unmanned Aerial Systems Laser Doppler Vibrometer (UAS-LDV): Development and Field Validation. *Sensors*, 20(21), 6051. https://doi.org/10.3390/s20216051
38. Mascareñas, D. D., Ballor, J. P., McClain, O. L., Mellor, M. A., Shen, C. Y., Bleck, B., ... & **Moreu, F.** (2020). Augmented reality for next generation infrastructure inspections. Structural Health Monitoring, 1475921720953846. https://journals.sagepub.com/doi/full/10.1177/1475921720953846
39. **Moreu, F.**, Maharjan, D., Wyckoff, E., & Zhu, C. (2020). Monitoring Human Induced Floor Vibrations for Quantifying Dance Moves. *Frontiers in Built Environment*, 6, 36. https://www.frontiersin.org/articles/10.3389/fbuil.2020.00036/full
40. Taylor, R.M., Maharjan, D., **Moreu, F.** et al. (2020); Parametric study of 3D printed microneedle (MN) holders for interstitial fluid (ISF) extraction. Microsyst. Technol. https://doi.org/10.1007/s00542-020-04758-0
41. Aguero, M., Maharjan, D., Rodriguez, M. D. P., Mascarenas, D. D. L., & **Moreu, F.** (2020). Design and Implementation of a Connection between Augmented Reality and Sensors. *Robotics*, *9*(1), 3. https://doi.org/10.3390/robotics9010003
42. Ozdagli, A. I., **Moreu, F.**, Xu, D., & Wang, T. (2020). Experimental Analysis on Effectiveness of Crash Beams for Impact Attenuation of Overheight Vehicle Collisions on Railroad Bridges. *Journal of Bridge Engineering*, *25*(1), 04019133. https://doi.org/10.1061/(ASCE)BE.1943-5592.0001503
43. Garg, P., **Moreu, F.**, Ozdagli, A., Taha, M. R., & Mascareñas, D. (2019). Noncontact Dynamic Displacement Measurement of Structures Using a Moving Laser Doppler Vibrometer. *Journal of Bridge Engineering*, *24*(9), 04019089. https://doi.org/10.1061/(ASCE)BE.1943-5592.0001472
44. Mascarenas, David Dennis Lee, Harden, Troy Anthony, Morales Garcia, John Evan, Boardman, Beth Leigh, Sosebee, Erin Marie, Blackhart, Craig, Cattaneo, Alessandro, Krebs, Matthew Scott, Tockstein,

Jameson John, Green, Andre Walter, Dasari, Sudeep Rao, Bleck, Brian Mark, Katko, Benjamin Joseph, **Moreu, Fernando**, Maharjan, Dilendra, Aguero, Marlon, Fernandez, Ricardo, Trujillo, Julio B., and Wysong, Andrew Russell. *Augmented Reality for Enabling Smart Nuclear Infrastructure*. United States: N. p., 2019. https://www.frontiersin.org/articles/10.3389/fbuil.2019.00082/full

45. Liu, B., Ozdagli, A. I., **Moreu, F.**, & Chi, Q. (2019). Hybrid reference-free total displacement for railroad bridge campaign monitoring. *Measurement Science and Technology*. https://doi.org/10.1088/1361-6501/ab2091
46. Gomez, J. A., Ozdagli, A. I., & **Moreu, F.** (2019). Reference-free dynamic displacements of railroad bridges using low-cost sensors. *Journal of Intelligent Material Systems and Structures*, *30*(9), 1291-1305. https://doi.org/10.1177/1045389X17721375
47. Aguero, M., Ozdagli, A., & **Moreu, F.** (2019). Measuring Reference-Free Total Displacements of Piles and Columns Using Low-Cost, Battery-Powered, Efficient Wireless Intelligent Sensors (LEWIS2). *Sensors*, *19*(7), 1549. https://doi.org/10.3390/s19071549
48. **Moreu, F.**, Li, X., Li, S., & Zhang, D. (2018). Technical specifications of structural health monitoring for highway bridges: new Chinese structural health monitoring code. *Frontiers in Built Environment*, *4*, 10. https://www.frontiersin.org/articles/10.3389/fbuil.2018.00010/full
49. Liu, B.; Ozdagli, A.; **Moreu, F.** (2018); "Direct reference-free measurement of displacements for railroad bridge management"; *Structural Control and Health Monitoring*. https://doi.org/10.1002/stc.2241
50. Ozdagli, A. I., Liu, B., & **Moreu, F.** (2018). "Measuring Total Transverse Reference-Free Displacements for Condition Assessment of Timber Railroad Bridges: Experimental Validation." *Journal of Structural Engineering*, *144*(6), 04018047. https://doi.org/10.1061/(ASCE)ST.1943-541X.0002041
51. Ozdagli, Ali I.; Liu, Bideng; **Moreu, F.**; (2018); "Low-cost, efficient wireless intelligent sensors (LEWIS) measuring real-time reference-free dynamic displacements." *Mechanical Systems and Signal Processing* Volume 107, July, Pg. 343–356. https://doi.org/10.1016/j.ymssp.2018.01.034
52. **Moreu, F.**; Ayorinde, E.; Mason, J.; Farrar, C.; and Mascarenas, D.D.L. (2017); "Remote Railroad Bridge Structural Tap Testing Using Aerial Robots"; *International Journal of Intelligent Robotics and Applications*, 1-14. https://doi.org/10.1007/s41315-017-0041-7
53. D. D. L. Mascarenas, **F. Moreu**, P. Cantu, D. Shields, J. Wadden, M. El Hadedy, C. Farrar (2017) "A compliant mechanism for inspecting extremely confined spaces". *Smart Materials and Structures*, 26(11), 115028. https://doi.org/10.1088/1361-665X/aa9195
54. Ozdagli, Ali I.; Gomez, Jose A.; **Moreu, F.**; (2017); "Total reference-free displacements for condition assessment of timber railroad bridges using tilt"; *Smart Structures and Systems*; Volume 20, Number 5, November; pages 549-562. https://doi.org/10.12989/sss.2017.20.5.549
55. Ozdagli, A. I., Gomez, J. A., & **Moreu, F.** (2017). "Real-Time Reference-Free Displacement of Railroad Bridges during Train-Crossing Events". *Journal of Bridge Engineering*, 22 (10), 04017073. https://doi.org/10.1061/(ASCE)BE.1943-5592.0001113
56. Hoag, A., Hoult, N., Take, A., **Moreu, F.**, Le, H. and Tolikonda, V. (2017); "Measuring displacements of a railroad bridge using DIC and accelerometers"; Smart Structures and Systems *Smart Structures and Systems*; Volume 19, Number 2, February 2017. https://doi.org/10.12989/sss.2017.19.2.225
57. **Moreu, F.**, Spencer Jr, B. F., Foutch, D. A., & Scola, S. (2017). Consequence-based management of railroad bridge networks. *Structure and Infrastructure Engineering*, 1-14. https://doi.org/10.1080/15732479.2016.1162817

58. **Moreu, F.**; Kim, R. E.; and Spencer, Jr., B. F. (2017); "Railroad Bridge Monitoring Using Wireless Smart Sensors"; *Structural Control and Health Monitoring*. https://doi.org/10.1061/(ASCE)ST.1943-541X.0001530
59. Kim, R. E.; **Moreu, F.**; and Spencer, Jr., B. F. (2016); "Hybrid Model for Railroad Bridge Dynamics"; Journal of Structural Engineering Volume 142 Issue 10 – October 2016. https://doi.org/10.1061/(ASCE)ST.1943-541X.0001530
60. **Moreu, F.**; Jo, H.; Li, J.; Kim, R. E., Scola, S.; Spencer, Jr., B. F.; and LaFave, J. M. (2016); "Reference-Free Displacement Estimation and Assessment for Railroad Bridges using Wireless Smart Sensors"; ASCE Journal of Bridge Engineering. Volume 21 Issue 2 - February 2016 https://doi.org/10.1061/(ASCE)BE.1943-5592.0000805
61. Kim, R. E.; **Moreu, F.**; and Spencer, Jr., B. F. (2015); "System identification of an in-service railroad bridge using wireless smart sensors"; *Smart Structures and Systems,* 15(3), 683-698. https://doi.org/10.12989/sss.2015.15.3.683
62. **Moreu, F.**; Jo, H.; Li, J.; Kim, R.; Cho, S.; Kimmle, A.; Scola, S.; Le, H.; Spencer, Jr., B. F.; and LaFave, J. M. (2015); "Dynamic Assessment of Timber Railroad Bridges using Displacements"; ASCE Journal of Bridge Engineering, Volume 20 Issue 10 - October 2015. https://doi.org/10.1061/(ASCE)BE.1943-5592.0000726

Several journal papers in preparation for 2023:

- One paper submitted after first review, awaiting response from reviewers.
- One paper ongoing first review.
- Two papers submitted awaiting response from reviewers.
- Two papers ready to be submitted by November 15th 2023.
- Three papers in preparation to be submitted by December 31st 2023.

PUBLICATIONS IN CONFERENCE PROCEEDINGS

1. **Moreu, F.**, Wyckoff, E. (2024). Human-Structural Dynamics Interfaces Using Augmented Reality. In: Noh, H.Y., Whelan, M., Harvey, P.S. (eds) Dynamics of Civil Structures, Volume 2. SEM 2023. Conference Proceedings of the Society for Experimental Mechanics Series. Springer, Cham. https://doi.org/10.1007/978-3-031-36663-5_11
2. **Moreu, F**. "Railroad Infrastructure Inspections using Augmented Reality" (2023). AREMA 2023 Annual Conference & Exposition, Indianapolis, IN, September.
3. Baca, Anistasia, Ria Mukerji, Lauren Vigil, Lindsey Rotche, Su Zhang, Carolyn Hushman, Mark C. Stone, **Fernando Moreu**, and Yolanda C. Lin. "Developing Fragility Curves Towards Assessing Flood Risk in Ohkay Owingeh." In *AGU Fall Meeting Abstracts*, vol. 2022, pp. NH35C-0502. 2022.
4. Zheng, K., Sorensen, J., DeVilliers, C., Cattaneo, A., **Moreu, F.**, Taylor, G., & Mascareñas, D. (2023). Neuromorphic Data Processing for Event-Driven Imagery for Acoustic Measurements. In *Rotating Machinery, Optical Methods & Scanning LDV Methods, Volume 6* (pp. 37-41). Springer, Cham.
5. Mojidra, R., Li, J., Mohammadkhorasani, A., **Moreu, F.**, Collins, W., Bennett, C., & Taher, S. A. (2022, April). Vision-based inspection of out-of-plane fatigue cracks in steel structures. In Sensors and Smart Structures Technologies for Civil, Mechanical, and Aerospace Systems 2022 (Vol. 12046, pp. 145-151). SPIE.
6. Restrepo, J., Nasimi, R., and **Moreu, F.**, "Accessing Pedestrian Bridge Serviceability and Displacement using Low-cost Sensors" Transportation Research Board 100th Annual Meeting, Washington, DC, January 2022.
7. Thompson, D., Nasimi, R., Atcitty, S., Murillo, J., and **Moreu, F.**, "Use of Remote Structural Tap

Testing Devices deployed via Ground Vehicle for Health Monitoring of Transportation Infrastructure" Transportation Research Board 100th Annual Meeting, Washington, DC, January 2022.

8. Robbins, E., Schreiber, T., Malla, A., Pacini, B. R., Kuether, R. J., Manzato, S., ... & **Moreu, F.** (2022). Pre-test Predictions of Next-Level Assembly Using Calibrated Nonlinear Subcomponent Model. In *Nonlinear Structures & Systems, Volume 1* (pp. 1-13). Springer, Cham.
9. Wyckoff, E., Ball, M., & **Moreu, F.** (2022). Real-Time Human Cognition of Nearby Vibrations Using Augmented Reality. In *Dynamics of Civil Structures*, Volume 2 (pp. 139-145). Springer, Cham.
10. **Moreu, F.**, Woodall, J., & Maji, A. (2022). Understanding Errors from Multi-Input-Multi-Output (MIMO) Testing of a Cantilever Beam. In *Dynamics of Civil Structures, Volume 2* (pp. 147-152). Springer, Cham.
11. Roya Nasimi; Fernando **Moreu**; John Stormont; and Amir Bagherieh. Automated Classification of Surface Properties of Rocks Tran-SET 2021 (June 3-4) Virtual Conference.
12. Xinxing Yuan, Fernando **Moreu**, Christopher D Lippitt. Bridge Construction Monitoring Using LiDAR Data. Tran-SET 2021 (June 3-4) Virtual Conference.
13. Hossain, M., Hanson, J. W., & **Moreu, F.** (2021). Real-Time Theoretical and Experimental Dynamic Mode Shapes for Structural Analysis Using Augmented Reality. In *Topics in Modal Analysis & Testing, Volume 8* (pp. 351-356). Springer, Cham.
14. Woodall, J., Hossain, M., Maji, A., Pott, J., & **Moreu, F.** (2021). Exploring Uncertainties in Multi-Input-Multi-Output (MIMO) Testing. In *Special Topics in Structural Dynamics & Experimental Techniques, Volume 5* (pp. 197-204). Springer, Cham.
15. Murillo, Joshua S.; **Moreu**, Fernando; Ball, Marlan (2021); "Invited Student Paper - 5th Generation Low-cost Efficient Wireless Intelligent Sensors (LEWIS 5) for Transportation", Transportation Research Board 100th Annual Meeting, Washington, DC, January 2021.
16. Martins, C., Ghanbari, L., Wang, C., & **Moreu, F.** (2019, April). Development of a Conceptual Model for Accelerated Project Prioritization after Disaster Event. In *MATEC Web of Conferences* (Vol. 271, p. 08001). EDP Sciences.
17. Agüero, M., Ozdagli, A., & **Moreu, F.** (2019, April). Low-cost, Battery-Powered, Efficient Wireless Intelligent Sensor (LEWIS2): Outdoors and Remote Sensing Applications. In *MATEC Web of Conferences* (Vol. 271, p. 01007). EDP Sciences.
18. Maharjan, D., Wyckoff, E., Agüero, M., Martinez, S., Zhou, L., & **Moreu, F.** (2019, March). Monitoring induced floor vibrations: dance performance and bridge engineering. In *Sensors and Smart Structures Technologies for Civil, Mechanical, and Aerospace Systems 2019* (Vol. 10970, p. 109701E). International Society for Optics and Photonics.
19. Maharjan, D., Agüero, M., Lippitt, C., & **Moreu, F.** (2019). Infrastructure Stakeholders' Perspective in Development and Implementation of New Structural Health Monitoring (SHM) Technologies for Maintenance and Management of Transportation Infrastructure. In *MATEC Web of Conferences* (Vol. 271, p. 01010). EDP Sciences.
20. Pirayesh, R., Naseri, A., **Moreu, F.**, Stochaj, S., Shah, N., & Krizmanic, J. (2019). Attitude Control Optimization of a Two-CubeSat Virtual Telescope in a Highly Elliptical Orbit. In *Space Operations: Inspiring Humankind's Future* (pp. 233-258). Springer, Cham.
21. Ballor, J. P., McClain, O. L., Mellor, M. A., Cattaneo, A., Harden, T. A., Shelton, P., Martinez, E., Narushof, B., Moreu, F. & Mascareñas, D. D. (2019). Augmented Reality for Next Generation Infrastructure Inspections. In *Model Validation and Uncertainty Quantification, Volume 3* (pp. 185-192). Springer, Cham.

22. Liu, B., Ozdagli, A., & **Moreu, F.** (2018, May). Direct Reference-Free Dynamic Deflection Measurement of Railroad Bridge under Service Load. In *Sensors and Instrumentation, Aircraft/Aerospace and Energy Harvesting, Volume 8: Proceedings of the 36th IMAC, A Conference and Exposition on Structural Dynamics 2018* (p. 83). Springer.
23. Ozdagli, A., Liu, B., & **Moreu, F.** (2018, May). Real-Time Low-Cost Wireless Reference-Free Displacement Sensing of Railroad Bridges. In *Sensors and Instrumentation, Aircraft/Aerospace and Energy Harvesting, Volume 8: Proceedings of the 36th IMAC, A Conference and Exposition on Structural Dynamics 2018* (p. 103). Springer.
24. Ozdagli, A., Liu, B., & **Moreu, F.** (2018). Low-cost wireless smart sensors for measuring real-time reference-free dynamic displacements of railroad bridges. *The 7th World Conference on Structural Control and Monitoring*, Qingdao, China, July 22-25.
25. **Moreu, F.**, Garg, P, Ozdagli, A. (2018). Transverse bridge displacement measurement using a laser carried by unmanned aerial system. *The 7th World Conference on Structural Control and Monitoring*, Qingdao, China, July 22-25.
26. Ayorinde, E., Benjamin, I., **Moreu, F.** (2018); "Investigating the Use of Wireless Sensors to Measure the Performance of Launch Vehicles". 2018 American Institute of Aeronautics and Astronautics Region IV Student Paper Conference, Albuquerque, NM, April 13-14.
27. **Moreu, F.**, Lippitt, C., Soni, R., Ozdagli, A., Liu, B., Li, X., Ayorinde, E., Zhang, S. (2018); "High School Students Building and Using Sensors Towards Smart Management of Transportation Systems". 2018 Tran-SET Conference, New Orleans, LA, April 3-4.
28. Ozdagli, A. I., Vemuganti, S., Liu, B., **Moreu, F**. "Impact Rating of Semi-Trailer Truck – Railway Through Plate Girder (TPG) Bridge". AREMA 2017 Annual Conference & Exposition, Indianapolis, IN, September.
29. **Moreu, F**. Bleck, B., Vemuganti, S., Mascarenas, D. "Enhancing Structural Visual Inspection of Railroad Bridges Using HoloLens". AREMA 2017 Annual Conference & Exposition, Indianapolis, IN, September.
30. Liu, B., Gomez, J., Ozdagli, A.I., **Moreu, F.** (2017); "Cost-Effective Monitoring of Railroad Bridge Performance", In ASME 2017 Conference on Smart Materials, Adaptive Structures and Intelligent Systems, September.
31. Ozdagli, A., Gomez, J., **Moreu, F.** (2017). Measuring lateral displacements of railroad bridges susceptible to asymmetric loading; 3rd Huixian International Forum on Earthquake Engineering for Young Researchers. Champ., Illinois, August.
32. **Moreu, F.**, Liu, B., Ozdagli, A. I. (2017). Observation and monitoring of total reference-free displacements; 3rd Huixian International Forum on Earthquake Engineering for Young Researchers. Champ., Illinois, August.
33. Liu, B., Ozdagli, A. I., **Moreu, F.** (2017). Measurement of direct reference-free dynamic displacements of railroad bridges under train-crossing and ground motion excitations; 3rd Huixian International Forum on Earthquake Engineering for Young Researchers. Champ. Illinois, August.
34. Jafari, A., Pérez, G., **Moreu, F.**, & Valentin, V. *Optimizing Railroad Bridge Networks Management Using Mixed Integer Linear Programming and Genetic Algorithm*. In Computing in Civil Engineering 2017 (pp. 1-9).
35. **Moreu, F.**, Bleck, B., Vemuganti, S., Rogers, D., & Mascarenas, D. (2017). Augmented Reality Tools for Enhanced Structural Inspection. *Structural Health Monitoring 2017*.
36. Mascarenas, D., **Moreu, F.**, Cantu, P., Shields, D., Wadden, J., El Hadedy, Mohamed, & Farrar, C.

(2017). A Steerable-Needle Inspired Mechanism for Inspecting Extremely Confined Spaces. *Structural Health Monitoring 2017*.

37. Vemuganti, S., **Moreu, F**., Ozdagli, O., Bajric, A., Liu, B., Brake, M., Troyer, K., *Sensing and Rating of vehicle-bridge collisions*, IMAC XXXV conference by Society of Experimental Mechanics (SEM). Garden Grove, CA, USA, January 30-February 2 2017.
38. Garg, P., Ozdagli, A., **Moreu, F**. (2017). *Optimal Bridge Displacement Controlled by Train Speed on Real-Time*. IMAC XXXV conference by Society of Experimental Mechanics (SEM). Garden Grove, CA, USA, January 30-February 2 2017
39. Vemuganti, S., Ozdagli, A., **Moreu F.**, Survey Bottom Surface Abrasion of Concrete Crossties, TRB 96th Annual Meeting, 2017.
40. Lauren G., Shreya V., **Moreu, F.** (2017, January). Cyber-physical systems related to historic infrastructure maintenance, TRB 96th Annual Meeting, 2017.
41. **Moreu, F.**; Altwood, T. J.; Jo, H.; Kim, R.; Cho, S.; LaFave, J.M.; and Spencer Jr., B.F. (2016, August). Displacements of Steel Railroad Bridges under Revenue Service Traffic for Performance-Based Assessment. In Proc., AREMA 2016 Annual Conf. and Exposition (pp. 1- 20). Lanham, MD: American Railway Engineering and Maintenance-of-Way Association (AREMA).
42. Gomez, J. A., Ozdagli, A. I., & **Moreu, F.** (2016, September). Application of Low-Cost Sensors for Estimation of Reference-Free Displacements Under Dynamic Loading for Railroad Bridges Safety. In ASME 2016 Conference on Smart Materials, Adaptive Structures and Intelligent Systems (pp. V001T05A021-V001T05A021). American Society of Mechanical Engineers (click here)
43. Garg, P., Gomez, J., Ozdagli, A., **Moreu, F**. (2016). Non-Contact, Reference-Free Measurement of Bridge Displacement Using Viberometer. 2nd Huixian International Forum on Earthquake Engineering for Young Researchers. Beijing, China, August 19-21 2016
44. **Moreu, F.**, and Spencer Jr, B. F. (2015). *Consequence-Based Management of Railroad Bridge Infrastructure enabled by Structural Health Monitoring*. 2015 World Congress on Advances in Structural Engineering and Mechanics (ASEM15). Incheon, South Korea, August 25-29 2015.
45. Spencer, Jr., B.F., **Moreu, F.**, Kim, R. (2014); "Structural Health Monitoring of Railroad Bridges Using Wireless Smart Sensors (WSSs): Recent Real-world Experiences in North America"; Fourth International Symposium on Life-Cycle Civil Engineering (IALCEE 2014); Waseda University, Tokyo, Japan, November 16-19 (click here)
46. **Moreu, F.**; Jo, H.; Li, J. Cho, S.; Kim, R.; Spencer, B.; and LaFave, J.; (2012); "Reference-free displacement estimation for structural health monitoring of railroad bridges"; AREMA 2012 Annual Conference & Exposition, Chicago, IL, September (click here)
47. **Moreu, F.**; LaFave, J.; Spencer, B. (2012); "Structural health monitoring of railroad bridges – research needs and preliminary results"; Structures Congress (ASCE-SEI 2012), Chicago, IL, March (click here)
48. **Moreu, F.**; LaFave, J.; Spencer, B. (2012); "New regulations on railroad bridge safety: opportunities and challenges for railroad bridge monitoring"; SPIE, Smart Structures and Nondestructive Evaluation and Health Monitoring, San Diego, CA, March (click here)
49. Ren, J. J.; Wang, P.; Xiang, R.; **Moreu, F.** (2011); "Rub-plate length influence on longitudinal coupled slab track forces and displacements in railroad bridges turnouts", Transportation Research Board (TRB) Annual Meeting, Washington, DC, January (click here)
50. **Moreu, F.** (2008); "Young Structural Engineers Building Structures for the Poor"; Proceedings of the 17th Congress of IABSE (International Association for Bridge and Structural Engineering): "Creating and Renewing Urban Structures. Tall Buildings, Bridges and Infrastructure", Chicago, IL, September (click here)

51. **Moreu, F.**, Nagayama, T., Zeman, J., Rus, G., Lee, S.Y., and Park, T. (2008); "Railroad Bridge Replacement in the US Today: Current Technology and Future Possibilities"; Proceedings of the Fourth International Conference on Bridge Maintenance, Safety and Management, IABMAS (International Association for Bridge Maintenance and Safety), Seoul, South Korea, July (click here)
52. **Moreu, F.** (2008); "Upgrading Railroads Infrastructure with Prestressed Concrete Bridges"; Proceedings of the 2008 Concrete Bridge Conference. HPC – Safe, Affordable and Efficient. NCBC (National Concrete Bridge Council), Saint Louis, MO, April
53. **Moreu, F.** and Nagayama, T. (2008); "Use of Wireless Sensors for Timber Trestle Railroad Bridges Health Monitoring Assessment"; ASCE Conf. Proc. 314, 36; Proceedings of the 2008 Structures Congress: Crossing Borders; DOI:10.1061/41016 (314) 36, April (click here)
54. **Moreu, F.** and Nagayama, T. (2007); "Possibilities of Using Sensing Technology For Railroad Bridges Maintenance and Repair"; Proceedings of the IABSE Symposium 'Improving Infrastructure Worldwide – Bringing People Closer'; Weimar, Germany, September 19-21. ISBN: 978-385748-116-1 (click here)
55. **Moreu, F.** (2007); "Building US Railroad Bridges Within Hours a.k.a. "Railroad Bridge Change-Outs"; Proceedings of the IABSE Symposium 'Improving Infrastructure Worldwide – Bringing People Closer'; Weimar, Germany, September 19-21. ISBN: 978-385748-116-1 (click here)
56. **Moreu, F.** (2007); "Consulting Engineering, Research and Innovation in Civil Engineering in the United Status. Potential Applications to Engineering Practice in Spain". Proceedings of the II Nacional Consulting Engineering Congress. Madrid, Spain. April 23, 24 [In Spanish]
57. **Moreu, F.** (2006); "Construction of a New 80'– 0" Steel Girder Span. Mile U5.6 Edgewood Subdivision, Cruse, IL"; Proceedings of the 7th International Conference on Short and Medium Span Bridges 2006, Montreal, Canada, August
58. **Moreu, F.** (2006); "New Memphis Super Terminal (MST) Intermodal Railroad. Bridge over Horn Lake Cut-off Ditch Design and Construction"; Proceedings of the 7th International Conference on Short and Medium Span Bridges 2006, Montreal, Canada, August
59. **Moreu, F**.; Gagnon, E.; Edwards, R. (2006); "Railroad Bridges in the Service of Society"; Fernando Moreu, Eric Gagnon, Riley Edwards. Proceedings of the 3rd National Congress of Civil Engineering, Zaragoza, Spain, October
60. **Moreu, F.** (2005); "Prestressed Concrete Railroad Bridges on Driven H-Piles: The Mile Bridge, KY (USA)"; Proceedings of the Structural Engineering Seminar 2004-2005. Seminario José Antonio García García. University of Granada (Spain), May.

TECHNICAL REPORTS

1. **Moreu, F.**, Law, V., Khorasani, A., Malek, K., and Wyckoff, E. (2023). Augmenting Reality for Safer Inspections of Railroad Infrastructure and Operations (No. Rail Safety IDEA Project 43). https://trid.trb.org/view/2154956
2. Li, J., Bennett, C., Collins, W. & **Moreu, F.** (2022). Fatigue Crack Inspection Using Computer Vision and Augmented Reality (NCHRP IDEA Project 223). https://trid.trb.org/view/2110661
3. **Moreu, F.**, & Nasimi, R. (2022). Measuring Behavior of Railroad Bridges under Revenue Traffic using Lasers and Unmanned Aerial Vehicles (UAVs) for Safer Operations: Implementation (No. Rail Safety IDEA Project 37). https://trid.trb.org/view/1938473
4. **Moreu, F.**, Stormont, J., Nasimi, R., Bagherieh, A., & Atcitty, S. (2021). An Automated System for Inspecting Rock Faces and Detecting Potential Rock Falls Using Machine Learning (No. 20GTUNM31). Transportation Consortium of South-Central States. https://rosap.ntl.bts.gov/view/dot/61741
5. **Moreu, F.**, & Malek, K. (2021). Bridge Cracks Monitoring: Detection, Measurement, and Comparison

using Augmented Reality (No. 20STUNM33). Transportation Consortium of South-Central States. https://rosap.ntl.bts.gov/view/dot/61831

6. **Moreu, F.**, Lippitt, C., & Yuan, X. (2020). Bridge Construction Monitoring using LIDAR for Quantified, Objective Quality-Control Quality-Assurance (QOQCQA). https://digitalcommons.lsu.edu/transet_pubs/76/
7. Spencer, B. F., Gomez, F., Park, J., Yoon, H., & **Moreu, F.** (2020). *Reference-Free Estimates of Railroad Bridge Displacement Under Revenue Service Traffic* (No. DOT/FRA/ORD-20/21). United States. Department of Transportation. Federal Railroad Administration.
8. Mascarenas, D. D. L., Harden, T. A., Morales Garcia, J. E., Boardman, B. L., Sosebee, E. M., Blackhart, C., **Moreu, F.**, ... & Dasari, S. R. (2019). Augmented Reality for Enabling Smart Nuclear Infrastructure. *Frontiers in Built Environment*, *5*(LA-UR-18-30914).
9. **Moreu, F.**, Lippitt, C., Maharjan, D., Aguero, M., & Yuan, X. (2019). Augmented Reality Enhancing the Inspections of Transportation Infrastructure: Research, Education, and Industry Implementation. https://digitalcommons.lsu.edu/transet_pubs/55/
10. **Moreu, F.**, Wang, C., Yuan, X., Ghanbari, L., & Garrido, C. (2019). Strategies for Prioritizing Needs for Accelerated Construction after Hazard Events. https://digitalcommons.lsu.edu/transet_pubs/49/
11. **Moreu, F.**, Lippitt, C., Maharjan, D., Aguero, M., & Nasimi, R. (2018). Development, Training, Education, and Implementation of Low-Cost Sensing Technologies for Bridge Structural Health Monitoring (SHM). https://digitalcommons.lsu.edu/transet_pubs/16/
12. **Moreu, F.**, & Taha, M. R. (2018). Railroad bridge inspections for maintenance and replacement prioritization using unmanned aerial vehicles (UAVs) with laser scanning capabilities (No. Rail Safety IDEA Project 32) (click here)
13. **Moreu, F.**, Kim, R., Mechitov, K., and Spencer Jr, B. F. (2016). *Railroad Bridge Monitoring Case Study: Little Calumet River Bridge*. Structural Health Monitoring Applications Case Studies Archive, Tufts University, School of Engineering, ASCE SEI (click here)
14. **Moreu, F.**, and Spencer Jr, B. F. (2015). *Framework for Consequence-based Management and Safety of Railroad Bridge Infrastructure Using Wireless Smart Sensors (WSS)*. Newmark Structural Engineering Laboratory. University of Illinois at Urbana-Champaign (click here)
15. Spencer Jr, B. F., **Moreu, F.**, and Kim, R. E. (2015). *Campaign Monitoring of Railroad Bridges in High-Speed Rail Shared Corridors using Wireless Smart Sensors*. Newmark Structural Engineering Laboratory. University of Illinois at Urbana-Champaign (click here)
16. **Moreu, F.** and LaFave, J. (2012); "Current Research Topics: Railroad Bridges and Structural Engineering"; Newmark Structural Engineering Laboratory (NSEL) Report Series 032; University of Illinois at Urbana-Champaign (UIUC), Urbana, IL (click here)

MAGAZINE ARTICLES

1. **Moreu, F.**, Malek, K., Wyckoff, E., Mohammadkhorasani, A. (2022) "Augmented Reality: Existing Capabilities and Future Opportunities" TR News, 340m pp 16-21. July (click here)
2. **Moreu, F.** (2022) "Exceeding the Dream: Wireless sensor networks build resilience in a Native community — and in our research team"; *Winds of Change* Summer Issue. August 8 (click here)
3. **Moreu, F.**, Nasimi, R., Taha, M.R, Garg, P., Basemera-Fitzpatrick, V., Mascarenas, D., Mullen, M. (2020) "Rail Safety IDEA Project 32: Drones and Lasers Enable Safe Railroad Bridges Operations" TR News, 326m pp 38-39. May (click here)
4. **Moreu, F.** (2020); "Ralph B. Peck, PhD, PE, NAE, Hon. M. ASCE" *Geo-Strata —Geo Institute of ASCE*, 2020, Vol. 24, Issue 2, Pg. 16-18, 20-22, 24-27. https://doi.org/10.1061/geosek.0000061
5. **Moreu, F.** (2014); "China Ministry OKs Code for Structural Health Monitoring Systems for Large

Bridges"; ASCE Technical Notes (October) (click here)

6. **Moreu, F.** and LaFave, J. (2011); "Survey of current research topics-Railroad Bridges and Structural Engineering"; Railway Track & Structures, September, pgs. 65-70 (click here)
7. **Moreu, F.** (2007); "Seminar by Martita Mullen in the Civil Engineering College at the University of Granada". The engineer's activity. "Young & Engineer". Revista de Obras Públicas. Number 3480. Colegio de Ingenieros de Caminos, Canales y Puertos. September [In Spanish] (click here)

BOOK CHAPTERS

1. Mascareñas, D., **Moreu, F.**, Wyckoff, E., Susmita, S., & Morales, J. (2022). Augmented Reality for Cradle-to-Grave Infrastructure Monitoring, and Inspection. In Recent Developments in Structural Health Monitoring and Assessment–Opportunities and Challenges: Bridges, Buildings and Other Infrastructures (pp. 407-428).
2. Flanigan, K. A., Aguero, M., Nasimi, R., **Moreu, F.**, Lynch, J. P., & Ettouney, M. (2022). Objective resilience monitoring for railroad systems. In Objective Resilience: Technology (pp. 75-120). Reston, VA: American Society of Civil Engineers.
3. **Moreu, F.** (2001); Seismic Performance of the non-linear new element 08 for DRAIN-2DX, analysis software for non-linear elements under seismic demands; University of Granada, Granada (Spain) [In Spanish] (click here)

GUEST EDITOR

1. Loh, K., Noh, H., **Moreu, F.** "Human Performance Sensing and Human-Structure Interactions"; Journal of Sensors (submissions open until January 31st 2024) (click here)
2. Guo, Y., **Moreu, F.**, Lu, H., Zhu. X., Xu. Z. "Smart Sensing Technology and Infrastructure Health Monitoring"; Journal of Sensors (submissions open until January 15th 2024) (click here)
3. Chang, C., Lin, T., **Moreu, F.** "Methods and Applications of Machine/Deep Learning for Structural Monitoring and Sensing"; Journal of Sensors (submissions closed August 15th 2023) (click here)
4. **Moreu, F.**; "Structural Sensing and Sustainable Infrastructure Maintenance"; Journal of Sustainability (submissions closed July 30th 2023) (click here)
5. **Moreu, F.**, Noh, Haeyoung, Mascarenas, D., Zhang, P. "Understanding Human-Infrastructure Interactions: Context-Aware Structures and Interfaces", Frontiers in Built Environment, Structural Sensing, Control and Asset Management (submissions closed Spring 2020) (click here)

OTHER PUBLICATIONS

1. **Moreu, F.**, Noh, H. Y., Zhang, P., & Mascarenas, D. (2021). Editorial: Understanding Human-Infrastructure Interactions: Context-Aware Structures and Interfaces. *Frontiers in Built Environment*, *7*, 87. https://doi.org/10.3389/fbuil.2021.698620

OTHER PAPERS AND POSTERS PRESENTED AT PROFESSIONAL MEETINGS

1. Wyckoff, E., Khorasani, A., Malek, K. and **Moreu, F.** (2022) "Increasing the use of Human-Machine Interfaces with Augmented Reality for Inspectors" 11th International Association for Bridge Maintenance, Safety and Management (IABMAS 2022) July 10-13, Barcelona, Spain
2. Murillo, J. and **Moreu, F.** "Smart and Connected Communities informed against Floods with Low-cost Sensors (LEWIS 5)" 11th International Association for Bridge Maintenance, Safety and Management (IABMAS 2022) July 10-13, Barcelona, Spain.
3. Malek, K., Mohammadkhorasani, A., **Moreu, F.** (2022) "Augmented Reality Software Development

for Infrastructure Inspection and Characterization"; 8th World Conference in Structural Control and Monitoring, Orlando, Florida, June 6-8.

4. Sanei, M. & **Moreu, F.** (2022) "Measuring Reinforced Concrete Spacing Using RGB Camera and Unmanned Aerial Vehicle (UAV)"; 8th World Conference in Structural Control and Monitoring, Orlando, Florida, June 6-8.
5. Mojidra, R., Mohammadkhorasani, A., **Moreu, F.**, Collins, W., Bennett, C. Li, J. (2022) "Computer Vision and Augmented Reality for Human centered Fatigue Crack Inspection of Steel Bridges"; 8th World Conference in Structural Control and Monitoring, Orlando, Florida, June 6-8.
6. Mustari, S., Hanson, J., Mohammadkhorasani, A., and **Moreu, F.** (2022) "Augmented Reality Application to Analyze Eye Movement during Structural Inspection"; 8th World Conference in Structural Control and Monitoring, Orlando, Florida, June 6-8.
7. Li, J., Mojidra, R., Khorasani, A., **Moreu, F.**, Collins, W., Bennett, C. (2022) "Human-Centered Steel Bridge Inspection using Computer Vision and Augmented Reality"; American Society of Civil Engineers, Engineering Mechanics Institute, Annual Conference, Baltimore, Maryland, May 31-June 3 (mini-symposium keynote presentation).
8. Wyckoff, E., Ball, M., **Moreu, F.** (2022) "Augmented Reality for Feedback and Control in Vibratory Experiments"; American Society of Civil Engineers, Engineering Mechanics Institute, Annual Conference, Baltimore, Maryland, May 31-June 3.
9. Robbins, E., **Moreu, F.** (2022) "Investigating Shaker-System Stability for Strong and Weak Nonlinear Systems"; American Society of Civil Engineers, Engineering Mechanics Institute, Annual Conference, Baltimore, Maryland, May 31-June 3.
10. Yousef, O., **Moreu, F.** (2022) "Evaluation of Event-Based Camera for Structural Dynamic Measurement and Control"; American Society of Civil Engineers, Engineering Mechanics Institute, Annual Conference, Baltimore, Maryland, May 31-June 3.
11. Yuan, X.., Lippitt, C., & **Moreu, F.** (2021.) "LIDAR for rebar spacing determination using structural indexes" SHMII, Lisbon, Portugal (July 29) (presented in Zoom.)
12. Wyckoff, E., Ball, M., Doyle, D., Petersen, C., Fierro, R., **Moreu, F.** (2021) "Augmented Reality Tools for Enhanced Structural Inspection Using Wireless Smart Sensors" American Society of Civil Engineers, Engineering Mechanics Institute, Annual Conference (Virtual), New York, New York, May 25-28.
13. **Moreu, F.**, Wyckoff, E., Hossain, M., Ball, M., Doyle, D., Tubb, M., Petersen, C., Fierro, R. (2021) "Augmented Reality Tools for Agile Manufacturing of Space Vehicles" American Society of Civil Engineers, Engineering Mechanics Institute, Annual Conference (Online), New York, NY, May 25-28.
14. Yousef, O., Komijama, S., **Moreu, F.** (2021) "Programming AI and AR for Safety of Inspectors in Railroad Maintenance and Management Operations" American Society of Civil Engineers, Engineering Mechanics Institute, Annual Conference (Virtual), New York, New York, May 25-28.
15. Khorasani, A., Mustari, S., Cowan, A., D. Law, V., **Moreu, F.** (2021) "Increasing the Understanding Structures through Augmented Reality" American Society of Civil Engineers, Engineering Mechanics Institute, Annual Conference (Virtual), New York, New York, May 25-28.
16. **Moreu, F.**, "Augmented Human-Infrastructure Interfaces for Monitoring Critical Structures" Remote Sensing Techniques for Track Condition and Performance, Standing Committee on Railroad Track Structure System Design (AR050), TRB 99th Annual Meeting, 2020.
17. **Moreu, F.**, "Using Artificial Intelligence to Unlock the Hidden Value of Asset Management Data: Transforming Data into Advanced Decision Making". Panel Discussion: Transforming Data into Advanced Decision Making, TRB 99th Annual Meeting, 2020.

18. **Moreu, F.**, Nasimi, R. and Mullen, M. (2019); "3D Displacement Measurement of Railroad Bridges Using Drones: Implementation" AREMA annual Conference, Minneapolis, Minnesota, September 24, 2019.
19. Aguero, M., Chavez, S., Maharjan, D., M., Mascarenas, D., **Moreu, F.** (2019) "Sensor Data Visualization using Augmented Reality and Database" American Society of Civil Engineers, Engineering Mechanics Institute, Annual Conference, Pasadena, California, June 18-21.
20. Maharjan, D., Hossain, M., Rodriguez, M., **Moreu, F.** (2019) " Structural vulnerability of roof structures in nepali pagoda temples due to load path discontinuity"; American Society of Civil Engineers, Engineering Mechanics Institute, Annual Conference, Pasadena, California, June 18-21.
21. Maharjan, D., Rodriguez, M., Aguero, M., Mascarenas, D., **Moreu, F.** (2019) "Use of Augmented Reality for time critical decision making in hazardous built environment" American Society of Civil Engineers, Engineering Mechanics Institute, Annual Conference, Pasadena, California, June 18-21.
22. Robbins, E., Aguero, M., Maharjan, D., Ayorinde, E., **Moreu, F.** (2019) "Low Cost Wireless Smart Strain Sensors for Structural Health Monitoring of Launching Operations on Aerospace Vehicles" American Society of Civil Engineers, Engineering Mechanics Institute, Annual Conference, Pasadena, California, June 18-21.
23. Maharjan, D., Aguero, M., and **Moreu, F.** (2019) "Augmented Reality for Structural Inspections", Annual Structures Congress Conference of the American Society of Civil Engineers, Orlando, Florida (April).
24. **Moreu, F.** (2019) "Inspection of Bridges Using Augmented Reality", Annual Structures Congress Conference of the American Society of Civil Engineers, Orlando, Florida (April).
25. Maharjan, D., Garg, P., and **Moreu, F.** (2018) "Dynamic Displacement of Railroad Bridges Using UAV and Lasers", Annual Engineering Mechanics Institute Conference of the American Society of Civil Engineers, Massachusetts Institute of Technology (M.I.T.) Cambridge, Massachusetts (May).
26. Diaz, S., Garg, P., Aguero, M., and **Moreu, F.** (2018) "Dancing and Engineering: real-time visualization of data for dancers' performance", Annual Engineering Mechanics Institute Conference of the American Society of Civil Engineers, Massachusetts Institute of Technology (M.I.T.) Cambridge, Massachusetts (May.)
27. **Moreu, F.**, Mascarenas, D. (2018) "Human-infrastructure Interfaces using Augmented Reality", Annual Engineering Mechanics Institute Conference of the American Society of Civil Engineers, Massachusetts Institute of Technology (M.I.T.) Cambridge, Massachusetts (May.)
28. **Moreu, F.**, Ayorinde, E., Benjamin, (2018) "Selecting, Designing and Testing of Low-Cost Sensing of Commercial Space Launch Vehicles", Annual Engineering Mechanics Institute Conference of the American Society of Civil Engineers, Massachusetts Institute of Technology (M.I.T.) Cambridge, Massachusetts (May.)
29. **Moreu, F.**, Garg, P. (2018) "P18-20231 - Rail Safety IDEA Project 32: Railroad Bridge Inspections for Maintenance and Replacement Prioritization Using Unmanned Aerial Vehicles (UAVs) with Laser Scanning Capabilities" TRB 97th Annual Meeting (poster).
30. Garg, P., **Moreu, F.** (2018) "Railroad Bridge Inspections for Maintenance and Replacement Prioritization Using Unmanned Aerial Vehicles (UAVs) with Laser" TRB 97th Annual Meeting.
31. **Moreu, F.** Li, X. (2017); "New Chinese SHM code for large bridges monitoring and safety and USA implications" 7th International Conference on Experimental Vibration Analysis for Civil Engineering Structures, July 12-14. San Diego, University of San Diego, California.
32. **Moreu, F.** Ozdagli, Ali I.; Gomez, Jose A. (2017); "Total Reference-free Displacement of Bridges under Train Crossings" 2017 Rail Infrastructure and Vehicle Inspection Technology Conference. University of Illinois at Urbana-Champaign, June 20-21.

33. Bleck, B., **Moreu, F.** (2017); "New Augmented Reality for Change Detection of Railroad Infrastructure" 2017 Rail Infrastructure and Vehicle Inspection Technology Conference. University of Illinois at Urbana-Champaign, June 20-21.
34. **Moreu, F.**, Lynch, J., and Ettourney, M. (2017); "Objective Resiliency Framework for Ensuring Railroad Network Safety and Efficiency". American Society of Civil Engineers, Engineering Mechanics Institute Conference, June 4-7, 2017.
35. Bleck, B., Vemuganti, S., Farrar, C., Polli, A. & Mascarenas, D., **Moreu, F.** (2017). "Enhancing Structural Visual Inspection Using HoloLens". American Society of Civil Engineers, Engineering Mechanics Institute Conference, June 4-7, 2017.
36. **Moreu, F.**, Ozdagli, A.I., Gomez, J. "Experimental assessment of railroad bridge critical infrastructure using shake tables". American Society of Civil Engineers, Engineering Mechanics Institute Conference, June 4-7, 2017.
37. **Moreu, F**., Garg, P., Vemuganti, S., Ozdagli, A., (2017) "Real-time Displacements of Railroad Bridges Under Train Crossing Events Using Non-contact Reference-free Vibrometers" Mini-symposium, chair, structural performance monitoring of railroad infrastructure, ASCE-SEI Annual Congress, Denver, Colorado, April 6-8.
38. **Moreu, F.**, Ayorinde, E., Mason, J., Mascarenas, D. "Remote Railroad Bridge Structural Tap Testing using Aerial Robots", Los Alamos Summer Symposium (winners of the student poster competition).
39. Vemuganti, S., Ozdagli, A., **Moreu F.**, Survey Bottom Surface Abrasion of Concrete Crossties, AREMA Annual Conference, Orlando, Florida (2nd place in the student competition).
40. **Moreu, F.**; Spencer, Jr., B. F.; Foutch, D. A.; and Scola, S. (2015); "Consequence-Based Management of Railroad Bridges"; 6th International Conference on Advances in Experimental Structural Engineering, 11th International Workshop on Advanced Smart Materials and Smart Structures Technology, University of Illinois, Urbana-Champaign, Urbana, Illinois. August 1-2
41. **Moreu, F.**, Li, J., Jo, H., Kim, R. E., Scola, S., Spencer Jr., B.F., LaFave, J.M. (2015); "Reference-free Displacements for Condition Assessment of Railroad Bridges"; 6th International Conference on Advances in Experimental Structural Engineering, 11th International Workshop on Advanced Smart Materials and Smart Structures Technology, University of Illinois, Urbana- Champaign, Urbana, Illinois. August 1-2
42. Kim, R. and **Moreu, F.** (2014): "Model Development and Identification for a Railroad Bridge using Wireless Smart Sensors"; Computational Science and Engineering Annual Meeting, National Center for Super Computer Applications (NCSA), Urbana, IL, April 7
43. **Moreu, F.** (2014): "Campaign Monitoring of Railroad Bridges using Wireless Smart Sensors: Past, Present, and Future"; EKS Research Retreat, Allerton Conference Center, University of Illinois, Monticello, IL, February
44. **Moreu, F.** (2013): "Structural Health Monitoring of Railroad Bridges"; EKS Research Retreat, Allerton Conference Center, University of Illinois, Monticello, IL, February
45. **Moreu, F.** and LaFave, J. M. (2012): "Wireless Sensing Technology to Enhance Safety and Reliability for Railroad Bridges"; Association of American Railroads (AAR) Annual Research Review, Pueblo, CO, March
46. **Moreu, F.** (2012): "Railroad Bridge Replacement Prioritization"; EKS Research Retreat, Allerton Conference Center, University of Illinois, Monticello, IL, February
47. **Moreu, F.** (2012); "Structural Health Monitoring of Timber Railroad Bridges"; AREMA Committee 10 meeting, Burlington, IA, June 18-20
48. **Moreu, F.** and LaFave, J. M. (2010): "Bridge Performance Assessment using Simplified Field

Monitoring"; Association of American Railroads (AAR) Annual Research Review, Pueblo, CO, February

PATENTS

One patent awarded:

1. **Moreu, F.** & Taha, M. R. (2020). *U.S. Patent No. 10,641,898*. Washington, DC: U.S. Patent and Trademark Office.

Four patents under review and marketing:

1. **Moreu, F.**, Lippitt, C., Yuan, X., Sanei, M. (2022); " The Automatic RGBD-AR-UAV Rebar Inspection" (under evaluation)
2. **Moreu, F.**, Aguero, M., Maharjan, D. Rodriguez, P., Mascarenas, D. (2018); "Augmented Sensing for Real-time Inspections" (marketing)
3. **Moreu, F.**, Mascarenas, D. (2017); "Remote Structural Tap Testing using Aerial Robots"; (marketing)
4. **Moreu, F.**, Taha, M., Garg, P. (2016); "Assessing the condition of railroad bridges enabled by reference-free, non-contact displacement under revenue service train loads using Unmanned Aerial Vehicles (UAVs) and laser cameras" (marketing)
5. **Moreu, F.**, Taha, M., Chirstodoulou, C. (2016); "Assessing the condition of railroad bridges enabled by reference-free, non-contact displacement under revenue service train loads using Unmanned Aerial Vehicles (UAVs) and laser cameras" (marketing)

AWARDS AND HONOR SOCIETIES

Winner SHM in Action Competition, International Workshop in SHM (IWSHM)	2023
Fulbright-Hays Award 2022-2023 (@ National Taiwan University, Taiwan)	2023
UNM Department of Civil Engineering Best Research Paper Spring Semester	2023
UNM School of Engineering Outstanding Junior Faculty Research Award	2022
UNM Department of Civil Engineering Best Research Paper Spring Semester	2022
UNM Department of Civil Engineering Best Research Paper Fall Semester	2021
UNM Department of Civil Engineering Stamm Excellence in Research	2021
ASCE EXCEED, Excellence in Civil Engineering Education	2019
UNM Department of Civil Engineering Stamm Excellence in Education	2019
UNM Department of Civil Engineering Best Research Paper Spring Semester	2016
Center for East Asian and Pacific Studies (CEAPS) Graduate Fellow	2014-2015
Foreign Language and Area Studies (FLAS) Graduate Fellow (click here)	Summer 2014
ASCE SEI Structures Congress Poster Selected as "Best of the Best Voting"	April 2012
Graduate College Dissertation Travel Grant, University of Illinois	2011-2012
Talentia Graduate Fellow, Spanish Government	2010-2011
O. H. Ammann Research Fellow, ASCE (click here)	2010
ASCE Young Engineer of the Year Award Central Illinois Section (click here)	2010
Spanish Society of Civil Engineers Young Engineer of the Year Award (click here)	2010
Max Zar Scholarship, Structural Engineering Foundation	Fall 2009

National Science Foundation (NSF) Scholarship July 2009

STUDENTS AWARDS

TRB Minority Fellow, Marielly Rodriguez (Undergraduate Student) 2023
TRB Minority Fellow, Christian Torres (Undergraduate Student) 2023
TRB Minority Fellow, Timothy Thiegart (Undergraduate Student) 2022
TRB Minority Fellow, Eric Olaguir (Undergraduate Student) 2022
McNair Scholar, Eric Olaguir (Undergraduate Student) 2022
ASCE EMI, SHMC Paper Competition (top five finalist), Odey Yousef (Graduate Student) 2022
TRB Minority Fellow, Jennifer Restrepo (Graduate Student) 2022
TRB Minority Fellow, Dominic Thompson (Undergraduate Student) 2022
AFRL Summer Outstanding Scholar Award, Elijah Wyckoff (Graduate Student) 2021
Nationwide Solar Splash Student competition (3rd place), Jennifer Restrepo (Graduate Student) 2021
TRB Minority Fellow, Joshua Murillo (Undergraduate Student) 2021
ASCE EMI, SHMC Paper Competition (2nd place), Roya Nasimi (Graduate Student) 2020
Sandia National Lab Critical Skills Part-Time Program, Angela Montoya (Graduate Student) 2020
TRB Minority Fellow, Jason Aldaz (Graduate Student) 2020
AFRL Summer Outstanding Scholar Award, Maimuna Hossain (Graduate Student) 2019
TRB Minority Fellow, Emmanuel Ayorinde (Undergraduate Student) 2018
TRB Minority Fellow, Lauren Gomez (Undergraduate Student) 2017

OTHER RECOGNITIONS

Guest interviewed at Geotracks: Students Designing and Deploying Sensors to Improve Flood Prediction in New Mexico (click here) Summer 2022
Keynote paper at EMI Mini-Symposium in Computer Vision Summer 2022
TV News: Researchers at UNM create robot to safely inspect rockslide sites (click here). Spring 2022
Best of Albuquerque Interview/Article for Cybersecurity (click here) Spring 2021
Guest speaker at UNM Lighting Round (click here) Fall 2020
Guest speaker at SOE Engineering in Action (LoboDrome Proposal) (click here) Fall 2020
TV link (click here)

GRANTS, CONTRACTS

Extramural funded grants and projects to date at UNM (all awarded), total: 41 projects ($6,396,374)

(PI of the project unless it is noted otherwise)

1. Sandia National Laboratories, "Non-linear Mechanics and Dynamics Structural Sensing and Damage Assessment" (Co-PI Tariq Khraishi, ME) (October 1st, 2023-September 30th, 2028) ($84,368/year 1)
2. Southern Plains Transportation Center (SPTC) U.S. Department of Transportation (USDOT), "Increasing understanding to climate emergencies and enhancing safety of rural and tribal areas using

wireless smart sensors and human-environment-data interfaces using Augmented Reality (AR)" (06/01/2023 – 05/31/2024) ($160,000.)

3. New Mexico Regional Development Corporation, "Post-wildfire Flooding Monitoring using Low-Cost Efficient Wireless Intelligent Sensors in New Mexico Tribal Land" (June 1st 2023-May 31st 2024.) ($33,903.)

4. Department of Energy (Florida International University, PI): MSIPP WIPP: "Time Machine for underground inspection using Augmented Reality"; (October 1st 2021 -September 30th 2023) (Co-PI John Stormont) ($75,000.)

5. Michigan Tech University, "Expanding Summer Youth Programs in Rail through Virtual Learning and a National Campus Network" (June 1st-July 31st 2023) ($8,922.)

6. Sandia National Laboratories, "Investigation of the Multi-Input Multiple-Output Dynamic Testing: Numerical Investigation" (October 2021-September 2024) ($450,000.)

7. Sandia National Laboratories, "Experimental Techniques for the Control of Nonlinear Dynamical Structures" (October 2022-June 2024) ($148,500.)

8. Office of Naval Research "Scanning and Visualizing Damage connecting Augmented Reality (AR) with LiDAR, Models and Databases" (August 2022-April 2024) ($69,385.00)

9. Tran-SET Program, Louisiana State University U.S. Department of Transportation (USDOT), "TranSET 6: Bridge Inspection Training and Enhanced Operations using Augmented Reality (21-052-ST)", (August 2022-February 2024) ($130,000.)

10. Federal Railway Administration BAA; Research Initiatives in Support of Making Railroading a Career of Choice: "The Railroader of the Mid-Century". (Co-PI Haeyoung Noh, Stanford University, and Sungmoon Jung, Florida State University) (September 23, 2021-September 22, 2024) ($475,375.)

11. National Science Foundation; SCC-CIVIC-FA Track B: Low-Cost Efficient Wireless Intelligent Sensors (LEWIS) for Greater Preparedness and Resilience to Post-Wildfire Flooding in Native American Communities (Co-PI: Mark Stone, CCEE; Su Zhang, EDAC; Yolanda Lin, Geography; Carolyn Hushman, Educational Psychology.) (October 1, 2021-December 31, 2023) ($1,032,000 to date.)

12. National Science Foundation (PI: Mark Stone, CCEE): SRS RN: Transforming Rural-Urban Systems: Trajectories for Sustainability in the Intermountain West (eight Universities total), contributing as senior personnel (September 15th 2021-October 31st 2026) ($30,000.)

13. Office of Naval Research, "Measuring Damage Outdoors while Flying (MDOF)" (September 13, 2021- March 31st, 2024) (Co-PI Rafael Fierro, ECE) ($425,365.)

14. National Science Foundation (PI: Rebekah Napolitano, PSU), "Collaborative Research: HDR DSC: Infusing community-centered data science into undergraduate engineering curricula"; (October 1st 2021-September 30th 2024.) ($130,000.)

15. Sandia National Laboratories; Sandia UNM ENGR 2019 NMSBA; "Wearable Fall Protection Sensor Market Feasibility"; (August 20th 2021-December 31st 2021) ($8,500.)

16. Tran-SET Program, Louisiana State University U.S. Department of Transportation (USDOT), "TranSET 5: Increasing Bridge Durability and Service Life with LIDAR Enhanced Unmanned Aerial Systems (UAS)", (Co-PI Chris Lippitt, Geography) (August 2021-February 2023) ($100,000.)

17. Department of Energy BENEFIT (PI: Rebekah Napolitano, PSU): (July 1st 2021 -June 30th 2023) ($12,500.)

18. Tetra Tech Inc.: “Crash Beam Attenuation”; (March 23th 2021– October 31st 2021) ($40,657.)

19. National Science Foundation; SCC-CIVIC-PG Track B: Low-Cost Efficient Wireless Intelligent Sensors (LEWIS) for Greater Preparedness and Resilience to Post-Wildfire Flooding in Native American Communities (Co-PI: Mark Stone, CCEE; Su Zhang, EDAC; Yolanda Lin, Geography; Carolyn Hushman, Educational Psychology.) (January 15, 2021-June 30 2021) ($50,000.)

20. National Academy of Sciences, NCHRP IDEA (University of Kansas): “Fatigue crack monitoring using AR” (February 1st 2021-January 31st 2023.) ($60,000.)

21. Federal Railway Administration BAA; Research Initiatives in Support of Rail Safety; FRA-HF-004, Research Initiatives in Support of Rail Safety: “Automation and the Human-Machine Interface” (Co-PI Victor Law, OILS) (July 1, 2020-June 30 2021) ($209,258.)

22. National Academy of Sciences, Transportation Research Board (TRB) IDEA Safety: “Augmenting Reality for Safer Inspections of Railroad Infrastructure and Operations” (Co-PI Victor Law, OILS) (January 2021-November 2022) ($99,000.)

23. National Aeronautics and Space Administration (NASA) and New Mexico Space Grant Consortium (NMSGC); “Safe and Augmented Human-Robotic Interaction for Space (SAHRIS)." (April 8, 2020-February 28, 2021) ($30,000.)

24. Office of Naval Research; “Engaging University of New Mexico ROTC Cadets in Cybersecurity Research” (Co-PI Francesco Sorrentino, ME) (January 1, 2020-July 8th, 2022) ($500,000.)

25. New Mexico Consortium, Los Alamos National Laboratory “Cybersecurity of Cyber-physical Systems Using Wireless Smart Sensors” (Fall 2020-Fall 2021) ($32,824.)

26. Air Force Research Laboratory: “Agile Manufacturing for High Value, Low Volume Production” (PI Rafael Fierro, ECE) (April 2018-April 2028) ($194,891 allocated to date.)

27. Tran-SET Program, Louisiana State University U.S. Department of Transportation (USDOT), “20GTUNM31 - An automated system for inspecting rock faces and detecting potential rock falls using machine learning” (PI John Stormont, CCEE) (Summer 2020-Fall 2021) ($100,000.)

28. Tran-SET Program, Louisiana State University U.S. Department of Transportation (USDOT), "20STUNM04 - Bridge Cracks Monitoring: Detection, Measurement, and Comparison using Augmented Reality ", Summer 2020-Fall 2021 ($120,000.)

29. National Academy of Sciences, Transportation Research Board (TRB) IDEA Safety: “Measuring Behavior of Railroad Bridges under Revenue Traffic using Lasers and Unmanned Aerial Vehicles (UAVs) for Safer Operations: Implementation” (Nov 2018-August 2020) ($99,187.)

30. Sandia National Laboratories, “Investigation of the Multi-Input Dynamic Testing” (October 2018-September 2021) ($690,000.)

31. Sandia National Laboratories, “Control of Nonlinear Dynamical Structures under Extreme Normal Environments” (October 2019-September 2022) ($220,500.)

32. New Mexico Consortium, Los Alamos National Laboratory “Smart management of infrastructure using human-infrastructure interfaces” (Spring 2019-Spring 2020) ($47,590.)

33. Tran-SET Program, Louisiana State University U.S. Department of Transportation (USDOT), “TranSET 3: Bridge Construction Monitoring using LIDAR for Quantified, Objective Quality-Control Quality-Assurance (QOQCQA)”, (Co-PI Chris Lippitt, Geography) (Summer 2019-Spring 2021) ($120,000.)

34. Tran-SET Program, Louisiana State University U.S. Department of Transportation (USDOT),

"TranSET 2: Strategies for Prioritizing Needs for Accelerated Construction after Hazard Events", (PI Vanessa Valentin) (Spring 2018-Summer 2019) ($50,000.)

35. Los Alamos County, "Augmented inspection to assist existing design and maintenance of infrastructure" (Summer 2017-Spring 2020) ($65,000.)
36. Los Alamos National Laboratory, "Augmented Reality for inspections" (May 2018-September 2018) ($81,318.)
37. New Mexico Consortium, Los Alamos National Laboratory "Augmenting Human Assessment of Infrastructures Performance Through New Technologies" (Spring 2017-Spring 2018) ($31,944.)
38. Tran-SET Program, Louisiana State University U.S. Department of Transportation (USDOT), "Tran-SET 17STUNM02: Development, Training, Education, and Implementation of Low-cost Sensing Technologies for Bridge Structural Health Monitoring (SHM)", (Co-PI Chris Lippitt, Geography) (Summer 2017-Fall 2018) ($150,000.)
39. National Aeronautics and Space Administration (NASA) and New Mexico Space Grant Consortium (NMSGC); "Structural Performance Monitoring Using Wireless Sensors (WSW) for Cost-Efficient Management and Development of Commercial Space Vehicles" (Spring 2017- Spring 2018) ($25,000.)
40. National Academy of Sciences, Transportation Research Board (TRB) IDEA Safety: "Railroad Bridge Inspections for Replacement Prioritization Using Unmanned Aerial Vehicles (UAVs) with 3D Laser Scanning Capabilities" (Co-PI Mahmoud Taha, CCEE) (November 2016-March 2018) ($99,400.)
41. New Mexico Consortium, Los Alamos National Laboratory "Ensuring the Sustainability and Resilience of Timber Bridge Railroad Infrastructure Using Remotely Deployed Sensor Nodes", Summer 2016 ($38,811.)

Internally funded grants and projects to date at UNM (all awarded), <u>total: 8 projects ($125,831.36)</u>

1. NSF I-Corps Program: Low-cost Efficient Wireless Intelligent Sensors Field Deployments at California and Tramway (fall 2022) ($5,000)
2. Fall 2021 Program for Enhancing Research Capacity (PERC): Light Detection and Ranging (LiDAR) for Terrain and Vegetation analysis; PI Chris Lippitt, Co-PI Moreu (summer 2021) ($35,931.36)
3. UNM Summer 2021 WeR1 Investing in Faculty Success Program: PhD support ($4,400.)
4. OVPR UNM Sandia Alliance, LDRD-ACORN: "Nonlinear Dynamic Vibrations Instrumentation"; (December 2020) ($40,000.)
5. Department of Civil Engineering at UNM, Major Teaching Instrumentation (MTI) Proposal, "Shake Table repair" Spring 2017 ($30,000.)
6. UNM Center for Teaching Excellence. Teaching Allocation Grant. Fall 2016. "Augmented Reality for Structural Inspection: Teleportation" ($2,500.)
7. Department of Civil Engineering at UNM, Curriculum Committee and Chair. Spring 2016. "Shake Table for Research of Dynamic Loads" ($5,000.)
8. UNM Center for Teaching Excellence. Teaching Allocation Grant. Fall 2015. "Shake Table for Teaching Experimental Structural Dynamics" ($2,000.)
9. UNM Chair Competition on Innovative Educational Tools. Fall 2015. "UAV for Infrastructure Monitoring" ($1,000.)

Grants and contracts I formulated and wrote proposals for on behalf of the PIs prior to UNM (all awarded), total: 7 projects ($486,737).

1. Federal Railroad Administration (FRA): Condition Assessment of Railroad Bridges using Reference-free Estimates of Bridge Displacement under In-service Train Loads (PI B. F. Spencer, Jr.), May 2015-May 2016. Research and Demonstration Projects Supporting the Development of Reference-free Displacement Estimations under Live Loads, FRA BAA-2014-2 ($144,281.)
2. Association of American Railroads (AAR), Technology Scanning Program: Structural Health Monitoring of Railroad Bridges for Impact Detection (PI B. F. Spencer, Jr.), January 2015-December 2015 ($30,000.)
3. Federal Railroad Administration (FRA): Campaign Monitoring of Railroad Bridges in High- Speed Rail Shared Corridors using Wireless Smart Sensors (PI B. F. Spencer, Jr.), February 2013-February 2014. Research and Demonstration Projects Supporting the Development of High Speed and Intercity Passenger Rail Service, FRA BAA-2010-1 ($164,456.)
4. Association of American Railroads (AAR), Technology Scanning Program: Structural Health Monitoring of Railroad Bridges for Impact Detection (PI B. F. Spencer, Jr.), January 2014-December 2014 ($30,000.)
5. Association of American Railroads (AAR), Technology Scanning Program: Wireless Sensing Technology to Enhance Safety and Reliability for Railroad Bridges (PI James M. LaFave), January 2013-December 2013 ($39,000.)
6. Association of American Railroads (AAR), Technology Scanning Program: Wireless Sensing Technology to Enhance Safety and Reliability for Railroad Bridges (PI James M. LaFave), January 2012-December 2012 ($34,000.)
7. Association of American Railroads (AAR), Technology Scanning Program: Bridge Performance Assessment using Simplified Field Monitoring (PI James M. LaFave), January 2011-December 2011 ($45,000.)

PROFESSIONAL SERVICE

Professional committee leadership:

- American Society of Civil Engineers (ASCE) - Engineering Mechanics Institute (EMI) Structural Health Monitoring and Control (SHMC) Committee Secretary (September 2023-present.)
- Society of Engineering Mechanics, Dynamics of Civil Structures Technical Division Secretary (February 2023-present.)
- American Railway Engineering and Maintenance-of-way Association (AREMA) Committee 10: Construction, Management and Maintenance of Railroad Bridges. Research and Advancement Subcommittee: Assistant to the Chairman (June 2010-present).
- American Society of Civil Engineer New Mexico Section, Structures and Mechanics Chair (Fall 2015-present.)
- American Society of Civil Engineers (ASCE) “Fly-In New Mexico Leader (Captain)” (Fall 2015-Fall 2022.)

Professional committee memberships:

- Transportation Research Board, Standing Committee on Testing and Evaluation of Transportation Structures - AKB40.
- American Society of Mechanical Engineers (ASME.)

- International Structural Health Monitoring of Intelligent Infrastructure (ISHMII.)
- UAS/Remote Sensing Cluster of the NM CRDC.
- NU Rail faculty member representative (UNM.)
- AREMA Committee 7: Guest participant on railroad steel bridge design and rating committees.
- AREMA Committee 24: Guest participant on education and training.

Technical reviewer for (in the last two years):

- Journal of Structural Health Monitoring.
- Journal of Mechanical Systems and System Processing.
- Journal of Measurement.
- Journal of Building Engineering.
- Journal of Computer-Aided Civil and Infrastructure Engineering.
- Journal of Civil Structural Health Monitoring.
- Journal of Vibration and Acoustics (ASME.)
- Journal of Sensors.
- Journal of Automation in Construction.
- Journal of Engineering Computations.
- Journal of Vibration and Control.
- Journal of Control and Health Monitoring.
- Journal of Smart Structures and Systems.
- Journal of Performance of Constructed Facilities, ASCE.
- Journal of Bridge Engineering, ASCE.
- Journal of Engineering Structures, ASCE.
- Journal of Engineering Mechanics, ASCE.

Service at professional venues:

- October 17th, 2023, 2023 NSF HDR Ecosystem Conference, panel presenter "Expanding the Engineer's Toolbox: Lessons in Data Science Education", Denver, CO.
- September 14th, 2023, International Workshop of Structural Health Monitoring, Panel Member of the panel "New Technologies and Artificial Intelligence for Highway Bridge Monitoring: A Panel Discussion". Stanford, Palo Alto, CA.
- May 31st 2022, ASCE EMI Structural Health Monitoring & Control (SHMC) Committee Meeting, ad-hoc secretary for minutes (on behalf of secretary Noh joining remotely)
- Fall Conference Coordinator; ASCE New Mexico Fall Conference, Albuquerque, NM. October 15, 2021 (Zoom, over 50 participants.)
- American Society of Civil Engineers, EMI SHMC Committee Student Competition (SHMC-SC) 2021. Sponsored by: The EMI SHMC Committee. Student paper competition, chair (June 2020-May 2021.)
- Fall Conference Chair and Masters of Ceremonies; ASCE New Mexico Fall Conference, Albuquerque, NM. October 16, 2020 (Zoom, over 100 participants.)
- AREMA Committee 10: Construction, Management and Maintenance of Railroad Bridges. Spring

2020 National Meeting, Host at UNM SOE (supported by CCEE Department) (30 attendants from railroad industry hosted in Stamm Room for 1 day.)

- American Society of Civil Engineers Fly-In: Representing New Mexico with the Legislators at Washington DC, March 12-13, 2019.
- Super STEM AFRL Outreach, Smart Sensors and Technology Booth (February 23rd 2019.)
- Fall Conference Chair and Masters of Ceremonies; ASCE New Mexico Fall Conference, Albuquerque, NM. September 28, 2018 (in person, over 100 participants.)
- Technical reviewer of multiple programs and panel reviews at the National Science Foundation related to Cyber-Physical Systems, Civil Infrastructure Monitoring, and Controls (2017 to present.)
- American Society of Civil Engineers, Engineering Mechanics Institute, EMI Objective Resilience Committee Student Competition (ORC-SC) 2017. Sponsored by: The EMI Objective Resilience Committee (ORC.) Student best-paper competition, judge (June 2017.)
- American Society of Civil Engineers State Leaders: Representing New Mexico with ASCE Headquarters for leadership positions, meeting at Washington DC, June 13, 2017.
- American Society of Civil Engineers Fly-In: Representing New Mexico with the Legislators at Washington DC, March 13-14, 2017.
- American Society of Civil Engineers Fly-In: Representing New Mexico with the Legislators at Washington DC, March 14-18, 2016.
- Fulbright Scholarship Candidates Interview Committee, University of Illinois at Urbana-Champaign, September 2014.
- Delegate of the Spanish Society of Civil Engineers, International Meeting with Board of Directors, ASCE Annual Conference, Charlotte, NC, October 15-17, 2013.
- Delegate of the Spanish Society of Civil Engineers, International Agreement with the Canadian Society of Civil Engineers (CSCE), International Heritage Landmark in Civil Engineering, Niagara Falls, ON (Canada), September 28-30, 2010.
- Host from the Spanish Society of Civil Engineers to Stefan Jaeger (ASCE), ASCE 2025 Vision presentation to the Spanish Civil Engineering Associations, Madrid (Spain) June 21-23, 2010.
- Delegate of the Spanish Society of Civil Engineers, International Heritage Landmark in Civil Engineering, with ASCE President Blaine Leonard and Washington State Governor Christine Gregoire, Port Townsend, WA (US), April 20-23, 2010 (click here)

Symposium/Session Chair

- Session co-chair, “Human Performance Sensing and Human-Structure Interactions” International Workshop in Structural Health Monitoring, Stanford, CA, September 12-15 2023.
- Session chair, Mini-symposium, “Assessing Human-Infrastructure Interactions and their Performance”, ASCE-EMI Annual Conference, Georgia Tech, Atlanta, GA, June 7-9 2023 (PhD student M. Sanei chaired on my behalf).
- Session chair, Mini-symposium, “Session chair, Mini-symposium, "Assessing Human-Infrastructure Interactions and their Performance", ASCE-EMI Annual Conference, Georgia Tech, Atlanta, GA, June 7-9 2023 (PhD student A. Khorasani chaired on my behalf).
- Session chair, Session Civil Engineering SHM, International Modal Analysis Conference, Austin, Texas, February 13-16, 2023.
- Session chair, Mini-symposium, “Innovative Solution of Classic Problems in Bridge Design,

Construction and Maintenance with Artificial Intelligence", Eleventh International Conference on Bridge Maintenance, Safety and Management, by International Association for Bridge Maintenance and Safety (IABMAS), University Politec of Catalunya, Spain, July 11-15, 2022.

- Session chair, Mini-symposium, "Assessing Human-Infrastructure Interactions and Interfaces", Eighth World Conference on Structural Control and Monitoring (8WCSCM), University of Central Florida, Orlando, Florida, July 6-8, 2022.
- Session chair, Mini-symposium, "Assessing Human-Infrastructure Interactions and their Performance", ASCE-EMI Annual Conference, John Hopkins University, Maryland, May 31-June 3 2022.
- Session chair, Session Civil Engineering SHM, International Modal Analysis Conference, Orlando, Florida, February 6-9, 2022.
- Session chair, Mini-symposium, "Computer Vision and Structural Health Monitoring", ASCE-EMI Annual Conference, Columbia, NY, May 25-28 2021.
- Session chair, Mini-symposium, "Augmented Reality and Human-structure Interfaces", ASCE-EMI Annual Conference, Columbia, NY, May 25-28 2021.
- Session chair, Session Civil Engineering SHM, International Modal Analysis Conference, February 8-11, 2021 (online).
- Fall conference structures chair; ASCE New Mexico Fall Conference, Socorro, NM. October 18, 2019.
- Session chair, "Augmented Reality and Structural Health Monitoring" International Workshop in Structural Health Monitoring, Stanford, CA, September 10-12 2019.
- Session chair; Mini-symposium, "human and structures interfaces and machine learning", ASCE-EMI Annual Conferences, Pasadena, CA, June 18-21 2019.
- Session chair; Industry Applications of SHM; 9th International Conference on Structural Health Monitoring of Intelligent Structures", Saint Louis, MO. August 4-7, 2019.
- Session chair, Mini-symposium, "Human-structures interfaces", ASCE-EMI Annual Conference, Boston, MA, May 27-30 2018.
- Session chair, Innovation in displacement measurement: 3rd Huixian International Forum on Earthquake Engineering for Young Researchers. Champaign, Illinois, August 11-12, 2017.
- Session chair, 7th International Conference on Experimental Vibration Analysis for Civil Engineering Structures, July 12-14, 2017. San Diego, University of San Diego, California.
- Session chair: Panel review, structural performance monitoring of railroad infrastructure: an stakeholder point of view, ASCE-SEI Annual Congress, Fort Worth, Texas, April 19-21 2018.
- Mini-symposium, chair, structural performance monitoring of railroad infrastructure, ASCE-SEI Annual Congress, Denver, Colorado, April 6-8 2017.
- Mini-symposium, chair, structural health monitoring for bridges, European Workshop for Structural Health Monitoring, Bilbao, Spain, July 7, 2016.
- Mini-symposium, co-chair, structural health monitoring, 6th International Conference on Advances in Experimental Structural Engineering, 11th International Workshop on Advanced Smart Materials and Smart Structures Technology, University of Illinois, Urbana-Champaign, Urbana, Illinois. August 1-2, 2015.
- Mini-symposium, co-chair, afternoon session, EKS retreat, Allerton Park Retreat Center, Monticello, IL, February 1-2 2014.

- Chairman, Second Meeting of Civil Engineers from Spain in the US, Illini Center, Chicago, IL November 10-11, 2012.
- Chairman, First Meeting of Civil Engineers from Spain in the US, Urbana Country Club, Urbana, IL, April 27, 2012.

UNM, School of Engineering

- New Chair Search Committee, Department of Civil, Construction and Environmental Engineering, member (August 2023-present.)
- Lobo-Drome PI (design, fundraising, and dissemination of a new UAS facility for SOE, including applying and receiving support from ONR DURIP and presenting to donors, meeting with architects, and UNM Foundation).
- Mentor of 2-3 minority students each summer supported by Engineering Student Success Center (ESSC) (2019- present)
- World Engineering Deans Conference, Civil Engineering Research, booth, November 13, 2018.
- Coordinator, Shake Out day, October 18, 2018.
- Congressional Challenge, Design an App, expert panel at Explora, October 13th 2017.
- Dean Search committee, member (October 2016-January 2017.)

UNM, Prince of Asturias Chair Endowment

- Advisory Board, member (December 2015- present.)

UNM, Department of Civil, Construction and Environmental Engineering

- Two new faculty search committee, member (August 2023-present.)
- One new faculty search committee, member (August 2020- March 2021.)
- Four new faculty search committee, member (August 2019 –March 2020.)
- Structures faculty search committee, member (August 2018-March 2019.)
- Structures Area: faculty coordinator
- Graduate Committee, member (August 2015- present.)
- Graduate recruitment week: organized CCEE seminar and tours for prospective CCEE applicants.
- Collaborate with CE160 with lectures, or those of my graduate students and postdocs (since 2020.)
- American Society of Civil Engineers (ASCE) student chapter, faculty mentor (August 2021-present)
- American Institute Steel Construction (AISC) Bridge Competition student chapter, faculty mentor (January 2023-present)
- Earthquake Engineering Research Institute (EERI) student chapter, faculty mentor: organized seminars including: Dr. Nakai and the Fukushima Daiichi Nuclear Plant (click here)

UNM, Outreach

- Summer Transportation Institute 2016 to present (click here)
- Smart Management of Infrastructure Summer Camp, 2016 to present (click here)
- Visiting local high school and middle schools throughout the year (two-three per semester.)
- Mentoring 1-2 high school students throughout the year for their senior project (2016-present.)
- UNM SOE Booth at the 7th World Conference on Structural Control and Monitoring (WCSCM), Qingdao, China, July 22-25 2018.

- UNM SOE Engineering Open House 2015 to present (both Civil Engineering and Mechanical Engineering Open Houses): approximately ten students of my research group present about six demonstrations including, but not limited to: robots, AR, sensors, computer vision, and dynamics.

INVITED WORKSHOP PRESENTER

1. "HDR DSC: Infusion of data science and computation into engineering curricula: Human-Machine-Dynamics Collaboration using Augmented Reality" NSF HDR Ecosystem Conference, Denver, CO. October 15-18, 2023.
2. "Augmented Reality for Human-Centered Structural Health Monitoring", Sandia National Laboratory 4th Annual XR Conference: Augmented, Virtual and Mixed Reality, July 12th (click here)
3. "Structural Dynamics and Low-cost Sensors" Sandia National Laboratory Short Course on Strutural Dynamics, Non-linear Mechanic and Dynamics (NOMAD) Summer School, June 23rd 2022 (17 students).
4. Monitoring for sAfe and Resilient Systems (MARS) SHM Workshop, "Advancing Human-Infrastructure Interfaces: New Frontiers and Opportunities", Chair of Structural Mechanics & Monitoring, ETH Zurich, March 28th, 2022 (online)
5. Transportation Research Board (2020) Artificial Intelligence for Infrastructure Management, 99th Annual TRB Conference, Washington DC, January.
6. TRANSET Webinar Series: "Innovative Technology, Techniques, and Processes in Transportation Infrastructure Inspection" (Section 2) "Augmented Reality for Infrastructure Inspections" September 26, 2020.
7. TRANSET Webinar Series: "Innovative Technology, Techniques, and Processes in Transportation Infrastructure Inspection" (Section 1): "Cyber Physical Systems for Maintenance of Critical Infrastructure", June 27, 2020.
8. Resilience Infrastructure with New Cyber physical Systems, Universidad de Sonora, Mexico, Hermosillo, Mexico, November 23-27, 2019.
9. Artificial Intelligence and Machine Learning for Civil Infrastructure; South East University, Nanjing, China, September 4-6, 2019.
10. Presenter/coordinator: AFRL Technological Showcase for Industry and National Laboratories, February 28th 2018 (over 100 attendees), STC UNM, Albuquerque, NM
11. Young Researchers Symposium in Earthquake Engineering, Chinese Earthquake Administration, Institute of Engineering Mechanics. August 17-18, 2016.
12. New Mexico Collaborative Research and Development Council, Feb 16 2016, Albuquerque, New Mexico." Unmanned Aerial Systems (UAS) and Remote Sensing (RS) Cluster."
13. New Mexico Collaborative Research and Development Council, December 11th 2015, Santa Ana Pueblo, New Mexico." Unmanned Aerial Systems (UAS) and Remote Sensing (RS) Cluster."
14. Bridge Weigh-in-Motion (BWIM); University of Connecticut, FHWA and Connecticut Department of Transportation, Storrs, CT, October 26-27, 2015.
15. UNM COSMIAC Region Technical Workforce Study, Albuquerque, NM. September 18, 2015.

INVITED ORAL PRESENTATIONS / TECHNICAL SEMINARS

1. "New Human-Machine-Structure Interfaces Enabling Structural Health Monitoring, Digital Twin",

Iowa State University, Structural Health Monitoring Seminar for thirty students and faculty. Ames, IA. October 26th 2023.

2. "Human-Machine-Digital Twin Interfaces using Augmented Reality", Purdue University, Seminar for ten students and faculty, West Lafayette, IN, October 2nd 2023.
3. Taiwan High Speed Railways, Taipei, Taiwan. "Advancing New Human-Machine-Structure Interfaces with Potential Applications for High-Speed Rail Management" (3 hours meeting with managers of the Taiwan HSR to discuss railroad operations, management, and monitoring. Discussion on practical implementation of research for HSR infrastructure management and monitoring.)
4. Taoyuan Metro Rail Company, Taoyuan, Taiwan. "Structural Health Monitoring of Railroads using Human-Machine-Data Interfaces" (3 hours meeting with metro engineering team and tour of locomotive shop and engineering buildings for passenger transportation between the airport and Taipei. Discussion of practical research for infrastructure monitoring and management with new technologies.)
5. "Practical Implementation of Structural Health Monitoring for Infrastructure Safety" Department of Civil Engineering, Chung Hsign University, Taichung, Taiwan, June 1st 2023.
6. "New Technologies for the Understanding of Structural Complexity and Disasters" Department of Civil Engineering, Taiwan Tech, Taipei, Taiwan, May 31st 2023.
7. "Structural Health Monitoring of Railroads using Human-Machine-Data Interfaces" Department of Transportation Logistics and Management, National Yang Ming Chiao Tung University (NYCU), Hsinchu, Taiwan, April 17th 2023.
8. "High Speed Rail and Infrastructure Maintenance, Assessment, and Post-Earthquake Damage Evaluation: Studying Chinese Language to Advance Engineering Understanding"; Fulbright Kick-off Project Presentation. Taiwan Fulbright Foundation, Taipei, Taiwan, April 10th 2023.
9. "Advancing Safety during Disasters: New Human-Machine-Structure Interfaces" National Center for Research on Earthquake Engineering, National Taiwan University, Taipei, Taiwan, April 6th 2023.
10. "Professional Applications of Structural Dynamics and Structural Health Monitoring", Structural Dynamics Lecture at the Department of Civil and Environmental Engineering, National Taiwan University, Taipei, Taiwan, April 4th 2023 (10 students).
11. "Advancing Civil Infrastructure Safety and Management with New Human-Data-Structure Interfaces", Computer Aided Program, Department of Civil and Environmental Engineering, National Taiwan University, Taipei, Taiwan, March 21st, 2023 (online).
12. "Human-Infrastructure Interfaces in Structural Health Monitoring" Department of Mechanical Engineering, National Sun Yat-sen University, Kaishung, Taiwan, March 7th 2023 (online).
13. "New Structural Health Monitoring Techniques for Infrastructure Management", Department of Civil Architectural and Environmental Engineering, University of Texas at Austin, February 15th 2023.
14. "Advancing Infrastructure Design, Safety and Maintenance with New Human-Structure Interfaces", Department of Civil and Environmental Engineering, Virginia Tech, February 7th 2023.
15. "Construction inspection of reinforced concrete using Lidar and UAVs". Testing and Evaluation of Transportation Structures Committee, AKT40, January 12th, TRB 102th Annual Meeting, Washington DC, 2023.
16. "Augmented Reality investigation for underwater bridge inspection of bridges" AKT40(2) Structure Coatings and Linings Subcommittee, January 13th, TRB 102th Annual Meeting, Washington DC, 2023.
17. "New Human-Infrastructure Interfaces in Structural Dynamics" University of Bologna, Department of Civil Engineering, December 13th 2022.

18. "Emergency responses after disasters using Augmented Reality and New Sensing Interfaces" University of Granada, Department of Civil Engineering, October 7th 2022.
19. "New Robot-enabled Human-Machine Interfaces (HMI) for Structural Health Monitoring (SHM)"; Chair of Structural Mechanics & Monitoring, ETH Zurich, September 16th, 2022 (click here)
20. "Augmented Reality for Railroad Infrastructure Critical Inspection"; AREMA Technical Committee 10 Bridge Maintenance; 2022 AREMA Annual Meeting, Denver, Colorado, August 28th.
21. "The Railroaders of the Mid-Century"; AREMA Technical Committee 24 Education and Training; 2022 AREMA Annual Meeting, Denver, Colorado, August 27th .
22. "Human-Machine Interfaces with SHM Applications" 11th International Conference on Structural Health Monitoring of Intelligent Infrastructure, August 12th, 2022, Montreal, Quebec, Canada.
23. "Structural Health Monitoring and Human-Infrastructure Interfaces"; 2022 Los Alamos Dynamics Summer School (LADSS); Los Alamos National Laboratory, Los Alamos, NM, June 21st 2022.
24. "Intelligent Human-Infrastructure Interfaces for Inspectors and Decision-Makers" INSPIRE University Center of Transportation Webinar, June 21st 2022 (click here).
25. "The Railroads of the Future: SmartRailroads.org" Department of Civil, Construction and Environmental Engineering, University of New Mexico, Graduate Seminar, May 4th 2022.
26. "UNM ROTC Cybersecurity program: training our UNM ROTC cadets and students" Rotary Club of Albuquerque, March 16th 2022 (click here)
27. "Human-machine Interfaces for SHM using Unmanned Aerial Systems: applications" SHM class, hosted by Dr. Simon LaFlamme, University of Iowa, February 24th 2022.
28. "Low-cost Efficient Wireless Intelligent Sensors (LEWIS) for Reserve Officer Training Corps (ROTC) Cyber Physical Cyber Security Training (CPCST)" Structural Health Monitoring Subcommittee, AKT40(3) Safety and Security of Bridges and Structures, January 11th, TRB 101th Annual Meeting, Washington DC.
29. "New Machine Learning Waterfront Inspection Capabilities and Interfaces: Indoor and Outdoor Validations" AKT40(2) Structure Coatings and Linings Subcommittee, January 11th, TRB 101th Annual Meeting, Washington DC.
30. "New Bridge Inspection and Monitoring Enabled by Using Human-Structure Interfaces" AKT40 Structures Maintenance, January 11, TRB 101th Annual Meeting, Washington DC.
31. "Human-structures interfaces for inspection of structures". Testing and Evaluation of Transportation Structures Committee, AKT40, January 10th, TRB 101th Annual Meeting, Washington DC.
32. "Human-machine interfaces for structural inspection and augmented reality" CEE Workshop on "Civil Digital Transformation and Beyond"; Virtual Workshop, KAIST, November 19th 2021.
33. "Wearable sensors and research opportunities for ROTC Cadets Using Wireless Sensors"; ROTC weekly briefing, UNM ROTC Marines and Navy students (over 80 students), November 18th 2021.
34. "Civil, Structural, and Cyber-physical research for high school students", Menaul Academy, Albuquerque, NM. November 2nd, 2021 (200 students)
35. "Cyber physical systems for ROTC Cadets Using Wireless Sensors"; ROTC weekly briefing, UNM ROTC Marines and Navy students (over 80 students), September 9th 2021.
36. "New Human-Infrastructure Solutions for Augmented Inspection and Maintenance of Structures" HNTB Technology Group, August 27th 2021.
37. "Augmented Reality Enabling New Human-Infrastructure Interfaces" IABMAS International Society, July 21st, 2021.
38. "The Future of Work for Resilient Management of Disasters"; Department of Civil and Environmental

Engineering. Florida State University, Tallahassee, FL, May 24th 2021.

39. "Cyber Physical Systems for Structural Dynamics with Structural Health Monitoring Applications", Department of CCEE, University of New Mexico, Departmental Seminar, May 5th 2021.
40. "Smart Management of Infrastructure: New Interfaces in Structural Health Monitoring (SHM)" Department of Civil and Environmental Engineering Departmental Seminar, University of South Carolina, March 10th, 2021.
41. "Advancing Human-Infrastructure Interfaces: The New Frontiers"; Smart Structures Webinar Series, Department of Civil and Environmental Engineering, University of Kentucky, March 9th, 2021.
42. "2021 STEAM Virtual: Augmented Reality: New Human-Infrastructure Interfaces", National Museum of Nuclear Science and History, February 23rd, 2021 (click here)
43. "Augmenting Human-Infrastructure Interfaces", Computer Science Departmental Seminar, University of New Mexico, October 28th 2020.
44. "Low-Cost Efficient Wireless Intelligent Sensors (LEWIS) Towards Smart Management of Infrastructure" Electrical and Computer Engineering Departmental Seminar, University of New Mexico, May 7th 2020.
45. "Human-Infrastructure Interfaces for Critical Infrastructure and Disasters"; Department of Civil and Environmental Engineering. Florida State University, Tallahassee, FL, November 8, 2019.
46. "Human-Infrastructure Interfaces for Engineering Inspections"; Department of Civil and Environmental Engineering. University of Minnesota, Minneapolis, September 23, 2019.
47. "Structural Health Monitoring of Civil Infrastructure"; Southern East University, Department of Civil Engineering, Nanjing, China, September 6th 2019.
48. "Augmented Reality for Structural Health Monitoring"; APEES 2019 Summer School, University of La Sapienza, Rome, Italy, July 31st 2019.
49. "Structural Health Monitoring New Technologies and Paradigms"; American Institute of Aeronautics and Astronautics NM Chapter; April 19, 2019.
50. "Human-Infrastructure Interfaces and Augmented Reality"; Department of Civil, Environmental and Infrastructure Engineering, Mason University, April 4th 2019, Fairfax, VA.
51. "Augmented Reality for Transportation Infrastructure"; 56th Pavement and Transportation Conference, UNM and NMDOT, January 10, 2019, Albuquerque, NM.
52. "Structural Dynamics and Structural Health Monitoring." Yangzhou University, China. November 18-22, 2018.
53. "Human-Infrastructure Interfaces for Civil Engineering", September 19th 2018. Department of Civil and Environmental Engineering. University of Michigan, Ann Arbor, MI.
54. "Structural Health Monitoring of Critical Infrastructure", July 26th 2018. Nanjing Forestry University and Southeast University, Nanjing, China.
55. "Advanced Systems for Infrastructure Inspection through Machine Learning, Artificial Intelligence, and Augmented Reality", May 29th, 2018. Tuffs University, Department of Civil and Environmental Engineering, Boston, Massachusetts.
56. "Protection of bridge spans against lateral impact by truck vehicles" (2018) TRB Subcommittee AHD 35(1) Safety and Security of Bridges and Structures, January 9, TRB 97th Annual Meeting, Washington DC.
57. "Augmented Reality Tools for Enhanced Structural Inspections" Committee AFF40 "Testing and Evaluation of Transportation Structures", January 9, TRB 97th Annual Meeting, Washington DC.

58. "Wireless Smart Sensors for Structural Health Monitoring". Department of Civil and Environmental Engineering, Institute of Disaster Prevention, Yanjiao, Hefei Province, China. December 29, 2017.
59. "Advanced Sensing for Structural Safety, Smart Cities, and Connected Communities". Institute of Engineering Mechanics, Chinese Earthquake Administration. Yanjiao, Hefei Province, China. November 20-25, 2017.
60. "Augmented Sensing and Augmented Reality for Structural Health Monitoring". Department of Civil and Environmental Engineering, Institute of Disaster Prevention, Yanjiao, Hefei Province, China. November 24, 2017.
61. New Mexico Society of Professional Engineers; November 10, 2017; Albuquerque, New Mexico; "2017 NMSPE Issues Conference"
62. STEM: SIPI Community College, Albuquerque. "Augmented Reality and Low-cost sensors for Infrastructure", November 2nd 2017 (20 students).
63. STEM: CNM, Albuquerque. "Structural Health Monitoring for Transportation Infrastructure and engineering studies." Both class seminar and laboratory demonstration.
64. BD Spokes: PLANNING: MIDWEST: Big Data Innovations for Bridge Health: Omaha, Nebraska: "Using Unmanned Aerial Systems (UAS) with Lasers to Assess Structural Performance", October 4th, 2017.
65. STEM: Menaul School, Albuquerque. "Augmented Reality for Safer Infrastructure", September 5th 2017 (200 students) (click here)
66. Department of Civil and Environmental Engineering, University of Omaha, Nebraska: "Structural Health Monitoring of Railroad Bridges", July 31st, 2017.
67. Department of Civil Engineering, Lanzhou University of Technology, Lanzhou, Gansu Province, China. Wireless Smart Sensors for Structural Health Monitoring. July 20, 2017.
68. STEAM: Dream Builders at the National Hispanic Cultural Center; Augmented Reality for the Future Engineers; April 13, 2017.
69. Native American Community Academy; Technology and Engineering Applications Using Augmented Reality; March 27, 2017.
70. Transportation Research Board Committee AFF40 Nugget Presentation: Railroad Bridge Monitoring and Inspection under Live Loads: Current State of the Art and Future Trends; Washington DC, January 11, 2017.
71. American Society of Civil Engineers, Engineering of Mechanics Institute (EMI), Objective Resilience Group: Performance Monitoring of Railroad Infrastructure; Washington DC, January 10, 2017.
72. New Mexico Department of Transportation (NMDOT) Annual Transportation and Paving Conference: "Consequence-based management of complex bridge networks using wireless smart sensors"; January 5, 2017.
73. New Mexico Tech, Department of Mechanical Engineering (seminar): "Cost-effective Remote Sensing and Rating of Critical Infrastructure", October 4, 2016.
74. University of Tennessee at Knoxville, Department of Civil and Environmental Engineering (seminar); "Structural Health Monitoring of Railroad Bridges in North America" May 27, 2016
75. American Society of Civil Engineers, Engineering Mechanics Institute (EMI); "wireless smart sensors monitoring railroad bridge networks" Annual Conference, Nashville, TN, May 23-26.
76. American Society of Civil Engineers New Mexico Section Annual Conference, Socorro, New Mexico, April 29, 2016;" Consequence-based Monitoring of Infrastructure for Decision-making"

77. University of Kansas, Department of Civil, Environmental and Architectural Engineering (seminar), April 15, 2016; "Structural Health Monitoring Using Wireless Smart Sensors (WSSs): Performance Assessment and Decision Tools Applications"
78. University of New Mexico, Department of Mechanical Engineering (seminar); March 25, 2016; Albuquerque, New Mexico; "Hybrid Sensing for Structural Health Monitoring"
79. New Mexico Collaborative Research and Development Council, February 26, 2016, Albuquerque, New Mexico. Unmanned Aerial Systems (UAS) and Remote Sensing (RS) Cluster. "UNM Research Opportunities for UAS and Infrastructure Consequence-Based Assessment"
80. American Society of Civil Engineers, Annual Structural Congress, February 17, 2016, Phoenix, Arizona; Committee in System Identification; Southwest panel in Structural Health Monitoring, representing UNM: "SHM in the Southwest: State of the Art and Future Opportunities"
81. University of New Mexico. Department of Civil Engineering Graduate Seminar; February 3, 2016; "Structural Health Monitoring Using Wireless Smart Sensors"
82. Computational Sustainability at the University of New Mexico (guest lecturer); November 16, 2015; Albuquerque, New Mexico; "Wireless Smart Sensors for Structural Health Monitoring"
83. New Mexico Society of Professional Engineers; November 13, 2015; Albuquerque, New Mexico; "2015 NMSPE Issues Conference"
84. West Point US Military Academy; October 28; "Railroad Bridge Maintenance, Repairs, and Replacement Prioritization Using Wireless Smart Sensors"
85. Department of Civil and Environmental Engineering, University of Arizona, October 23, 2015; Tucson, Arizona; "Management of Railroad Bridges Using Wireless Smart Sensors"
86. Department of Civil Engineering, University of New Mexico, March 26, 2015; "Critical Infrastructure Management using Wireless Smart Sensors"
87. Institute of Disaster Prevention, Beijing (China), August 4, 2014: "Structural Health Monitoring (SHM) of Railroad Bridges"
88. Institute of Engineering Mechanics, China Earthquake Administration, Harbin (China), July 14, 2014: "Structural Health Monitoring (SHM) for Railroad Bridges using Wireless Smart Sensor (WSSs) in North America"
89. Department of Transportation Engineering, Harbin Institute of Technology (HIT), Harbin (China), July 9, 2014: "Railroad Bridges Replacement Projects in North America: Why, What, and How?"
90. Department of Civil Engineering, Northeast Forestry University, Harbin (China), July 7, 2014: "New Smart Technologies for Safely Designing and Maintaining Civil Engineering Structures: The Illinois Approach" (click here)
91. Department of Civil Engineering, Harbin Institute of Technology, Harbin (China), July 4, 2014: "Campaign Monitoring of Railroad Bridges using Wireless Smart Sensors: Past, Present, and Future" (click here)
92. Society of Civil Engineers of Spain, Granada (Spain), December 30, 2011: "Civil Engineering Professional Developments in United States"
93. University of Granada and Society of Civil Engineers of Spain, Granada, Spain, December 30, 2010: "Civil Engineering Education in United States"
94. Engineering Week, LaSalle Bajío University, León (Mexico), Teleconference, October 12, 2010: "Young and Engineer: Is there any Future?"
95. Institute of Engineering Mechanics, China Earthquake Administration, Beijing (China), August 2, 2010: "Railroad Bridges and Structural Health Monitoring"

96. Employment Fair Expo, University of Granada, Granada (Spain), May 20, 2010: "Engineering Education in the Global Market"
97. Maintenance of Way Club of Chicago, Chicago, IL, January 18, 2010: "Railroad Bridges Maintenance"
98. Department of Structural Engineering and Mechanics, University of Granada, Granada (Spain), January 12, 2010: "Railroad Bridges and Structural Health Monitoring"
99. Society of Civil Engineers of Spain, Granada (Spain), December 31, 2009: "Young & Engineering, the American Experience"
100. ASCE Eastern Illinois Professional Chapter, Champaign, IL, December 15, 2009: "Railroad Bridges in the US inspection, maintenance and management"
101. Institute of Engineering Mechanics, China Earthquake Administration (Harbin, China), August 6, 2007: "US Midwest bridges and other structures"
102. Bridges and Structures Laboratory, Department of Civil Engineering, University of Tokyo, Tokyo (Japan), August 2, 2007: "Bridges Connecting Society"
103. Department of Civil and Environmental Engineering, Christian Brothers University, Memphis, TN, March 2007: "Structural Engineering: Projects and Examples"
104. Ecole Nationale des Ponts et Chaussées, Paris (France), May 2006: "USA railroad intermodal facilities"
105. Maintenance of Way Club of Chicago, Chicago, IL, May 2006: "Edgewood Railroad Bridge Design and Construction Particularities"
106. ASCE student chapter, Civil Engineering Department, Santa Clara University, Santa Clara, CA, May 2005: "Midwest Structures Design and Construction"
107. Department of Structural Engineering and Mechanics, University of Granada, Granada (Spain), Dec. 2004: "Prestressed Concrete Railroad Bridges on Driven H-piles: The Mile Bridge, KY (USA)"
108. Bridges and Structures Laboratory, Department of Civil Engineering, University of Tokyo, Tokyo (Japan), May 2004: "USA Structures throughout their Design"

RELEVANT LINKS (MEDIA/NEWS)

- National Chung Hsing University and College of Engineering collaborates with The University of New Mexico and Fulbright Hays Faculty Research Abroad with STEM Education

  https://www2.nchu.edu.tw/en-news-detail/id/788/title/National_Chung_Hsing_University_and_College_of_Engineering_collaborates_with_The_University_of_New_Mexico_and_Fulbright_Hays_Faculty_Research_Abroad_with_STEM_Education

- UNM wins international contest in Structural Health Monitoring

  https://civil.unm.edu/news/2023/10/unm-wins-international-contest-in-structural-health-monitoring.html

- Moreu spending semester in Taiwan as a Fulbright Fellow

  https://engineering.unm.edu/news/2023/01/moreu-spending-semester-in-taiwan-as-a-fulbright-fellow.html

- School of Engineering summer program hits the rails to attract middle and high schoolers to STEM (2022)

  https://news.unm.edu/news/school-of-engineering-summer-program-hits-the-rails-to-attract-middle-and-high-schoolers-to-stem

- UNM group designs rock-tapping remote-control robot to detect potential slides (2022)

  https://news.unm.edu/news/unm-group-designs-rock-tapping-remote-control-robot-to-detect-potential-slides

- Researchers at UNM create robot to safely inspect rockslide sites (2022)

  https://youtu.be/lMKpTQ_PPnQ

- SMILab at UNM presents results on cyber security research and training for safer Wireless Sensor Networks, Structural Health Monitoring and Secure Digital Twins

  https://newmexicoconsortium.org/smilab-presents-results-for-safer-wireless-sensor-networks/

- UNM's School of Engineering looking to build 'LoboDrome' (2021)

  https://youtu.be/TJHMmAVffbA

- UNM’s SMILab develops marine and underwater smart sensing in NSF/ONR project (2021)

  https://news.unm.edu/news/unms-smilab-develops-marine-and-underwater-smart-sensing-in-nsfonr-project

- SMILab works with ROTC to train cadets in cybersecurity (2021)

  https://news.unm.edu/news/smilab-works-with-rotc-to-train-cadets-in-cybersecurity

- SMILab research assistant receives national recognition

  http://news.unm.edu/news/smilab-research-assistant-receives-national-recognition

- Dance and engineering form unique collaboration (2020)

  http://news.unm.edu/news/dance-and-engineering-form-unique-collaboration

- UNM researchers using drones to examine aging bridges (2019)

  https://www.krqe.com/news/albuquerque-metro/unm-researchers-using-drones-to-examine-aging-bridges/

  https://innovations.unm.edu/unm-inventors-to-showcase-drone-technology-at-the-transportation-research-board/

  https://youtu.be/XHqFZBGjptU

  https://nmpartnership.com/unm-researchers-using-drones-to-examine-aging-bridges-2/

- Drone researchers covered in news, will present at #TRBAM (2019)

  https://www.trb.org/main/blurbs/179961.aspx

- UNM researchers partner with Sandia Peak to collect data (2019)

  http://news.unm.edu/news/unm-researchers-partner-with-sandia-peak-to-collect-data

- CCEE alumni met in Washington, DC, at the ASCE Fly-In meeting last week to request more funding for infrastructure

  https://civil.unm.edu/news/2019/03/ccee-alumni-met-in-washington-dc-at-the-asce-fly-in-meeting-last-week-to-request-more-funding-for-infrastructure.html

- Researchers look for ways to prevent railroad overpass crashes (2018)

  https://carc.unm.edu/research/researchers-look-for-ways-to-prevent-railroad-overpass-crashes.html

- Connecting “wires, improving an industry” Moreu, Fernando; Wanek-Libman, Mischa. Railway Track & Structures; New York Vol. 114, Iss. 9, (Sep 2018): 22-24,26. (2018)

https://www.proquest.com/docview/2120140486

- Launch of wireless sensors for SHM of commercial space vehicles (2017)

  https://youtu.be/_uNTT5IS6Co

- NASA Supports UNM Using Wireless Sensors for SHM of Commercial Space Vehicles (2017)

  https://civil.unm.edu/news/2017/11/nasa-supports-unm-using-wireless-sensors-for-shm-of-commercial-space-vehicles.html

- High schoolers build sensors, test them at Sandia crest

  http://engineering.unm.edu/news/2017/06/high-schoolers-to-build-sensors,-test-them-at-sandia-crest.html

- Summer Transportation Institute 2017 (2017)

  https://youtu.be/Id60RZNKVLs

- Six High Schoolers Present Results of Their Internship to UNM Mentors, Faculty, and Stephanie Kean, Field Representative of Congresswoman Michelle Lujan-Grisham (2017)

  http://civil.unm.edu/news/2017/07/six-high-schoolers-present-results-of-their-internship-to-unm-mentors,-faculty,-and-stephanie-kean,-field-representative-of-congresswoman-michelle-lujan-grisham.html

- Congresswoman Lujan-Grisham support SMILab Summer Camp Diploma Ceremony (2017)

  https://www.instagram.com/p/BWfiVY3jquU/?taken-by=replujangrisham
  https://twitter.com/RepLujanGrisham/status/885529664864702466

- UNM CE 410 students learn how to design structures “under the bridge” (2016)

  https://www.nurailcenter.org/resources/docs/unm.pdf

- Dr. Moreu is NM Lead Representative for ASCE Program (2016)

  https://civil.unm.edu/news/2016/03/dr.-moreu-is-nm-lead-representative-for-asce-program.html

WORKSHOP ORGANIZER

- Low-cost Efficient Wireless Sensors for STEM, Teaching 30 teachers from New Mexico building sensors in the classroom, New Mexico Science Teachers Association (NMSTA) Annual Conference, Farmington, NM, October 21st 2023.
- Low-cost Efficient Wireless Intelligent Sensors Workshop at National Research Center of Earthquake Engineering (NCREE) and National Taiwan University (NTU), with students from Keelung Ocean University and Taiwan Tech. Hosted at Taipei, Taiwan (twenty-five students, two days), hosted by NTU and Professor Chang. August 24-25th 2023.
- Low-cost Efficient Wireless Intelligent Sensors Workshop at College of Engineering of National Chung Hsing Univeristy, Taichung, Taiwan (twenty five students, five hours), hosted by the Dean of the College of Engineering. August 18th 2023.
- Low-cost Efficient Wireless Intelligent Sensors Workshop with High Water Mark LLC staff, six staff members learned to use long-term sensor deployments for post-wildfire flooding, server access, and assisted developing business model (five hours), January 25th 2023.
- Elementary School Workshop for Smart Railroads, in collaboration with Federal Railway Administration, Florida State University and Stanford University. Attendees included BNSF, Rail Runner, School teachers, QPEC, Sandia National Laboratories, NM DOT, and New Mexico Consortium. 54 elementary school students built sensors and took the rail runner mentored by industry

(9 hours), January 20th, 2023.

- Low-cost Efficient Wireless Intelligent Sensors Workshop for Sonora University (Mexico) at Albuquerque, New Mexico, as part of the Program of the Americas, seven students (nine hours), August 31st 2022.
- Low-cost Efficient Wireless Intelligent Sensors Workshop with High Water Mark LLC staff, nine staff members learned to build low-cost sensors and learned long-term sensor deployments for post-wildfire flooding (three hours), July 26th 2022.
- Ohkay Owingeh Government and CIVIC Partners Workshop, including members of UNM, Stantec, BHI, and collaborators for planning Year one CIVIC grant at Ohkay Owingeh Government Building, December 13th 2021: over thirty attendees.
- Ohkay Owingeh Government Sensor Opening Workshop, discussing locations, low-cost sensor technology, and the value of data: ten members of Ohkay Owingeh and five members from UNM.
- First Smart Management of Infrastructure Laboratory Webinar, July 9th 2020, over one hundred participants national and international (click here)
- Workshop in Augmented Reality for Bridge Inspection, March 1st 2019, Albuquerque, New Mexico, for NMDOT Bridge Inspectors (15 attendees) (planner, instructor and host)
- Workshop in Augmented Sensing of Critical Energy and Industrial Facilities, May 9th 2018, Albuquerque, New Mexico, for Electric Power Research Institute (EPRI) (45 attendees) (instructor and host)
- High School Workshop on Sensors, Infrastructure, and Monitoring, June 27th 2018: 30 sensors were built by 30 high schoolers who tested them in the pedestrian bridge dance competition the day after.
- Workshop in industry acceptance of new technologies in decisions, April 18th, 2018, ASCE SEI, Forth Worth, Texas (25 attendees) (instructor and host)
- Workshop in low-costs sensors, human-machine interfaces, machine learning, International Modal Analysis Conference (IMAC), Orlando, Florida, February 10, 2018 (12 attendees) (instructor and host).
- High School Workshop on Sensors, Infrastructure, and Monitoring, June 17th 2017: over 14 sensors were built by high schoolers who tested them in the Tramway in the same day.

WORKSHOP PARTICIPATION - ATTENDEE

- P-Waver Company: Sense Ahead For Possibilities. Workshop organized by National Taiwan Unviersity at P-Waver headquarters in Taipei: “New Technologies for advanced inspection and monitoring” (10 minutes presentation.) July 3rd 2023 (2 hours.)
- National Science Foundation, NHERI University of Florida Boundary Layer Wind Tunnel User Workshop, Gainsville, Florida, January 6-7, 2022 (14 selected participants.)
- National Science Foundation Florida International University Wall of Wind Experimental Facility User Workshop, Miami, Florida, December 2-3, 2022 (12 selected participants.)
- National Science Foundation, funded workshop, NHERI RAPID Workshop for Users, Seattle, Washington, July 26-30, 2021 (24 selected participants.)
- National Science Foundation, funded workshop, NSF ENG CAREER Workshop, Arlington, VA, April 1-2, 2019.
- National Science Foundation, funded workshop, Aspiring PI CPS Workshop, Arlington, VA, August 3-4, 2017.
- National Science Foundation -funded workshop NHERI@UC San Diego User Training Workshop, Dec 12-13, 2016.

- National Science Foundation -funded workshop NHERI Wall of Wind Experimental Facility User Workshop, November 18, 2016.
- National Science Foundation NSF-funded workshop on teaching 'structural art', University of Massachusetts (UMass Amherst), June 13-14 2016.
- Workshop on Cyber-Physical Co-Design of Wireless Monitoring and Control for Civil Infrastructure, Thomas M. Siebel Center for Computer Science, University of Illinois, Urbana, IL, February 17-18, 2011.
- Interactive Workshop on Bridge Inspection and Rating, University of Illinois, Urbana, IL, February 24, 2010.
- Design of Deep Foundations, Ensoft, Inc. Austin, TX, November 11-13, 2003.
- Bridge Construction Inspection, Technology Transfer Program, Illinois Department of Transportation (IDOT), 2003.

OTHER MENTORING / CERTIFICATION

Los Alamos National Laboratory 2016, 2021, 2022

Los Alamos, New Mexico Faculty Mentor

- Collaborated with the Los Alamos Dynamics Summer School (LADSS) as faculty mentor.
- Developed the research project and coordinated with LANL mentors throughout the project.
- Includes instruction and training related to hardware, software, development, and programming.
- Mentored students during the summer and in the following Spring for IMAC participation (conference supported by LADSS as part of the summer Program.)

(not mentoring in Summer 2023 during Fulbright, will resume on Summer 2024)

Air Force Research Laboratory 2019-2022

Albuquerque, New Mexico Faculty Mentor

- Collaborated with the AFRL Scholars Program as a lead faculty mentor for three students (PhD, Undergraduate, and Community College Levels.)
- Developed the research project and coordinated with external industry throughout the project.
- Includes training hardware, software, development, and programming.
- Selected students to participate in the project.

(not mentoring in Summer 2023 during Fulbright, will resume on Summer 2024)

Sandia National Laboratory 2016, 2020, 2022

Albuquerque, New Mexico Faculty Mentor

- Collaborated with the Non Linear Mechanics and Dynamics (NOMAD) as faculty mentor.
- Developed the research project and coordinated with external industry throughout the project.
- Includes instruction and training related to hardware, software, development, and programming.
- Selected students to participate in the project.

(not mentoring in Summer 2023 during Fulbright, will resume on Summer 2024)

Professional Development Certificate May 2015
Department of Civil and Environmental Engineering University of Illinois at Urbana-Champaign

- Three years program.
- Assisting senior undergraduate students and junior graduate students to grow academically and professionally through mentoring.
- Involves at least meeting once a month to monitor students' progress towards their academic program.
- Includes regular service to the community through regular service hours.

Certificate in Foundations of Teaching April 2015
Center for Innovation in Teaching and Learning (CITL)
University of Illinois at Urbana-Champaign

- Attending and evaluating the teaching of a professor and discussing teaching methodology after the lecture.
- Reading one textbook about teaching philosophy and presenting results to a consultant in teaching.
- Attending more than 8 hours of workshops in teaching
- Preparing teaching materials for a large audience of students, being evaluated by a teaching consultant, and receiving feedback and implementing lessons learned for a second lecture.

PROFESSIONAL MEMBERSHIP

- American Society of Mechanical Engineers (ASME.)
- ASME Structural Engineering Mechanics (SEM.)
- American Railway Engineering and Maintenance-of-Way Association (AREMA.)
- American Society of Civil Engineers (ASCE.)
- ASCE NM Section; Chair of structures at the New Mexico Section.
- ASCE Engineering Mechanics Institute (EMI.)
- National Society of Professional Engineers (NSPE.)
- Transportation Research Board (TRB.)
- New Mexico Society of Professional Engineers (NMSPE.)
- Chi Epsilon, Civil Engineering Honor Society.

UNM STUDENTS (current)

Post-doctorate students

None at this moment.

PhD students

Angela Montoya	*PhD in Civil, Construction and Environmental Engineering* *Proposal defended November 2020* *Thesis Tittle: "Detection of Transient Pulses in the Response of Single Degree of Freedom Harmonic Systems Subject to Random Excitation"* *Thesis defense planned for December 2023*	2023
Eric Robbins	*PhD in Civil, Construction and Environmental Engineering*	2024

	Thesis defense planned for March 2024	
Kaveh Malek	*PhD in Mechanical Engineering* *Comprehensive exam planned for November 2023*	2024
Ali Khorasani	*PhD in Civil, Construction and Environmental Engineering* *Comprehensive exam planned for January 2024*	2024
Masha Sanei	*PhD in Civil, Construction and Environmental Engineering* *Qualifier defended and passed April 2022*	2025
Saiqa Mutari	*PhD in Civil, Construction and Environmental Engineering* *Qualifier defended and passed November 2021*	2025
Maimuna Hossain	*PhD in Mechanical Engineering* *Qualifier planned for Fall 2023*	2025

Master students

Odey Yousef	*MS in Civil, Construction and Environmental Engineering* *"Event-based Sensing for Augmented Structural Control"*	2023
Jennifer Restrepo	*MS in Civil, Construction and Environmental Engineering* *"Quantification of Multiple Input Multiple Output Experimental Uncertainties"*	2023
Shivaleela Macharla	*MS in Mechanical Engineering* *"Solar Panel Structural Design and Optimization"*	2024
Wyatt Seager	*MS in Civil, Construction and Environmental Engineering* *"Multiple-Input Multiple-Output for Structural Control"*	2025

Undergraduate students

Dungan Garner (CE, 2024)

Dalton Berry (CS, 2024)

Daniel Gavin (ED, MATH, 2024)

Timothy Thiergart (NGS, 2024)

Morgan Merrill (CE, 2026)

Elias Mosco (CS, 2026)

Ronan Reza (CE, 2027)

Visiting scholars

Marielly Rodriguez Gauthier	Summer 22 and 23
Christian Torres	May-August 2023

High school students

Aaron Atcitty	July 2022-present

UNM STUDENT (former)

Former Post-doctorate students

Jiaqi Xu	January 2020-April 2021
Ali I. Ozdagli	December 2015-May 2018

Former visiting scholars

Yi-Syuan Chen, Junior in Civil Engineering, National Taiwan University — June-July 2022

Chih-Han Chung, Junior in Mechanical Engineering, National Taiwan University — June-July 2022

Yi-Chen Lee, Senior in Civil Engineering, National Taiwan University — June-July 2022

Xiang Xu, MS student in Structural Engineering — September 2019-August 2020
Yangzhou University, Jiangsu Province, China

Marlan Ballard, Post-CNM student in Computer Science — January 2020-June 2021

Bideng Liu, Institute of Disaster Prevention, Beijing, China — December 2016-January 2018
Associate Professor

Ronny Moreano, ESPE, Quito, Ecuador — October 2017-December 2017
Senior, Civil Engineering

Former graduate students

<u>Two PhD thesis total to date</u>

Roya Nasimi — August 2018- Dec 2021
"Condition Monitoring of Structures Enabled with Vision-based Sensor Fusion on Cyber Physical Systems"
(CCEE student)
Graduated with distinctions
Currently tenure-track assistant professor at California State University East Bay (San Francisco, CA)

Xinxing Yuan — Dec 2018- May 2022
"Monitoring of Structural Construction Quality Using 3D Point Cloud Data"
(CCEE student)
Currently structural engineer at Stantec (Manhattan, NY)

<u>Seven MS thesis total to date</u>

Elijah Wyckoff — August 2020 – July 2022
"Augmented Reality for Human Control of Engineering Tasks"
(ME student)

Eric Robbins — June 2019- May 2021
"Non-linear Dynamics Control Using Wireless Smart Sensors"
(CCEE student)

James Woodall — January 2019-May 2021
"Multiple-Input Multiple-Output Uncertainties Quantification"
(CCEE student)

Marlon Aguero — January 2018-Dec 2020
"Real-time Displacement with Augmented Reality for Structural Health Monitoring"
(CCEE student)

Dilendra Maharjan — January 2018-Dec 2019
"Augmented Reality for Structural Health Monitoring"
(CCEE student)

Piyush Garg — December 2015-Dec 2017
"Non-contact monitoring of railroad bridge performance using UAS"
(ECE student)

Jose A. Gomez — August 2015-May 2017
"Cost-effective monitoring of railroad bridge performance"
(CCEE student) (click here)

Two MS thesis defended in other institutions as main director of research

Rafa Cardona

"Low Cost Sensors for Long-term deployment Monitoring" — January 2019-June 2019
(CCEE student in Exchange with University of Castilla La Mancha in Spain)

Can Zhu

"Total Displacement Monitoring of Railroad Bridges using 2DOF" — June 2018-June 2019
(CCEE student in Exchange with Yangzhou University, China)

Other graduate students supervised without MS Thesis

Joshua Murillo	*Masters in National and Global Security*	2022
Maimuna Hossain	*Masters in Mechanical Engineering*	2021
Adam Baros	*MEng in Civil, Construction and Environmental Engineering*	2020
Jason Aldaz	*MEng in Civil, Construction and Environmental Engineering*	2020
Tony Lampert	*MEng in Civil, Construction and Environmental Engineering*	2019

Former undergraduate students

(CCEE unless noted otherwise)

Solomon Atcitty (ME, 2023)

Jack Hanson (CS, 2024)

Connor Miller (Economy, 2024) (ROTC student 2021-2022)

Zane Dudney (History, 2025) (ROTC student 2021-2022)

Porter Yang (CS, 2025) (ROTC student 2021-2022)

Gabriel Zelaya (ECE, 2025) (ROTC student 2021-2022)

Hector Valenzuela (CS, 2025) (ROTC student 2021-2022)

Dominic Thompson *(graduated May 2022) (ME student)*

Jennifer Restrepo *(graduated May 2021) (ME student)*

Casie Elizondo *(graduated May 2021) (ROTC, ECE student)*

Joshua Murillo *(graduated May 2021)(ROTC, NGS student)*

Odey Yousef *(graduated December 2020)*

Somie Chavez (*graduated May 2020*)

Benjamin Narushof *(graduated May 2020)*

Emmanuel Ayorinde *(graduated May 2020) (ME student)*
Brian Bleck *(graduated May 2020) (CS student)*
Laura Gomez *(graduated May 2018)*
Cassy Mcclintock *(graduated May 2018)*
Sharon Shen *(graduated May 2018) (CS student)*
Ian Benjamin *(graduated May 2018) (ME student)*
Emily Scrimshaw *(graduated May 2018) (ME student)*
Michael Schuh *(graduated May 2018) (ME student)*

Former high school students

Ronan Reza, junior and senior, La Cueva High School	July 2022-August 2023
Aaron Atcitty, sophomore, Home School	July 2022-August 2022
Morgan Merrill, senior, El Dorado High School	June 2022-August 2022
Aldo Morelli, junior, Bosque High School	June 2021 - July 2021
Nehan Tarefder, sophomore, La Cueva High School	June 2021 - July 2021
Malak Elbaz, senior, Menaul School	Octob. 2020-May 2021
Sho Komijama, senior, Menaul School	Octob. 2019-May 2020
Selene Diaz, senior, Menaul School (click here, page 10)	Octob. 2017-May 2018
Douglas Natseway, Native American Community Academy, junior	Novem. 2016-July 2017
Valentino Pettis, Native American Community Academy, junior	Novem. 2016-July 2017
Erik Moreno, Los Lunas Academy of Dreams, junior	May 2017-July 2017
Sunjeev Salomon, La Cueva High School, senior	January 2016-May 2016
Clayon Bliss, Saint Pius the 10th, senior	June 2016-July 2016
Manny Rivas, South Valley Academy, junior	June 2016-July 2016

STUDENT COMMITTEE SERVICE

PhD students

Md Parvez Molla (adviser Dr. Abdullah Mueen , CS) *Roadside LiDAR Data Processing for Intelligent Transportation System*	November 2023
Zafrul Akim Khan (adviser Dr. Rafi Tarefder) *Modeling of Asphalt Concrete for Cross-Anisotropic Viscoelasticity and Heterogeneity*	October 2023
Biswajit Bairgi (adviser Dr. Rafi Tarefder) *"Characterization of Foamed Warm-Mix Asphalt for Workability and Moisture Damage"*	August 2021
Krishna Chaitanya Jagadeesh Simma (adviser Dr. Susan Bogus) *"Monitoring of Energy Efficient Buildings"*	May 2021
Razieh Nadafianshahamabadi (adviser Dr. Greg Rowangould) *"Is Transportation Planning Effective? A Critical Review of Long-range Regional Transportation Planning in the United States"*	June 2019
Gauhar Sabih (adviser Dr. Rafi Tarefder)	May 2019

"Effects of Coefficient of Thermal Expansion on Unbonded Concrete Overlay Design and Performance"

Darren Luke (advisor Dr. Percy Ng) May 2018
"Elevated Temperature Progressive Damage and Failure of Duplex Stainless Steel"

MS students

Ryan Dow (adviser Dr. Susan Bogus) May 2019
"Drivable Space Datasets Created by Airborne LiDAR and Aerial Images"

Cheikhna Sy (adviser Dr. Rafael Fierro) May 2019
"UAS Control with Heterogenous Communication"

Anima Bista (adviser Dr. Walter Gerstle) February 2019
"Validation of the state based peridynamic lattice model"

Bipesh Shrestha (adviser Dr. Walter Gerstle) April 2018
"Study of building vibrations caused by machinery"

Siavash Kazeroni (advisor Dr. Walter Gerstle) December 2017
"State-based Peridynamic Particle Method"

Sushil Ghimire (advisor Dr. Walter Gerstle) May 2017
"Nuclear plants vibration analysis using non-contact sensors"

Mojgan Maadandar (advisor Dr. Mahmoud R. Taha) May 2017
"Composite materials for resilient structures"

Jaime Adroher (advisor Rafael Palacios, ICAI, Madrid, Spain) June 2017
"Analysis of railroad bridge data using advanced wavelet sensors"

Guillermo Perez (advisor Vanesa Valentin, University of Valencia, Spain) June 2017
"Optimizing Railroad Bridge Networks Management Using Mixed Integer Linear Programming and Genetic Algorithm"

TEACHING

Engineering Statics Spring 2020
CE202, University of New Mexico

- New interactive lectures with Polls and Kahoot
- Half of the semester was offered online due to COVID-19
- Students were able to participate in tutoring sessions with Zoom

Design of Metals Fall 2018, 2019, 2020, 2023
CE424, University of New Mexico

- Offered for both seniors and graduate students
- Incorporated a real bridge design
- Students have to present their bridge design to state, city and county engineers

Structural Dynamics Spring 2017, 2018, 2021
CE521, University of New Mexico

- New course adapted for the Civil Engineering Department
- Directed to seniors and graduate students

Bio-design Fall 2016
ME 561 section 001, University of New Mexico

- New multi-disciplinary course developed at UNM
- To provide experience in innovating medical technologies
- Combines concepts of both engineering and medicine
- Directed to seniors and graduate students

Structural Design Fall 2015, 2016, 2017

CE410, University of New Mexico

- New course developed for the Civil Engineering Department
- Combines concepts of both concrete and steel design
- Includes 3D printing
- Directed to senior students

Advanced Structural Dynamics Spring 2016, 2019, 2022

CE598, University of New Mexico

- New course developed for the Civil Engineering Department
- Combines concepts of both theory and experimental dynamics
- Directed to graduate students
- First time this course is offered

Introduction to Remote Shake Table Experiments Spring 2016

STEM, University of New Mexico

- New course developed for the STEM School of Engineering
- Combines creating a website, running experiments, drone technology
- Directed to freshmen and sophomore students
- First time this course is offered

PROFESSIONAL REFERENCES AVAILABLE UPON REQUEST

Automation in Construction 143 (2022) 104542

Contents lists available at ScienceDirect

Automation in Construction

journal homepage: www.elsevier.com/locate/autcon

Realtime conversion of cracks from pixel to engineering scale using Augmented Reality

Kaveh Malek [a], Fernando Moreu [b,*]

[a] Department of Mechanical Engineering, University of New Mexico, NM, United States
[b] Department of Civil, Construction and Environmental Engineering, University of New Mexico, NM, United States

ARTICLE INFO

Keywords:
Augmented reality
Crack characterization
Pixel unit conversion
Euler angles
Edge extraction

ABSTRACT

A key step in image-based crack characterization techniques is pixel to engineering scale conversion. The conversion factor corresponds to Camera-to-Crack-Distance (CCD) and camera obliquity angle. To date, nonstationary image-based crack characterization methods are not designed for real-time unit conversion. This study develops a new crack characterization algorithm for Augmented Reality (AR) headsets; then implements it in Unity-game-software on a computer; and finally deploys and validates it in AR headsets. The proposed algorithm includes: (1) the transformation of pixel information to AR platform; (2) edge extraction utilizing Canny algorithm; (3) crack measurement at the pixel level adopting the horizontal approach; (4) CCD and camera angle measurement using AR orientation capabilities and applying this information for perspective correction; (5) Engineering scale dimensions computation using the results of (3)–(4). A scaler equation for perspective correction streamlines the algorithm toward real-time implementation. The results show maximum errors of 8.45% and 12.05% for laboratory and field experiments, respectively.

1. Introduction

Crack formation and propagation in concrete structures are key issues during their service life. Crack characteristics can reveal information on concrete models, facilitating damage assessment and maintenance planning [1]. From surface crack shape and positional attributes, the internal damage pattern of a concrete structure and the source of it can be deducted, imparting relevant information on

Abbreviations: X, X-axis in the world coordinate system (X); Y, X-axis in the world coordinate system (Y); Z, X-axis in the world coordinate system (Z); i_1, the index of the first processed row in image; i_2, the index of the last processed row in image; N_k, The number of pixels between two edges at the kth row in image; β_k, $arctan\left(\frac{\text{X-gradient}}{\text{Y-gradient}}\right)$ at the crack edge in the kth row of image; α, $arctan\left(\frac{\text{Y-gradient}}{\text{X-gradient}}\right)$ at the crack edge in the kth row of image; θ_x, pitch (around X); θ_y, `yaw (around Y); $\theta_z$, roll (around Z); $\theta_y$, `yaw (around Y′); $\theta_{z''}$, roll (around Z"); X_0, X-axis at initial state; Y_0, Y-axis at initial state; Z_0, *Z*-axis at initial state; X_1, X-axis at final state; Y_1, Y-axis at final state; Z_1, *Z*-axis at final state; C, center of the intersection of concrete surface and camera FOV; V_C, axis in the direction of projection of camera optical axis on concrete surface that passes through C; U_C, axis vertical to V_C on the concrete surface; X_I, axis of image coordinate system in the direction of image width; YI, axis of image coordinate system in the direction of image height; ΔX, size of X-pixel in engineering units; ΔXI, size of X-pixel in pixel units (i.e., 1 pixel); ΔY, size of Y-pixel in engineering units; ΔYI, size of Y-pixel in pixel units (i.e., 1 pixel); ΔX_{CP}, size of the central X-pixel in engineering units for perpendicular camera angle; ΔX_C, size of the central X-pixel in engineering units; ΔXI_C, size of the central X-pixel in pixel units (i.e., 1 pixel); ΔY_C, size of the central Y-pixel in engineering units; ΔYI_C, size of the central Y-pixel in pixel units (i.e., 1 pixel); ΔX_{VC}, V_C-component of ΔX_C; ΔX_{UC}, U_C-component of ΔX_C; ΔXI_{VC}, V_C-component of ΔXI_C; ΔXI_{UC}, U_C-component of ΔXI_C; CCD, Camera-Crack-Distance; d_C, CCD in direction of camera optical axis; *d*, CCD at an arbitrary angle; α_X,α_Y, coefficients accounting for camera intrinsic parameters and d_C that is estimated in calibration process; θ_C, angle between the camera optical axis and the vector normal to concrete surface; θ_Z, rotation angle of the picture around Z-axis; θ_{xyC}, angle between U_C and X_C; A, arbitrary point in the world coordinate system (A); A', arbitrary point in the world coordinate system (A'); A", arbitrary point in the world coordinate system (A"); B, arbitrary point in the world coordinate system (B); B′, arbitrary point in the world coordinate system (B′); B″, arbitrary point in the world coordinate system (B″); OA, arbitrary line in the world coordinate system (OA); A'B′, arbitrary line in the world coordinate system (A'B′); $\theta_{Z'}$, rotation of AB around *Z*-axis after two rotations around X and Y′-axes; $\theta_{Z''}$, rotation of AB around Z"-axis; θ, camera angle for an arbitrary pixel; θ_{xy}, angle between the projection of camera angle on concrete surface and X- axis; η, slope of the line interpolating the data of pixel size according to distance.

* Corresponding author at: Department of Civil, Construction and Environmental Engineering, University of New Mexico, 210 University Blvd, NE, MSC01 1070, Albuquerque, NM 87131, United States.
E-mail address: fmoreu@unm.edu (F. Moreu).

https://doi.org/10.1016/j.autcon.2022.104542
Received 28 March 2022; Received in revised form 5 August 2022; Accepted 19 August 2022

Table 1
The past attempts to overcome pixel unit conversion limitations compared to the present approach

Publication	Processing Method	Orienting Technique	Illustration of Orienting Technique
Shan et al., [6]	Canny edge detection and Zernike subpixel evaluation algorithms	Distortion correction using CCD and image obliquity angle measured by applying parallax theory to images of two cameras fixed at two locations	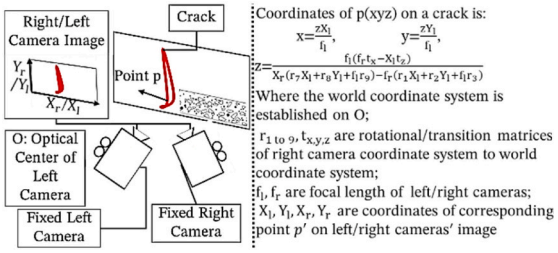
Lei et al., [14]	Diverse image arithmetic operators and adaptive partition	Real-time pixel-size measurement at perpendicular angle using reference comparison. Application of a parallel projection device as the conversion reference	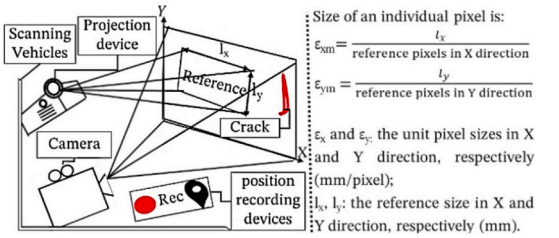
Valença et al., [13]	Point cloud segmentation	Distortion correction for images of large structures (e.g., large bridges) using TLS for CCD and image obliquity angle calculation	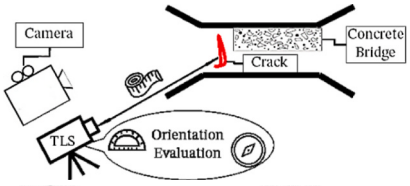
Kim et al., [12] Lei et al. [17] Choi et al. [16] Wang et al. [18] Liu et al. [19]	Image binarization with grayscale thresholding Support Vector Machine Convolutional Neural Network (CNN) Niblack local binarization	Pixel-size measurement at perpendicular angle; Ultrasonic Displacement Sensor (UDS) or range sensor for CCD calculation Measurement at fixed camera distance Distortion correction using 3D scene reconstruction	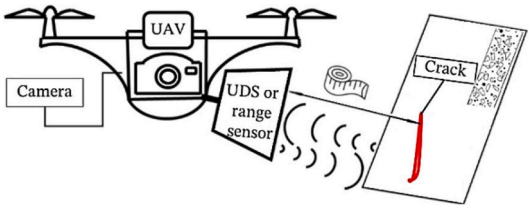
Li and Zhao, [2]	New encoder-decoder network (CedNet) based on deep-learning (DL)	Online pixel-size calculation at vertical angle; Physical attachment of a laser range finder to a smartphone for real-time CCD sizing	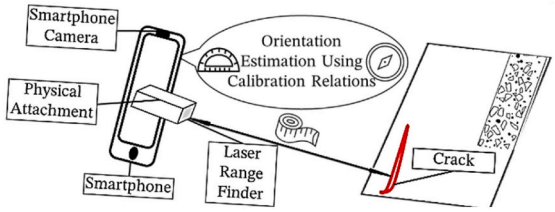
Ni et al., [15]	Smartphone measuring app called SADIPT	Real-time pixel-size measurement at perpendicular angle; Combination of smartphone and a fixed laser distance measurer for real-time CCD measurement	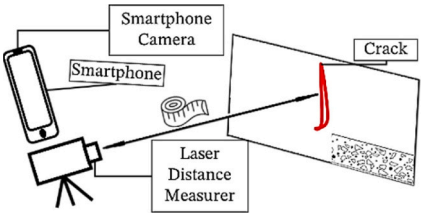
State of the art	Canny algorithm and horizontal scale pixel evaluation	Real-time distortion correction at any distance and angle of camera; CCD and image obliquity angle measurement using AR headset capabilities	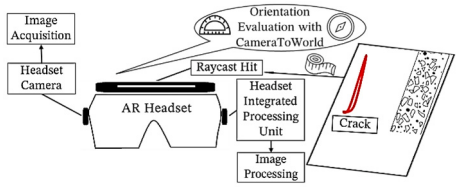

infrastructure evaluation and planning [2]. The dimensional characteristics of surface cracks such as width and length are significant in the fracture mechanism of concrete structures. For example: the stress intensity factor of the cracks is proportionate to the square root of crack size, based on conventional fracture mechanism theories available in the mechanics of material textbooks (e.g. [3,4]). In addition, inspection codes and standards evaluate the concrete structures using their crack dimensional properties [5] and specify the nominal limit values of the crack width.

The widths of concrete cracks are traditionally sized using a magnifying glass and a simple comparator consisting of a plastic or metallic strip with fixed-width lines [6]. However, the manual

assessment of cracks with comparators is slow, hard to conduct, and suffers from human subjectivity and sampling errors [5,6,7]. Therefore, developing new technology for crack measurement is essential in infrastructure safety management.

Several studies propose substituting traditional crack measurement techniques, with image-based methods. Past studies [8] address the inherent limitations of image-processing concrete cracks, such as the non-uniform shape and size of cracks, and random variation in the brightness and color of images. Wang et al. [7] provided a new comprehensive definition of crack width using Laplace's Equation to resolve the ambiguity of the previous concept and then developed a width measurement algorithm using the new definition. Yang et al., [9] and Ni et al., [10] proposed image-processing techniques enabling the extraction and width measurement of thin cracks with sub-pixel size on concrete surfaces. Shao et al., [11] used PTZ (Pan/Tilt/Zoom) cameras for feeding the image processing systems to resolve budget limitations in crack characterization image-based methods.

Several past studies have addressed the conversion of crack dimensional characteristics from pixel units to engineering units at different camera orientations. The computation of the conversion factor is one of the most prominent limitations of width quantification in camera image-processing systems [12,13]. Table 1 shows the previous studies which have addressed pixel-unit conversion. Shan et al. [6] dealt with the pixel-scale conversion issue of fixed-camera setups by adding an auxiliary camera, and thereby eliminated the dependence of stationary methodologies on unit converter scales attached to the concrete surfaces. Lei et al., [14] addressed unit conversion limitations under a mobile camera setup for tunnel crack characterization. They applied a real-time automatic calibration system for single-pixel sizing by including a parallel projection device to lining-scanning vehicles. This device projected a reference on tunnel lining surfaces that functioned as a comparator for transforming the crack characters from pixel to engineering units at a perpendicular camera angle. Meanwhile, Li and Zhao, [2] and Ni et al., [15] evaluated pixel-scale conversion for smartphone image-processing methods using a laser rangefinder for CCD evaluation. While the former anchored the rangefinder to the smartphone, the latter used an unattached device for CCD measurement. Both studies evaluated their crack characterization methods for a camera angle perpendicular to the concrete surfaces. Methodologies for crack characterization systems carried by Unmanned Aerial Vehicles (UAV) have significantly contributed to pixel unit conversion because of their nonstationary nature. For example, Choi et al., [16], Kim et al., [12], Lei et al., [17], and Wang et al., [18] proposed new methodologies for crack characterization via UAV that could measure the cracks at perpendicular camera angles.

Liu et al., [19] and Valença et al., [13] proposed methodologies that could correct geometry and perspective distortion for nonstationary setups with changing camera angles and positions. Liu et al., [19] designed a 3D reconstruction of the environment using 2D images captured by an UAV image acquisition system. Valença et al., [13] used the data obtained by Terrestrial Laser Scanning (TLS) to create 3D models of the structure and used that model to locate and orient the crack in relation to the camera. The locating/orienting processes in the two mentioned studies were time-consuming because of the long execution time associated with 3D scene reconstruction and TLS implementation.

Each of the mentioned past studies implemented their methodologies using a crack characterization system separated into an image acquisition device, an orientating element, and a processing unit which is usually stationary. Previous research excluded the user interface for visual inspection processes conducted by humans in the field [20]. Further, normal human inspection is essential in the field to enable necessary on-the-spot decisions that experts need to conduct in person (S. [21]). For example, in human visual inspections, the evaluation criteria for concrete structures in technical codes and standards is the characteristics of surface cracks which can be gauged more objectively by the integration of human visual inspection and image-based methods. Additionally, in real-life civil/infrastructure inspections, the experts need to judge and evaluate the severity of cracks in real-time. Immediate quantification of cracks during field inspections using image-based methods can provide inspectors with a decision-assistance tool. Therefore, research and industry communities have been recently studying real-time crack characterization methods with human-in-the-loop approaches. This solution transforms the job of inspectors by supplying a decision-assistance tool based on image-processing, enabling necessary on-the-spot choices that experts conduct in person during their inspection.

Fig. 1 classifies the discussed publications based on processing time, portability, and capability for angle distortion correction. Liu et al., [19], Choi et al., [16], Wang et al., [18], and Kim et al., [12] developed non-stationary crack characterization methodologies at a vertical camera angle which are implemented in non-real-time. Ni et al., [15] have proposed a real-time stationary means for crack characterization at a vertical camera angle. Lei et al., [14] and Li and Zhao, [2] developed non-stationary real-time crack characterization methods at a vertical camera angle. Shan et al., [6]'s methodology measured the crack in non-real-time at different camera angles using a stationary camera setup. Valença et al., [13] and Liu et al., [19] proposed non-real-time non-stationary systems for crack characterization at different camera angles and distances. The authors find no evidence of real-time portable system for pixel unit conversion at any camera angle and position.

This study develops a crack characterization tool based on image-processing for AR headsets and addresses real-time conversion from pixel units to engineering units at any camera position and angle. The processes of image acquisition, image processing, and pixel-unit conversion is performed inside the platform of AR headsets, and the method is applicable for any AR headset with integrated computational power. Deploying image-based measurement systems in the AR headset platform requires dealing with several challenges that include [22]: (1) limitations in terms of software packages and libraries compatible with AR headsets and (2) limited processing capability of AR headsets that prevents the implementation of codes with high memory complexity. The research team manages the challenge 1 by coding a crack measurement algorithm in C# with no auxiliary packages; implementing it in Unity-game-software; and deploying it in AR headsets. After the image acquisition is completed in the AR headset camera, the algorithm transforms the two-dimensional image data into the single-dimensional mathematical environment of headsets. Next, Canny edge detection technique with the Sobel-Feldman operator and median filter extract the crack edges from the transformed image data. The number of pixels between crack edges and the angle of the crack at the centerline is then calculated using the horizontal approach pixel analysis. Afterwards, the capabilities of AR headsets measure camera's distance and obliquity angle by which image perspective correction is accomplished in real-time. The algorithm then computes the crack's engineering scale dimensions from the crack characteristics at pixel level, the corresponding CCD, and camera intrinsic parameters obtained in calibration process. Finally, the developed tool retransforms the processed image data into image format and displays the processed image and the calculated dimensions to the user. To address challenge 2 i.e., to reduce the memory complexity of the algorithm, a scalar formula for correction of perspective distortion in image of cracks existing on the flat surfaces, is proposed. Additionally, in the edge extraction and pixel analysis phase, several simplifications are made in the initial algorithm to streamline the algorithm toward lower processing time. The scalar equation for distortion correction and the simplifications enable a near real-time image-processing in this study.

2. Crack identification methodology

Two crucial phases of edge extraction and dimensional quantification form the main skeleton of image-based crack characterization

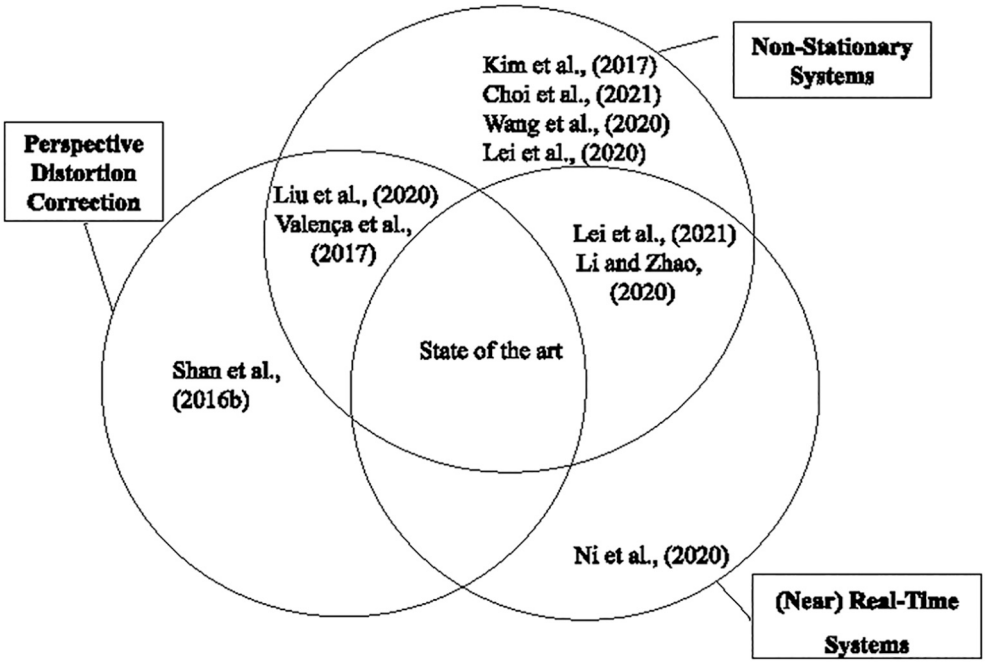

Fig. 1. Comparison of the past studies in terms of processing time distance and angle measurement and portability.

algorithms. Image-processing that search for an assumed pattern and Artificial Neural Network (ANN) are two common approaches for crack edge extraction [2]. Furthermore, the dimensional quantification phase requires a pixel or sub-pixel analysis [2]. This section first outlines the developed crack characterization algorithm and describes the algorithm's steps in chronological order, then details the edge extraction, and finally explains dimensional quantification methods.

2.1. Outline of methodology

Fig. 2 outlines the crack characterization algorithm and shows its primary steps. After image acquisition (step 1), pixel values of the image that involve the information required for image-processing are transformed into the AR headset platform (step 2). Then an edge detection algorithm (step 3) finds and stores the positions of crack edges and the

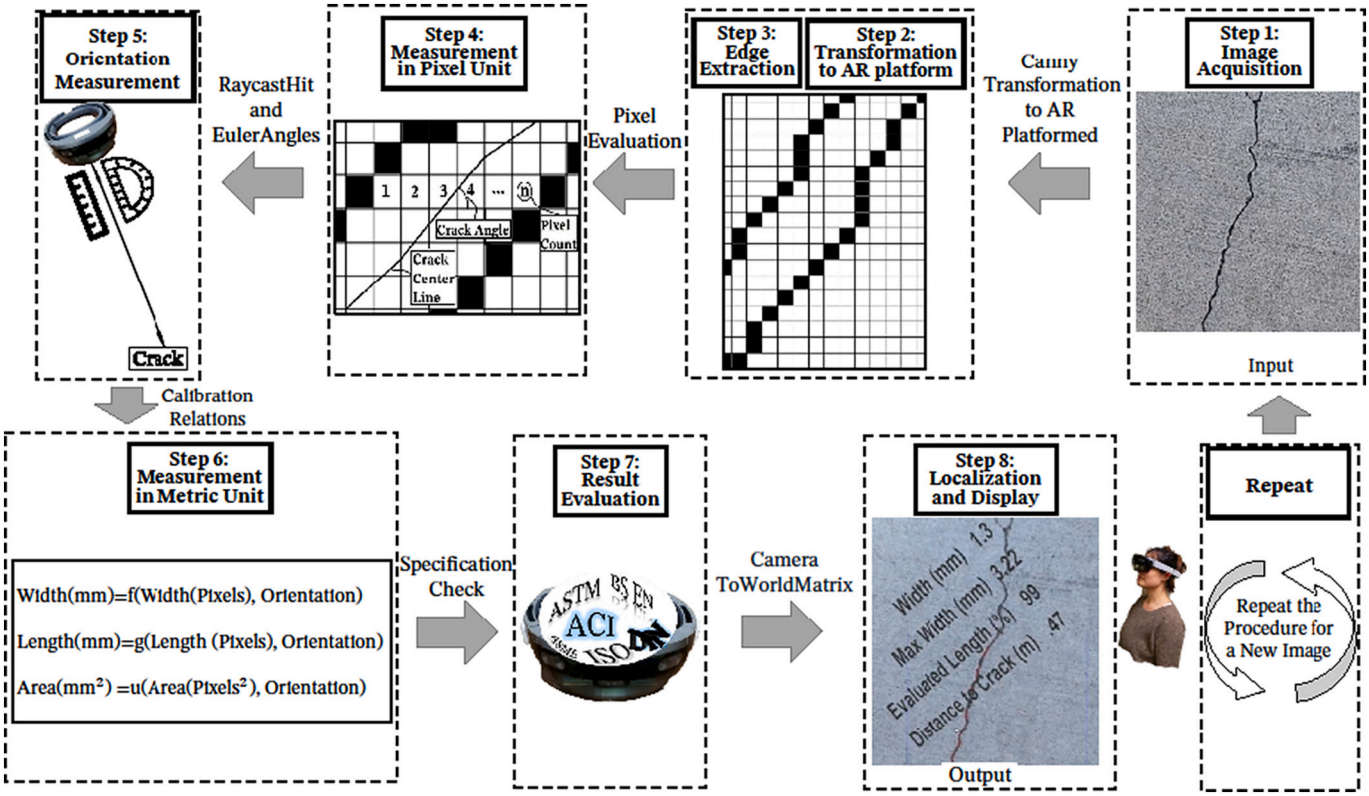

Fig. 2. The outline of AR crack characterization.

gradient of the picture at crack edges. The information achieved in the edge detection step provides sufficient data for in-pixel crack measurement using pixel evaluation (step 4). Then, the headset measures CCD and the camera obliquity angle using AR headset orienting capabilities (step 5). The AR headset capability for distance and angle measurement are respectively called "RaycastHit" and "TransformeulerAngle". The engineering dimensions of cracks, e.g., in metric or imperial units are the function of camera intrinsic parameters, CCD, camera angle and in-pixel dimensions. The crack dimensions are measured in metric units using in-pixel measurements, CCD, camera angles, and camera intrinsic parameters achieved in a calibration process (step 6). Afterwards, the algorithm evaluates the crack dimensions based on the criteria in the relevant specification (step 7). An overlay of the crack image with a noticeable color on the real crack, the crack dimensions in the engineering unit, and a technical proposal on the crack condition are finally demonstrated to the user (step 8). The headset capability for localization is called "cameraToWorldMatrix". It should be noted that this study limits the processing to a rectangular part in the center of the image to reduce the implementation time. The final results presented to the user corresponds to the results of the mentioned processed part.

2.2. Edge extraction

Among the traditional edge detection methods, the Canny algorithm has the fastest processing speed [6]. Canny is a multistep algorithm, and each step has a specific function in edge detection performance [23]. Fig. 3 shows the step used in this study. First, the acquired RGB image goes through a grey-scaling procedure that transforms images from multi-color (red, green, and blue) to single-color (grey) space. This study uses a weighted method for greying the image in that the greyscale pixel value is the sum of each primary color multiplied by a coefficient established on the color's wavelengths [24]. The Canny algorithm basically employs a Gaussian filter for reducing noise in the image [23] but the combination of Canny with other filters is also explored [25]. Because median filter effectively accomplishes our desired noise removal and edge preservation simultaneously [26], this study employs a median filter for smoothing AR headset images. The algorithm involves a Sobel Kernel to find image gradient in two orthogonal directions i.e., image length and width directions, and thereby computes image gradient magnitude and direction as mentioned in Fig. 3. In the non-maximum suppression step, the algorithm thins the edges by keeping the pixels in the local maximum gradient and discarding the other pixels. Afterward, the algorithm contains a gradient evaluation based on an upper and a lower threshold. Pixels exceeding the upper threshold in gradient amplitude are preserved and pixels failing to reach the minimum threshold are deleted. Judgement on pixels with gradient amplitude between the two thresholds, called hysteresis edge linking, depends on their connectivity to pixels surpassing the upper threshold [23].

The Canny algorithm's efficiency depends on the median filter size and the upper and lower thresholds applied for edge tracking. The research team conducted several preliminary tests to explore the optimum Canny parameters [27]. The result shows that growing the size of median Kernel matrix to greater than [3 × 3] does not considerably improve the Canny Algorithm's performance. To lower algorithmic complexity, a 3 × 3 median filter was selected to reduce the noise in the

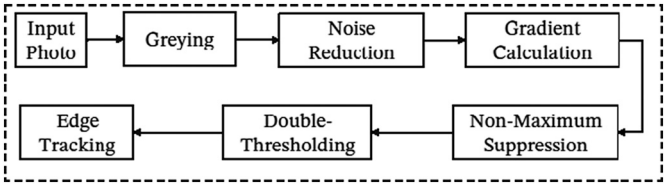

Fig. 3. Edge extraction using Canny algorithm.

images during laboratory and field tests. In addition, the results of preliminary trials demonstrate that the optimal Canny thresholds mainly depends on CCD i.e., optimization of Canny performance requires adjustment of the upper and lower threshold based on CCD. This study first explores optimal Canny thresholds at different distances using a dataset of 15 cracks during preliminary experiment [27] and then use this information to train the algorithm. The algorithm finally applies the capability of AR headset for CCD measurement and automatically adjusts the Canny threshold in real-time.

2.3. Characterization algorithm

2.3.1. Pixel-level measurement

Fig. 4 describes the in-pixel measurement procedure employed in this study for in-pixel crack measurement. After image acquisition (Fig. 4a) and edge detection (Fig. 4b), this study conducts a pixel evaluation in the binary image as shown in Fig. 4c. This study takes a horizontal scale approach for the measurement and computes the pixels between crack edges on each pixel row to obtain crack width. The conventional horizontal scale approach lacks accuracy for inclined and horizontal cracks because it neglects crack slope [6]. By applying the Canny algorithm, the gradient direction at crack edges is fully extracted. The research team use this information to mitigate the mentioned problem for inclined and horizontal cracks. The algorithm estimates the crack centerline gradient by averaging the gradients on the edges and applying it as the crack slope. The schematic view of pixels between the edges of cracks in the image coordinate system is magnified in Fig. 4d. Eqs. (1)–(3) are used to quantify the crack at pixel level in the processed part:

$$\text{Average Width } (\text{X}-\text{pixels}) = \frac{\sum_{i1}^{i2} N_k \times cos(\alpha_k)}{i2-i1} = \frac{\sum_{i1}^{i2} N_k \times sin(\beta_k)}{i2-i1} \tag{1}$$

$$\text{Length}_{\text{i1 to i2}} \ (\text{Y}-\text{pixels}) = \sum_{i1}^{i2} \frac{1}{sin(\beta_k)} = \sum_{i1}^{i2} \frac{1}{cos(\alpha_k)} \tag{2}$$

$$\text{Area}_{\text{i1 to i2}} \ (\text{X}-\text{pixels} \times \text{Y}-\text{pixels}) = \sum_{i1}^{i2} \frac{N_k \times \text{Cos}(\alpha_k)}{Cos(\alpha_k)} = \sum_{i1}^{i2} \frac{N_k \times \text{Sin}(\beta_k)}{\text{Sin}(\beta_k)} = \sum_{i1}^{i2} N_k \times 1 \tag{3}$$

Where i_1 and i_2 are respectively the index of the first and the last processed row in image, N_k is the number of pixels between two edges at the kth row, $\beta_k$is $arctan\left(\frac{\text{X-gradient)}}{\text{Y-gradient}}\right)$ at the crack edge in the kth row of image and α is $arctan\left(\frac{\text{Y-gradient)}}{\text{X-gradient}}\right)$ at the crack edge in the kth row of image. The crack dimensions in pixel units are calculated using Eqs. (1)–(3) as shown in Fig. 4e. The pixel-level measurement is in the image coordinate system and quantifies the cracks in the pixel units. The crack measurement in the engineering unit involves a further step that transforms from the image to the world coordinate system and shows the results in metric units to the user as demonstrated in Fig. 4 f. the next section describes the methodology to achieve this transformation.

2.3.2. Perspective distortion correction

The methodology includes a lightweight algorithm for perspective transformation using a scalar equation based on three Euler angles of the camera and CCD in direction of the camera optical axis. This study integrates this algorithm into crack characterization code to correct perspective distortion for crack on flat surface in real-time. Fig. 5 describes the three Euler angles in AR platform. The X-Y-Z are the three Cartesian axes of AR headset world coordinate system. Fig. 5a demonstrates the three components of the Euler angle vector around the three

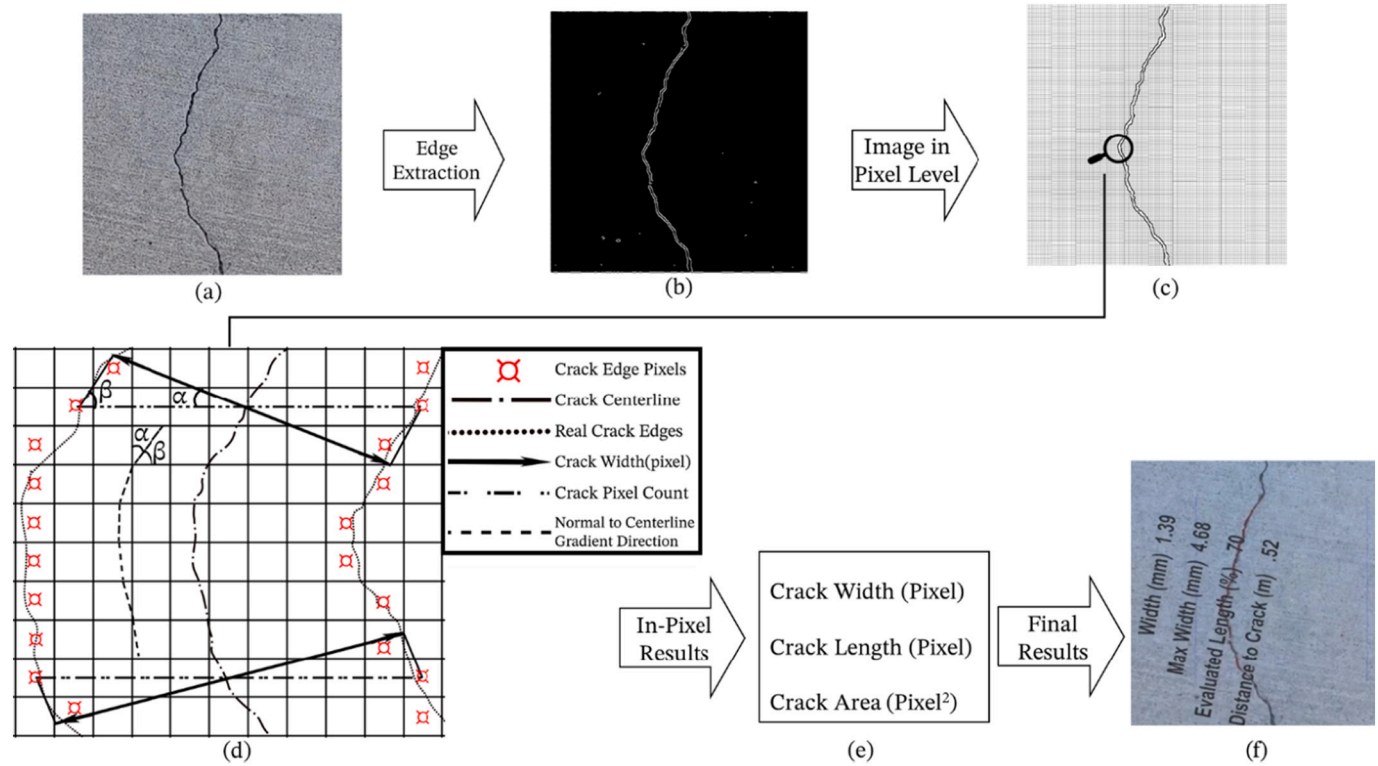

Fig. 4. Pixel level measurement methodology (a) acquired image (b) binary image (c) pixel-level image (d) magnified pixel-level image (e) results in pixel units (f) results in metric units.

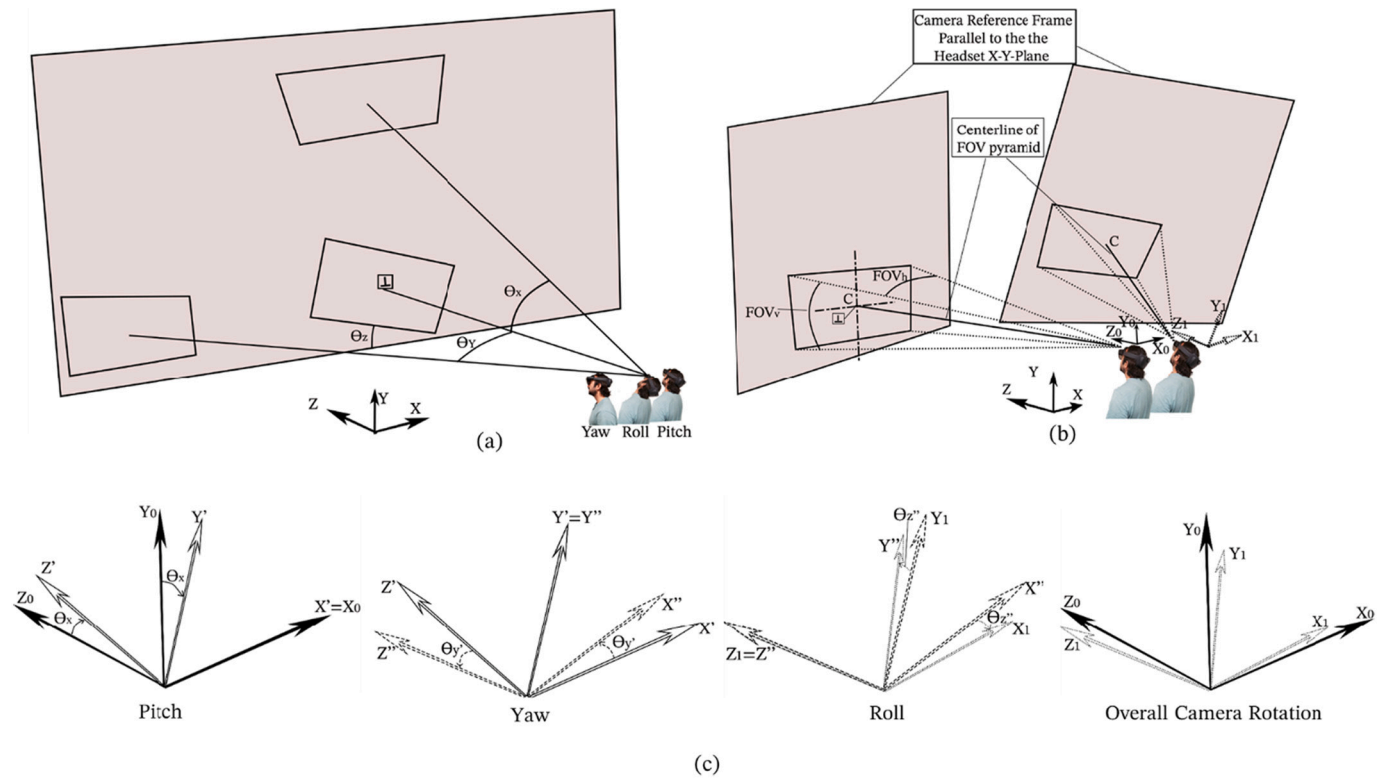

Fig. 5. Illustration of Euler angles (a) the demonstration of yaw, roll, pitch in AR platform (b) an arbitrary rotation of the AR headset coordinate system (c) using the three Euler angles to formulate the arbitrary rotation.

axes of the world coordinate system i.e., pitch θ_X around X, yaw θ_Y around Y, and roll θ_Z around Z. To have a clear understanding of Euler angles, each angle is shown when the other two angles are set to zero. Fig. 5b shows two consecutive states in the motion of an AR headset. The left-hand side of Fig. 5b shows that the camera coordinate system (X_0, Y_0, Z_0) and the world coordinate system (X, Y, Z) are initially in the same direction. The headset user then turns his head in an arbitrary position with an updated camera coordinate system (X_1, Y_1, Z_1) as shown on the right-hand side of Fig. 5b. The camera coordinate system and its reference plane undergo the same rotation as the headset. Horizontal and vertical Fields Of Views (FOV) are also demonstrated in this figure (FOV_h and FOV_v, respectively). Fig. 5c demonstrates that any arbitrary rotation of the AR headset can be decomposed to three Euler angles with the sequence of XYZ namely, $\theta_X - \theta_{Y'} - \theta_{Z''}$ (from left to right of the figure).

Fig. 6 describes the approach employed by this study to correct image distortion resulting from the camera oblique angles at image center. The camera of AR headset is assumed to have a closed box with a narrow hole on it and to be without a lens. The X-Y-Z are the three Cartesian axes of the world coordinate system. The *Z*-axis and XY-plane are respectively normal and parallel to the concrete surface. C is the center of the intersection between concrete surface and camera FOV which corresponds to the center of image. Fig. 6a shows a small imaginary square at the center of image. One side of this square is in the direction of projection of the camera optical axis on concrete surface that passes through C. This direction is entitled V_C in Fig. 6. The angle between the camera optical axis and the axis normal to concrete surface (Z-axis) is called θ_C. The size of ΔV_C which is an arbitrary small line at C in V_C direction is contracted proportional to cos (θ_C) in the image coordinate system. The camera angle does not affect pixel size in vertical direction to V_C because the camera optical axis is perpendicular to this direction. Therefore, the side of imaginary square in U_C direction, which is in vertical direction to V_C axis, is not affected by camera oblique angle. Fig. 6b magnifies the center of the image and shows the pixels encompassed by the given square. Fig. 6c shows the pixel located at the center of the image. This further magnification of the central pixel at C in Fig. 6c provides enough details to correlate the image coordinate system with V_C-U_C directions. This correlation provides a relationship between the size of the central pixel with the actual size of corresponding surface. The center of the image plane in the code is translated from bottom left to the center of the image. Therefore, X_I and Y_I are the axes of image coordinate system in the direction of image width and height, respectively. The U_C/V_C-components of a pixel in X_I direction (ΔXI) and the corresponding real size (ΔX_C) have the following relations:

$$\Delta X_{VC} = \alpha_X \Delta XI_{VC} cos\theta_C \; \Delta X_{UC} = \alpha_X \Delta XI_{UC}$$

Where ΔXI_C=1 pixel and $\alpha_X \left(\frac{mm}{pixel}\right)$ is a function of intrinsic parameters and d_C that is estimated in calibration process. ΔX_C is then calculated as follows:

$$\Delta XI_C = \sqrt{\Delta XI_{UC}{}^2 + \Delta XI_{VC}{}^2} = \sqrt{\frac{\Delta X_{UC}{}^2}{(\alpha_X)^2} + \frac{\Delta X_{VC}{}^2}{(\alpha_X cos\theta_C)^2}}$$
$$= \frac{\Delta X_C}{\alpha_X}\sqrt{sin^2\left(\frac{\pi}{2} - \theta_Z - \theta_{xyC}\right) + \frac{cos^2\left(\frac{\pi}{2} - \theta_Z - \theta_{xyC}\right)}{cos\theta_C}}$$

$$\Delta X_C = \frac{\alpha_X \Delta XI_C}{\sqrt{\frac{sin^2\left(\theta_Z + \theta_{xyC}\right)}{cos\theta_C} + cos^2\left(\theta_Z + \theta_{xyC}\right)}} \quad (4)$$

And by repeating this procedure for the pixel in the direction of Y_I:

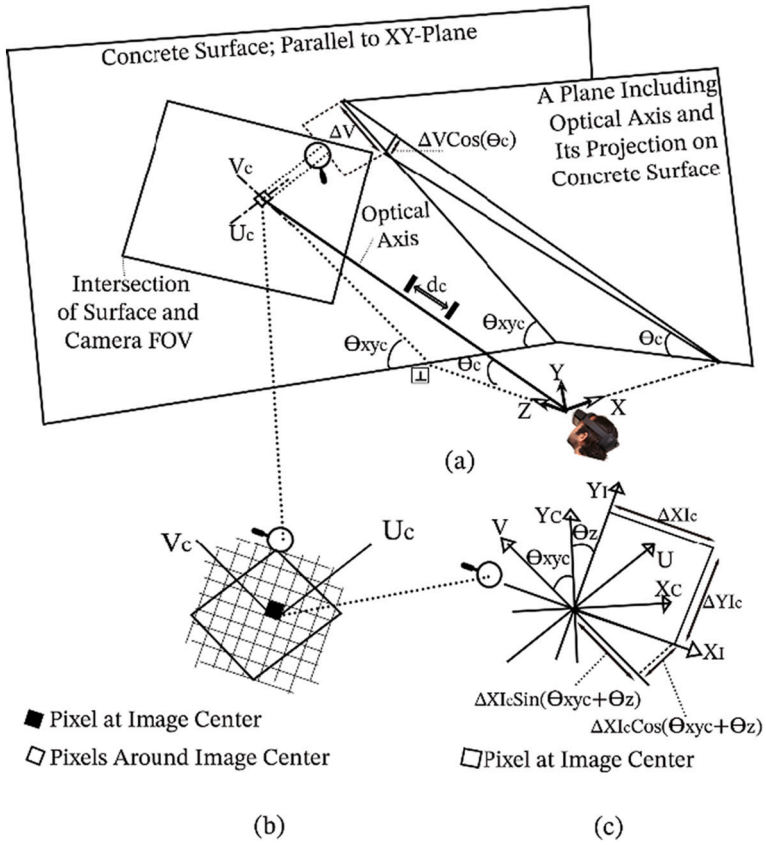

Fig. 6. Approach for image distortion correction for the pixel at the center of camera FOV (a) the effect of camera angle on the size of an imaginary square is evaluated at two different directions i.e., V_C and U_C (b) magnification of the mentioned rectangle (c) further magnification of the pixel at the center of image used to correlate image coordinate system with V_C/U_C directions.

$$\Delta Y_C = \frac{\alpha_Y \Delta YI_C}{\sqrt{\frac{cos^2(\theta_Z+\theta_{xyC})}{cos\theta_C} + sin^2(\theta_Z+\theta_{xyC})}} \quad (5)$$

Where ΔYI_C=1 pixel, $\alpha_{Y\left(\frac{mm}{pixel}\right)}$ is a function of camera intrinsic parameters and d_C that is achievable from the calibration process, θ_{xyC} is the angle between U_C and X_C (X_C and Y_C are two axes that are parallel to X and Y axes, respectively and pass through C), and θ_Z is the rotation angle of the picture around *Z*-axis.

Fig. 7 shows the rotation of two imaginary lines i.e., OA and AB subjected to an arbitrary rotation used to calculate θ_C, θ_{xyC} and θ_Z. O is the center of the coordinate system, A is fixed to *Z*-axis at an arbitrary distance to O, and B is selected so that AB is initially parallel to Y-axis in ZY-plane. This study decomposes an arbitrary rotation of a coordinate system subjected to three rotations of Euler angles with the sequence of XY'Z" as shown in Fig. 7. The coordinates of A after rotation around X and Y′ axes are A' and A", respectively:

$$A = \begin{bmatrix} 0 \\ 0 \\ OA \end{bmatrix} \quad A' = \begin{bmatrix} 0 \\ OAsin\theta_X \\ OACos\theta_X \end{bmatrix} \quad A'' = \begin{bmatrix} -OAsin\theta_{Y'} \\ OAsin\theta_X cos\theta_{Y'} \\ OACos\theta_X cos\theta_{Y'} \end{bmatrix}$$

θ_{xyC} and θ_C can be calculated using the XYZ-coordinates of A, A' and A". Considering that the rotation around Z" does not change the θ and θ_{xy}, these angles are:

$$\theta_{xyC} = arctan\left(\frac{sin\theta_X cos\theta_{Y'}}{sin\theta_{Y'}}\right) \quad (6)$$

$$\theta_C = arcsin\sqrt{sin^2\theta_{Y'} + sin^2\theta_X cos^2\theta_{Y'}} \quad (7)$$

Rotation of AR headset around Z-axis (θ_Z) is achievable by evaluating the rotation of the line AB around Z-axis. The coordinates of B after the rotation around X and Y′ axes are B′ and B″, respectively. Rotation around X-axis does not rotate AB around Z axis and therefore A'B′, is parallel to Y-axis. The rotation of AB around Z-axis after two rotations around X and Y′-axes ($\theta_{Z'}$) is:

$$\theta_{Z'} = arctan\left(\frac{X_{B''} - X_{A''}}{Y_{B''} - Y_{A''}}\right)$$

And:

$$B' = \begin{bmatrix} 0 \\ OAsin\theta_X + A'B' \\ OACos\theta_X \end{bmatrix} B''$$
$$= \begin{bmatrix} -(OA - A'B'sin\theta_X)sin\theta_{Y'} \\ A'B'cos^2\theta_X + (OA - A'B'sin\theta_X)cos\theta_{Y'}sin\theta_X \\ \cdots \end{bmatrix}$$

Therefore:

$$\theta_{Z'} = arctan\left(\frac{sin\theta_X sin\theta_{Y'}}{cos^2\theta_X - sin^2\theta_X cos^2\theta_{Y'}}\right)$$

θ_Z is then formulated as:

$$\theta_Z = \theta_{Z'} + \theta_{Z''}cos\theta_C = arctan\left(\frac{sin\theta_X sin\theta_{Y'}}{cos^2\theta_X - sin^2\theta_X cos^2\theta_{Y'}}\right) + \theta_{Z''}cos\theta_C \quad (8)$$

Substitution of Eqs. (6)–(8) in Eqs. (4) and (5) provides the pixel size at the center of the image.

Fig. 8 shows the approach proposed to calculate the pixel size at any position in the image. The analysis of a random pixel results in the same relationship for pixel size as Eqs. (4) and (5) but with different θ_{xy}, θ and d as shown in Fig. 8a. To calculate θ_{xy}, θ and d for an arbitrary pixel first the location of C in the world coordinate system (XYZ) is calculated as follows:

$$X_C = -d_C sin\theta_C cos\theta_{xyC}\ Y_C = d_C sin\theta_C sin\theta_{xyC}\ Z_C = d_C cos\theta_C$$

Next, the algorithm estimates the location of the given pixel by applying the pixel size at C (ΔX_C and ΔY_C) as an initial approximation for all pixels throughout image as demonstrated in Fig. 8b. Therefore, the coordinates of the pixel in the world coordinate system are:

$$X = -d sin\theta_C cos\theta_{xyC} + n\Delta X_C cos\theta_Z + m\Delta Y_C sin\theta_Z\ Y$$
$$= d sin\theta_C sin\theta_{xyC} + m\Delta Y_C cos\theta_Z - n\Delta X_C sin\theta_Z Z = d_C cos\theta_C$$

Where n and m are the integer indices of the pixel in new image coordinate system centering at C. The algorithm subsequently calculates the angles θ_{xy}, θ and the distance d:

$$d = \sqrt{X^2 + Y^2 + Z^2} \quad (10)$$

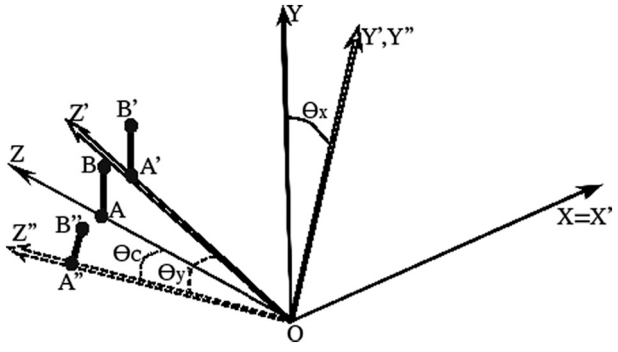

Fig. 7. The method for calculation of angles θ_C, θ_{xyC} and θ_Z based on the rotation of the lines OA and AB.

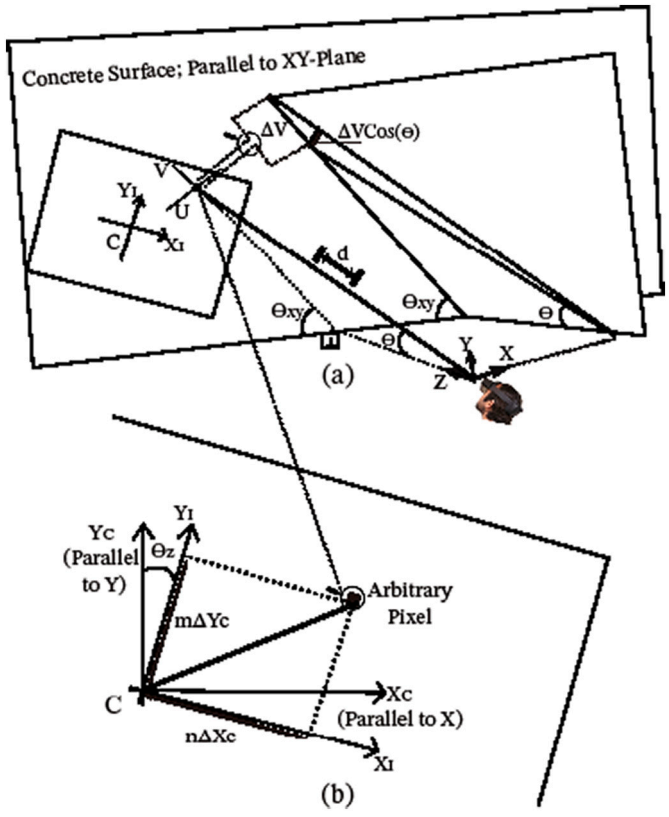

Fig. 8. Perspective correction for any arbitrary pixel in the image (a) the intersection of camera FOV with concrete surface at any arbitrary pixel gives the angles required for perspective transformation (b) the position of the pixel in image coordinate system is calculated based on the size of the central pixel.

$$\theta = arctan\frac{\sqrt{X^2 + Y^2}}{Z} \tag{11}$$

$$\theta_{xy} = arctan\frac{X}{Y} \tag{12}$$

Finally, generalizing of Eqs. (4) and (5) gives the pixel size of any pixel in the image:

$$\Delta X = \frac{\alpha_X \Delta \mathrm{XI}}{\sqrt{\frac{sin^2(\theta_Z+\theta_{xy})}{cos\theta} + cos^2(\theta_Z + \theta_{xy})}} \tag{13}$$

$$\Delta Y = \frac{\alpha_Y \Delta \mathrm{YI}}{\sqrt{\frac{cos^2(\theta_Z+\theta_{xy})}{cos\theta} + sin^2(\theta_Z + \theta_{xy})}} \tag{14}$$

It should be mentioned that the application of Euler angles for distortion correction can inherently cause gimbal lock problem. Gimbal lock will result in the loss of control over the angle in three-dimensional coordinate system when using Euler angles. The angle quantification can be affected by gimbal lock when one of the Euler angles reaches 90 degrees [28]. This study assumes the rotation of head around each of the Euler angles does not reach 90° in normal head positions. This assumption excludes the possibility of gimbal lock from the proposed distortion correction method.

3. Algorithmic transformation

This section describes the methodology of this study for deploying the discussed measurement algorithm in the AR platform. The authors first discuss the AR headset platform, then explore its capabilities and limitations regarding image processing, and finally explain the step for implementation of the algorithm in the AR platform.

3.1. AR headset platform

The developed algorithm for crack characterization is implementable in AR headsets with the following capabilities: (1) headset angle computation, (2) distance measurement, (3) integrated processing unit, and (4) see-through display. This study uses the Microsoft HoloLens headset for crack characterization. The researchers implement the pixel level algorithm in both generations of the headset, but only the newer version (the 2nd generation) is employed for the final crack characterization in the engineering unit. To provide a clear insight about this AR headset some of the properties of the headset are quoted from its manufacturer website as presented in Table 2. The feature improvement from the 1st to 2nd generation includes memory, CPU and storage increase, weight reduction, and integration of new features such as Scene understanding and eye-tracking.

Unreal and Unity engines are two software platforms for developing applications for AR-headsets with integrated computing capabilities [22]. The AR developers integrate C# codes with Unity projects to have more variable design parameters [29] but C^{++} and Visual Studio can also be attached to Unity for developing AR apps [30]. This study employs Unity platform and C# programming languages to develop the crack measurement tool.

Table 2
Comparing the two generations of the employed AR headset

Feature	1st generation	2nd generation
Stationary frame of reference	✓	✓
Attached frame of reference	✓	✓
Spatial anchors	✓	✓
Spatial mapping	✓	✓
Scene understanding	×	✓
Eye-tracking	×	✓
Weight	579 g	566 g
CPU Cores	4	8
Memory	1GB	4GB
Storage	64 GB	64 GB

3.2. AR coding challenges

Matrices are normally used to save the pixel information in image processing with computer. Furthermore, in image processing, diverse athematic operators are required to achieve useful information from the image. However, the authors cannot find high-dimensional matrix capability and enough image arithmetic functions in the Unity-C# platform. The OpenCVSharp, as a library of powerful arithmetic functions for online image processing in C#, is tested to make up for the mentioned shortcomings. However, our entire attempt to deploy any Unity project, which includes OpenCVSharp libraries, in AR headsets has not succeeded. Therefore, this study excludes OpenCVSharp and other auxiliary packages from the Unity project. Instead, the methodology includes saving and processing of the pixel values of the photos in 1D arrays and employs the limited arithmetic operators available in Unity-C# to implement the measurement algorithm. The project is then deployed in the AR headset but because of the limited processing speed of the device, the implementation time was impractical for real-time or near-real-time applications. This study uses a scalar formula for perspective correction to shorten the processing time. Additionally, streamlining of the initial code reduces the complexity of the algorithm toward real-time processing. The efforts for streamlining the code toward lower processing times are discussed in Section 5.2.

3.3. Crack characterization algorithm

Fig. 9 details the steps of crack characterization algorithm. The first step in the algorithm is automatic image acquisition using the headset's Web Camera Application Programming Interface (API). Two image acquisition means are available in the AR headset platform i.e., the PhotoCapturing and VideoCapturing (Webcam) modes. While the PhotoCapturing camera mode of AR headsets provides a single-step image acquisition strategy, the VideoCapturing mode requires an additional step that is restoring the webcam texture resulting from a video sequence to a two-dimensional texture. The second step includes employing a one-dimensional array to store and codify the pixel information. To make the algorithm implementable inside the AR digital platform, the processing must be inside arrays. The traceability of the pixels in the arrays is essential for image processing. Additionally, to make the algorithm compatible with the AR platform, supplementary packages such as OpenCVSharp are removed from the Unity project. The third step in the algorithm is edge detection using Canny operator. In the fourth step the algorithm utilizes the information obtained from Canny operator to conduct crack measurement in pixel units. After crack measurement at pixel level, the algorithm takes the fifth step in which AR headset orients the Web Camera relative to the flat concrete surface undergoing inspection. In C#-unity environment two commands enable the AR-headset to receive the orientation information which are called "RaycastHit" and "TransformeulerAngle". The "RaycastHit" command provides CCD in direction of camera optical axis (d_C in Fig. 6a) and "TransformeulerAngle" measures the headset Euler angles ($\theta_X - \theta_{Y'} - \theta_{Z''}$ in Fig. 5c). Additionally, this step includes a perspective transformation to correct the distortion caused by oblique camera angles. The sixth step is the transformation from in-pixel measurement to measurement in the engineering unit. This step includes the substitution of the calibration relations in the results of pixel level measurement (fourth step) using the information of the camera angles and CCD (fifth step). In the seventh step, the algorithm can compare the crack dimensions with the crack criteria stated in the relevant specifications to assist the decision-making process. In the eighth step, the AR tool overlay cracks with the processed photo where the cracks are marked with a noticeable color and displays the characterization results to the user.

The algorithm is summarized in the following pseudo code:

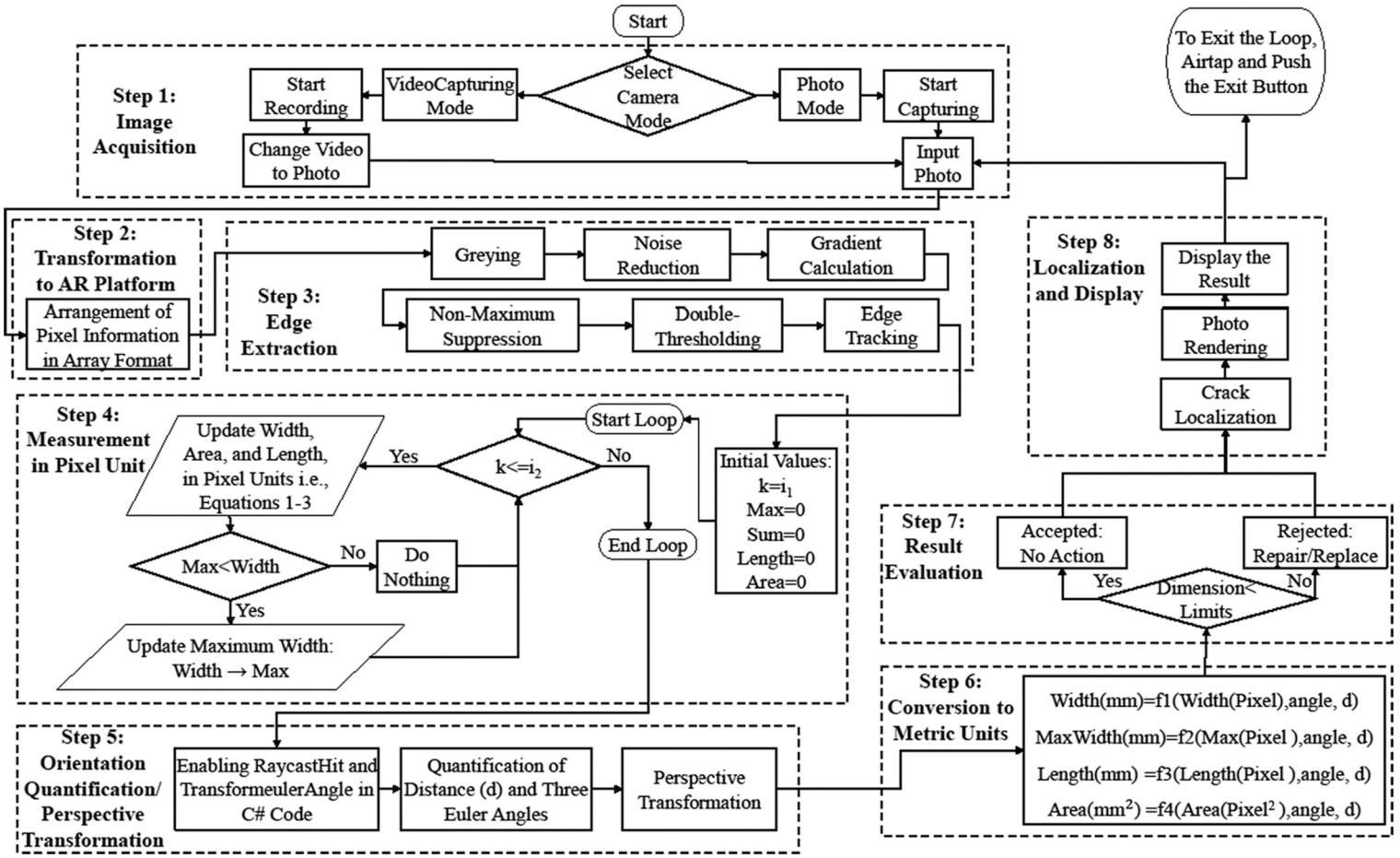

Fig. 9. Crack Characterization Algorithm.

4. Calibration process and resolution

However, this information should be validated through experiment to ensure the accurate measurement. To fact-check the theorical pixel size calculated from geometry and manufacturer specification, this study conducts a calibration process in which the pixel size at different distances is calculated. The AR crack measurement tool is usable by human

- Algorithm title: Crack characterization
- Method: Canny edge detection and pixel analysis
- Input: AR headset image
- Output: Maximum crack width (mm), average crack width (mm), crack length (mm), crack area (mm^2)

```
1. Update at every time step,
2.        Acquire an image,
3.        Transform the pixel information into the AR platforms,
4.        For every pixel inside the processed part,
5.              Apply Canny algorithm to extract:
                    (1) pixels on the crack edges (2) image gradient direction at the crack edges,
6.        End for,
7.        Set initial values:
                maximum width=0, average width=0; length=0; area=0,
8         For each row k inside the processed part,
9               Apply Equations 1-3 to calculate:
                    (1) average width (pixels) (2) length (pixels) (3) area (pixels 2),
10.             If maximum width< width_k then,
11.                 maximum width =width_k,
12.             End if,
13.       End for,
14.       Measure CCD by applying RaycastHit,
15.       Measure camera obliquity angle by applying Transform.eulerAngles,
16.       Apply perspective transformation,
17.       Apply pixel information into Equations 13-14 to quantify the crack in standard units,
18.       Evaluate the structure by comparing the defect dimensions with the specification criteria,
19.       Display the results to the inspector,
20. End update.
```

The proposed methodology necessitates updating the algorithm with the coefficients $\alpha_X$and α_Y at every time-step as described by Eqs. (4), (5), (13) and (14). The knowledge of individual pixel size at vertical camera angle is required at different CCDs to update $\alpha_X$and $\alpha_Y$at every time step. The estimation of pixel size at different CCDs is performable by using a geometrical relationship based on the intrinsic parameters of the headset camera achieved from the manufacturer specification. users who wear AR headset. Therefore, in the calibration experiment, the measurement error because of the deviations in users' position and angle from the set-condition was controlled by the test operators. The AR tool alerted the operators to adjust their positions if they violated the set-limits for the experiments. The research team selected these tolerances lenient enough so that the test was applicable to human operators. The range of motion in *Z*-direction, the tolerance of motion in X,Y-

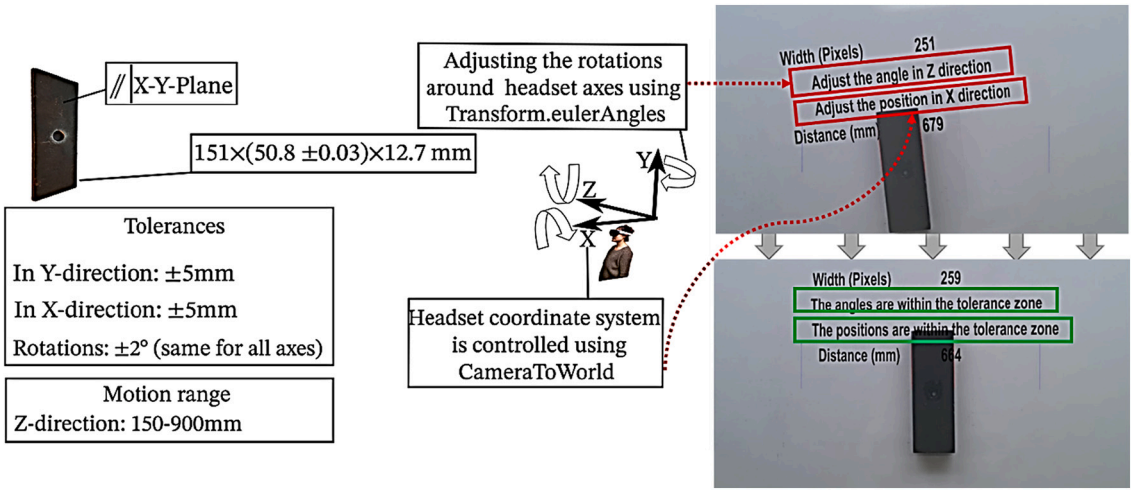

Fig. 10. Calibration experiment illustration.

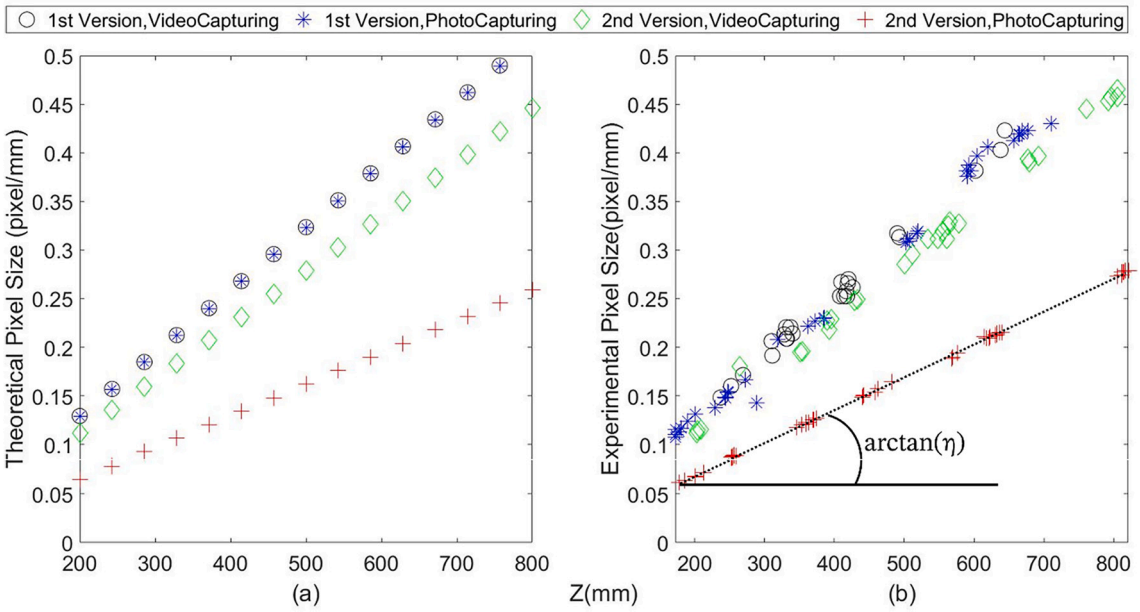

Fig. 11. Resolution of the AR headsets (a) theoretical (b) experimental.

Table 3
The resolution and FOVh of the two generations of AR headset

	Resolution (pixel2)		FOVh (°)	
	1st	2nd	1st	2nd
Photo	2048 × 1152	1280 × 720	67	64.69
Webcam	3904 × 2196	2272 × 1278	45	64.69

directions, and the tolerance or rotations in X,Y,Z- directions are demonstrated in Fig. 10. Additionally, Fig. 10 shows the size of the gauge used for the calibration. The test operators moved in the Z direction during the experiment and recorded the data of pixel count and CCD when their positions were within the set tolerances. The same calibration experiment was repeated for the two versions and for the two camera modes of the AR headset to have a wider evaluation of measurement potential in the headsets.

Fig. 11 (a) and (b), respectively show the theoretical and experimental pixel size of the two generations of the AR headset and the two available camera modes. Eq. (15) provides the theoretical pixel size in X_I and Y_I direction at the center of image for perpendicular camera angle (X_I and Y_I are the direction of image width and height, respectively):

$$\Delta X_{CP} = \frac{2 \times Z \times tan(FOV_h/2)}{X_I - \text{Resolution}} \text{ and} \Delta Y_{CP} = \frac{2 \times Z \times tan(FOV_v/2)}{Y_I - \text{Resolution}} \quad (15)$$

The FOVh of the headset and their resolution in X_I and Y_I directions are also shown in Table 3. A smaller pixel size implies a smaller resolution and a higher accuracy. This implies that the PhotoCapturing mode of the 2nd generation has the highest accuracy. Additionally, the VideoCapturing and PhotoCapturing modes of the 1st generation (both are similar in pixel size) has the lowest accuracy and the accuracy of the VideoCapturing mode of the 2nd generation lies between them. The results of the calibration experiments for all headset versions and camera modes are consistent with the theoretical linear relations between pixel size and CCD achieved from Eq. (15) as shown in Fig. 11.

The results of calibration are essential for achieving the coefficients of α_x and α_y in Eqs. (13) and (14). Applying Eq. (4) for calibration experiment with the following values:

$$\theta_C = 0\ \theta_Z = 0\ \theta_{xyC} = 0\ Z = d_C$$

shows that α_x *is equal to* ηd_C where η is the slope of the line interpolating the data in Fig. 11b as shown for PhotoCapturing mode of the 2nd generation.

Substituting the FOVh and resolutions of the headsets in XI and YI directions in Eq. (15) shows that the pixel size is the same in these directions for perpendicular camera angle. Applying calibration angles (θ_C, θ_Z, θ_{xyC}) in Eq. (5) shows that $\alpha_y = \alpha_x$.

5. Accuracy and time quantification

5.1. Benchmark accuracy study

The research team assessed the accuracy of the AR tool using three machined metallic gauges with maximum tolerance of ±0.03 mm on their width and compared the app measurement with the measurement of a digital caliper with the resolution of 0.01 mm. Fig. 12 shows the experimental setup used for the accuracy evaluation of the AR tool. The experiment was performed at UNM Center for Advanced Research Computing (CARC). The test was conducted using the PhotoCapturing mode of the 2nd generation headset that has the highest resolution compared to the other combinations of headsets and camera modes (see Fig. 11). The research team fixed the gauges to a magnetic board with several magnets. Fig. 12a demonstrates the metallic gauges and the magnetic board used in the experiments. To reduce the error caused by the protruding edges of the gauges in testing the AR tool at obliqued camera angles, the researchers made the two following efforts: (1) using two narrow gauges with a thickness of 0.5 ± 0.1 mm during the experiments with obliqued camera angles. (2) beveling their edges in the experiments with obliqued camera angles.

Like the calibration experiments, the test was performed by human operators. The test operators changed position in X and Z direction (see Fig. 5a) and their angles in Y direction (θ_Y in Fig. 5a) during the experiment and adjusted their positions and angles by the feedback received from the AR tool. While the test operators reached a new test position, they recorded the data of pixel count, CCD and θ_Y at least for three app measurements. Therefore, the experiments evaluate the accuracy of the AR tool at different CCDs and headset angles (gauge angle i.e., α in Fig. 4a is not a test parameter). Fig. 12b shows three positions of a test operator during the experiments and demonstrates the head angles in Y direction (θ_Y). Fig. 12c shows the result of AR tool measurement for

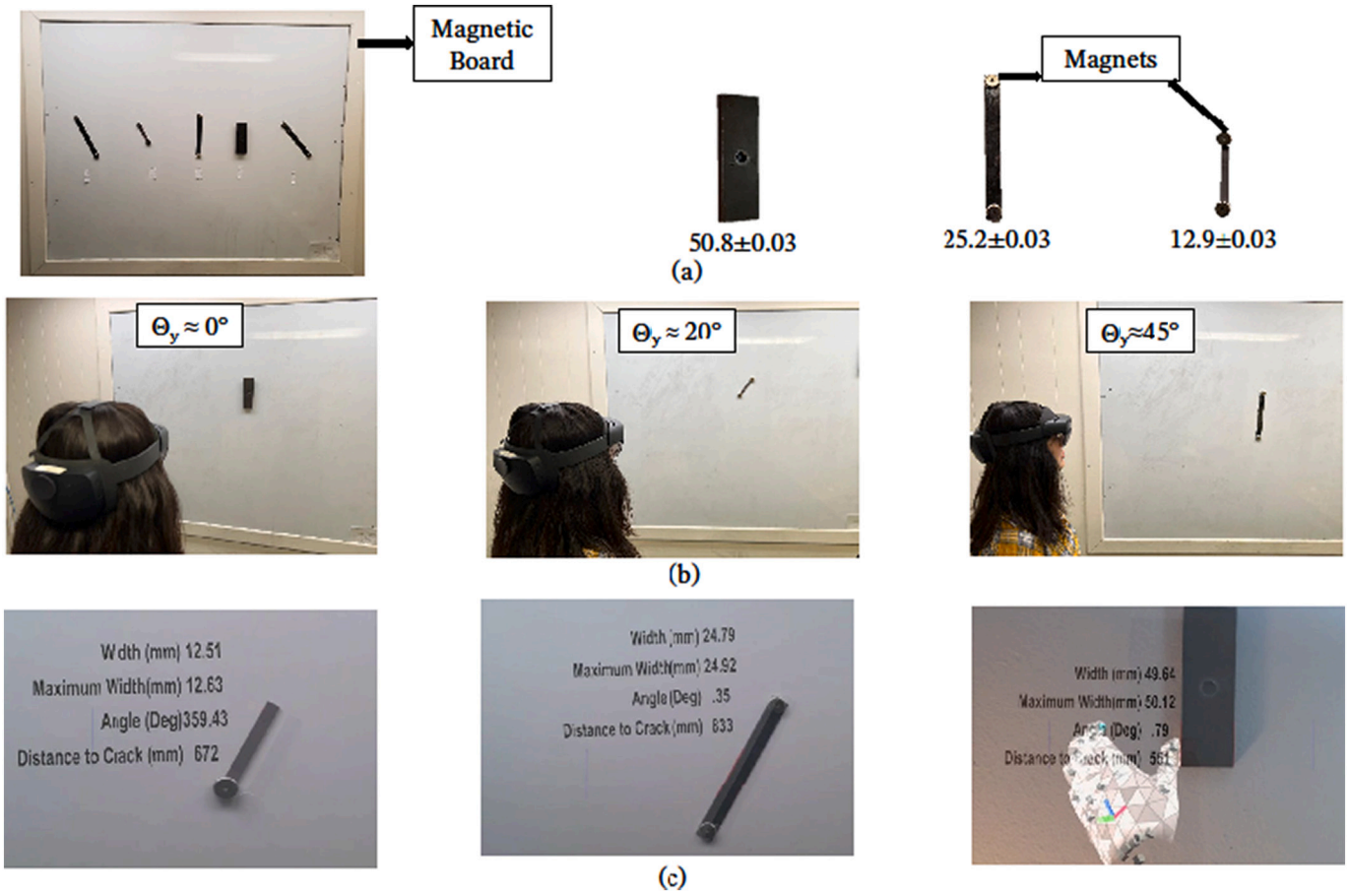

Fig. 12. The experimental setup used for accuracy benchmark study (a) the magnetic board and metallic gauges (b) illustration of the processed part in the image (c) the change in the processing time with the size of the processed part.

three experiments conducted with different gauges at different angles and CCDs.

Fig. 13 shows the results of the laboratory experiments. Each point represents 3 or more measurements approximately at its nominal angle and CCD. The maximum deviations of angle and distance from the nominal values are similar to the calibration experiments which are shown in Fig. 10. While the change in CCD does not show a significant effect on measurement errors, the higher errors appeared to occur at sharper headset angles i.e., θ_Y between 35° - 47.5°. The maximum relative error during the laboratory experiments was 8.45%. This maximum relative error corresponds to the gauge with the nominal width of 12.9 mm when the CCD and head angle in Y direction (θ_Y) are approximately 635 mm and 45°, respectively.

The existing crack characterization methodologies which establish a network between their acquisition, orientation, and processing units can have comparable accuracy or supersede the proposed integrated system in accuracy because they benefit from free choice of processing power. Those methodologies can implement more complex algorithms such as video processing or artificial neural network to achieve higher accuracies. Two examples of network-based characterization methodologies with higher and lower accuracies compared to the proposed system are respectively Shan et al. [6] with the maximum relative error of 5.4% and Shao et al. [11] with the maximum relative error of 14.54%. The networking approach, however, results in nonrealtime processing because of the latency in connection establishment between different elements i.e., image acquisition device, orientation system, and processing unit. For example, Mojidra et al. [31] proposed a crack identification system using network-based AR. They developed a CNN model using a short video of cracked surfaces as the input and made a database and internet connection between AR headset and MATLAB software on a computer. They detected cracks with significant accuracy and streamlined the processing time to approximately 30 s. The following section quantifies the time of the proposed method and demonstrates its capability to achieve near real-time processing.

5.2. Processing time

For correction of perspective and geometrical distortion in the processed image, reconstruction of 3D model of structures is proposed by the past studies (e.g., [19,13]). However, implementation of 3D model reconstruction is time consuming [13]. Specifically, the processing capability of AR headsets prevents implementation of the algorithms with high memory complexity [22]. This study develops a lightweight algorithm based on scalar equations (Eqs. (13) and (14)) for perspective transformation and implements it to reduce the memory complexity toward real-time processing. In addition, to reduce the algorithm complexity of the edge detection step, the algorithm excludes the edge thinning steps of the Canny operator, which does not contribute to the crack measurement task. Additionally, the algorithm limits the processing to a rectangular part in the center of the image to reduce the processing time. This study assumes this rectangle as the users' field of attention and excludes the photo's off-center from the image-processing. The human field of attention can differ between different users and therefore the algorithm enables the user to change the size of the mentioned rectangle based on their preference. The user can adjust the size of this rectangle to create a proper balance between the crack characterization area and the processing time.

The research team conducted an experiment on the campus of the

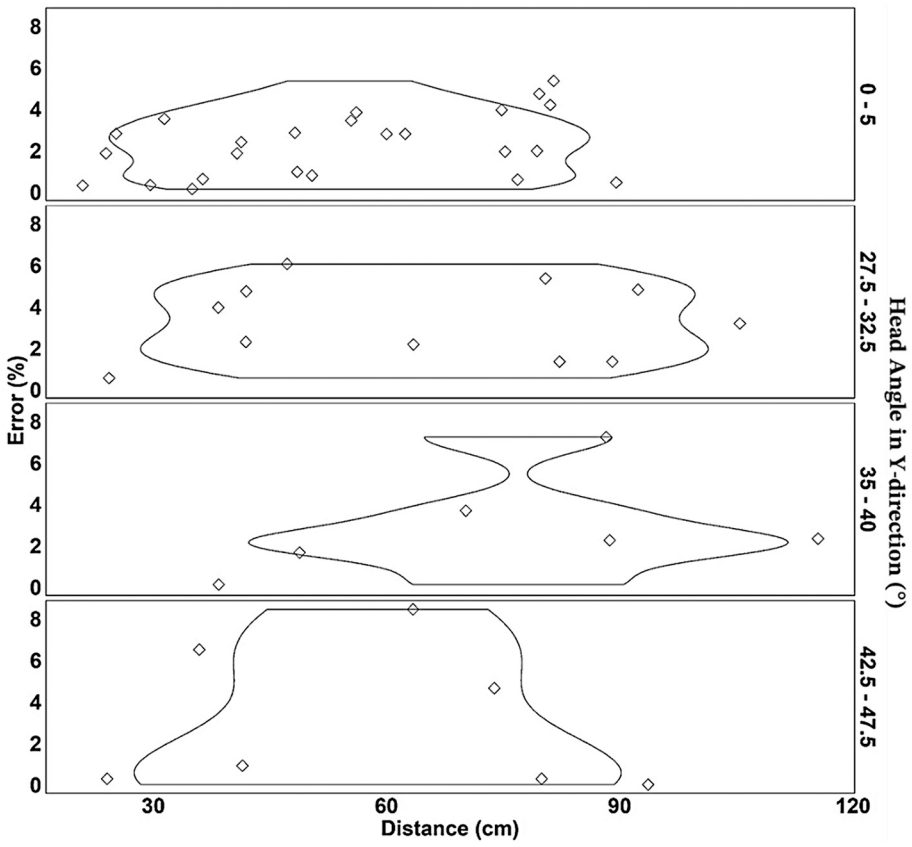

Fig. 13. The results of the laboratory experiment.

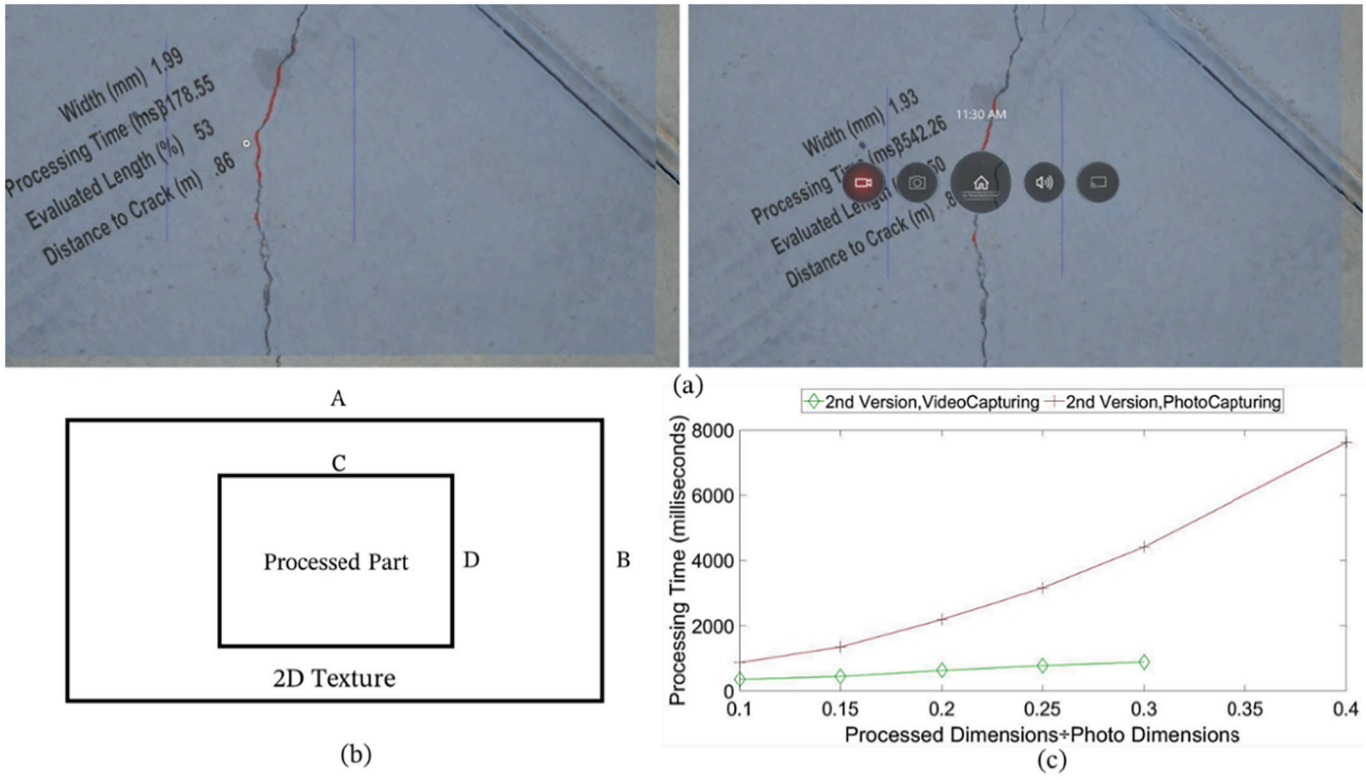

Fig. 14. Processing time description (a) examples of processing time evaluation tests on the 2nd generation headset (b) illustration of the processed part in the image (c) the change in the processing time with the size of the processed part.

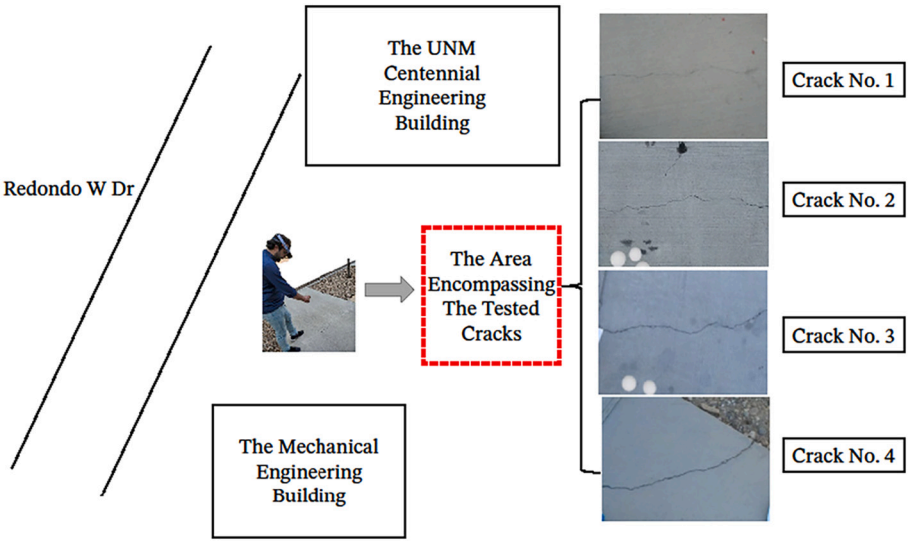

Fig. 15. Illustration of the tested cracks and their locations.

University of New Mexico (UNM) in which the processing time was evaluated for different sizes of the processed rectangle. Fig. 14a shows two instances of data collection corresponding to the processing time evaluation of the PhotoCapturing mode of the 2nd generation. Fig. 14b shows the position of the processing part inside an 2D texture representing an image. Fig. 14c illustrates the change in the processing time of the 2nd generation headset with the size of the processed part for the two available camera modes i.e., VideoCapturing and PhotoCapturing.

Crack No. 1

Distance (m)	Width (mm) AR	Caliper	Average AR	Error (%)	Exemplar Image
0.45	0.83	0.81	0.82	0.10	
0.44	0.80				
0.45	0.86				
0.45	0.80				
0.46	0.79				
0.46	0.81				
0.35	0.81	0.78	0.81	3.09	
0.38	0.84				
0.33	0.77				

Crack No. 2

Distance (m)	Width (mm) AR	Caliper	AR Average	Error (%)	Exemplar Image
0.53	1.07	1.03	1.07	3.47	
0.54	1.05				
0.54	1.08				
0.64	0.91	1.03	0.98	4.94	
0.66	1.08				
0.64	0.95				

Crack No. 3

Distance (m)	Width (mm) AR	Caliper	AR average	Error (%)	Exemplar Image
0.81	1.23	1.36	1.24	9.02	
0.80	1.23				
0.82	1.25				
0.52	1.32	1.34	1.37	2.63	
0.52	1.36				
0.52	1.40				
0.52	1.36				
0.52	1.39				
0.53	1.36				
0.53	1.40				
0.53	1.34				
0.54	1.38				
0.55	1.40				

Crack No. 4

Distance (m)	Width (mm) AR	Caliper	AR average	Error (%)	Exemplar Image
0.99	1.96	2.24	1.97	12.05	
0.99	1.97				
0.99	1.94				
0.99	2.01				
0.66	2.02	2.24	1.972	11.98	
0.66	1.91				
0.69	2.02				
0.69	1.97				
0.68	1.97				
0.68	1.94				

Fig. 16. The results of the case study for the four tested cracks.

In the experiment, the dimensions of the processed rectangle to the image's dimensions were the same for both length and width i.e., $\frac{C}{A} = \frac{D}{B}$. While the processing time of PhotoCapturing mode appears to increase drastically with the size of the processed part, in VideoCapturing mode the increase is moderate. Overall, the processing time is less in the VideoCapturing mode than the PhotoCapturing mode. However, VideoCapturing mode is not applicable for complex algorithm for example, if the processed part exceeds 30% of the image in size, the only workable mode is PhotoCapturing. The processing-times of the two headsets were also evaluated and compared. The processing time of the 2nd generation is generally greater than the first generation. For example, for a special size of processed rectangle where C is 25% of A and D is 45% of B the processing time for the PhotoCapturing and VideoCapturing modes of the 2nd generation are 3185 and 770 milliseconds, respectively. The processing time of the PhotoCapturing and VideoCapturing modes of the 1st generation for the mentioned size are respectively 1676 and 377 milliseconds.

6. Field experiment

The researchers tested the final version of the AR app on the cracks on the pavements of the UNM campus as a case study to evaluate the usability of the method for real-world crack inspections. First the research team tested the AR tool on real cracks with diverse patterns and sizes and adjusted the tools' features and thresholds for real crack measurement. Next, four surface cracks on the pavement between the Mechanical Engineering and the Centennial building at UNM were selected as shown in Fig. 15. The research team first measured the cracks with a digital caliper of 0.01 mm resolution and used the caliper measurement as the ground truth for accuracy analysis. The caliper measurement included three or more measurements at every centimeter of the cracks. The widths of the selected cracks ranged approximately from 0.8 mm to 2 mm.

The research team then used the AR tool to quantify the cracks. Similar to the calibration and accuracy measurement tests, the field experiment was conducted by human operators. Based on the results of the calibration tests (Section 4), the PhotoCapturing mode of the second generation has the highest resolution compared to the other combinations of headsets and camera modes. Therefore, to increase the measurement accuracy, that mode and generation was selected for conducting the field measurement. The operators moved in different directions around the cracks during the tests and recorded the crack width at different arbitrary distance and head angles. To increase the repeatability of the experiment, each measurement included a minimum number of three app readings. Fig. 16 shows the results of the AR app measurements for the four cracks at different distance and includes a comparison between the caliper measurement and the app measurement. The AR tool measures the crack width at two different positions for each crack. Additionally, the final value of the AR app is the average of three or more than three measurements of the cracks at the two positions. To enhance the validity of the results, the test operators adjusted their distance from each crack based on the resolution of the headset's camera and the size of the crack. For example, they measured the width of the narrowest cracks i.e., crack No.1 at closer positions compared to the other cracks.

The comparison of the app measurement with the caliper measurement as the ground truth shows a maximum of 12.05% relative errors for the measurements.

7. Conclusion

This study deals with one of the most significant knowledge-gaps in online crack width quantification through image-based methods. This gap includes the real-time translation of the pixel-level information to engineering knowledge at different camera positions and angles. The research team uses AR headset capabilities and thereby integrates entire crack characterization devices i.e., image acquisition, image processing, distance measurer and orienting device into one single platform. Additionally, this study develops a lightweight algorithm for perspective correction that reduces the memory complexity toward real-time processing. The authors consider addressing the following limitations of the proposed method as the future direction of this study:

1. Limitation for concrete with curved surface: The algorithm does not deal with the geometry distortion in the images caused by non-flat structural surfaces.
2. Distortion correction limitations: Application of Euler for distortion correction causes inherent issues such as gimbal lock. Using quaternion matrix instead of Euler angles for angle measurement is a possible future work of this study.
3. Multiple crack limitations: The crack measurement system used during the experiments can measure a single crack in horizontal direction (the direction of image's width). The algorithm is adjustable for multiple crack measurement with the same accuracy but with different processing time.

Additionally, the following limitation of AR headset can affect the performance of this methodology:

1. Vision limitation of AR headset: The AR headset employed in this study gives the user an unclear view under direct sunlight.
2. Limitation of camera resolution: The developed methodology utilizes camera of AR headset for input image acquisition whose resolution is limited based on the headset manufacturer specification.

Declaration of Competing Interest

The authors declare no conflicts of interest.

Data availability

The data that support the findings of this study are available from the corresponding author, FM, upon reasonable request.

Acknowledgments

This work is funded by the New Mexico Department of Transportation (NMDOT), the Transportation Consortium of South-Central States (Tran-SET), project number 69A3551747106, and the National Academic of Science Transportation Research Board (TRB) Rail Safety IDEA RS-43, project number A21-0277. In addition, the authors appreciate the efforts of John-Wesley Hanson, Xinxing Yuan, Ali Mohammadkhorasani, Daniel Gavin, Aaron Atcitty, and Roya Nasimi for improving the quality of this study.

References

[1] E.L. Labib, Y.L. Mo, T.T.C. Hsu, Shear cracking of prestressed girders with high strength concrete, Int. J. Concr. Struct. Mater. 7 (2013) 71–78, https://doi.org/10.1007/s40069-013-0033-4.
[2] S. Li, X. Zhao, Automatic crack detection and measurement of concrete structure using convolutional encoder-decoder network, IEEE Access 8 (2020) 134602–134618, https://doi.org/10.1109/ACCESS.2020.3011106.
[3] A.P. Boresi, R.J. Schmidt, Advanced Mechanics of Materials, 6th edition, Wiley, New York, 2002.
[4] Introduction, Unified Theory of Concrete Structures, John Wiley & Sons, Ltd, 2010, pp. 1–21, https://doi.org/10.1002/9780470688892.ch1.
[5] N. Gehri, J. Mata-Falcón, W. Kaufmann, Automated crack detection and measurement based on digital image correlation, Constr. Build. Mater. 256 (2020), 119383, https://doi.org/10.1016/j.conbuildmat.2020.119383.
[6] B. Shan, S. Zheng, J. Ou, A stereovision-based crack width detection approach for concrete surface assessment, KSCE J. Civ. Eng. 20 (2016) 803–812, https://doi.org/10.1007/s12205-015-0461-6.
[7] W. Wang, A. Zhang, K.C.P. Wang, A.F. Braham, S. Qiu, Pavement crack width measurement based on Laplace's equation for continuity and unambiguity,

Comput. Aid. Civ. Infrastruct. Eng. 33 (2018) 110–123, https://doi.org/10.1111/mice.12319.
[8] A. Mohan, S. Poobal, Crack detection using image processing: a critical review and analysis, Alexandria Eng. J. 57 (2) (2018) 787–798, https://doi.org/10.1016/j.aej.2017.01.020.
[9] Y.S. Yang, C.L. Wu, T.T.C. Hsu, H.C. Yang, H.J. Lu, Image analysis method for crack distribution and width estimation for reinforced concrete structures, Autom. Constr. 91 (2018) 120–132.
[10] F.T. Ni, J. Zhang, Z.Q. Chen, Zernike-moment measurement of thin-crack width in images enabled by dual-scale deep learning, Comput. Aided Civil Infrastruct. Eng. 34 (2019) 367–384, https://doi.org/10.1111/mice.12421.
[11] C. Shao, L. Zhang, W. Pan, PTZ camera-based image processing for automatic crack size measurement in expressways, IEEE Sensors J. 21 (2021) 23352–23361, https://doi.org/10.1109/JSEN.2021.3112005.
[12] H. Kim, J. Lee, E. Ahn, S. Cho, M. Shin, S.-H. Sim, Concrete crack identification using a UAV incorporating hybrid image processing, Sensors 17 (2017) 2052, https://doi.org/10.3390/s17092052.
[13] J. Valença, I. Puente, E. Júlio, H. González-Jorge, P. Arias-Sánchez, Assessment of cracks on concrete bridges using image processing supported by laser scanning survey, Constr. Build. Mater. 146 (2017) 668–678, https://doi.org/10.1016/j.conbuildmat.2017.04.096.
[14] M. Lei, L. Liu, C. Shi, Y. Tan, Y. Lin, W. Wang, A novel tunnel-lining crack recognition system based on digital image technology, Tunn. Undergr. Space Technol. Inc. Trenchl. Technol. Res. 108 (2021), https://doi.org/10.1016/j.tust.2020.103724.
[15] T. Ni, R. Zhou, C. Gu, Y. Yang, Measurement of concrete crack feature with android smartphone APP based on digital image processing techniques, Measurement 150 (2020) 107093–107100, https://doi.org/10.1016/j.measurement.2019.107093.
[16] D. Choi, W. Bell, D. Kim, J. Kim, UAV-driven structural crack detection and location determination using convolutional neural networks, Sensors 21 (2021) 2650, https://doi.org/10.3390/s21082650.
[17] B. Lei, Y. Ren, N. Wang, L. Huo, G. Song, Design of a new low-cost unmanned aerial vehicle and vision-based concrete crack inspection method, Struct. Health Monit. 19 (2020) 1871–1883, https://doi.org/10.1177/1475921719898862.
[18] H. Wang, L. Zhai, H. Huang, L. Guan, M. Kenan, W. Guiping, Measurement for Cracks at the Bottom of Bridges based on Tethered Creeping Unmanned Aerial Vehicle, 2020, https://doi.org/10.1016/j.autcon.2020.103330.
[19] Y.-F. Liu, X. Nie, J.-S. Fan, X.-G. Liu, Image-based crack assessment of bridge piers using unmanned aerial vehicles and three-dimensional scene reconstruction, Comput. Aid. Civ. Infrastruct. Eng. 35 (2020) 511–529, https://doi.org/10.1111/mice.12501.
[20] E. Karaaslan, U. Bagci, F.N. Catbas, Artificial intelligence assisted infrastructure assessment using mixed reality systems, Transp. Res. Rec. 2673 (2019) 413–424, https://doi.org/10.1177/0361198119839988.
[21] S. Wang, S.A. Zargar, F.-G. Yuan, Augmented reality for enhanced visual inspection through knowledge-based deep learning, Struct. Health Monit. 20 (2021) 426–442, https://doi.org/10.1177/1475921720976986.
[22] G.M. Santi, A. Ceruti, A. Liverani, F. Osti, Augmented reality in industry 4.0 and future innovation programs, Technologies 9 (2021) 33, https://doi.org/10.3390/technologies9020033.
[23] J. Canny, A Computational Approach to Edge Detection. IEEE Transactions on Pattern Analysis and Machine Intelligence PAMI-8, 1986, pp. 679–698, https://doi.org/10.1109/TPAMI.1986.4767851.
[24] S. Gopinathan, S. Gayathri, A Study on image enhancement techniques using YCbCr color space methods, Int. J. Adv. Eng. Res. Sci. 3 (8) (2016) 105–112.
[25] S. Beeran Kutty, S. Saaidin, P.N.A. Megat Yunus, S. Abu Hassan, Evaluation of canny and sobel operator for logo edge detection, in: 2014 International Symposium on Technology Management and Emerging Technologies. Presented at the 2014 International Symposium on Technology Management and Emerging Technologies, 2014, pp. 153–156, https://doi.org/10.1109/ISTMET.2014.6936497.
[26] S.M. Abid Hasan, K. Ko, Depth edge detection by image-based smoothing and morphological operations, J. Comput. Des. Eng. 3 (2016) 191–197, https://doi.org/10.1016/j.jcde.2016.02.002.
[27] F. Moreu, K. Malek, Transportation Consortium of South-Central States (Tran-SET), Louisiana State University (Baton Rouge, La.). U.T.C. for R. 6, 2021. Bridge Cracks Monitoring: Detection, Measurement, and Comparison Using Augmented Reality (No. 20STUNM33), Transportation Consortium of South-Central States, 2021.
[28] M. Kuang, J. Zhu, Hover control of a thrust-vectoring aircraft, SCIENCE CHINA Inf. Sci. 58 (2015) 1–5, https://doi.org/10.1007/s11432-015-5353-3.
[29] D. Maharjan, M. Agüero, D. Mascarenas, R. Fierro, F. Moreu, Enabling human–infrastructure interfaces for inspection using augmented reality, Struct. Health Monit. 20 (2021) 1980–1996, https://doi.org/10.1177/1475921720977017.
[30] D.D. Mascareñas, J.P. Ballor, O.L. McClain, M.A. Mellor, C.-Y. Shen, B. Bleck, J. Morales, L.-M.R. Yeong, B. Narushof, P. Shelton, E. Martinez, Y. Yang, A. Cattaneo, T.A. Harden, F. Moreu, Augmented reality for next generation infrastructure inspections, Struct. Health Monit. 20 (2021) 1957–1979, https://doi.org/10.1177/1475921720953846.
[31] R. Mojidra, J. Li, A. Mohammadkhorasani, F. Moreu, W. Collins, C. Bennett, S. A. Taher, Vision-based inspection of out-of-plane fatigue cracks in steel structures, in: Sensors and Smart Structures Technologies for Civil, Mechanical, and Aerospace Systems 2022. Presented at the Sensors and Smart Structures Technologies for Civil, Mechanical, and Aerospace Systems 2022, SPIE, 2022, pp. 145–151, https://doi.org/10.1117/12.2613188.

DOI: 10.1111/mice.12652

ORIGINAL ARTICLE

COMPUTER-AIDED CIVIL AND INFRASTRUCTURE ENGINEERING WILEY

A methodology for measuring the total displacements of structures using a laser–camera system

Roya Nasimi | **Fernando Moreu**

Department of Civil, Construction and Environmental Engineering, University of New Mexico, Albuquerque, NM, USA

Correspondence
Fernando Moreu, Department of Civil, Construction and Environmental Engineering, University of New Mexico, 210 University Blvd. NE, MSC01 1070, Albuquerque, NM 87131, USA.
Email: fmoreu@unm.edu

Abstract

Railroad bridge inspection manuals recommend measuring bridge displacements under train crossing events. Traditional displacement measurement methods require humans climbing the infrastructure for sensor installation, which is unsafe. Therefore, bridge inspectors are interested in noncontact methods. The authors of this paper developed a methodology that measures the noncontact, reference-free total transverse displacement of structures using a laser and a camera. Total displacement refers to both dynamic and pseudostatic components of displacement. The developed method can be implemented with off-the-shelf hardware components that are lightweight, and simple enough, so researchers can build their own system and test it in the field. First, the paper presents the methodology and tests it with a 1 degree of freedom (DOF) estimation with neither rotation nor elevation change. Subsequently, authors developed a new algorithm combining both laser and camera under arbitrary 6 DOF motion. The results of this research support noncontact reference-free total displacement measurements of railroad bridges.

1 | INTRODUCTION

North American railroads move 40% of total freight across the country by weight (FRA, 2020a). Today, North American railroads carry longer trains, heavier cars, and faster loads than they were initially designed for (Peterson & Gutkowski, 1999). Railroad companies regularly inspect and upgrade their infrastructure to safely increase speed, loads, and revenues (FRA, 2020b). Throughout the years, railroads have adopted different ways to monitor their infrastructure and increased their performance and serviceability levels (FRA, 2020b). Railroad bridge engineers consider the change of transverse displacement of railroad bridges under trains to be an indication of abnormal structural performance and capacity. Displacement can be an index of the structure's performance and the data collected from field showed that transverse displacement of old tresstle railroad bridges can reach 41.3 mm (Moreu et al., 2015; Robertson, 2005).

In recent decades, railroads have measured bridge transverse displacements under train crossing events with sensors. Personnel must climb the bridge and install the sensors to the bridge element, which is not safe. Furthermore, linear variable differential transformers (LVDTs) require the installation of scaffolds next to the bridge (Moreu et al., 2015) that may not be possible in some inaccessible locations. Wide range of sensors have been used by the experts in structural health monitoring (SHM) to inspect and assess structures remotely. For example, researchers used wireless smart sensors (WSS) or other sensors such as strain sensors' networks (Oh, Kim, Kim, Park, & Adeli, 2017). Amezquita-Sanchez, Valtierra-Rodriguez, and Adeli (2018) reviewed the recent advances in this field. Alternatively, researchers use accelerometers to measure

reference-free displacement of bridges (Hester, Brownjohn, Bocian, & Xu, 2017; Sekiya, Kimura, & Miki, 2016). However, the installation of accelerometers and wireless sensors needs mobilization in the site, and climbing the bridge for installation. Railroads are interested in new noncontact reference-free methods to measure the displacements.

To measure noncontact reference-free displacements from bridges or conducting a noncontact SHM, researchers have used digital cameras and lasers. As an example, cameras have been used by some researchers to obtain influence lines and estimate the weight of the vehicles crossing over the bridges. Ojio, Carey, OBrien, Doherty, and Taylor (2016) used one camera to monitor the traffic and another camera to find vertical deflection of a bridge. In robotics field, vehicle positioning is an important task for obstacle avoidance or autonomous navigation of the robot. They use several sensors depending on their application and objectives. Using Global Positioning System (GPS), Differential Global Positioning System (DGPS), inertial measurement units (IMU), and LiDAR, mono or stereo cameras for ego-motion are among the most preferred options. GPS is most common tool for positioning, but its precision can be within the range of meters. With invention of the DGPS, the accuracy of GPS improved to be within a few centimeters at its best and is not suitable for SHM. Beside accuracy issues, they cannot be used at all locations and DGPS suffers from signal outage, jamming, multipath effects (Aqel, Marhaban, Saripan, & Ismail, 2016; Jo, Sim, Tatkowski, Spencer, & Nelson, 2013; Maklouf & Adwaib, 2014). Inertial navigation systems (INS), IMU, and gyroscopes are other solutions to navigate the device of interest. They measure the relative position of the device from its starting point. However, the measurement error accumulates over time due to axis misalignment. Additionally, inertial sensors get affected by external magnetic fields. Finally, IMUs are different in grade and quality, and accurate models are expensive (Kok, Hol, & Schön, 2017; Woodman, 2007; Wang, Liang, Zhu, & Zhang, 2014). But IMUs can be used as a supplement sensor with other systems to improve their accuracy. Visual odometry (VO) using a monocular and stereo camera is another solution for navigation in robotics and they are also adopted by civil engineers for SHM purposes. Stereo cameras provide higher precision but have limitations including, but not limited to: additional calibration efforts and errors; limited baseline; volume/size; interface challenges; and higher costs when compared with monocular or consumer-grade cameras. In summary, stereo cameras are not an ideal option for commercial uses (Kitt et al., 2011; Sünderhauf & Protzel, 2007). Aqel et al. (2016) did a review of VO methods and discussed their advantages and disadvantages. Feature-based and appearance-based methods are used to find ego-motion. When the surface is textureless, for downward facing cameras, appearance-based methods such as template matching can be useful. However, density-based method can be noisy and get affected by the shadow or environment dynamics (Dille, Grocholsky, & Singh, 2010). Using an artificial target as a checkerboard enables a feature-based motion tracking with a limited number of data points and deals with the challenge of scale factor estimation in monocular VO methods by providing an even and solid surface (Kitt et al., 2011). Murray, Take, and Hoult (2015) used digital image correlation (DIC) to find the vertical and longitudinal absolute displacement of rails with two different subgrade conditions. Peddle, Goudreau, Carlson, and Santini-Bell (2011) used DIC to find the response of bridges with two field tests and validated their DIC results with LVDT measurements. There are several camera models transferring information from 3D world coordinates to 2D image coordinates and vice versa. The pinhole camera model (Sturm, 2014) is one well-known model to find the position of the camera. Xu and Brownjohn (2018) did a review on the vision-based methods for displacement measurements. They introduced the overall procedure, the various methods to go through the procedure, and the advantages or disadvantages of each method. Park, Park, Kim, and Adeli (2015) used multiple cameras and created a motion capture system (MCS) to obtain the accurate 3D displacement of certain markers on a structure. Alternatively, lasers have been one of the useful tools for structural displacement measurements. Zhao et al. (2015) developed a sensor system using a laser light to measure the displacement of a bridge accurately and quickly. They attached a laser to the structure to be monitored. The laser light was projected on a fixed board. They estimated the structure's displacement analyzing the images of the movement of laser on the projection board. Even though these are all noncontact methods, they still need some degree of access to the bridges and structures they measure. Park, Lee, Adeli, and Lee (2007) have used terrestrial laser scanner (TLS) with their displacement measurement model to collect the high-accuracy displacement of a steel beam in a laboratory. Additionally, Truong-Hong and Laefer (2014) used TLS to find bridges' vertical displacement under terrific load. LiDAR is a laser-based sensor. They are popular for their accuracy. However, their data set is very large and analyzing and interpreting can be challenging. LiDARs are useful to collect data in a large scale but for normal scale applications, VO is a cost-efficient solution (Fraundorfer & Scaramuzza, 2012). Moreover, Greenwood, Lynch, and Zekkos (2019) compared the use of cameras versus LiDAR on unmanned aerial systems (UAS). They mentioned that using LiDAR on a UAS requires knowing the position of the scanner that makes it challenging and cameras have the privilege of lighter weight compared to LiDAR

sensors. Finally, LiDAR sensors on UAS require immense data processing (Brooks et al., 2015; Hirose et al., 2015); therefore, single beam lasers become a good candidate for local monitoring. Radars are a well-established remote sensing system in several fields such as military, oceanography, and surveillance. However, their feasibility, efficiency, and use for civil engineering applications need further investigation. With emerging of commercial radar sensors, they have been used in more fields such as civil engineering. Researchers in SHM have used radars to monitor small displacement of bridges (Gentile, 2010; Rice, Li, Gu, & Hernandez, 2011). However, they used radar on a tripod. Other drawbacks of commercial radars are that they can be unreliable, require extensive signal processing, and they detect multiple targets that may require use of imaging radars that are expensive and heavy (Javadi & Farina, 2020; Pieraccini, 2013; Rice et al., 2011).

Researchers have used UAS to do vision-based assessment of bridges using images from camera (Liu, Nie, Fan, & Liu, 2020; Zhang & Elaksher, 2012). Chan, Guan, Jo, and Blumenstein (2015) discussed the benefits and challenges of UAS for vision-based bridge inspections. Additionally, Greenwood et al. (2019) prepared a review of the application of UAS for civil engineering infrastructure, describing several UAS technologies, sensors, and data acquisition systems. Yeum and Dyke (2015) did a vision-based inspection of a bridge using UAS to detect the cracks near the steel bolts. However, these methods were not intended to collect noncontact reference-free dynamic displacements.

Research teams have combined UAS with computer vision methods to find displacements of bridges and structures. A research reported the accuracy of three different types of displacement estimation of a mock-up bridge using a camera installed on a UAS (Jalinoos, Amjadian, Agrawal, Brooks, & Banach, 2020). They measured the change of location of certain points of the bridge after a hazard, in comparison with their original position. They estimated the translation and rotation with a fixed ground-based camera and the settlement with the UAS camera. Khuc, Nguyen, Dao, and Catbas (2020) used a UAS along with a computer vision method to estimate the displacement of a bridge. Yoon, Shin, and Spencer (2018) used a UAS and a camera in a laboratory setting to find absolute vertical displacements. Investigators used UAS along with cameras for SHM and vibration monitoring of wind turbines (Khadka, Fick, Afshar, Tavakoli, & Baqersad, 2020). For their work they used a stereo camera and accelerometers to determine the vibration and the mode shapes of the rotating blades of a wind turbine. However, all these methods focused on displacement algorithms collecting planar displacement with respect to the vision center and did not intend to measure transverse displacements of structures or bridges. In order to address this concern, Garg, Moreu, Ozdagli, Taha, and Mascareñas (2019) measured the dynamic transverse displacement of a bridge using a laser Doppler vibrometer (LDV). However, their method was not able to measure the total dynamic displacement caused by the hovering of the UAS and it is limited to dynamic transverse displacements. In addition, the LDV was expensive, heavy, and needed an additional module for operation that made it even heavier and was space demanding on UAS. In summary, as of today there is not a noncontact reference-free method to measure total transverse displacements.

This paper develops the design and validation of a new measurement methodology using a laser and a camera toward noncontact reference-free total transverse displacement that can be collected by a UAS in the field. This method uses a ground-based reference instead of any access or reference point on structure itself, which is a requirement in most of the methods. This paper describes the integration of both laser and computer vision to enable the estimation of the total dynamic transverse displacement. First, we describe the integration of both signals with a simple 1 degree of freedom (DOF) test enabling out of plane measurement of a mock-up railroad bridge pier cap. Initially, we used a pixel-based rotation-free method. In this test, laser and camera were sliding on a horizontal rail in both directions. The laser measured the perpendicular distance to the moving surface while the camera measured its own displacement with a simple pixel-based motion estimation approach. Results were validated against a fixed LVDT that was employed as ground truth. Secondly, the authors of this paper adopted the pinhole algorithm for camera displacement estimation considering rotation and out of plane movements of the camera, to enable precise displacement estimation in the field. Finally, we developed a new algorithm to account for laser–camera rotation and laser angle correction. The absolute dynamic transverse displacement was obtained calculating the relative displacement between the mock-up bridge pier cap displacement and a simulated drone motion. The novelty of this work resides in combining both laser and camera to obtain the total noncontact reference-free transverse displacement of structures that is original and does not exist to date. In the existing literature, researchers have used computer vision to obtain displacement from moving cameras (Yoon et al., 2018). However, they enable the determination of the two displacement components of structures that are parallel to the image plane. There is a shortage in the literature determining the out of plane displacement using computer vision in a noncontact way. Alternatively, lasers have been used to monitor the total displacement of structures, but they have been installed on a fixed location. In the past, researchers used lasers to obtain out of plane displacement

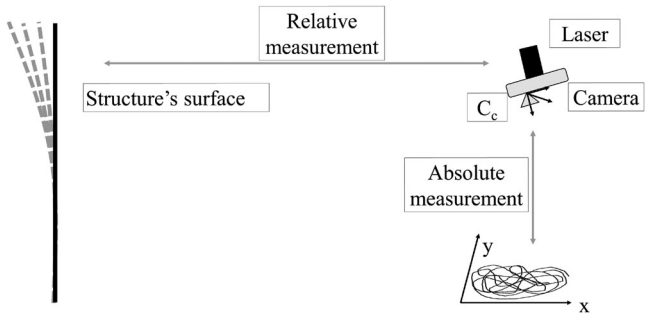

FIGURE 1 Total displacement estimation using laser and camera

of structures from a moving UAS, but because of the UAS's movement, they can only estimate the dynamic displacement of the structure, not the total displacement (Garg et al., 2019). There is no research theory or results today combining and integrating camera and laser together on a reference-free motion to obtain total noncontact transverse displacement of structures.

2 | METHODOLOGY

2.1 | Total displacement estimation using laser and camera

Figure 1 shows the proposed methodology, consisting of integrating measurements from two different sensing systems: a laser and a camera. Axes X and Y represent the projection of the two directions of the movement of the system motion relative to the ground or floor target. X is the axis of interest, transverse direction, perpendicular to Y axis, which is the direction of the rail. The authors of this paper propose using a laser to measure out of plane displacements, with an emphasis on total dynamics transverse displacements. Traditionally, long-range, high-profile lasers can measure displacements from a tripod in the vicinity of the structure, but the tripod installation is costly and sometimes not physically possible. If the laser could be attached to a UAS and hover next to the structure, affordable noncontact reference-free displacements would be enabled. However, the UAS hovering induces motion in 6 DOF altering the laser displacement measurement. The laser measures the relative displacement from the surface of interest. The camera attached to the laser can estimate the absolute movements of the laser. To determine the absolute total transverse displacement of the surface of interest, the translational and rotational motions detected by the camera are subtracted from the relative displacement measured by the laser. The total dynamic and pseudostatic transverse displacement of the structure can be obtained subtracting the calculated displacement of the camera in the direction of interest from the laser measurement.

2.2 | Movement measurement

Multiple UAS flights were conducted in the Multi-Agent, Robotics, and Heterogenous Systems Laboratory at the University of New Mexico (MARHES, 2020). The goal of these experiments was twofold: to cost-effectively select the laser range of interest based on the drone's hovering; and to know the range of translation and rotation that can be induced in a flight for algorithm development. Several tests were conducted with Intel AERO ready to fly drone (Intel, 2020), and the translation and rotation data were recorded using a Vicon MX system. The Vicon MX system includes eight MX-T10 cameras installed in a frame for high-precision 6 DOF motion tracking. The drone's hovering was generally measured under ± 50 cm and ± 5 degrees in translation and rotation, respectively. Authors selected their hardware and designed their algorithm and validation using this data.

2.3 | Hardware

The authors of this paper used the translation and rotation ranges obtained from the laboratory flights to select their hardware. Considering their weight, simplicity, and price lasers were a good option among other several sensor options. The research team used a Keyence IL-600 laser, with reference point and range of 600 and 800 mm, respectively, and 0.1 mm accuracy. Considering the range and the laser output voltage of ± 5, the sensitivity is 12.5 mV/mm. The laser data were collected with a sampling rate of 1,024 Hz. We used an APAMAN A100 action camera, with 4K resolution (2,160 $\times$ 3,840 pixels), and with a sampling rate of 30 fps.

2.4 | Research methodology

First, we developed and tested the total displacement estimation using laser and camera in a simple horizontal platform in order to validate the method with 1 DOF assumptions. Second, the algorithm to find the ego motion or camera motion was developed and validated using Vicon cameras, as well as the determination of the angle during flight for laser correction. Finally, the algorithm to find the noncontact reference-free total dynamic transverse displacement of a structure under loading was tested and validated. For validation purposes, the research team compared

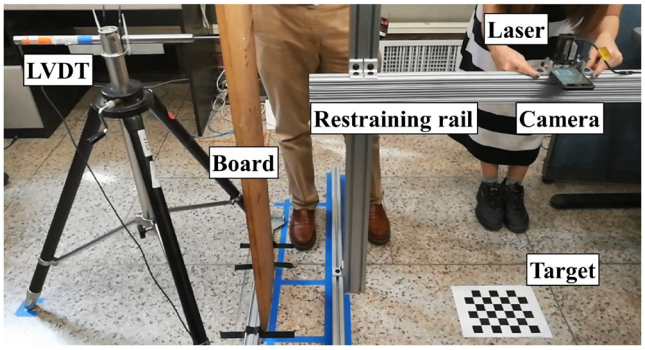

FIGURE 2 1 DOF laboratory rail test setup and instrumentation

displacement estimations with ground truth references using four indices: peak error (E1), peak error percentage (E2), root mean square error (E3), and root mean square error percentage (E4), expressed in Equations (1)–(4):

$$E_1 = \max(|\ \Delta_{est}(i) - \Delta_{meas}(i)\ |) \tag{1}$$

$$E_2 = \frac{E_1}{\max(|\ \Delta_{meas}(i)\ |)} \times 100 \tag{2}$$

$$E_3 = \sqrt{\frac{\sum_{i=1}^{N}(\Delta_{est}(i) - \Delta_{meas}(i))^2}{N}} \tag{3}$$

$$E_4 = \frac{E_3}{\max(|\ \Delta_{meas}(i)\ |)} \times 100, \tag{4}$$

where i is each time step, $\Delta_{est}(i)$ is the displacement value estimated by the proposed method, $\Delta_{meas}(i)$ is the displacement value measured by the reference sensor, and N is the total number of data points.

2.5 | Preliminary validation: 1 DOF

The laser–camera integration methodology was tested first moving both laser and camera in a 1 DOF rail test with no rotation or elevation change (Figure 2). During the experiments, one engineering student moved the laser and camera back and forth, while the structure moved similar to a railroad bridge crossing event, with both dynamic and pseudostatic displacements. In this test, the structure's motion was estimated subtracting the 1 DOF motion estimated by the camera from the laser data. For these experiments, the target was a checkerboard of 30 mm. The research team filmed the checkerboard target to estimate the movement of the camera using a pixel-based approach. First, the pixel values of the four checkerboard corners were obtained in every frame of the video. Second, the displacement of the camera was calculated in a pixel scale. Finally, the pixel measurements were converted to real-world motion using a scale factor in (mm/pixel). The scale factor of each frame was calculated from the known pattern size and its corresponding pixel numbers per pattern.

TABLE 1 Calculated performance indices for rail tests

Index	E_1	E_2	E_3	E_4
Test 1	3.0 mm	16.1%	1.2 mm	6.3%
Test 2	4.7 mm	23.4%	1.9 mm	9.8%

Figure 3 summarizes the results from one of the two experiments conducted to validate the methodology. There were three seconds of no movement followed by motions of both the laser (Figure 3a) and the camera (Figure 3b) with 2.5 cycles of approximately 60 mm and 0.5 Hz amplitude and frequency, respectively (Moreu et al., 2015). The board representing a railroad bridge pile moving transversally under two train cars started the motion after one cycle of the laser movement. As expected, both the laser signal and the camera estimation are identical before the board started the motion. After the second cycle of laser and camera motion, the board starts its motion under the first car crossing approximately at $t = 6$ s, and the laser's signal suddenly changes, whereas the camera continues measuring the absolute movement of both laser and camera. Similarly, the laser captures a sudden change at $t = 10$ s corresponding to the last movement of the board mimicking the last axle of the railroad car crossing the bridge. Figure 3c shows the noncontact board displacement estimation subtracting the camera displacement estimation from the laser measurement and the LVDT displacement measurement. For this validation, Table 1 summarizes the performance indices calculated for two experiments. The results show that this methodology is able to capture the peak displacement in 1 DOF with a peak error under 4 mm and 20%. Both RMS errors are under 2 mm and 10%. Railroad managers are interested in accuracy in the range of mm (Garg et al., 2019), so enabling noncontact reference-free measurement within these errors is a reasonable preliminary validation to advance this research toward total implementation. In practice, the laser and the camera on a UAS is expected to experience a 6 DOF motion. Both translation and rotation imposed on the camera can cause a change in the scale factor and affect the estimation of the pixel-based approach, providing incorrect values. Additionally, there is an error induced in the laser signal due to the laser rotation during the UAS hovering that is also ignored with the 1 DOF estimation approach. In order to develop a methodology that enables the use of laser–camera system on a UAS

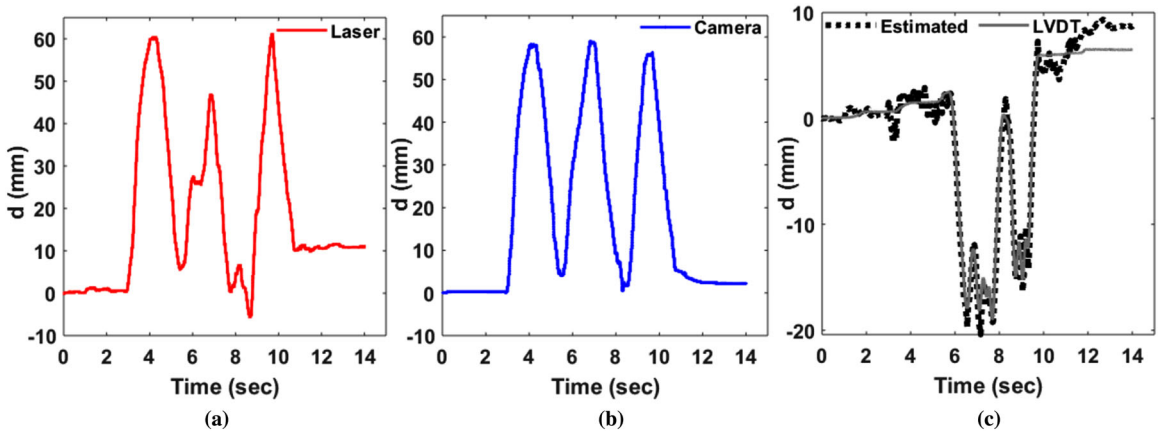

FIGURE 3 1 DOF total displacement estimation using laser and camera: (a) laser measurement, (b) camera displacement estimation, and (c) total displacement estimation and LVDT displacement measurement

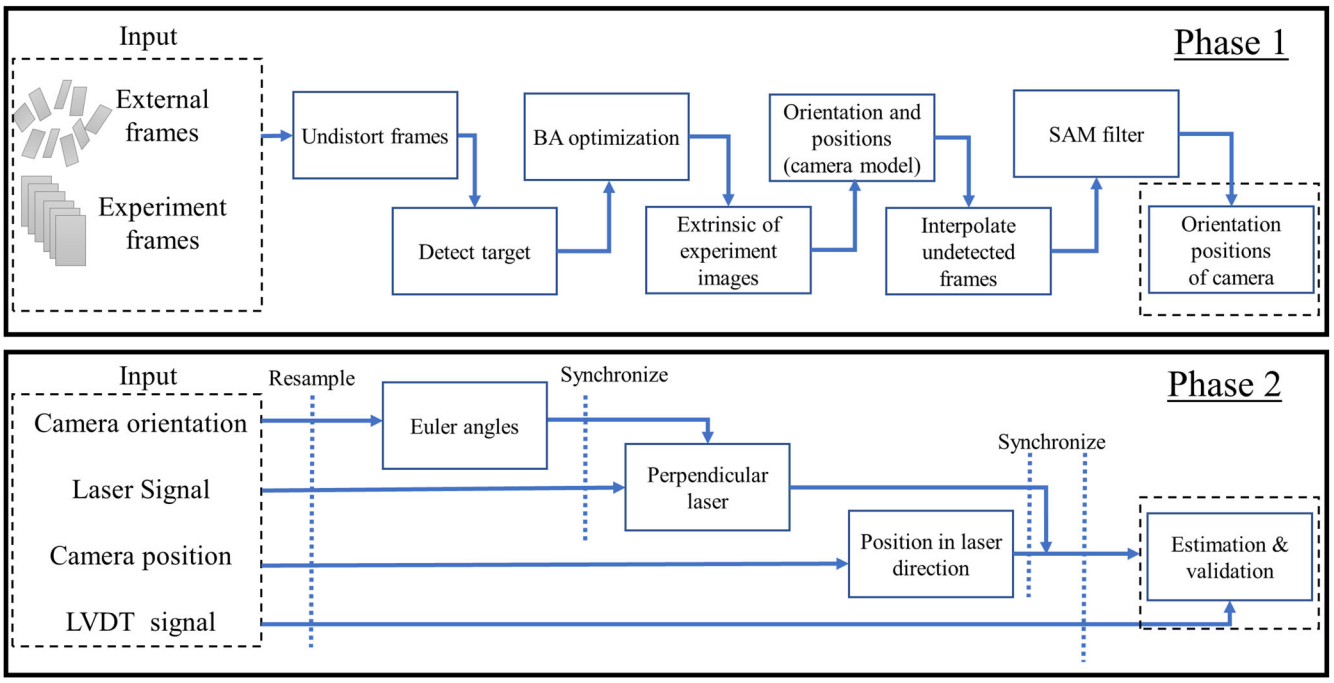

FIGURE 4 Laser–camera combination to measure noncontact, reference-free total dynamic transverse displacements

with 6 DOF motion, we developed an algorithm with a two-phase approach that provides a robust estimation of noncontact reference-free total displacement of structures.

3 | LASER–CAMERA SYSTEM UNDER ARBITRARY MOTION

Figure 4 separates the combination of the laser camera in Phase 1 and Phase 2. Phase 1 obtains the orientation and position of the camera. Phase 2 corrects the laser's angle and combines the laser and the camera data to measure noncontact, reference-free total dynamic transverse displacement of structures. The following sections describe both phases and their respective laboratory validation.

3.1 | Phase 1

3.1.1 | Pinhole camera model for 6 DOF motion estimation

The pinhole camera model describes the theory of perspective projection and maps the 3D world coordinate to 2D image coordinate (Figure 5). The algorithm is developed,

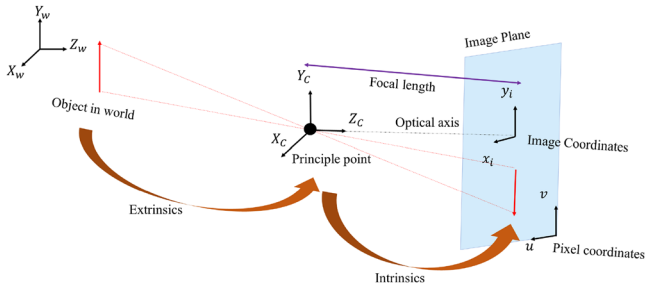

FIGURE 5 Pinhole camera model

assuming that the camera is a pinhole camera with a closed box and an extremely small hole on it and without the lens that normal cameras have. This point is considered as optical center (Sturm, 2014).

The 3D camera position is obtained using the pinhole camera algorithm, defined in Equation (5):

$$w\begin{bmatrix}x & y & 1\end{bmatrix} = \begin{bmatrix}X & Y & Z & 1\end{bmatrix} \times \begin{bmatrix}R\\ t\end{bmatrix} K \tag{5}$$

where w is the scale factor; x, y are the undistorted image points; X, Y, and Z are the world points; R and t are the rotation matrix and translation vector for each frame, respectively, which form the extrinsic matrix; and K is the intrinsic matrix that is a camera lens parameter and is constant for a camera. Camera calibration or camera resectioning is the act of finding pinhole camera intrinsic and extrinsic parameters by a video or images from the camera.

A camera calibration is required prior to the pinhole camera algorithm. For getting accurate results, several external reference frames are taken with considerable translation and rotations with regard to the target. These frames are used during the video process to conduct a joint optimization to minimize the reprojection error. This procedure of combining calibration and measuring frames together for increased accuracy is known as bundle adjustment. These external frames improve the accuracy and they act like additional eyes to create stereo effect and refine the estimation of the camera positions. Bundle adjustment minimizes the reprojection error by minimizing the Euclidean distance between the 3D ith point's projection into the jth frame and the point detected in the jth frame as given in Equation (6):

$$\sum_{i=1}^{n}\sum_{j=1}^{m} b_{ij}(D_{ij} - f(p_{ij}))^2 \tag{6}$$

where i represents the point number and j represents the frame number, $b_i j$ is a binary number and gets the value of 1 when the point i is visible in frame j and 0 when not visible, $D_i j$ represents the predicted or detected ith point in jth frame and $f(p_i j)$ represents the 3D projection of the ith point in jth frame (Furukawa & Ponce, 2009).

The pinhole camera model neglects some aspects of real cameras. Therefore, other models accompany the pinhole camera model to compensate the effect of those assumptions. First, in order to have a wide range of view, camera lenses have distortion effect. Tangential or geometric distortion occurs when the lens is not physically aligned parallel to the image plane. Usually geometric distortion does not exist in normal cameras; therefore, its coefficients are zero. On the other hand, radial distortion causes the rays to bend more in edges of the image and it becomes more severe when the lens is smaller

The research team of this project selected the division model proposed by Fitzgibbon (2001) for removing the camera distortions as defined in Equations (7)–(9):

$$x_u = \frac{x_d}{(1 + K_1 \times r_d^2 + K_2 \times r_d^4 + K_3 \times r_d^6)} \tag{7}$$

$$y_u = \frac{y_d}{(1 + K_1 \times r_d^2 + K_2 \times r_d^4 + K_3 \times r_d^6)} \tag{8}$$

$$r_d^2 = x_d^2 + y_d^2 \tag{9}$$

where x_u and y_u are the undistorted points; x_d and y_d are the distorted points; K_1, K_2, and K_3 are lens distortion coefficients obtained in calibration; and r_d is the Euclidean distance of the distorted point to the distortion center.

The pinhole camera model determines the camera positions for the experiment frames; however, some frames are lost in the process that need to be detected and located in the time domain. The proposed algorithm can interpolate between data points before and after each lost frame to have a continuous position estimation. The displacement and angle signals obtained from the camera were smoothened using a simple moving average (SMA) filter. The SMA filter proposes to remove the inaccuracies and noise of frame scale in the estimation not associated with the motion. This SMA filter relies on the knowledge of the dominant motion being monitored (Ozdagli, Gomez, & Moreu, 2017; Ozdagli, Liu, & Moreu, 2018). The SMA filter leads to a shift in the x axis of the signal, so both signals need to be synchronized for a second time. The characteristics of this SMA filter are shown in Equation (10):

$$y(i) = \frac{1}{N}\sum_{j=0}^{N-1} x(i+j) \tag{10}$$

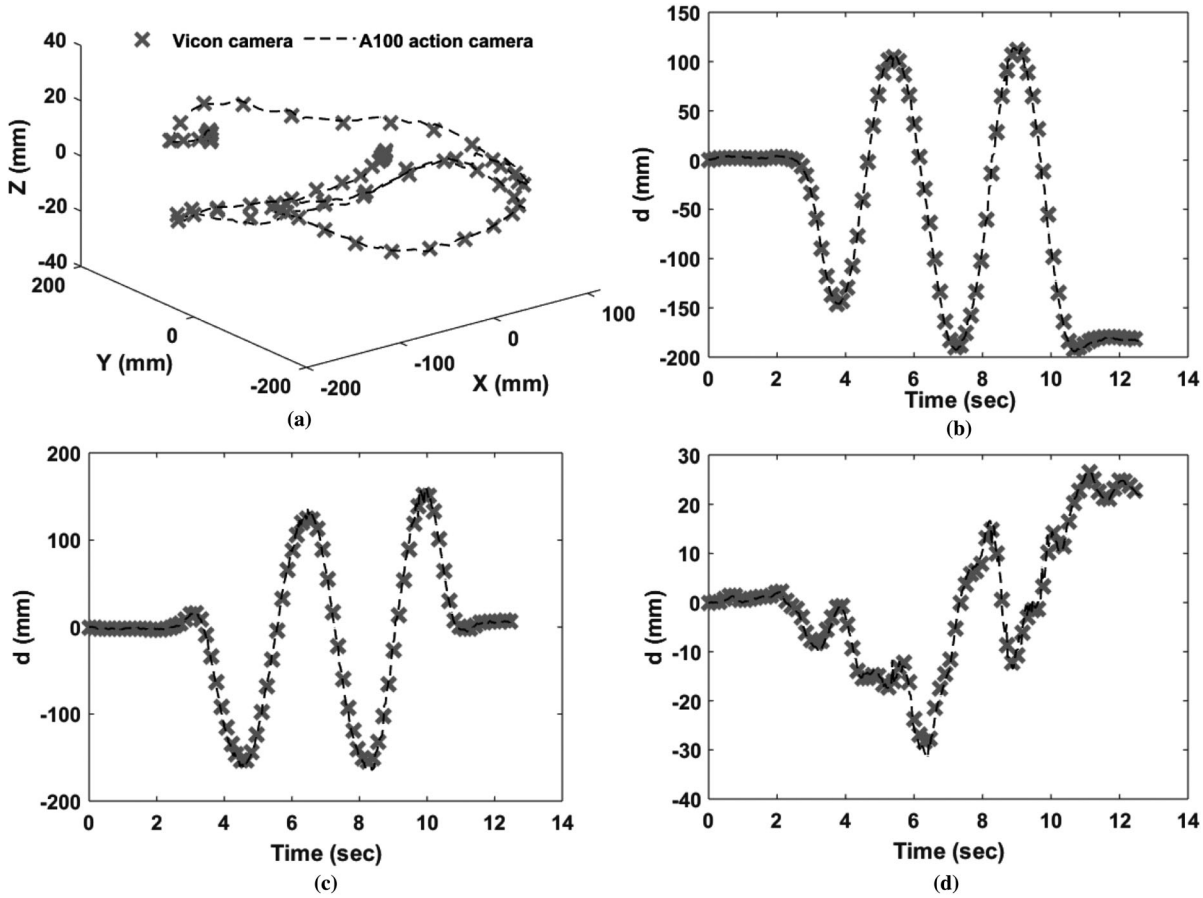

FIGURE 6 Displacement comparison between algorithm's estimation and VICON cameras' measurements: (a) 3D space view, (b) *X* direction, (c) *Y* direction, and (d) *Z* direction

where y is the filtered data, x is the unfiltered data, i is each time step, and N is the number of data points in the window size.

The output of Phase 1 is the continuous orientation and position of the camera that is validated in the next section using high-accuracy cameras.

3.1.2 | Camera motion validation

The authors of this paper evaluated the accuracy of the pinhole camera model for a 6 DOF motion estimation in an indoor laboratory in the UNM-AFRL Agile Manufacturing Laboratory (AgMan, 2020). AgMan is equipped with 16 Vicon Vantage V8 cameras. Each Vicon Vantage V8 has a custom 8 Megapixel sensor at 260 fps at full frame. The 16 Vicon V8 cameras are installed in the structural truss form of the Vicon system. The Vicon system is equipped to capture the 6 DOF motion of 14 mm pearls with high accuracy. In this experiment, three 14 mm pearls were attached to the moving camera for motion tracking using the Vicon system. The experiment of this section was conducted with a rate of 100 fps.

TABLE 2 Performance indices

Direction	E_1	E_2	E_3	E_4
X	16.3 mm	8.4%	2.9 mm	1.5%
Y	16.6 mm	10.7%	3.9 mm	2.5%
Z	3.1 mm	10.9%	1.0 mm	3.6%

The camera was moved in an arbitrary way in the laboratory space. The rotations and translations imposed on the camera were held within the ranges measured from the UAS flight and were estimated using the pinhole camera model algorithm. Figure 6 shows both measured and calculated displacements in the 3D space. Figure 6 shows that there is a good match between the estimated and measured positions in the three axes. To quantify the accuracy of the algorithm performance, indices are calculated. Displacement estimation of the camera and Vicon system is compared in each of the three directions, and the error indices are calculated for each direction. Table 2 summarizes the

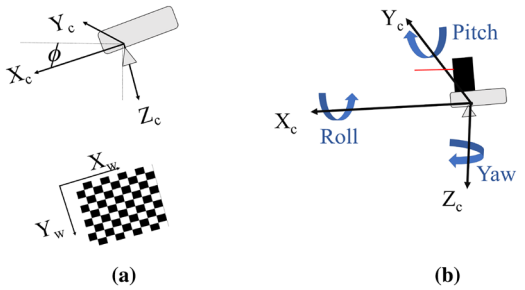

FIGURE 7 Coordinate systems for laser correction: (a) camera coordinate and world coordinate and (b) three laser rotations relative to three camera axes

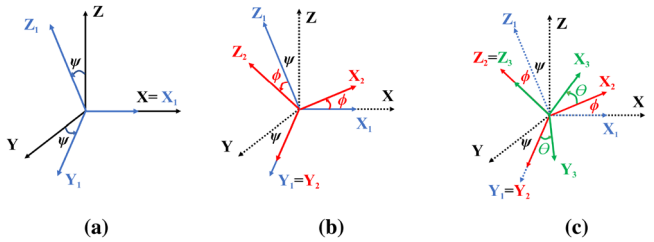

FIGURE 8 Rotation of coordinate systems with sequence of *XYZ*: (a) first global coordinate rotation about *X* axis, (b) second global coordinate rotation about *Y* axis, and (c) third global coordinate rotation about *Z* axis

three peak and RMS errors in mm and percentage. Peak errors in *X*, *Y*, and *Z* direction are 16.3 mm (8.4%), 16.6 mm (10.7%), and 3.1 mm (10.9%), respectively. RMS errors in *X*, *Y*, and *Z* direction are 2.9 mm (1.5%), 3.9 mm (2.5%), and 1 mm (3.6%), respectively. As we used a fixed ground-based target, the *X*, *Y*, and *Z* coordinates of the camera represent the location of the laser–camera system with regard to the ground reference. The peak estimation errors of the three axes are under 17 mm and 11% and the RMS estimation errors are under 4 mm and 4% error. These errors are reasonable for noncontact reference-free total displacement estimation.

3.2 | Phase 2

3.2.1 | Laser angle correction

Laser measurements provide the relative displacement between the drone and the structure, but when the laser is mounted on a drone, the measured signal contains an error induced by the drone's hovering. The laser movement has two components: translation and rotation. Using the camera displacement estimation method, the laser's translational displacement can be measured. The laser rotation induces an error in the estimation of the displacement that needs to be modified. To calculate the transverse movement of the structure of interest, researchers used the rotation matrices calculated for each camera frame. Figure 7 shows the coordinate systems used for the laser correction using the camera angles. Figure 7a shows the camera coordinate systems (X_c, Y_c, Z_c) relative to the world coordinate (X_w, Y_w). In this research, the objective is to estimate the movement of the camera in the *X* direction, which is in the direction of transverse displacement of the structure of interest. Figure 7b shows the coordinate systems and the rotation angles of the laser attached to the camera. Large pitch and yaw angles can lead to an increased laser signal in the *X* direction, which will result in inaccurate displacement estimations.

The algorithm determined the Euler angles using the rotation matrices of the camera extrinsic. The rotation angles about each axis can be found using the total rotation matrices of the camera frames. The total rotation matrices are determined considering an *XYZ* rotation sequence between frames. This means that the algorithm assumes that the frame is sequentially exposed to rotation about X_c, Y_c, and Z_c axes (Figures 8a, 8b, and 8c), respectively. ψ, ϕ, and θ are the rotation angles about X_c axis (roll), Y_c axis (pitch), and Z_c axis (yaw), respectively.

Researchers obtained the rotation matrices of the laser by synchronizing and resampling the measurements from both camera and laser. Equations (11), (12), and (13) show the rotation matrices when the coordinate systems rotate about *X*, *Y*, or *Z* axes, respectively. To calculate the total rotation matrix of each frame during the experiments with sequence of XYZ, the three matrices are combined. Equation (14) shows the total rotation matrix with three sequential rotations that enables the calculation of the three angles ψ, ϕ, and θ about *X*, *Y*, and *Z* axes, respectively.

$$R_{x,\psi} = \begin{bmatrix} 1 & 0 & 0 \\ 0 & \cos\psi & -\sin\psi \\ 0 & \sin\psi & \cos\psi \end{bmatrix} \tag{11}$$

$$R_{y,\phi} = \begin{bmatrix} \cos\phi & 0 & \sin\phi \\ 0 & 1 & 0 \\ -\sin\phi & 0 & \cos\phi \end{bmatrix} \tag{12}$$

$$R_{z,\theta} = \begin{bmatrix} \cos\theta & -\sin\theta & 0 \\ \sin\theta & \cos\theta & 0 \\ 0 & 0 & 1 \end{bmatrix} \tag{13}$$

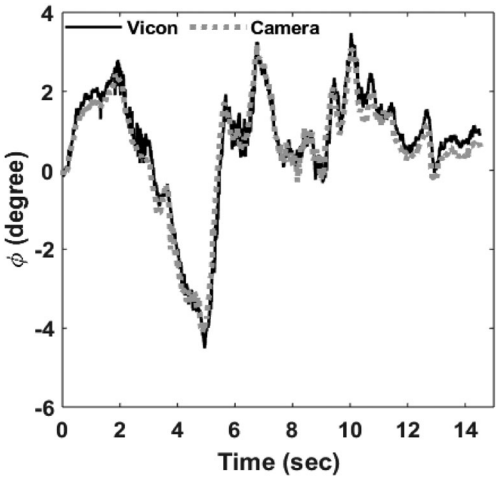

FIGURE 9 Rotation angle measured by Vicon system and estimation about camera's *Y* axis (pitch)

$$Rotation\,Matrix = R_{x,\psi} \times R_{y,\phi} \times R_{z,\theta} = \begin{bmatrix} \cos\phi\cos\theta & -\cos\phi\sin\theta & \sin\phi \\ \cos\psi\sin\theta + \sin\psi\sin\phi\cos\theta & \cos\psi\cos\theta - \sin\psi\sin\phi\sin\theta & -\sin\psi\cos\phi \\ \sin\psi\sin\theta - \cos\psi\sin\phi\cos\theta & \sin\psi\cos\theta + \cos\psi\sin\phi\sin\theta & \cos\psi\cos\theta \end{bmatrix}. \quad (14)$$

The research team estimated the three angles ψ, ϕ, and θ from the experiment conducted in the AgMan laboratory and compared them to the values obtained using the Vicon system. Figure 9 shows ϕ estimations and Vicon camera measurements. The angle estimations match well in phase and amplitude. Specifically, ϕ peak and RMS error are 1.4 and 0.3 degrees, respectively. This method is able to estimate the ϕ variation of the moving laser with high accuracy. Researchers estimated the ψ angle and also obtained a good match when compared with the Vicon camera data, but the result of ψ angle was not of interest as the roll angle has no effect in laser transverse displacement estimation. Finally, this methodology also estimated the θ angle and found Euler angle inaccuracies in the estimation. As a result, authors concluded that the Euler angle method is unable to estimate components that are not in the direction of gravity. Therefore, the results of this research recommend using a magnetometer or an additional accelerometer for field applications, to find the angle in nongravity direction.

3.2.2 | Laser motion compensation

We used the estimation of the angle and displacement to compensate the laser's 6 DOF motion. Once the laser signal was corrected, we calculated the total dynamic transverse displacement using laser and computer vision. To synchronize the laser and the camera, authors of this paper selected an event of reference in the time domain.

In general, this method proposes using the time history of both ϕ (pitch) and θ (yaw) angles to obtain the displacement perpendicular to the moving structures, and neglects the effect of ψ (roll), using Equation (15):

$$L_u = L \times \cos\phi \times \cos\theta \quad (15)$$

where L_u is the transverse displacement of the laser perpendicular to the surface, u indicates the direction of the transverse displacement, L is the displacement recorded with the laser that is moving with the camera, and ϕ and θ are laser's pitch and yaw angles, respectively, estimated with the camera's resampled rotation matrices. It is worth mentioning that the target is aligned parallel to the laser beam or the direction of the displacement that is being monitored. In the case of this paper, it is directed perpendicular to the rail direction, which coincides with the train traffic direction. Therefore, the camera's x coordinate is measured in direction of the transverse displacement. This method is developed for real inspections of timber railroad bridges, which are performed by inspectors observing the train crossing event when there is no water under the bridge.

3.2.3 | Displacement estimation

The total noncontact reference-free dynamic transverse displacement can be calculated subtracting the translational displacement of the camera in u direction from the perpendicular laser signal using Equation (16):

$$D_u(i) = -[(L_u(i) - L_u(R)) - (C_u(i) - C_u(R))] \quad (16)$$

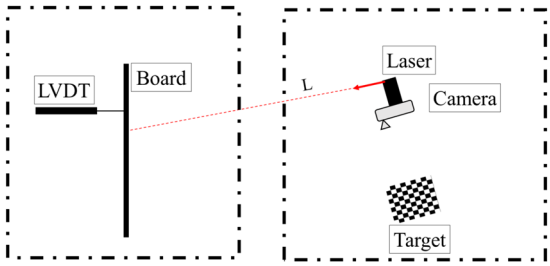

FIGURE 10 Laboratory experiment for validation of displacement estimation using laser–camera integration

where $D_u(i)$ is the ith total noncontact reference-free dynamic transverse displacement; u indicates the direction of the transverse displacement; $L_u(i)$ is the ith transverse distance measurement between the structure and the laser; $L_u(R)$ is the selected reference position for the transverse laser data; $C_u(i)$ is the ith camera position in the u direction; and $C_u(R)$ is the position of the camera in the u direction at the selected reference point. Displacements are considered to be negative when the structure is moving away from the monitoring area. Railroad managers and inspectors are interested in new methods to provide them with this information under railroad train bridge crossing events. The following section describes the validation and the experiment results.

3.3 | Total dynamic transverse displacement validation

A laboratory test was conducted adding a laser to a moving camera to find the noncontact reference-free total dynamic transverse displacement of a mock-up bridge pier. The bridge pier was manually stimulated with a pseudostatic and dynamic vibration representing a railroad bridge in need of repair (Moreu, Spencer, Foutch, & Scola, 2017). Figure 10 shows the layout of the experiment. One graduate student moved the laser and camera replicating a hovering UAS (right side of Figure 10), while another graduate student moved the board replicating a railroad bridge (left side of Figure 10). An LVDT measured the displacement of the board for validation purposes. The board was pinned at the bottom and the rotation effect was negligible in the horizontal displacement; hence, only one LVDT was needed for validation. Both laser and LVDT signals were collected using Vib-Pilot data acquisition (DAQ) with a sampling rate of 1,024 Hz. The signals need to be resampled to obtain a single sampling rate before processing data.

Target detection can be affected by the light and target size. After several experiments, we concluded that larger checkerboard size and natural light on the target can minimize the undetected frames. The research team determined the effect of both light conditions and target size in the target detection. After conducting various experiments, researchers determined that both natural light condition and a larger size checkerboard minimizes the number of undetected targets during the experiment. Therefore, researchers conducted the experiment under daylight conditions and used a checkerboard with a square size of 100 mm × 100 mm. In real field tests, this target size can obtain adequate accuracy for 10–20 ft tall timber trestle railroad bridges. However, user may choose a larger checkerboard for better target detection in other types of bridges, including taller bridges. Figure 10 shows the layout of the experiment.

The motivation of the study is to provide the railroad owner with the total transverse displacement of the timber railroad bridge under force vibration caused by the weight of a train crossing the bridge. The objective of this experiment is not to conduct modal analysis or to obtain dynamic properties of the bridge, but rather to replicate low-frequency responses similar to those observed in the field before by researchers deemed to be excessive by the railroad. Therefore, one student moved the board with amplitudes between 45 and 75 mm at approximately 0.6 Hz, replicating observed displacements under two locomotive cars. The authors chose to replicate field data obtained from 29 timber railroad bridge train crossing events, which all showed standard excessive movements at low frequencies. More specifically, this field data showed a dominant frequency of 0.6 Hz for 20 mph trains, and always under 2 Hz. According to the railroad owners, they are interested in displacements caused by train crossings (Moreu et al., 2015). The laser and the camera moved together in rotational and translational motion, while the board's movement was recorded by an LVDT with a fixed reference. Authors of this paper moved the laser camera with approximately 500 mm peak to peak in translation, and with a pitch angle of ±15 degrees, and a negligible yaw angle. There was an approximate vertical movement of 100 mm of the laser camera as opposed to the 1D experiment. The experiment lasted approximately 25 s. A window size of 0.25 s was selected for the SMA filter to keep the dominant period of the moving camera in the direction of interest, while canceling the noise caused by the estimation. Researchers applied a shift correction to account for the delay in the time domain. Figure 11(a) shows the laser signal recorded during the experiment, Figure 11(b) shows the pitch angle, and Figure 11(c) shows the perpendicular laser signal determined by angle correction.

The research team conducted various experiments in order to confirm the repeatability of the methodology. Figure 12 shows the results from one of the experiments using the video data (Figure 12a) and the laser data (Figure 12b). We estimated the noncontact total

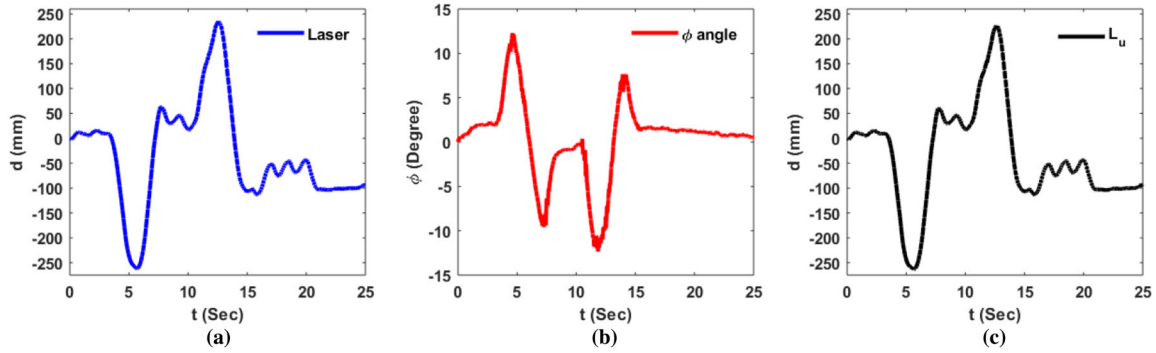

FIGURE 11 Laser's angular correction: (a) recorded laser signal, (b) laser's pitch angel estimation determined by synchronized camera data, and (c) perpendicular laser signal

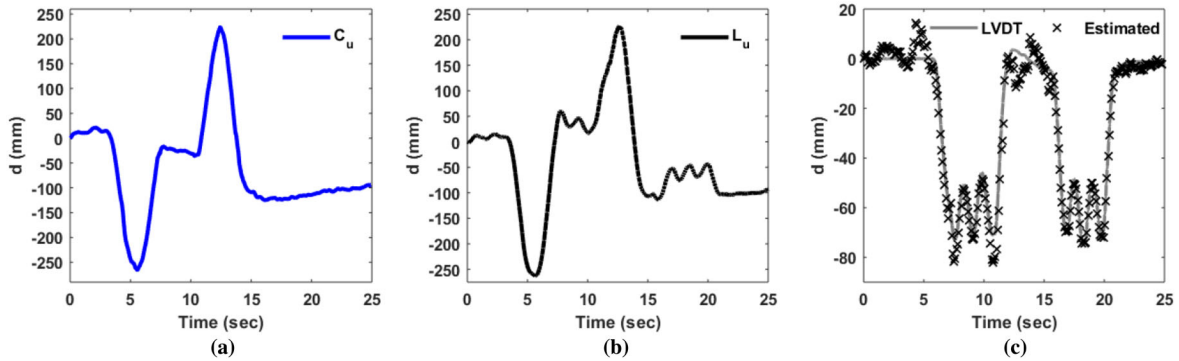

FIGURE 12 Noncontact total dynamic displacement estimation: (a) camera displacement in laser direction, (b) perpendicular laser signal, and (c) total displacement estimation and LVDT displacement measurement

dynamic transverse displacement of the mock-up pier by subtracting the camera motion from the laser signal to compensate for laser's translational motion, and compared it with the LVDT data (Figure 12c). The LVDT signal shows the motion of a bridge pier cap under force vibration of bridge that was simulated manually and in one direction as explained previously. We analyzed the results from two different experiments. The peak and RMS errors were 15.2 mm (20.5%) and 5.1 mm (6.9%), respectively. The methodology is able to estimate the structure's motion with a similar percentage error to the 1D estimation. Furthermore, during the observation of displacement changes of timber railroad bridges, inspectors are currently looking for changes of displacements above 12.7 mm (1/2 inch), with increasing increments of 6.3 mm (1/4 inch). In other words, railroad owners are not interested in displacements below 12.7 mm, and changes smaller than 6.3 mm. In this context, the error in displacement estimation is accepted by the railroad Class I managers as sufficient for timber railroad bridge monitoring. According to Figure 12(c) and the percentage of errors obtained in the various experiments, railroad owners and managers believe that the technical accuracy of the method is valid for timber railroad bridges' movements under train crossing events. According to these preliminary results and this error level being acceptable as a starting point, Class I railroad managers and owners recommend advancing this research toward field testing to further collect other factors that can advance its field implementation. Based on these results, the bridge inspector team could in the future test the suitability of this approach to measure noncontact, reference-free total dynamic transverse displacements in the field to test other limitations. The new method presented herein can complement or be an alternative to current approaches that successfully record displacements with terrestrial lasers from a tripod; using GPS; or sensor attachment to the structure. According to the railroad inspectors, it is beneficial to explore using lasers and drones to measure transverse displacements in the field for situations where the inspecting team would be limited to access to the structure or would not be able to be near the bridge during the train crossing. It is advantageous to explore displacement measurements with drones for field access limitations. Currently, there is

a trade-off between the cost efficiency and sampling rate of consumer-based cameras in structural monitoring, but in this research, the low cost was a primary objective. In the future, the accuracy of estimation of this method will be improved by employing cameras with higher accuracy and higher sampling rate, which will reduce the errors obtained in this laboratory experiment.

The outlined method combining laser and camera for field measurement of structures under loads provide a possible alternative for traditional sensing methods enabling the noncontact reference-free measurement of total dynamic structural displacement. Another value of the proposed methodology is that the measurement of displacement can be done without climbing or fouling the track that is a primary concern when adding sensors in the field. This research has identified future needs based on the current limitations, such as long processing time, light requirements for increased feature detection, and yaw calculation using external accelerometer. Future developments include laser–camera–accelerometer integration, low cost, low-energy development for field implementation, improved computer vision target detection, and target-free motion estimation, and taking advantage of data fusion techniques. The integration of this methodology with ongoing computer vision and UAS progress enables safer and viable alternatives for important collection of information in addition to traditional displacement sensors.

4 | DISCUSSION

The paper includes the method and validations in laboratory. However, for full implementation of the system, challenges and environmental effects need to be further investigated. For example, it is anticipated that the field implementation at first will be demanding when compared with other terrestrial approaches, such as terrestrial laser scanning, which are successfully used in the field from the ground. The complexity of enabling this new alternative today has inherent limitations. Therefore, this section provides complementary information concerning the limitations and future of the work. The methodology's concept is general enough to make it applicable for wider spectrum of sensors other than laser.

4.1 | Challenges and limitations

Table 3 lists, proposes solutions, and discusses expected challenges using the methodology in real field applications. Most of the challenges are hardware-related and will be solved with advent and availability of low-cost, high-quality sensors.

TABLE 3 List of existing challenges

Challenge	Description
Single point method	This method only measures transverse displacement at one fixed location, assuming that this single-point movement is a critical parameter of timber and railroad bridge performance
Target	This method depends on a fixed physical target on ground; target size should be adjusted for higher flight altitude
Weather conditions	Cannot be performed in windy and stormy weather
Accuracy	The accuracy is about 5–6 mm, and it cannot obtain submilliliter displacement like LVDT. However, using an inertial sensor like inertial measurement unit (IMU) can enhance estimation accuracy
Camera	Low sampling rate, computationally demanding, and long processing time, limited resolution
Low-cost sensors	Have limited capabilities such as short-range laser but cost-efficient development is vital for industry adoption
Untether flights	Appropriate low-cost data loggers should be provided for actual flights

4.2 | Outdoor experiment with UAS

Several field experiments were conducted to understand the dynamics and vibrations induced by UAS on the proposed system. Data were collected to recognize the capability and behavior of the system to inform the future of the work. The video of the camera installed on the UAS was analyzed. The camera was installed appropriately and firmly on the UAS along with other sensors. The video data showed that with the appropriate sensor placement, the vibrations of the UAS did not cause a problematic blur in experiment frames (Figure 13). The experiments conducted in field had better pattern detection performance than the ones conducted at indoor laboratory medium. The frames of the experiments conducted at better time of the day were fully detected and no blur issue was observed. Authors of this paper will discuss the field implementation, system design, and data analyses of the field experiments in an upcoming paper, because discussion of the variations is out of the scope of current paper.

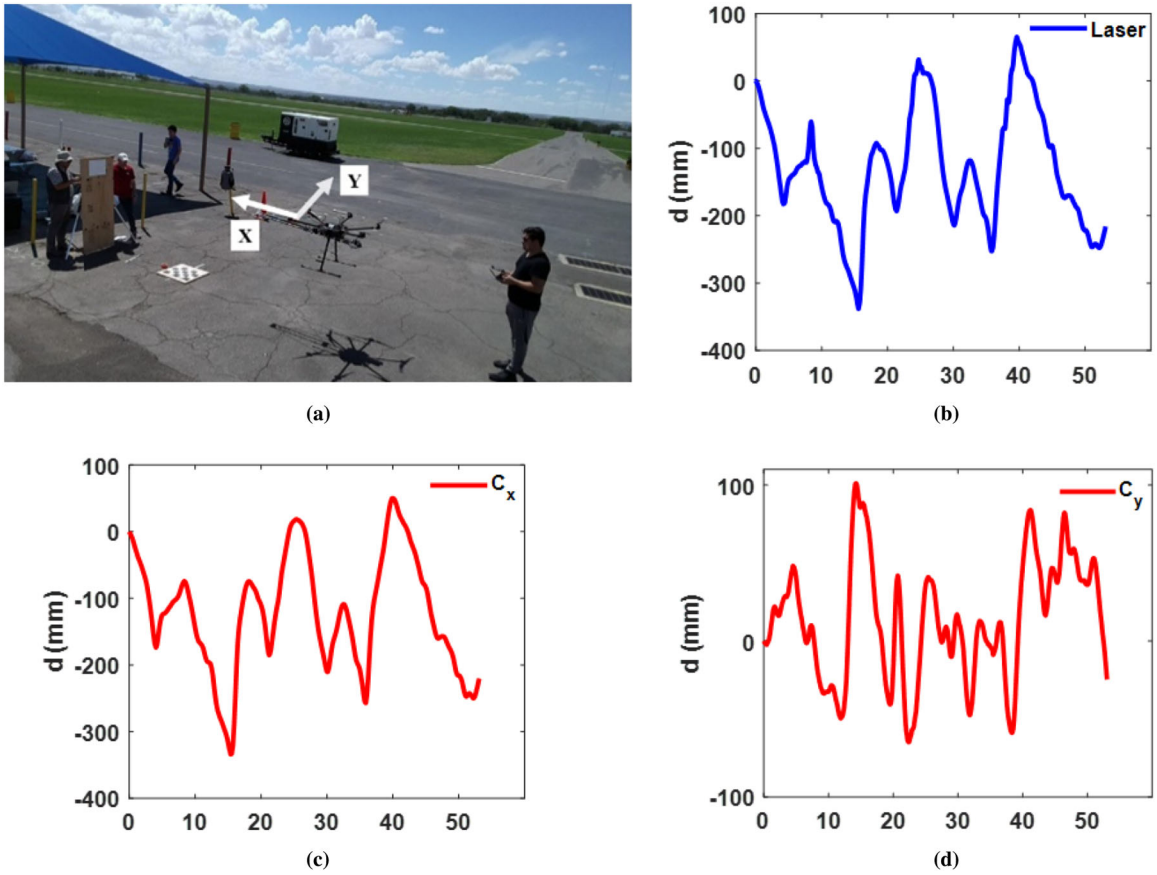

FIGURE 13 Field test: (a) field test using the system on UAS, (b) laser data collected in field, (c) processed camera data in *x* direction, and (d) processed camera data in *y* direction

4.3 | Error discussion

4.3.1 | System's evaluation

The method combines the signals of a camera and a laser to acquire out of plane displacement component for trestle railroad bridges. The RMS error was within the range of few millimeters (5.1 mm) and the peak or maximum error was 15.2 mm. It is worth mentioning that the maximum error occurred in the regions of zero LVDT displacements and not under trains, which could be in the future removed by the inspector observing those events without traffic.

To understand the error distribution, we needed to identify the error sources. The authors of the paper conducted the experiments of Section 3.1.1 to obtain the errors induced by camera only. The results showed that the RMSE varied between 1 and 3.9 mm and the maximum errors varied between 3.1 and 16.6 mm. On the other hand, the laser is accurate enough to capture small motions under 0.1 mm. The second source of the error is time-related. We needed to synchronize the data of the camera and laser to process them and there was a large sampling rate gap between camera and laser; furthermore, the camera's time stamps were not completely uniform. Thus, the synchronized data lacked a perfect match of time instants between sensors. The method's dependency on an accurate synchronization of data makes the synchronization the second source of error after camera position estimation. As discussed in Section 4.1, the accuracy of the method could be improved by integrating the camera with an IMU sensor, gyroscope, and using more capable sensors in future. This method is a first effort to offer a new laser–camera system for UAS to measure total dynamic displacement. The accuracy achieved with the proposed off-the-shelf hardware components can be increased in the future. The uncertainties associated with the combination of UAS, cameras, and lasers can be reduced exploring alternative hardware options for further development and improvement in the future.

4.3.2 | Environmental effects

Researchers conducted four field experiments to understand the challenges related to environmental factors, with an emphasis on the wind speed (Weather Underground,

2020). The authors tracked the effect of different wind and light conditions for each test. Specifically, wind and wind gust speeds had a clear affect on the flying conditions for the four experiments conducted. One field experiment demonstrated that the system successfully operated with wind and wind gusts at 2 mph or less. Later, researchers successfully run this experiment with winds of 5 mph and wind gusts of 7 mph, and also with winds of 8 mph and wind gusts of 10 mph. However, one field test was canceled due to winds of 11 mph and wind gusts of 16 mph and rain, causing safety concerns. Regarding light effects, the results of the preliminary analysis of the field experiments showed that the evening was the best time to conduct tests and obtain optimal camera resolution during the experiment. The tests with direct sunlight on the target lost approximately 1 fps, which was overcome by the interpolation suggested in the algorithm described earlier. The frames of the experiments conducted during the late afternoon hours were fully detected, and no blur issue was observed. Researchers designed the remote DAQ on the UAS to collect laser data with a precision of 0.8 mm. However, in addition to that 0.8 mm, environmental effects like wind and vibration induced noise in the results. More specifically, each mV of noise led to 0.15 mm of error in the signal. Based on the field experiments, high wind caused errors of a few millimeters in the displacement estimation of laser. Specifically, high wind during the field experiments caused the loss of individual frames, which the algorithm was able to identify, and correct accordingly during postprocessing.

4.4 | Applications of the system

This method is the first effort to find transverse displacement combining a laser and a camera on UAS. The system is not a replacement for the existing accurate measurement methods but provides an alternative when the railroad bridge inspectors rely on visual inspection and avoid climbing the railroad bridge for sensor installation. The method can provide useful information when the structure's displacement is not small such as what can be seen in trestle railroad bridges.

The proposed method can also open other applications for bridge inspections using UAS beyond collecting displacements, enabling a new method to collect bridge data remotely complementary to computer-vision methods.

5 | CONCLUSIONS

This paper describes a new methodology that integrates a moving laser and a camera to find the total noncontact reference-free dynamic transverse displacement of a structure. The proposed method can be implemented using an UAS, based on the validation of the estimations using drone movements in laboratory settings. The proposed methodology corrects laser's translation and rotation during measurements and estimates total dynamic transverse displacements, which cannot be collected with camera or laser alone. The algorithm was tested with laboratory experiments. The authors tested the laser-camera integration in a 1D configuration to evaluate the accuracy of the laser measurement without rotation or vertical translation, and they concluded that 1D method can estimate transverse total dynamic displacement with peak and RMS errors of 3.0 mm (16.1%) and 1.2 mm (6.3%), respectively. In order to account for rotation, the authors developed an estimation of the 6 DOF motion of the laser considering rotational motions of the camera. The results of the algorithm were validated using high precision cameras, with peak and RMS errors of 12.0 mm (10.0%) and 2.6 mm (2.5%), respectively. Using the rotation matrices of the camera, authors determined the history of the laser angle, enabling the estimation of the total noncontact reference-free dynamic transverse displacement. The results of the transverse displacement estimation had peak and RMS errors of 15.2 mm (20.5%) and 5.1 mm (6.9%), respectively. Railroad managers are interested in alternative methods to measure displacements with accuracy in the range of mm, so the results provide a first approach toward advancing and further improving the noncontact reference-free measurement for implementation. Using the successful evidence for displacement estimation, the next step of this research is the field implementation, which involves both hardware and software development. Finally, the hardware and software development need to consider low cost and low weight, which according to industry is a requirement in addition to the technical validation of the method. The proposed method in this paper has its limitations but offers an affordable and safe alternative for inspectors to do their displacement measurements with inaccessible locations and does not require sensor installation.

ACKNOWLEDGMENTS

This work was funded by the Transportation Research Board (TRB), Rail Safety IDEA Project 37: Measuring Behavior of Railroad Bridges under Revenue Traffic using Lasers and Unmanned Aerial Vehicles (UAVs) for Safer Operations: Implementation, Project 163418-0399. The authors greatly acknowledge this support and the feedback from project manager Dr. Velvet Basemera-Fitzpatrick. Authors extend their thanks to the TRB expert review panel for their input and constructive feedback: Dr. Rafael Fierro, Dr. Duane Otter, Dr. David Mascarenas, Martita Mullen, and Sandro Scola; and to the Smart Management

of Infrastructure Laboratory (SMILab) affiliates Nicolas Cobo, Jorshua Diaz, Odey Yousef, James Woodall, Marlan Ball, and Dr. Su Zhang for their assistance in both indoor and outdoor laboratory experiments.

REFERENCES

AgMan. (2020). Agile manufacturing laboratory, UNM. Retrieved from https://agile-mfg.unm.edu/people/.

Amezquita-Sanchez, J., Valtierra-Rodriguez, M., & Adeli, H. (2018). Wireless smart sensors for monitoring the health condition of civil infrastructure. *Scientia Iranica*, *25*(6), 2913–2925.

Aqel, M. O., Marhaban, M. H., Saripan, M. I., & Ismail, N. B. (2016). Review of visual odometry: Types, approaches, challenges, and applications. *SpringerPlus*, *5*(1), 1897.

Brooks, C., Dobson, R., Banach, D., Dean, D., Oommen, T., Wolf, R., … Hart, B. (2015). *Evaluating the use of unmanned aerial vehicles for transportation purposes*. Report No. RC-1616, Michigan Department of Transportation, Michigan.

Chan, B., Guan, H., Jo, J., & Blumenstein, M. (2015). Towards UAV-based bridge inspection systems: A review and an application perspective. *Structural Monitoring and Maintenance*, *2*(3), 283–300.

Dille, M., Grocholsky, B., & Singh, S. (2010). Outdoor downward-facing optical flow odometry with commodity sensors. In A. Zelinsky (Ed.), *Field and service robotics* (pp. 183–193). Cham: Springer.

Fitzgibbon, A. W. (2001). Simultaneous linear estimation of multiple view geometry and lens distortion. In *Proceedings of the 2001 IEEE Computer Society Conference on Computer Vision and Pattern Recognition (CVPR 2001)*, (Vol. *1*, pp. 125–132). IEEE.

FRA. (2020a). Federal railroad administration. Retrieved from https://www.fra.dot.gov/eLib/Details/L02696.

FRA. (2020b). Federal railroad administration. Retrieved from https://railroads.dot.gov/elibrary/bridge-safety-standards.

Fraundorfer, F., & Scaramuzza, D. (2012). Visual odometry: Part ii: Matching, robustness, optimization, and applications. *IEEE Robotics & Automation Magazine*, *19*(2), 78–90.

Furukawa, Y., & Ponce, J. (2009). Accurate camera calibration from multi-view stereo and bundle adjustment. *International Journal of Computer Vision*, *84*(3), 257–268.

Garg, P., Moreu, F., Ozdagli, A., Taha, M. R., & Mascareñas, D. (2019). Noncontact dynamic displacement measurement of structures using a moving laser doppler vibrometer. *Journal of Bridge Engineering*, *24*(9), 04019089.

Gentile, C. (2010). Deflection measurement on vibrating stay cables by non-contact microwave interferometer. *NDT & E International*, *43*(3), 231–240.

Greenwood, W. W., Lynch, J. P., & Zekkos, D. (2019). Applications of UAVs in civil infrastructure. *Journal of Infrastructure Systems*, *25*(2), 04019002.

Hester, D., Brownjohn, J., Bocian, M., & Xu, Y. (2017). Low cost bridge load test: Calculating bridge displacement from acceleration for load assessment calculations. *Engineering Structures*, *143*, 358–374.

Hirose, M., Xiao, Y., Zuo, Z., Kamat, V. R., Zekkos, D., & Lynch, J. (2015). Implementation of UAV localization methods for a mobile post-earthquake monitoring system. In *2015 IEEE Workshop on Environmental, Energy, and Structural Monitoring Systems (EESMS) Proceedings* (pp. 66–71). IEEE.

Intel. (2020). Intel aero ready to fly drone. Retrieved from https://www.intel.com/content/www/us/en/support/articles/000023271/drones/development-drones.html.

Jalinoos, F., Amjadian, M., Agrawal, A. K., Brooks, C., & Banach, D. (2020). Experimental evaluation of unmanned aerial system for measuring bridge movement. *Journal of Bridge Engineering*, *25*(1), 04019132.

Javadi, S. H., & Farina, A. (2020). Radar networks: A review of features and challenges. *Information Fusion*, *61*, 48–55.

Jo, H., Sim, S.-H., Tatkowski, A., Spencer, B. J., & Nelson, M. E. (2013). Feasibility of displacement monitoring using low-cost GPS receivers. *Structural Control and Health Monitoring*, *20*(9), 1240–1254.

Khadka, A., Fick, B., Afshar, A., Tavakoli, M., & Baqersad, J. (2020). Non-contact vibration monitoring of rotating wind turbines using a semi-autonomous UAV. *Mechanical Systems and Signal Processing*, *138*, 106446.

Khuc, T., Nguyen, T. A., Dao, H., & Catbas, F. N. (2020). Swaying displacement measurement for structural monitoring using computer vision and an unmanned aerial vehicle. *Measurement*, *159*, 107769.

Kitt, B. M., Rehder, J., Chambers, A. D., Schonbein, M., Lategahn, H., & Singh, S. (2011). Monocular visual odometry using a planar road model to solve scale ambiguity. In *Proceedings of the European Conference on Mobile Robots*, (pp. 43–48).

Kok, M., Hol, J. D., & Schön, T. B. (2017). *Using inertial sensors for position and orientation estimation*. arXiv preprint arXiv:1704.06053.

Liu, Y.-F., Nie, X., Fan, J.-S., & Liu, X.-G. (2020). Image-based crack assessment of bridge piers using unmanned aerial vehicles and three-dimensional scene reconstruction. *Computer-Aided Civil and Infrastructure Engineering*, *35*(5), 511–529.

Maklouf, O., & Adwaib, A. (2014). Performance evaluation of gps\ins main integration approach. *International Journal of Aerospace and Mechanical Engineering*, *8*(2), 476–484.

MARHES. (2020). Multi-agent, robotics, and heterogeneous systems laboratory, UNM. Retrieved from http://marhes.ece.unm.edu/.

Moreu, F., Jo, H., Li, J., Kim, R. E., Cho, S., Kimmle, A., … LaFave, J. M. (2015). Dynamic assessment of timber railroad bridges using displacements. *Journal of Bridge Engineering*, *20*(10), 0401 4114.

Moreu, F., Spencer, B. F., Foutch, D. A., & Scola, S. (2017). Consequence-based management of railroad bridge networks. *Structure and Infrastructure Engineering*, *13*(2), 273–286.

Murray, C. A., Take, W. A., & Hoult, N. A. (2015). Measurement of vertical and longitudinal rail displacements using digital image correlation. *Canadian Geotechnical Journal*, *52*(2), 141–155.

Oh, B. K., Kim, K. J., Kim, Y., Park, H. S., & Adeli, H. (2017). Evolutionary learning based sustainable strain sensing model for structural health monitoring of high-rise buildings. *Applied Soft Computing*, *58*, 576–585.

Ojio, T., Carey, C., OBrien, E. J., Doherty, C., & Taylor, S. E. (2016). Contactless bridge weigh-in-motion. *Journal of Bridge Engineering*, *21*(7), 04016032.

Ozdagli, A., Gomez, J., & Moreu, F. (2017). Real-time reference-free displacement of railroad bridges during train-crossing events. *Journal of Bridge Engineering*, *22*(10), 04017073.

Ozdagli, A., Liu, B., & Moreu, F. (2018). Measuring total transverse reference-free displacements for condition assessment of timber

railroad bridges: Experimental validation. *Journal of Structural Engineering*, *144*(6), 04018047.

Park, H. S., Lee, H., Adeli, H., & Lee, I. (2007). A new approach for health monitoring of structures: Terrestrial laser scanning. *Computer-Aided Civil and Infrastructure Engineering*, *22*(1), 19–30.

Park, S., Park, H. S., Kim, J., & Adeli, H. (2015). 3D displacement measurement model for health monitoring of structures using a motion capture system. *Measurement*, *59*, 352–362.

Peddle, J., Goudreau, A., Carlson, E., & Santini-Bell, E. (2011). Bridge displacement measurement through digital image correlation. *Bridge Structures*, *7*(4), 165–173.

Peterson, M., & Gutkowski, R. (1999). Evaluation of the structural integrity of timber bridges. *NDT & E International*, *32*(1), 43–48.

Pieraccini, M. (2013). Monitoring of civil infrastructures by interferometric radar: A review. *The Scientific World Journal*, *2013*, 1–8.

Rice, J. A., Li, C., Gu, C., & Hernandez, J. C. (2011). A wireless multifunctional radar-based displacement sensor for structural health monitoring. In *Sensors and Smart Structures Technologies for Civil, Mechanical, and Aerospace Systems 2011*, volume *7981* (pp. 79810K). International Society for Optics and Photonics.

Robertson, I. N. (2005). Prediction of vertical deflections for a long-span prestressed concrete bridge structure. *Engineering Structures*, *27*(12), 1820–1827.

Sekiya, H., Kimura, K., & Miki, C. (2016). Technique for determining bridge displacement response using MEMS accelerometers. *Sensors*, *16*(2), 257.

Sturm, P. (2014). Pinhole camera model. In *Computer Vision*; (pp. 610–613). New York, NY: Springer US.

Sünderhauf, N., & Protzel, P. (2007). *Stereo odometry.a review of approaches*. (Technical Report 3/07). Chemnitz University of Technology.

Truong-Hong, L., & Laefer, D. (2014). Using terrestrial laser scanning for dynamic bridge deflection measurement (paper 060). In *Istanbul Bridge Conference (IABSE)*.

Wang, D., Liang, H., Zhu, H., & Zhang, S. (2014). A bionic camera-based polarization navigation sensor. *Sensors*, *14*(7), 13006–13023.

Woodman, O. J. (2007). *An introduction to inertial navigation*. (Technical Report UCAMCL-TR-696). Computer Laboratory, University of Cambridge.

Xu, Y., & Brownjohn, J. M. (2018). Review of machine-vision based methodologies for displacement measurement in civil structures. *Journal of Civil Structural Health Monitoring*, *8*(1), 91–110.

Yeum, C. M., & Dyke, S. J. (2015). Vision-based automated crack detection for bridge inspection. *Computer-Aided Civil and Infrastructure Engineering*, *30*(10), 759–770.

Yoon, H., Shin, J., & Spencer, B. F., Jr. (2018). Structural displacement measurement using an unmanned aerial system. *Computer-Aided Civil and Infrastructure Engineering*, *33*(3), 183–192.

Zhang, C., & Elaksher, A. (2012). An unmanned aerial vehicle-based imaging system for 3D measurement of unpaved road surface distresses 1. *Computer-Aided Civil and Infrastructure Engineering*, *27*(2), 118–129.

Zhao, X., Liu, H., Yu, Y., Xu, X., Hu, W., Li, M., & Ou, J. (2015). Bridge displacement monitoring method based on laser projection-sensing technology. *Sensors*, *15*(4), 8444–8463.

How to cite this article: Nasimi R, Moreu F. A methodology for measuring the total displacements of structures using a laser–camera system. *Comput Aided Civ Inf*. 2021;1–17.
https://doi.org/10.1111/mice.12652

Mechanical Systems and Signal Processing 190 (2023) 110118

Contents lists available at ScienceDirect

Mechanical Systems and Signal Processing

journal homepage: www.elsevier.com/locate/ymssp

Stabilizing a strongly nonlinear structure through shaker dynamics in fixed frequency voltage control tests

E. Robbins [a], R.J. Kuether [b], B.R. Pacini [b], F. Moreu [a,*]

[a] Department of Civil, Construction, and Environmental Engineering, University of New Mexico, Albuquerque, NM 87131, USA
[b] Sandia National Laboratories*, Albuquerque, NM 87185, USA

ARTICLE INFO

Keywords:
Nonlinear stability
Nonlinear structures
Force drop-out phenomenon
Shaker-structure dynamics
Stepped sine testing

ABSTRACT

Bifurcations are commonly encountered during force controlled swept and stepped sine testing of nonlinear structures, which generally leads to the so-called jump-down or jump-up phenomena between stable solutions. There are various experimental closed-loop control algorithms, such as control-based continuation and phase-locked loop, to stabilize dynamical systems through these bifurcations, but they generally rely on specialized control algorithms that are not readily available with many commercial data acquisition software packages. A recent method was developed to experimentally apply sequential continuation using the shaker voltage that can be readily deployed using commercially available software. By utilizing the stabilizing effects of electrodynamic shakers and the force dropout phenomena in fixed frequency voltage control sine tests, this approach has been demonstrated to stabilize the unstable branch of a nonlinear system with three branches, allowing for three multivalued solutions to be identified within a specific frequency bandwidth near resonance. Recent testing on a strongly nonlinear system with vibro-impact nonlinearity has revealed jumping behavior when performing sequential continuation along the voltage parameter, like the jump phenomena seen during more traditional force controlled swept and stepped sine testing. This paper investigates the stabilizing effects of an electrodynamic shaker on strongly nonlinear structures in fixed frequency voltage control tests using both numerical and experimental methods. The harmonic balance method is applied to the coupled shaker-structure system with an electromechanical model to simulate the fixed voltage control tests and predict the stabilization for different parameters of the model. The simulated results are leveraged to inform the design of a set of experiments to demonstrate the stabilization characteristics on a fixture-pylon assembly with a vibro-impact nonlinearity. Through numerical simulation and experimental testing on two different strongly nonlinear systems, the various parameters that influence the stability of the coupled shaker-structure are revealed to better understand the performance of fixed frequency voltage control tests.

1. Introduction

Controlled stepped and swept sine testing are experimental procedures commonly used to obtain the nonlinear response of a system for purposes of system identification. These methods provide near steady state responses at various frequencies and excitation levels and can be used to perform model updating with comparable experimental and computational results conveniently and directly

* Corresponding author.
E-mail address: fmoreu@unm.edu (F. Moreu).

https://doi.org/10.1016/j.ymssp.2023.110118
Received 29 September 2022; Received in revised form 22 December 2022; Accepted 7 January 2023
Available online 25 January 2023

[14,15]. Depending on the type of nonlinear system, many solutions may exist [34,41] but in consideration of nonlinear systems that have three branches, one characteristic of force and response controlled stepped and swept sine tests is the well-known jump phenomenon that occurs at or near the resonant frequency of the response curve [26]. Although a hysteresis phenomenon can be observed by changing the sweep or step direction to obtain solutions along the lower (upper) portion of the branch, jumping still occurs and the responses can only be realized along the stable branches, leaving the unstable branch unmeasured in many tests [25].

Closed-loop control schemes in experimental nonlinear dynamics can introduce various complications throughout testing, most notably including quality-loss of the control parameter. For example, closed-loop control schemes in force control near resonance may demand a decrease in force to compensate for higher amplitude responses resulting in imperfect force control amplitudes. This requires optimization of certain test parameters such as step and sweep rates and high delay times to ensure steady state responses and quality tests which can result in excessive test times. Furthermore, higher harmonics can be introduced into the structure from increased shaker-structure interactions resulting in multi-harmonic inputs into the system [2,7]. Often these higher harmonics are not included in the analogous modeling efforts, and thus complicate the usefulness of the data when not explicitly measuring the waveforms of the input force. One approach to mitigate this is to develop a closed-loop control scheme to cancel the higher harmonic forces [28,29]. However, this approach may still possess similar challenges associated with quality-loss of the control parameter.

Control algorithms such as control-based continuation [16,39,40] and phase-locked loop [17,24] (or other methods based on phase control) have been used to control through the turning point bifurcations during nonlinear testing to measure the unstable branch which is of interest for fully characterizing the nonlinear dynamics for the purpose of model validation and calibration. These methods generally require the use of specialized software which are not commonly available within commercial software. There are various computational approaches to calculate the complete nonlinear response curves through the turning point bifurcations to obtain the multivalued response of a mathematical model of a nonlinear system. Some common techniques include the harmonic balance method [19], shooting method [20], and orthogonal collocation method [21] in combination with numerical continuation techniques [18]. There have also been numerical methods introduced with experimental approaches such as the intelligent nonlinear coupling analysis (INCA) method which utilizes the arc length continuation method [22]. These methods can be used together to compare experimental tests to numerical results but still require the need for specialized experimental control software.

Recent research has demonstrated the successful development of a sine testing method to obtain the unstable portion of the multivalued response curves of strongly nonlinear systems utilizing open-loop voltage control [1,23]. Zhang et al. [1] measured multivalued response curves by leveraging the force drop-out phenomena through resonance in sine testing with fixed frequency voltage control (FFVC) tests. This approach utilizes the electromechanical shaker input voltage as a physical, sequential continuation parameter as the relationship between the voltage and force creates a multivalued mapping from the force drop-out phenomena. Resultingly, the tests can readily be deployed with most commercial data acquisition systems and the input voltage is simply described as a sinusoidal function at a single fixed frequency and varying amplitude. This method has been successfully used for parameter identification [10], identification of weak nonlinearities [11], and measurement of multivalued response curves [12]. Zhang et al. [1] and Ferreira [3] both attribute the stabilization of the unstable solutions to the resultant shaker-structure dynamics during the test method. Many research studies have investigated the inclusion of shaker dynamics in vibration testing, both experimentally [2,4,6–12,36,37] and computationally [2,13,33]. Several scholars investigated the various interactions and behaviors that arise from shaker dynamics such as force dropout [37], force distortion [7], and the vibration modes that arise from electromechanical shakers [9], to name a few. Various other research in this area has also considered the nonlinear effects from shaker-structure interaction [28] or the shaker-structure interaction on nonlinear systems [33,35,38]. However, it is still not well-understood how the shaker stabilizes the nonlinear responses during FFVC testing and under what conditions the stabilization occurs.

The present research investigates and identifies the stabilization effect of the electromechanical shaker during simulated and experimental FFVC tests. When deploying this strategy on a strongly nonlinear vibro-impact system, it is shown experimentally that the shaker does not stabilize the system and produces a jump phenomenon when sequentially continuing along the shaker voltage parameter. Based on this observation, a modeling approach is developed to simulate a strongly nonlinear system coupled with an electromechanical shaker using multi-harmonic balance (MHB) and pseudo-arclength continuation to numerically compute the solutions from FFVC testing. The simulated multivalued response curves, continued along the data acquisition (DAQ) voltage parameter, are computed to observe the force-voltage and response-voltage relationships and gain insight into the stability of the coupled shaker-structure assembly. A parametric study on the shaker reveals how the shaker-structure parameters influence the presence of turning point bifurcations along the force-voltagecurve. The insights of the parametric study motivate further experimental testing to parametrically investigate the stabilization properties of the test setup on a strongly nonlinear vibro-impact system, and thus achieve the desired stabilization of the coupled system in FFVC tests.

The paper is organized as follows. Section 2 reviews and introduces the theoretical background to understand the stabilization of shaker dynamics. This includes a review of the FFVC test method and electrodynamic shaker dynamic modeling, and introduces a simulation framework using the method of harmonic balance and pseudo-arclength continuation to study the stabilization of FFVC tests. Section 3 describes the simulation results of an electromechanical shaker-structure model and presents results from a parametric study to identify which parameters in the model most strongly influence the shaker stabilization. Section 4 introduces the experimental system with a strong vibro-impact nonlinearity and presents an experimental parametric investigation where the patterns observed during the simulated experiments are effectively observed experimentally. Lastly, Section 5 draws conclusions from the research and includes recommendations for future work.

2. Theoretical background

This research leverages two fundamental concepts to stabilize a nonlinear system during experimental testing. Specifically, the dynamics of electromechanical shakers and the FFVC passive control test strategy are utilized, which uses the force drop-out phenomenon from shaker-structure interactions. In the FFVC control strategy, the force drops out on the force-voltage curve from the electromechanical coupling in the same manner that the force drops out on the frequency response curves from the mechanical shaker-structure interaction. These two fundamental concepts were studied by Zhang et al. in [1] where the FFVC test strategy was first introduced. This research investigates the FFVC tests, and the force drop-out phenomenon previously studied with the inclusion of the shaker dynamics as it has been discovered that the stabilizing behavior of a nonlinear system varies contingent upon the shaker-system interaction parameters. The following subsections will briefly introduce the theoretical background and describe the concepts used in this work.

2.1. Fixed frequency voltage control tests

The fundamental phenomenon utilized for the open-loop controlled test strategy is the well-known force drop-out phenomena, which occurs near resonance for both linear and nonlinear structures. Zhang et al. [1] demonstrated when the excitation frequency of a sine test is fixed and the forcing and response amplitudes are uncontrolled, then the force amplitude, F and response amplitude, R are given as single valued functions of the prescribed input voltage amplitude, V. These functions are written as

$$F = F(V) \tag{1}$$

$$R = R(V) \tag{2}$$

When the excitation frequency is fixed, the force response curves can be written as an implicit function of force and response amplitudes as

$$f(F, R) = 0 \tag{3}$$

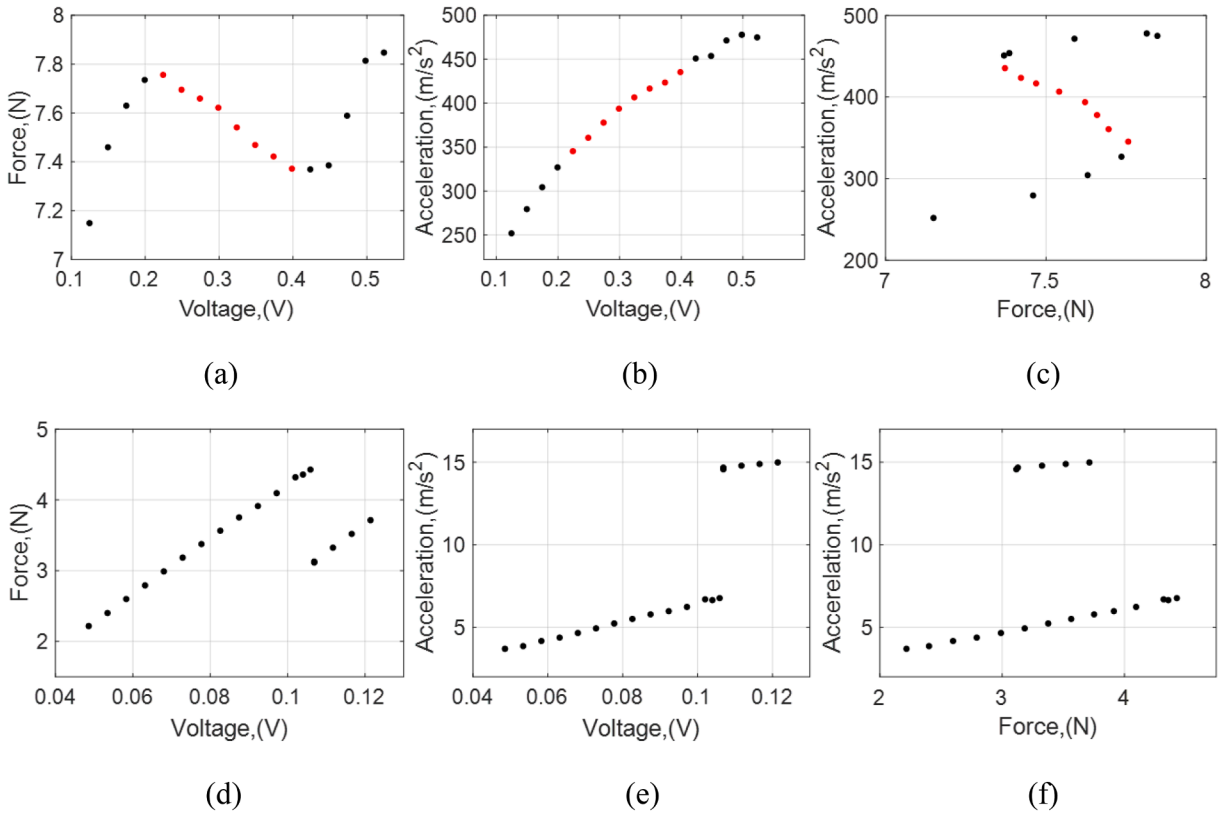

Fig. 1. The force drop-out curves (left column), monotonic voltage-amplitude response curves (middle column), and the force-amplitude response curves (S-curves) (right column) from FFVC tests on a weakly nonlinear structure (a-c) and a strongly nonlinear system (d-f). Note, the red points in (a-c) demonstrate the stabilized intermediate branch of the system. (For interpretation of the references to colour in this figure legend, the reader is referred to the web version of this article.)

The force and response are repeatedly measured as the amplitude of the sinusoidal voltage input is increased sequentially, up to a prescribed upper limit. To provide a more intuitive understanding of the differences between the expected stabilized and unexpected non-stabilized behavior of a shaker-nonlinear structure in FFVC tests, examples of experimental results of a stabilized weakly nonlinear structure and a non-stabilized strongly nonlinear structure are shown in Fig. 1. The experimental results of a stabilized structure similar to that shown in [1] are shown in Fig. 1 (a-c) and the results of a non-stabilized structure are shown in Fig. 1 (d-f).

The various relationships established between the voltage, force, and acceleration response amplitude presented in Eqs. (1) and (2) are shown in Fig. 1. Fig. 1 (a) shows the force dropout phenomenon where the force amplitude increases, decreases, and then increases again along a continuous curve as the voltage is incrementally increased. Fig. 1 (b) shows the monotonic relationship established between the response amplitude and the same incrementally increased voltage. Fig. 1 (c) shows the multivalued response curve (i.e. S-curve) between the force and response amplitudes described in Eq. (3), where unstable solutions of the system can be reconstructed with several tests performed at frequencies near the resonance of the structure. When the shaker-nonlinear structure is not stabilized, the results shown in Fig. 1 (d) and (e) show discontinuous jumps in the data rendering the reconstructed S-curve in Fig. 1 (f) discontinuous between the approximate points (4.4, 6.8) and (3.1, 14.6).

Although a multivalued relationship is established between the force and response amplitudes through the force dropout phenomena in FFVC tests, the underlying nonlinear structure still possesses the unstable dynamics within the multivalued response regions. In other words, the FFVC test strategy produces a stabilizing effect through the coupling of the shaker, stinger, and nonlinear structure such that the stability of the whole system is realized [3]. Reconstructing the response curves with the measured load cell force and response then allows for the nonlinear system dynamics to be recovered.

2.2. Electromechanical shaker dynamics

A dynamic shaker model is utilized to perform numerical simulations of coupled shaker-structure interactions, where the shaker model incorporates various mechanical and electrical parameters of the system. Lang and Snyder [9] introduced the matrix form of the lumped mass mechanical model and the cross coupled electrical model to describe the electromechanical shaker dynamics. Fig. 2 shows a general electromechanical model of a shaker and the internal circuit from [2,6,9]. The model is defined using Eqs. (4–9), where coupling occurs between the mechanical and electrical states within the model. The mechanical components shown in Fig. 2 (a) correspond to a three degree-of-freedom model of the shaker body mass M_1, the armature mass M_2, the load cell mass M_3, the armature stiffness and damping K_1 and C_1, and the stinger stiffness and damping K_2 and C_2. The displacements and external forces of the shaker body, armature mass, and load cell mass are given as x_1, x_2, x_3 and f_1, f_2, f_3 where the external forces are all assumed to be zero. The internal forces of the shaker are $F_{circuit}$ and $g(t)$, where $F_{circuit}$ is the force developed from the magnetic field and $g(t)$ is the reaction force from the shaker-structure interaction when the shaker is coupled to the structural model. The derivative of the states with respect to time are indicated with an overdot.

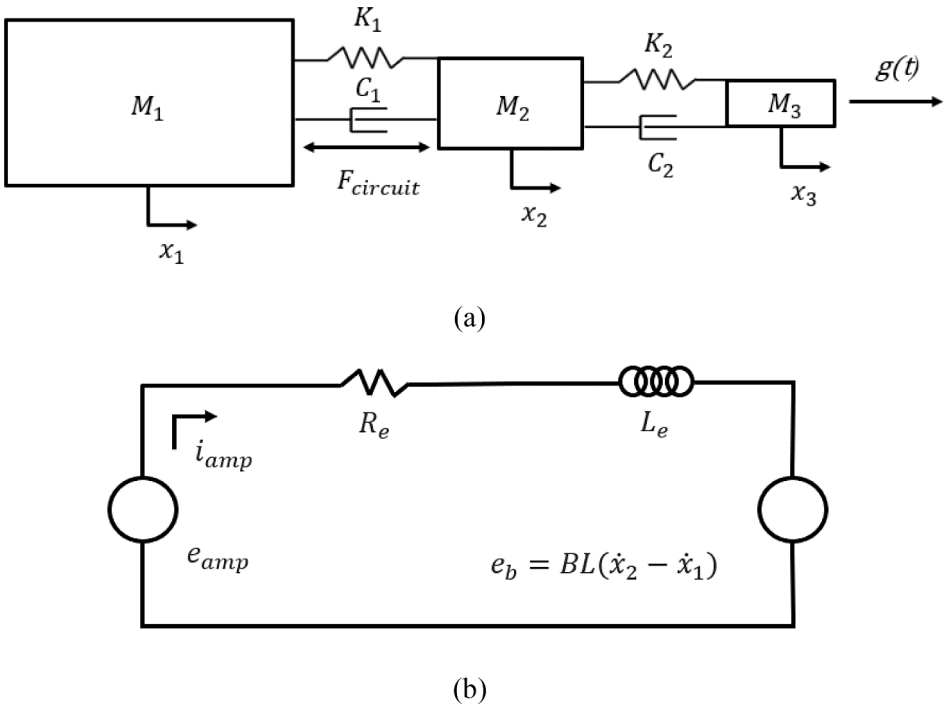

Fig. 2. Shaker (a) mechanical model and (b) electrical model.

To account for the dynamics of the shaker during testing, the mechanical and electrical parameters from Fig. 2 need to be included in the equation of motion (EOM). The general EOM of the shaker is described by Eq. (4) where the mass, damping, and stiffness matrices are given in Eqs. (5–7). The states and forces are given in Eqs. (8) and (9).

$$\mathbf{M}_{shaker}\ddot{\mathbf{x}} + \mathbf{C}_{shaker}\dot{\mathbf{x}} + \mathbf{K}_{shaker}\mathbf{x} = \mathbf{f}(t) \tag{4}$$

$$[\mathbf{M}_{shaker}] = \begin{bmatrix} M_1 & 0 & 0 & 0 & 0 \\ 0 & M_2 & 0 & 0 & 0 \\ 0 & 0 & M_3 & 0 & 0 \\ 0 & 0 & 0 & 0 & 0 \\ 0 & 0 & 0 & 0 & 0 \end{bmatrix} \tag{5}$$

$$[\mathbf{C}_{shaker}] = \begin{bmatrix} C_1 & -C_1 & 0 & 0 & 0 \\ -C_1 & (C_1 + C_2) & -C_2 & 0 & 0 \\ 0 & -C_2 & C_2 & 0 & 0 \\ -BL & BL & 0 & L_e & 0 \\ 0 & 0 & 0 & 0 & \dfrac{1}{G} \end{bmatrix} \tag{6}$$

$$[\mathbf{K}_{shaker}] = \begin{bmatrix} K_1 & -K_1 & 0 & BL & 0 \\ -K_1 & (K_1 + K_2) & -K_2 & -BL & 0 \\ 0 & -K_2 & K_2 & 0 & 0 \\ 0 & 0 & 0 & R_e & -1 \\ 0 & 0 & 0 & 0 & \dfrac{\omega_{brk}}{G} \end{bmatrix} \tag{7}$$

$$\{\mathbf{x}\} = \begin{bmatrix} x_1 \\ x_2 \\ x_3 \\ i_{amp} \\ e_{amp} \end{bmatrix} \tag{8}$$

$$\{\mathbf{f}\} = \begin{bmatrix} f_1 \\ f_2 \\ f_3 \\ 0 \\ e_{daq} \end{bmatrix} \tag{9}$$

The resulting mechanical force generated between the shaker body and armature mass $F_{circuit}$, is the electromotive force (EMF) and is proportional to the product of the current i_{amp}, the body's permanent magnetic flux density B, and the armature coil wire length L [2,6,9], which are shown in Fig. 2 (b). The amplifier current i_{amp}, links the EMF between Fig. 2 (a) and (b). Mathematically, the EMF is given as

$$F_{circuit} = BLi_{amp} \tag{10}$$

The voltage from the amplifier and data acquisition are given as e_{amp} and e_{daq}, where e_{daq} is the only nonzero external load in Eq (9). The shaker coupling factor BL, seen in Eqs. (10) and (11) links the current in the shaker to the force applied to the mechanical components as well as the back EMF to the relative velocity of the shaker armature and body, as seen in Fig. 2 (b). Note, the BL and R_e terms appear in the damping and stiffness matrices Eqs. (6) and (7), which makes them important parameters to consider in the equation of motion to properly account for shaker-system interactions.

The back EMF voltage, e_b, is defined in relation to the armature's velocity with respect to the shaker body velocity, $\dot{x}_2 - \dot{x}_1$ which can be seen in Eq. (11) and Fig. 2 (b). This decreases the voltage from the electrical circuit model as a function of the relative velocity of the armature and shaker body, and thus couples the mechanical motion to the circuit dynamics.

$$e_b = BL\left(\dot{x}_2 - \dot{x}_1\right) \tag{11}$$

This voltage drop influences the electrical current. The current influences the amount of force produced on the armature, thus completing the coupling relationship between the mechanical and electrical shaker components. Eqs. (12) and (13) show the expanded differential equations from the second and third rows of Eq. (4) which describe the dynamics of the armature and load cell masses. Eq. (13) includes the reaction force imparted on the shaker from the structure $g(t)$.

$$m_2\ddot{x}_2 - c_1\dot{x}_1 + (c_1 + c_2)\dot{x}_2 - c_2\dot{x}_3 - k_1x_1 + (k_1 + k_2)x_2 - k_2x_3 - BLi_{amp} = f_2 \tag{12}$$

$$m_3\ddot{x}_3 - c_2\left(\dot{x}_2 - \dot{x}_3\right) - k_2(x_2 - x_3) = g(t) \tag{13}$$

Substituting Eq. (13) into Eq. (12) produces the relationship between the load cell reaction force with respect to the mechanical and electrical parameters of the shaker given by Eq. (14).

$$g(t) = m_3\ddot{x}_3 + m_2\ddot{x}_2 + c_1\left(\dot{x}_2 - \dot{x}_1\right) - k_1(x_1 + x_2) - BLi_{amp} \tag{14}$$

Furthermore, Zhang et al. in [13] studied various shaker-structure interactions and indicated that the system damping of electromechanical shakers is the combination of the armature damping C_1 and electrical damping ξ_e. The electrical damping is given in Eq. (15) which is produced by the back EMF voltage and depends only on the shaker coupling factor and electrical resistance.

$$\xi_e = \frac{(BL)^2}{R_e} \tag{15}$$

For this research, the fundamental parameters for investigation are the qualitative behavior of the back EMF voltage from Eq. (11) and the electrical resistance from Eq. (15). Other parameters such as the armature damping and stiffness from Eqs. (6) and (7) will also be considered in the parametric study conducted in Section 3 as these parameters are all suspected to play an intricate role in the stability of nonlinear systems based on the interactive coupling established between the shaker and structure dynamics.

2.3. Harmonic balance algorithm for FFVC simulations

The electromechanical shaker model is coupled to a discretized model of the structure of interest to simulate the time-periodic solution for a harmonic voltage excitation supplied to the shaker. Taking the shaker model in Eq. (4), and denoting it with superscript (*sh*), the model can be appended to a structural model with superscript (*st*) to define the unconstrained, second order differential equation,

$$\begin{bmatrix} \mathbf{M}^{(\mathrm{st})} & 0 \\ 0 & \mathbf{M}^{(\mathrm{sh})} \end{bmatrix} \begin{Bmatrix} \ddot{\mathbf{x}}^{(\mathrm{st})} \\ \ddot{\mathbf{x}}^{(\mathrm{sh})} \end{Bmatrix} + \begin{bmatrix} \mathbf{C}^{(\mathrm{st})} & 0 \\ 0 & \mathbf{C}^{(\mathrm{sh})} \end{bmatrix} \begin{Bmatrix} \dot{\mathbf{x}}^{(\mathrm{st})} \\ \dot{\mathbf{x}}^{(\mathrm{sh})} \end{Bmatrix} + \begin{bmatrix} \mathbf{K}^{(\mathrm{st})} & 0 \\ 0 & \mathbf{K}^{(\mathrm{sh})} \end{bmatrix} \begin{Bmatrix} \mathbf{x}^{(\mathrm{st})} \\ \mathbf{x}^{(\mathrm{sh})} \end{Bmatrix} + \begin{Bmatrix} \mathbf{f}_{nl}^{(\mathrm{st})}\left(\mathbf{x}^{(\mathrm{st})}, \dot{\mathbf{x}}^{(\mathrm{st})}\right) \\ 0 \end{Bmatrix} = \begin{Bmatrix} 0 \\ \mathbf{f}^{(\mathrm{sh})}(t) \end{Bmatrix} + \begin{Bmatrix} \mathbf{g}^{(\mathrm{st})}(t) \\ \mathbf{g}^{(\mathrm{sh})}(t) \end{Bmatrix} \tag{16}$$

The structure and shaker matrices **M**, **C**, and **K** correspond to the mass, viscous damping and linear stiffness matrices, respectively. The nonlinear restoring force, $\mathbf{f}_{nl}^{(\mathrm{st})}\left(\mathbf{x}^{(\mathrm{st})}, \dot{\mathbf{x}}^{(\mathrm{st})}\right)$, is an $n \times 1$ vector containing the nonlinear elements in the structural model. The vectors $\mathbf{g}^{(\mathrm{st})}(t)$ and $\mathbf{g}^{(\mathrm{sh})}(t)$ are the reaction forces due to the coupling between the structural and shaker models, respectively, and are equal and opposite forces that are applied only at the connection DOF. The external load on the right side, denoted as $\mathbf{f}^{(\mathrm{sh})}(t)$, prescribe the time-varying voltage supplied from the DAQ. The shaker load vector in Eq. (9) assumes no external forces on the physical DOF and a sinusoidal voltage source from the DAQ. The voltage is written as

$$e_{daq} = \widetilde{v}_{ext}\sin(\omega t) \tag{17}$$

where the excitation frequency, ω, is prescribed and the voltage amplitude, $\widetilde{v}_{ext}$, is the unknown continuation parameter. Following the primal coupling formulation [42], the force equilibrium and compatibility conditions are satisfied by defining a unique set of interface DOF with the transformation,

$$\widetilde{\mathbf{x}} = \mathbf{L}\begin{Bmatrix} \mathbf{x}^{(\mathrm{st})} \\ \mathbf{x}^{(\mathrm{sh})} \end{Bmatrix} \tag{18}$$

Substituting this relation into the unconstrained model in Eq. (16) and premultiplying by the transpose of the transformation matrix, $\mathbf{L}^{\mathrm{T}}$, the constrained, primal assembly reduces to

$$\widetilde{\mathbf{M}}\ddot{\widetilde{\mathbf{x}}} + \widetilde{\mathbf{C}}\dot{\widetilde{\mathbf{x}}} + \widetilde{\mathbf{K}}\widetilde{\mathbf{x}} + \widetilde{\boldsymbol{f}}_{nl}\left(\widetilde{\mathbf{x}}, \dot{\widetilde{\mathbf{x}}}\right) = \widetilde{\mathbf{f}} \tag{19}$$

where

$$\widetilde{\mathbf{M}} = \mathbf{L}^{\mathrm{T}}\begin{bmatrix} \mathbf{M}^{(\mathrm{st})} & 0 \\ 0 & \mathbf{M}^{(\mathrm{sh})} \end{bmatrix}\mathbf{L} \tag{20}$$

$$\widetilde{\mathbf{C}} = \mathbf{L}^{\mathrm{T}}\begin{bmatrix} \mathbf{C}^{(\mathrm{st})} & 0 \\ 0 & \mathbf{C}^{(\mathrm{sh})} \end{bmatrix}\mathbf{L} \tag{21}$$

$$\widetilde{\mathbf{K}} = \mathbf{L}^{\mathrm{T}}\begin{bmatrix} \mathbf{K}^{(\mathrm{st})} & 0 \\ 0 & \mathbf{K}^{(\mathrm{sh})} \end{bmatrix}\mathbf{L} \tag{22}$$

$$\widetilde{\boldsymbol{f}}_{nl}\left(\widetilde{\mathbf{x}},\dot{\widetilde{\mathbf{x}}}\right)=\mathbf{L}^{\mathrm{T}}\left\{\begin{array}{c}\mathbf{f}_{nl}^{(\mathrm{st})}\left(\mathbf{x}^{(\mathrm{st})},\dot{\mathbf{x}}^{(\mathrm{st})}\right)\\0\end{array}\right\} \tag{23}$$

$$\widetilde{\mathbf{f}}=\mathbf{L}^{\mathrm{T}}\left\{\begin{array}{c}0\\\mathbf{f}^{(\mathrm{sh})}(t)\end{array}\right\} \tag{24}$$

$$\mathbf{L}^{\mathrm{T}}\left\{\begin{array}{c}\mathbf{g}^{(\mathrm{st})}(t)\\\mathbf{g}^{(\mathrm{sh})}(t)\end{array}\right\}=0 \tag{25}$$

Following the harmonic balance formulation [43], the assumed time-periodic solution to the constrained assembly in Eq. (19) and the nonlinear restoring force is approximated as a finite Fourier series,

$$\widetilde{\mathbf{x}}(t)=\frac{c_0^x}{\sqrt{2}}+\sum\nolimits_{k=1}^{N_h}\mathbf{s}_k^x\sin(k\omega t)+\mathbf{c}_k^x\cos(k\omega t) \tag{26}$$

$$\widetilde{\boldsymbol{f}}_{nl}\left(\widetilde{\mathbf{x}},\dot{\widetilde{\mathbf{x}}}\right)=\frac{c_0^{nl}}{\sqrt{2}}+\sum\nolimits_{k=1}^{N_h}\mathbf{s}_k^{nl}\sin(k\omega t)+\mathbf{c}_k^{nl}\cos(k\omega t) \tag{27}$$

Here the fundamental frequency, ω, of the forcing is assumed to be a known, prescribed value, while the Fourier coefficients of the displacements and nonlinear restoring force are unknowns. These terms are gathered into $(2N_h+1)\widetilde{n}\times 1$ vectors

$$\mathbf{z}=\left[\begin{array}{ccccccc}\left(\mathbf{c}_0^x\right)^{\mathrm{T}} & \left(\mathbf{s}_1^x\right)^{\mathrm{T}} & \left(\mathbf{c}_1^x\right)^{\mathrm{T}} & \cdots & \left(\mathbf{s}_{N_h}^x\right)^{\mathrm{T}} & \left(\mathbf{c}_{N_h}^x\right)^{\mathrm{T}}\end{array}\right]^{\mathrm{T}} \tag{28}$$

$$\mathbf{b}(\mathbf{z})=\left[\begin{array}{ccccccc}\left(\mathbf{c}_0^{nl}\right)^{\mathrm{T}} & \left(\mathbf{s}_1^{nl}\right)^{\mathrm{T}} & \left(\mathbf{c}_1^{nl}\right)^{\mathrm{T}} & \cdots & \left(\mathbf{s}_{N_h}^{nl}\right)^{\mathrm{T}} & \left(\mathbf{c}_{N_h}^{nl}\right)^{\mathrm{T}}\end{array}\right]^{\mathrm{T}} \tag{29}$$

The harmonic voltage source can be written in a similar vector form with an additional unknown variable corresponding to the external voltage,$\widetilde{v}_{ext}$

$$\mathbf{b}_{ext}=\left[\begin{array}{ccccccc}(0)^{\mathrm{T}} & \left(\widetilde{v}_{ext}\mathbf{e}_j\right)^{\mathrm{T}} & (0)^{\mathrm{T}} & \cdots & (0)^{\mathrm{T}} & (0)^{\mathrm{T}}\end{array}\right]^{\mathrm{T}} \tag{30}$$

where $\mathbf{e}_j$ is a standard unit column vector with a single unity entry at the row corresponding to the voltage load in Eq. (24). Following the derivation in [31,32], a Fourier-Galerkin projection onto the orthogonal set of discrete periodic functions results in the MHB frequency domain governing equations,

$$\mathbf{r}\left(\mathbf{z},\widetilde{v}_{ext}\right)=\mathbf{A}(\omega)\mathbf{z}+\mathbf{b}(\mathbf{z})-\mathbf{b}_{ext} \tag{31}$$

where $\mathbf{A}(\omega)$ is the linear portion of the dynamic stiffness matrix of dimension $(2N_h+1)\widetilde{n}\times(2N_h+1)\widetilde{n}$

$$\mathbf{A}(\omega)=\left[\begin{array}{cccc}\widetilde{\mathbf{K}} & & & \\ & \widetilde{\mathbf{K}}-\omega^2\widetilde{\mathbf{M}} & -\omega\widetilde{\mathbf{C}} & \\ & \omega\widetilde{\mathbf{C}} & \widetilde{\mathbf{K}}-\omega^2\widetilde{\mathbf{M}} & \\ & & & \ddots \\ & & & \widetilde{\mathbf{K}}-(N_h\omega)^2\widetilde{\mathbf{M}} \\ & & & N_h\omega\widetilde{\mathbf{C}}\end{array}\right.\left.\begin{array}{c}\\ \\ \\ \\ -N_h\omega\widetilde{\mathbf{C}} \\ \widetilde{\mathbf{K}}-(N_h\omega)^2\widetilde{\mathbf{M}}\end{array}\right] \tag{32}$$

The alternating time–frequency method [30] is used to approximate the Fourier coefficients in Eq. (29) from the time-domain nonlinear restoring force vector. In this way, the Fourier coefficients of the nonlinear force, $\mathbf{b}(\mathbf{z})$, can be computed numerically by sampling the nonlinear restoring force in the time domain and transforming to the frequency domain using the discrete Fourier transform.

The unknowns for Eq. (31) correspond to those from the fixed-frequency voltage control simulations, which include the Fourier coefficients of the displacements, $\mathbf{z}$, and scalar corresponding to the external voltage, $\widetilde{v}_{ext}$. The unknown variables are collected as,

$$\mathbf{y}=\left[\begin{array}{cc}\mathbf{z} & \widetilde{v}_{ext}\end{array}\right]^{\mathrm{T}} \tag{33}$$

The roots of the residual function $\mathbf{r}\left(\mathbf{z},\widetilde{v}_{ext}\right)$ define the solutions to the nonlinear, algebraic system of equations that approximate the periodic solutions of Eq. (26). The pseudo-arclength continuation algorithm described in [18] allows for a solution branch to be traced with the external voltage treated as the continuation variable. The Jacobian matrix needed for the continuation scheme is computed using the same approach as outlined in [31,32]. From the described harmonic balance and pseudo-arclength continuation algorithm, the simulated FFVC response produces force-voltage and response-voltage curves, from which the force-response S-curves

can be obtained for a series of simulations at different forcing frequencies.

3. Simulations on a nonlinear cantilever beam

A series of FFVC simulations was performed on a nonlinear system to explore the shaker model parameters influencing the stability of a coupled shaker-structure nonlinear system. The structure utilized in the simulations was a finite element model of a cantilever beam with a cubic nonlinear spring at the free end, which is shown in Fig. 3. The nonlinear beam was selected for the FFVC simulations because it served as a simple structure with few DOF to allow for a focused investigation of the different parameters in the shaker model. This structure was leveraged to achieve the goal of investigating global insight on the parameters that influence stabilizing behaviors of nonlinear systems through shaker dynamics in FFVC tests. Therefore, the insight gained from the simulations in this section were used conceptually to design an experiment with a different nonlinear structure presented in Section 4.

The beam model was discretized with a total of 19 Euler-Bernoulli beam elements, had a total length of 0.7 m and a square cross-section with height and width of 1.4 cm. The beam is assumed to have steel material properties with a Young's Modulus of 205 GPa and density of 7800 kg/m^3. The identified electromechanical shaker model from [2] was attached to the beam at various locations along the length to represent the coupled system. The multi-harmonic balance method in Section 2.3 was used to obtain the steady state solutions from the coupled nonlinear system while continuing along the DAQ voltage parameter. The objective here is to simulate FFVC tests on the nonlinear cantilever beam and change different parameters in the shaker and system setup such as spring constants, damping constants, drive point location, electromechanical coupling factor, and others, to observe which parameters are most sensitive to the stabilization of the electromechanical shaker.

3.1. Drive point location

The first two modes of the cantilever beam were considered for the analysis but for the sake of brevity only the results near the first mode are presented here. The linearized natural frequency of the first mode of the beam was 23 Hz but was excited at 29 Hz in the simulated FFVC tests to obtain significant nonlinear responses of the hardening system. The resulting load cell force and DAQ voltage curves were simulated for three different drive point locations, namely, near the fixed end, at the midspan, and at the beam tip. The corresponding force drop-out curves are shown in Fig. 4 where the solid lines represent the magnitude of the first harmonic (1ω) and the dashed lines represent the third harmonic magnitude (3ω). These were the most dominant frequencies observed in the load cell force. Starting with the response for the shaker attached at the beam tip (node 20), the resultant curve produces the typical force drop-out behavior that has been observed in previously reported experiments [1] and in Fig. 1. Initially the force increases until it reaches a local maximum around 0.04 V, at which point the force decreases continuously until a local minimum is reached, and the force then proceeds to increase. The three regions of load cell forces with the same value, each at different voltages, indicates that the reconstructed S-curve can reproduce the three solutions along the forced response curve, namely the upper and lower stable branch, as well as the intermediate branch that is unstable in the absence of the shaker but is stabilized due to the shaker-structure interaction.

A fundamental characteristic that results from the shaker-structure interaction is the multi-harmonic forcing shown in Fig. 4. In this case, the force drop-out curve contains higher harmonics that distort the monoharmonic forcing around the local minimum value as the presence of the higher harmonics increases the force value at this location due to the transfer of loads between the structure and shaker. This interaction can easily be seen in Fig. 4 on the tip drive point curve where the third harmonic increases and eventually intersects the fundamental harmonic near the local minimum of the force dropout. In general, the force is multi-harmonic which can lead to discrepancies in the desired force drop-out curve and reconstructed S-curve generated from the fundamental forcing harmonic. Higher order harmonic interactions will be discussed further in the following section.

The results for the case when the shaker is attached at the midspan (node 11) reveal different drop-out behavior than the results obtained from the beam tip. It is observed that the load cell force increases initially with an increase in voltage. Around 0.025 V, the force begins to decrease, but now the force-voltage curve also turns back in voltage due to the presence of a turning point bifurcation. The force continues to decrease until reaching a local minimum, followed by an increase in force and another turning point bifurcation. As a result of this behavior, there are multi-valued responses at specific regions of excitation voltage. This type of behavior does not produce the continuous single valued response that is required to realize the multivalued force-response curves from FFVC tests, and hence in this case the shaker does not provide a stabilizing effect on the nonlinear dynamics. When performing FFVC experiments in the laboratory, the method applies experimental continuation with incrementally increasing voltage to the shaker. For the curves with turning point bifurcations, this would produce a jump phenomenon to another solution point, like the behavior observed in the force-controlled experiments. A simple experimental continuation strategy would not be able to traverse these bifurcations.

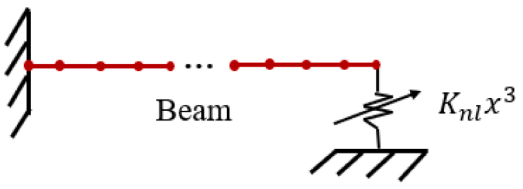

Fig. 3. Cantilever beam used in the simulation with a cubic spring at the free end.

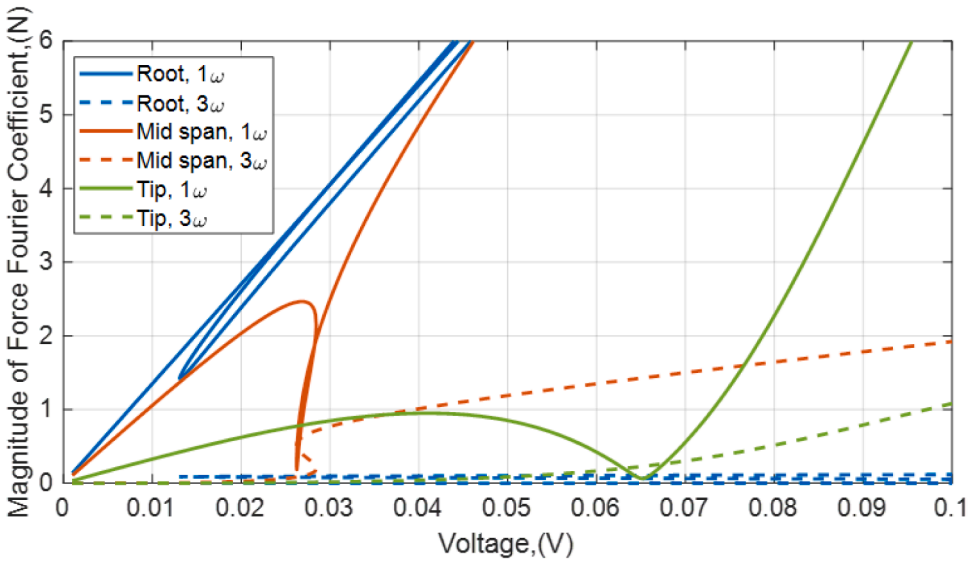

Fig. 4. The force drop-out curves with respect to voltage detailing the change in shaker drive points on the beam at the fixed end (root), the mid-span, and the free end (tip).

When the shaker is attached near the fixed end (node 3), the behavior of the force-dropout curves is similar to the midspan, except that the turning points are much sharper. The simulated results presented here provide insight into the experimental observations in Section 4. The electromechanical shaker does not necessarily provide a stabilization to the underlying structure's dynamics and is dependent on the elected drive point location in this example. The load cell force and voltage curves can produce bifurcations along the solution space, which present challenges when applying simple experimental continuation methods along the voltage parameter.

This force dropout behavior was further investigated with a more comprehensive simulation where the shaker was attached to every node along the length of the beam. Generally, it was observed that the turning point bifurcations persisted in the force drop-out curve when applying the force at locations between the fixed end at node 3 to the mid-span at node 11. When the shaker was attached to node 12 through node 20 the system demonstrated force drop-out behavior free of bifurcations and hence the shaker provided a stabilizing effect only at about half of the drive point locations in the model. When relating this to the mode shape of the first linearized mode of the system, it appears that the shaker stabilized the structure's dynamics when attached at more responsive points on the beam. Simulations on the second mode of the beam demonstrated similar behavior but are not included for brevity.

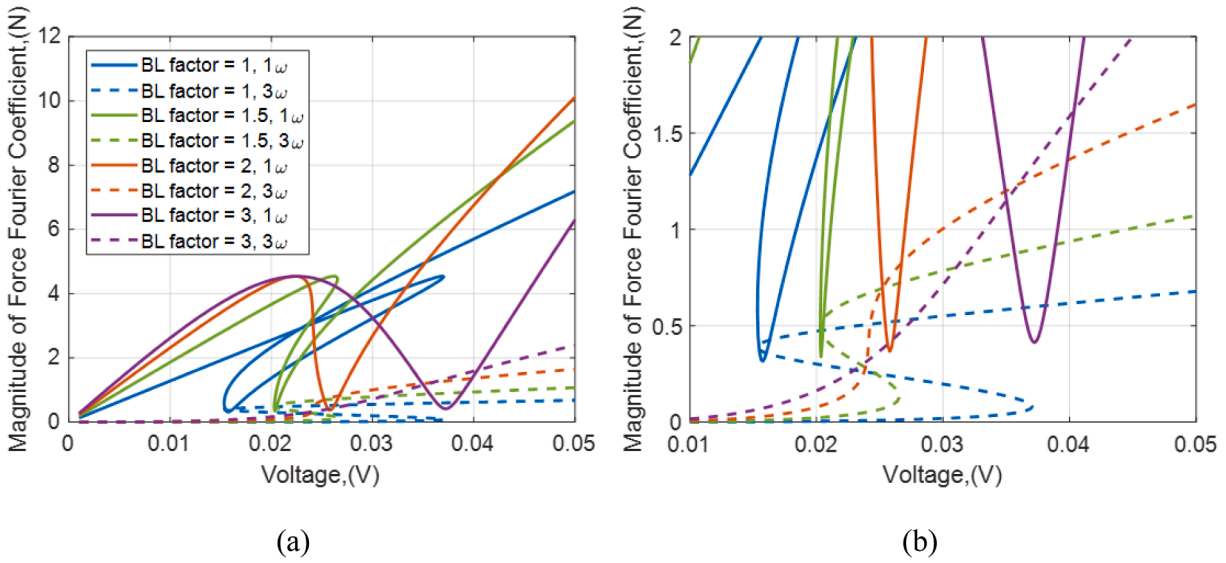

Fig. 5. *BL* constant parameter changes at shaker excitation drive points at (a) node 8. Note, (b) is a zoomed in window of (a) to show the details of the harmonic interactions at the second turning points.

3.2. Electromechanical shaker parameters

An observation from the previous section showed that the shaker had the greatest stabilizing effect for drive points that are active in the target mode. Therefore, it was hypothesized that the stabilizing effect of the shaker was due to the effect of the back EMF as an increase in this value results in an increase in the electrical damping. Reverting back to Eq. (11), the back EMF is proportional to the electromechanical coupling factor BL and the relative velocity between the shaker body and armature mass. It was therefore of interest to observe the effects of the coupling factor on the stabilizing effect of the system while keeping the relative velocity of the armature and shaker body unchanged (i.e. maintaining the same drive point location).

Fig. 5 (a) shows the effects of scaling the initial BL constant in the shaker model by different factors. In this case, the shaker is attached near the midspan at node 8 such that the nominal shaker-structure system produces force dropout curves with multivalued response and turning point bifurcations. Fig. 5 (a) shows that doubling and tripling the BL constant results in a stabilizing effect as the force-voltage curve no longer bifurcates along the branch. An incremental solution with BL scaled by 1.5 shows the evolution of the curve as the parameter is varied. By increasing the electromechanical coupling factor, the regions where the force as a function of voltage is no longer singular valued shrinks until the system no longer bifurcates. It is noted that the inverse is also true. Namely, when the shaker is attached at a node that stabilizes the system, decreasing the values of BL causes the system to transition to a multivalued response curve with bifurcations, hence losing the stabilization effect of the shaker. These results are not included for brevity.

Other electrical and mechanical parameter changes within the electromechanical shaker model were considered to further investigate the stabilizing behavior of the shaker. It was revealed that scaling the R_e, K_1, and C_1 parameters from the electromechanical model demonstrated similar results to those shown in Fig. 5 but generally required more extreme scaling factors. These results were also not included for brevity.

The reconstructed S-curves of the peak displacement and fundamental harmonic of the load cell force corresponding to the four BL constant parameter changes from Fig. 5 (a) and (b) are presented in Fig. 6. It can be observed in Fig. 6 (a) that the changes in the shaker parameters produce different reconstructions of the S-curve, which are supposed to represent the underlying dynamics of the system. These differences can be explained by the effects of the higher order harmonics from the force drop-out curves in Fig. 5 (a) and (b), which appear in the S-curve most notably near the second (upper) turning point. The third harmonics start to dominate near the local minimum in the force drop-out curves for increasing BL constants and results in different ratios of the fundamental force harmonic and the third harmonic. This reveals that the forcing is not monoharmonic and in fact the S-curves are computed from a multi-harmonic input force where the relative ratio of the input force harmonics varies along the curve for different BL constants. Alternatively, there is good agreement between the S-curves outside of the upper turning point region where the input force is dominated by the fundamental harmonic. This is further verified in Fig. 6 (b) which demonstrates overall good agreement in the reconstructed S-curves in consideration of only the magnitude of the fundamental harmonic. These observations lead to the conclusion that the reconstructed force-response S-curves from experimental data must account for the multi-harmonic nature of the excitation.

3.3. Multi-Harmonic balance and time integration simulation comparison

An experimental simulation was also conducted on the nonlinear cantilever beam where the results were compared directly to

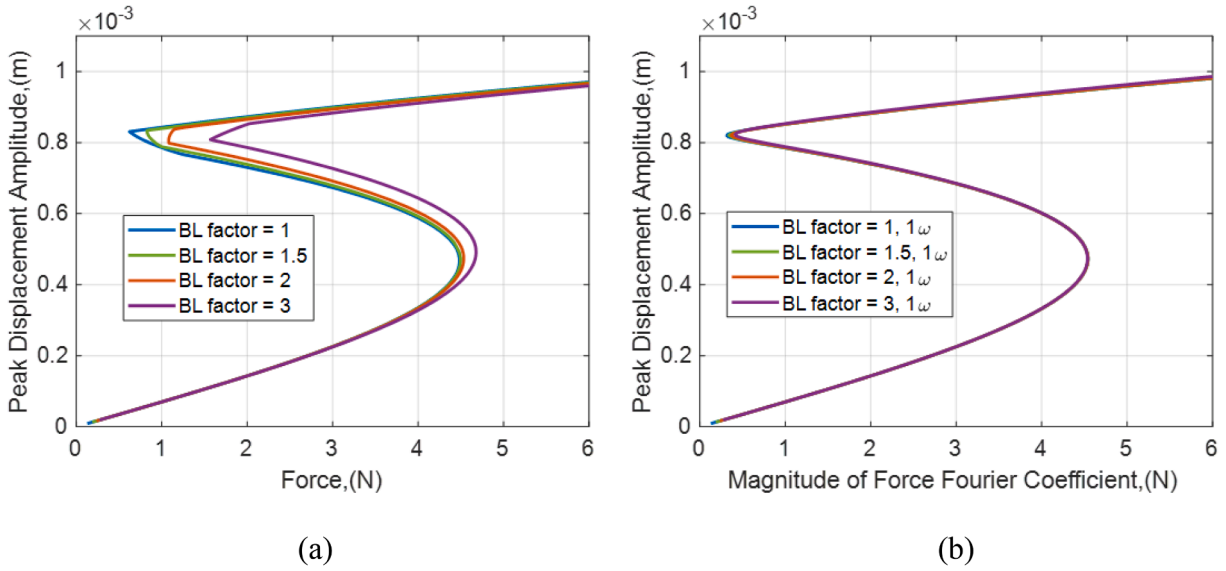

Fig. 6. Reconstructed S-curve from BL constant parameter changes shown in Fig. 5 (a) and (b) for the (a) peak force (multi-harmonic) and (b) magnitude of the fundamental harmonic of the force.

those computed by the MHB simulation. Numerical time integration using ODE45 in MATLAB was applied to perform FFVC tests on the beam. A sinusoidal voltage was applied to the coupled shaker-beam model with a fixed voltage amplitude and frequency, and the response was integrated to steady state conditions. Simulated data was collected at several discrete voltage amplitudes, just as is done in the physical experiments. The shaker was fixed to node 8 on the beam and *BL* scaling factors of one and three were used to compare the two extreme unstable and stable conditions, as shown in Fig. 5 (a). The comparison demonstrates that there is good agreement between the S-curves but more importantly, it highlights the stabilizing effect of scaling the *BL* shaker parameter. Fig. 7 (a) and (b) show the comparison of the S-curves corresponding to *BL* scaling factors of one and three. It can be seen in Fig. 7 (a) that a scaling factor of one results in jumping whereas in Fig. 7 (b) a scaling factor of three results in stabilized behavior. Relating this to the MHB results in Fig. 5, this confirms that the jump phenomena observed in the simulated FFVC test is caused by the turning point bifurcation in the force-voltage curve. The nonlinear forced response (NLFR) curves of the cantilever beam were also computed where the S-curves from harmonic balance and numerical time integration were overlaid. This is shown in Fig. 8. Notice that the S-curves intersect the NLFR curves at the upper and lower stable branches and the intermediate unstable branch. The reconstructed S-curve with the *BL* parameter scaled by one is unable to capture the intermediate unstable solutions of the NLFR curve, but by stabilizing the dynamics with a *BL* scale factor of three, the simulated FFVC tests are able to measure these unstable regions. A set of FFVC tests can be conducted at different discrete frequencies so the entire NLFR surface can be realized with the inclusion of the intermediate unstable solutions, assuming the shaker configuration used in the test stabilizes this region of the curve.

In practice, it is not immediately obvious to the authors how a practitioner could modify the shaker parameters such as the ones investigated here. These are inherent to the shaker selected for the test, and model parameters are identified empirically using methods such as those presented in [6,13,27]. It is more straightforward to change the drive point location on the structure when designing the FFVC test setup. This finding can be leveraged in FFVC tests so shakers or the excitation drive points can be optimized to produce stabilizing effects on a strongly nonlinear system, for the purpose of system identification. The next section presents results on a nonlinear vibro-impact system with different drive point locations to observe the resulting stabilizing effects of the coupled shaker-structure system and corroborate the findings from this section.

4. Experimental investigation on a strongly nonlinear system

Based on the insights gained from the simulated FFVC response on the coupled nonlinear cantilever beam, it was of interest to explore these findings experimentally. A different strongly nonlinear structure was used for the experimental tests to assess if the shaker stabilizes the structure's dynamics when attached at more responsive drive points along the structure. The hypothesis is that the back EMF voltage from Eq. (11) increases with increasing relative velocity between the shaker armature and body. A fixture-pylon assembly with a vibro-impact nonlinearity served as the experimental structure for the FFVC testing. The experimental testing consisted of four different FFVC tests corresponding to different excitation drive points along the structure where the force drop-out and reconstructed S-curves were compared for each drive point. Each excitation drive point was initially tested in a band-limited white noise sine test at low force levels to observe the linear behavior of the shaker armature and pylon FRFs.

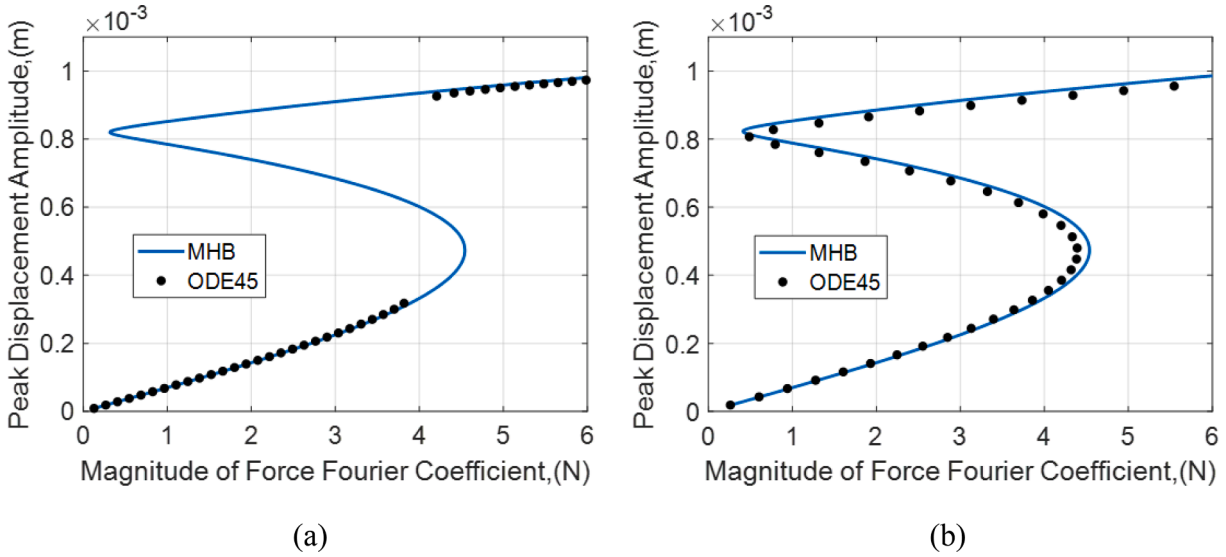

Fig. 7. MHB simulation and ODE45 experimental simulation comparison of the reconstructed S-curves for *BL* scaled at an integer of (a) one and (b) three, with the shaker excitation drive point fixed at node 8.

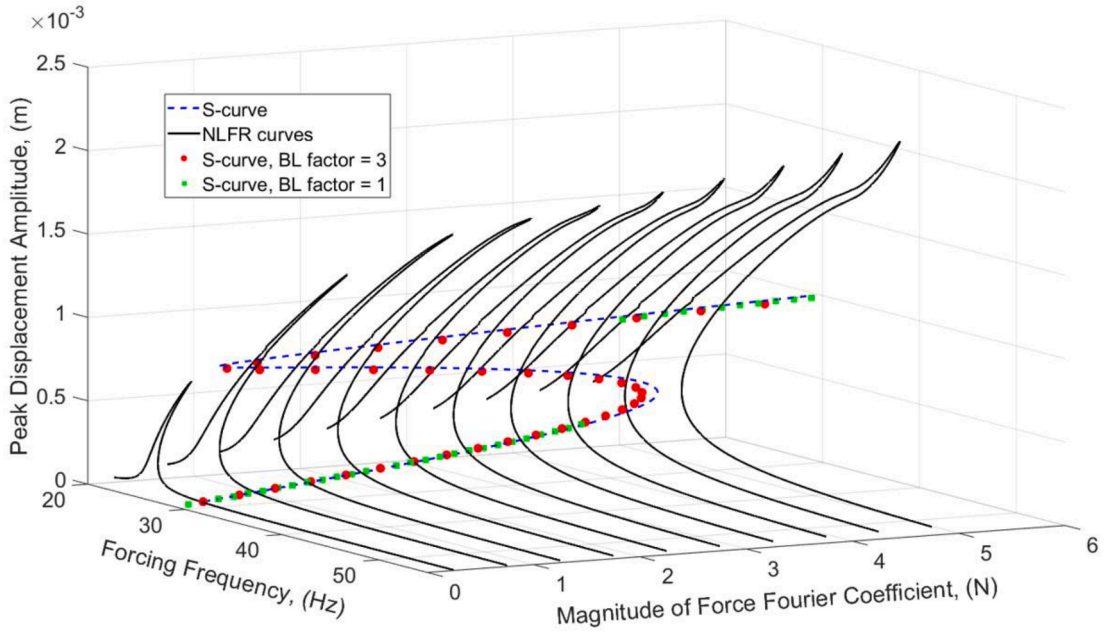

Fig. 8. The NLFR curves of the beam and the intersection of the S-curves from the MHB simulation and ODE45 experimental simulation for *BL* scaled at integers of one and three.

4.1. Strongly nonlinear System: Fixture-Pylon experimental setup

A fixture-pylon assembly from [5] was used as the strongly nonlinear system for this research. As detailed in Fig. 9, the mock pylon is bolted to a large fixture in order to isolate the nonlinearity for the purpose of nonlinear system identification. The pylon consists of two upper blocks and two washers which creates a small gap between the upper blocks and the vertical thin beam. The two lower blocks are glued to the thin beam to represent a payload mass. The gap created in between the upper blocks and beam can be modeled as a gap-spring-type nonlinearity as described in [5] where more details can be found. The mode of interest for this testing was the

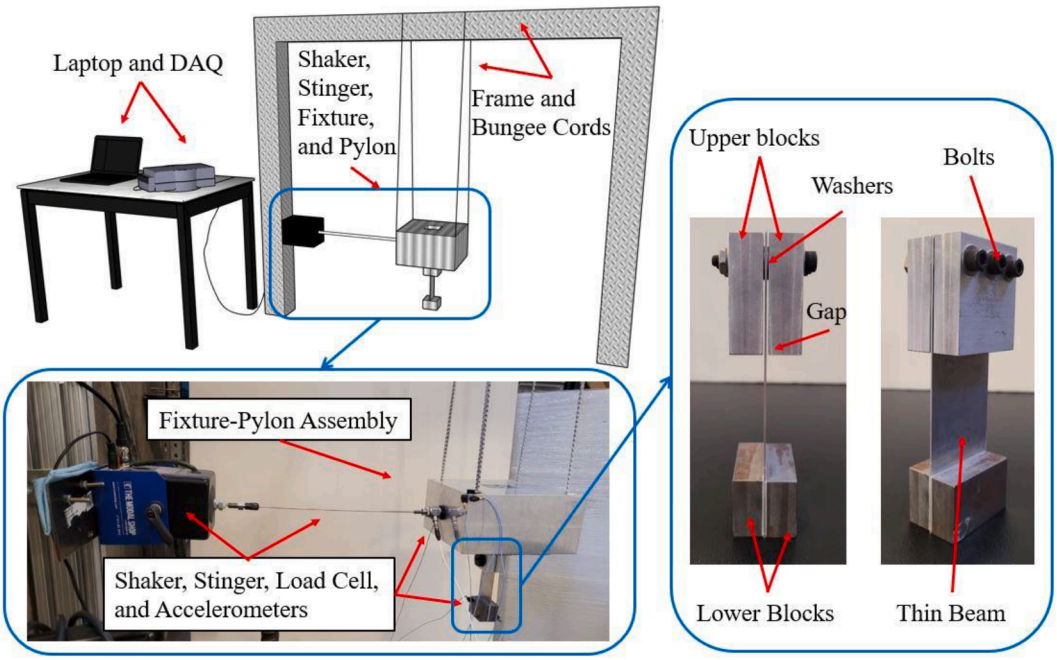

Fig. 9. Full schematic of experimental setup (top left), view of shaker-fixture-pylon setup (bottom left), and detailed diagram of pylon (right).

fundamental mode at 9.1 Hz which is a simple bending mode of the beam such that at low force levels the pylon acts as a linear system. At sufficiently higher force levels, the beam vibrates with a large enough amplitude such that the contacts within the upper blocks create a hardening response.

The fixture-pylon assembly was suspended by bungee cords to create a free boundary condition. The shaker was fixed to a rigid frame (implying $x_1 = 0$ in Fig. 2) and the stinger connected to a load cell that was attached to the center of the fixture block. Six accelerometers were used on the assembly, where one was mounted to the upper and lower blocks of the pylon. The bottom-most accelerometer as seen in Fig. 9 was used as the response location of interest for all testing conducted on the assembly as this was the point of maximum displacement for the bending mode of the pylon. The six accelerometers, the load cell, and the shaker were connected to an 8-channel m + p international VibPilot signal analyzer for signal source generation and acquistion. The electroctromechanical shaker used in this research was the Modal Shop K2007E01 SmartShaker with an integrated amplifier.

4.2. Changing shaker drive point locations

Fig. 10 shows the four different drive point locations on the assembly used in the testing. Note the load cell was glued to each drive point location, like that shown in Fig. 9, but is not shown explicitly in Fig. 10. Fig. 11 shows the FRFs corresponding to the four different excitation drive points on the assembly relating the load cell force to the response from the bottom pylon accelerometer. It can be seen in Fig. 11 that exciting at the bottom of the fixture and the upper pylon block resulted in higher peak magnitudes in the FRF. Thus, these more active drive points would drive the armature to higher velocities and introduce high levels of back EMF voltage than those on the upper and center fixture.

To further demonstrate the effect of drive point selection on the armature velocity, additional linear random vibration tests were conducted but with an accelerometer placed on the armature. Note, an accelerometer was not placed on the shaker body for this test because the shaker was in a fixed boundary condition and the response was assumed to be negligible. Fig. 12 compares the FRFs for the shaker armature corresponding to the four drive points. This result is consistent with the results shown in Fig. 11 in that the peak magnitudes occur when the drive point is at the bottom of the fixture and on the pylon block. Therefore, the armature velocity will be highest for these drive points. When referring to Section 2.2 where the shaker dynamics were discussed, higher relative armature velocities produce a larger back EMF voltage in the shaker. Thus, based on the observations of the simulated model, the shaker should be more likely to stabilize the dynamics when placed either at the bottom of the fixture or on the pylon block. This is evaluated in the next section.

4.3. FFVC experiments

The FFVC test strategy as described in [1] was applied to the fixture-pylon assembly at a constant frequency of 9.7 Hz. Note, the fixed frequency of 9.7 Hz was selected to operate in the nonlinear response regime without damaging the structure. Each data point in the experimental FFVC tests corresponded to an individual sine test that was started with zero initial conditions due to the single valued nature of the force and response amplitudes mentioned in Section 2. Each test was carried out for approximately 30 s until the steady state response was reached and the maximum magnitudes of the spectra were taken for the force and response amplitudes at each corresponding voltage increment.

FFVC tests were conducted on the pylon assembly for the four drive point locations from Fig. 10 and the results are shown in Fig. 13 for the upper (a), middle (b), and bottom (c) of the fixture as well as the upper pylon block (d). The relationship between the load cell force and input voltage shows that there is a sudden jump down during the force dropout that occurs at the upper and middle drive points on the fixture, shown in Fig. 13 (a) and (b). This behavior is inconsistent with the previously reported data from other researchers [1], along with the plot shown in Fig. 1 (a), where the load cell force produced smooth and continuous behavior along the voltage axis. It can be hypothesized that the unstable portion of the response curve has not been measured in these tests, and that the

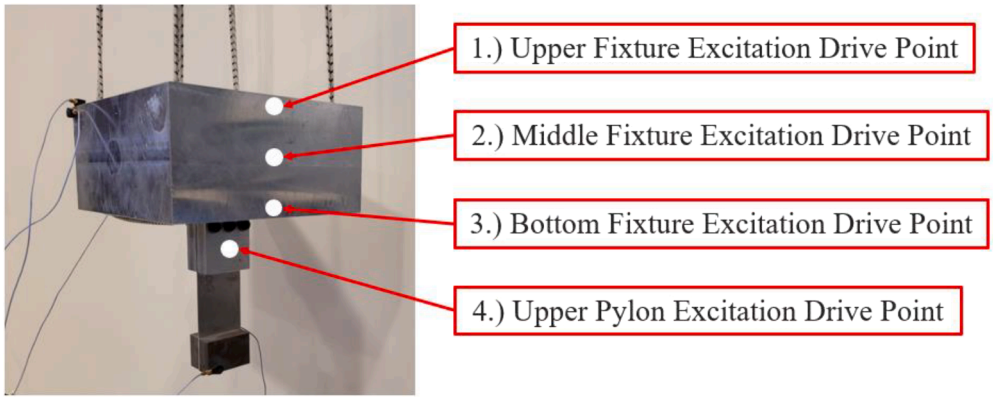

Fig. 10. Four different excitation drive point locations on fixture-pylon assembly used for linear random vibration and FFVC tests.

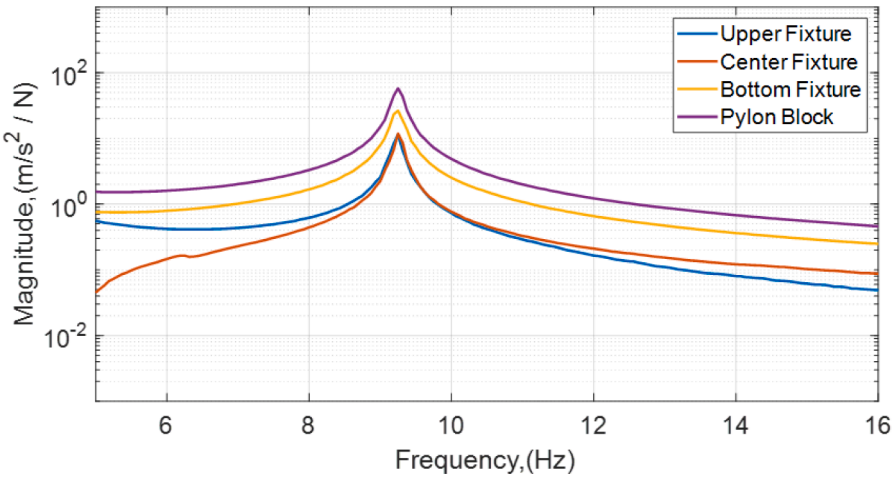

Fig. 11. FRFs corresponding to the changes of excitation drive points on the fixture-pylon assembly with respect to the bottom pylon accelerometer.

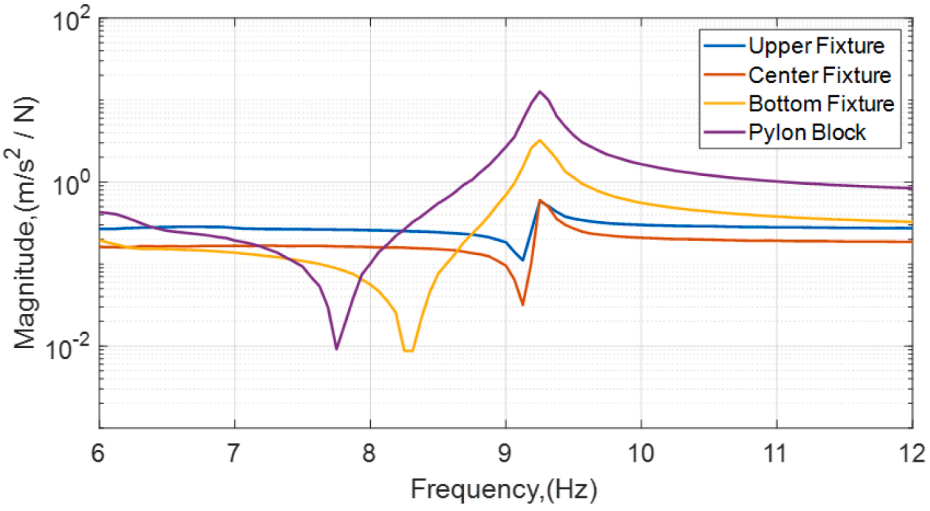

Fig. 12. FRFs corresponding to the changes of excitation drive points on the fixture-pylon assembly with respect to the shaker armature accelerometer.

shaker did not stabilize the unstable portion of the response of the underlying nonlinear structure. However, the two lower, more active excitation points show the desired multivalued force dropout curves which are shown in Fig. 13 (c) and (d). It can also be observed that the harmonics (the second harmonic in this case) of the force have significantly increased at the two lower drive points. The harmonics become more active near the local minimum of the force-voltage curve which is where the stabilization occurs. This observation is also consistent with the numerical study from Section 3.1 shown in Fig. 4, where it was observed that the third harmonic increased and intersected the force-voltage curve at the local minimum. The reconstructed S-curves corresponding to the data shown in Fig. 13 was plotted and are shown in Fig. 14. Similar behavior is observed where the upper and middle drive points on the fixture demonstrate the jumping behavior with only two stable solutions whereas the bottom fixture and upper pylon block drive points are able to trace all three solutions, including the unstable portion of the response.

It is noted here that the force drop-out curves seen in Fig. 13 have inherently different behaviors due to the excitations at different drive points along the structure. This was also observed in Figs. 11 and 12 where the four different excitation drive points resulted in different FRFs. It is reemphasized here that the purpose of exciting the structure at four different drive points was to investigate the locations that stabilized the intermediate solution of the nonlinear forced response curve. Therefore, the force drop-out curves shown in Fig. 13 are not directly compared based on the turning points and relative agreement but rather they are investigated in finding a stabilizing drive point for the purpose of system identification. This is also the case for the reconstructed S-curves shown in Fig. 14. It is only when the structure is excited at the same drive point that the force drop-out curves and reconstructed S-curves can be compared directly which was done in Fig. 6 and was useful for observing the effects of higher harmonics.

These results demonstrate similar trends to those observed in the simulated experiments in Section 3, where excitation applied at

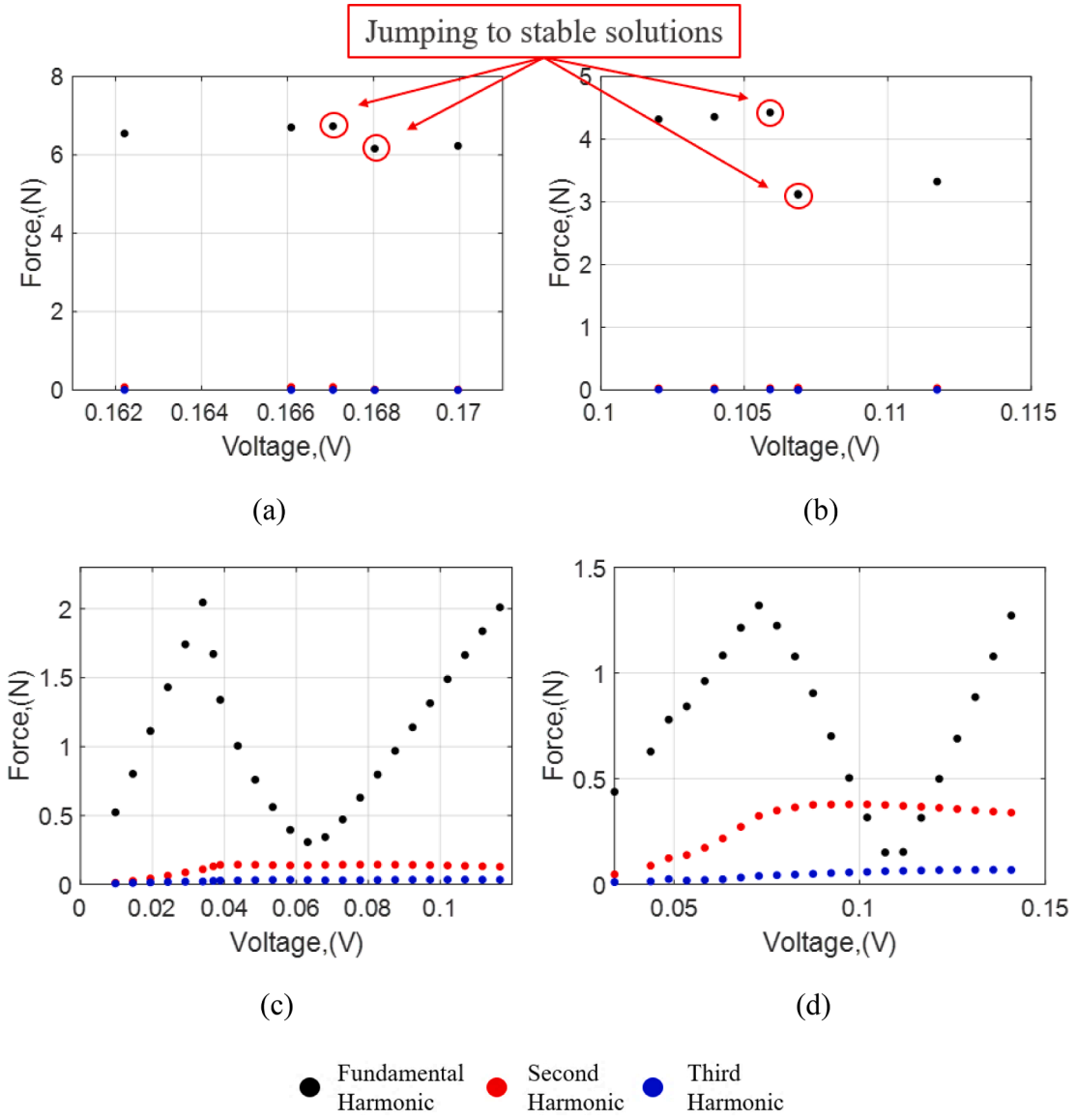

Fig. 13. Force-voltage curves corresponding to the change of excitation drive points at the (a) upper fixture, (b) middle fixture, (c) bottom fixture, and (d) upper pylon block.

active locations improves the stabilizing effect of the shaker and improves the ability to trace out a smooth S-curve that shows all three solutions along the multivalued response. Additionally, these results suggest that the back EMF is one effect responsible for the shaker to help stabilize the nonlinear response since the more active drive points were shown to have larger armature velocities.

5. Conclusions

In this research the stabilizing effects of an electromechanical shaker were explored by conducting FFVC sine tests on a strongly nonlinear structure. Motivating experimental results demonstrated that a strongly nonlinear system unexpectedly produced a jump phenomenon instead of tracing the unstable portions of the multivalued response curve as reported previously [1]. To explore this behavior, a parametric study was performed by connecting an electromechanical model of a shaker to a finite element model of a 20 node Euler-Bernoulli beam with a nonlinear cubic spring at the free end. Various shaker properties as well as different drive point locations were studied by conducting simulated experiments using harmonic balance to solve the nonlinear equations of motion.

The findings from the parametric study were explored experimentally by performing a series of FFVC tests at different drive points of a structure comprised of a strong vibro-impact nonlinearity. Four drive points were explored, two of which demonstrated notably higher armature responses. The results corroborated those from the parametric study of the model where the unstable portion of the

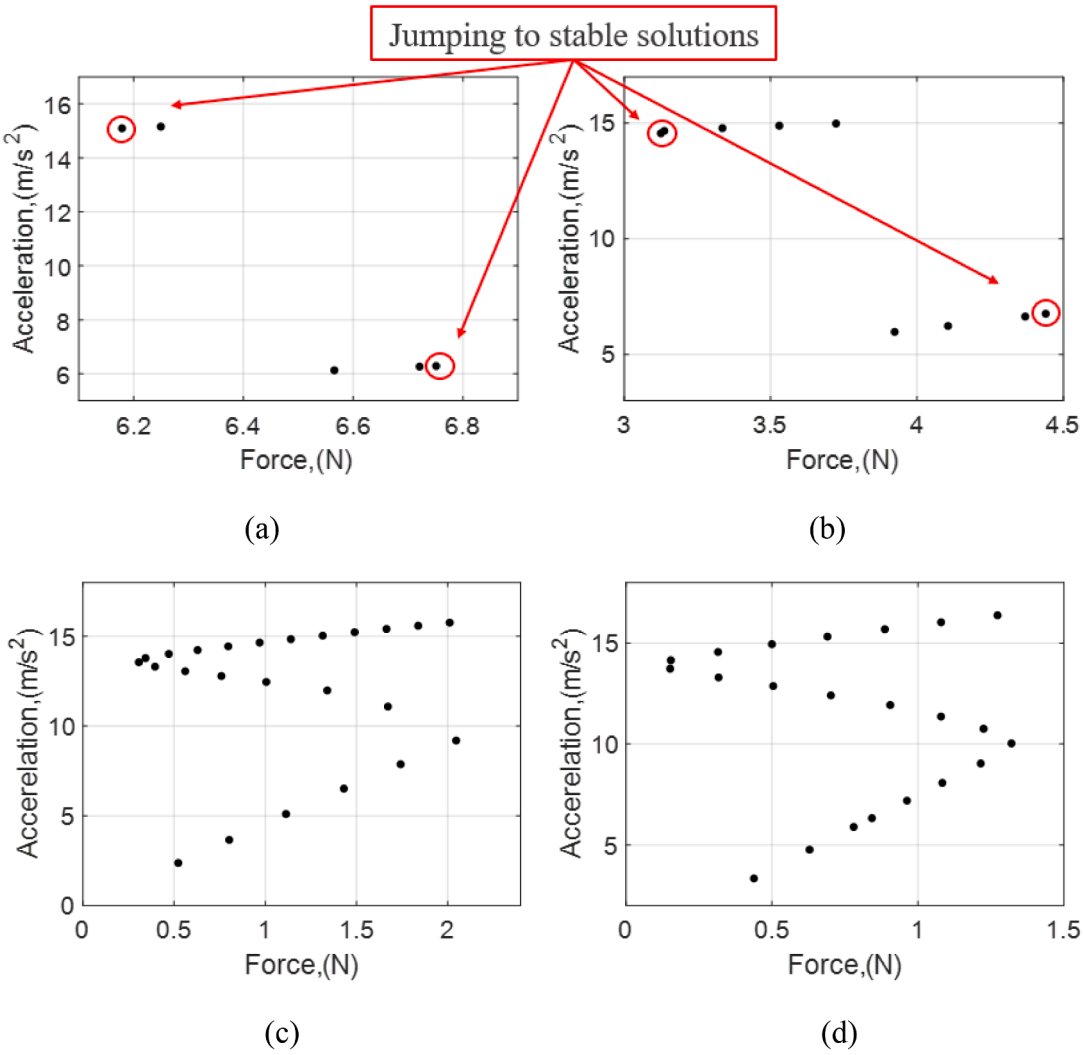

Fig. 14. S-curves of the magnitude of the fundamental harmonic of the force corresponding to the change of excitation drive points at the (a) upper fixture, (b) middle fixture, (c) bottom fixture, and (d) upper pylon block.

nonlinear force-response was achieved only for the more active drive point locations, i.e. those with higher shaker armature responses (and therefore larger back electromotive forces).

Through numerical and experimental testing on two different strongly nonlinear systems, it was demonstrated that there were various parameters that influenced the stability of the nonlinear systems through the electromechanical shaker dynamics in fixed frequency voltage control tests. Specifically, factoring the BL, R_e, K_1, and C_1 parameters from the electromechanical model resulted in stabilizing behaviors for which the BL and R_e parameters demonstrated the highest sensitivity to the shaker stability. It was also demonstrated that the back electromotive force on the shaker produced by the relative velocity of the shaker body and armature strongly influenced the stabilizing effect of the shaker. This value was sensitive to the shaker magnetic properties and the responsiveness of the drive point location for the target mode. Future modeling and testing on the fixture-pylon assembly in FFVC will be conducted to investigate the influence of each excitation drive point on the underlying linear mode, the influence of harmonic distortion, and the influence of the drive points on the behavior of the turning points in the force drop-out curves. Modeling the fixture-pylon assembly will also be considered for future work where the simulated and experimental results will be compared and assessed in a stability analysis.

Declaration of Competing Interest

The authors declare that they have no known competing financial interests or personal relationships that could have appeared to influence the work reported in this paper.

Data availability

The data will be available upon reasonable request

Acknowledgments

The authors acknowledge the financial support of the Laboratory Directed Research and Development program at Sandia National Laboratories, a multimission laboratory managed and operated by National Technology and Engineering Solutions of Sandia LLC, a wholly owned subsidiary of Honeywell International Inc. for the U.S. Department of Energy's National Nuclear Security Administration under contract DE-NA0003525. This paper describes objective technical results and analysis. Any subjective views or opinions that might be expressed in the paper do not necessarily represent the views of the U.S. Department of Energy or the United States Government. SAND Number:

References

[1] G. Zhang, C. Zang, M.I. Friswell, Measurement of multivalued response curves of a strongly nonlinear system by exploiting exciter dynamics, Mechanical Systems and Signal Processing, Volume 140,, 106474, ISSN 0888–3270 (2020), https://doi.org/10.1016/j.ymssp.2019.106474.
[2] B.R. Pacini, R.J. Kuether, D.R. Roettgen, Shaker-structure interaction modeling and analysis for nonlinear force appropriation testing, Mechanical Systems and Signal Processing 162 (2022) 108000.
[3] J.V. Ferreira, Dynamic response analysis of structures with nonlinear components, University of London, 1998. PhD thesis,.
[4] P. Varoto, L. de Oliveira, Interaction between a vibration exciter and the structure under test, Journal of Sound and Vibration. 36 (2002) (2002) 20–26.
[5] E. Robbins, et al., Pre-test Predictions of Next-Level Assembly using Calibrated Nonlinear Subcomponent Model, 39th International Modal Analysis Conference (IMAC), February 2021.
[6] Schultz, Ryan. (2021). Calibration of Shaker Electro-mechanical Models. 10.1007/978-3-030- 47709-7_12.
[7] G.R. Tomlinson, Force distortion in resonance testing of structures with electro-dynamic vibration exciters, Journal of Sound and Vibration. 63 (3) (1979) 337–350. ISSN 0022–460X.
[8] G.F. Lang, Electrodynamic shaker fundamentals, Journal of Sound and Vibration. 31 (1997) 14–23.
[9] Lang, George Fox and D. H. Snyder. Understanding the physics of electrodynamic shaker performance. Journal of Sound and Vibration. Volume 35 (2001): 24-33.
[10] G. Zhang, C. Zang, M.I. Friswell, Parameter Identification of a Strongly Nonlinear Rotor-Bearing System Based on Reconstructed Constant Response Tests, Journal of Engineering for Gas Turbines and Power 142 (2020) 8.
[11] G. Zhang, C. Zang, M.I. Friswell, Identification of weak nonlinearities in MDOF systems based on reconstructed constant response tests, Archive of Applied Mechanics 89 (10) (2019) 2053–2074.
[12] G. Zhang, C. Zang, M.I. Friswell, Measurement of the multivalued phase curves of a strongly nonlinear system by fixed frequency tests, Archive of Applied Mechanics 90 (11) (2020) 2543–2560.
[13] Z.H.A.N.G. Guiwei, W.A.N.G. Xiaochen, Y.A.N.G. Zhichun, Study on excitation force characteristics in a coupled shaker-structure system considering structure modes coupling, Chinese Journal of Aeronautics 35 (7) (2022) 227–245. ISSN 1000–9361.
[14] T. Dossogne, L. Masset, B. Peeters, J.P. Noël, Nonlinear dynamic model upgrading and updating using sine-sweep vibration data, Proc. R. Soc. 475 (2229) (2019) 20190166.
[15] G. Kerschen, K. Worden, A.F. Vakakis, J.-C. Golinval, Past, present and future of nonlinear system identification in structural dynamics, Mechanical Systems and Signal Processing 20 (3) (2006) 505–592, https://doi.org/10.1016/j.ymssp.2005.04.008. ISSN 0888–3270,.
[16] J. Sieber, B. Krauskopf, Control based bifurcation analysis for experiments, Nonlinear Dynamics 51 (2008) 365–377, https://doi.org/10.1007/s11071-007-9217-2.
[17] V. Denis, M. Jossic, C. Giraud-Audine, B. Chomette, A. Renault, O. Thomas, Identification of nonlinear modes using phase-locked-loop experimental continuation and normal form, Mechanical Systems and Signal Processing 106 (2018) 430–452.
[18] R. Seydel, Practical bifurcation and stability analysis, Springer Science & Business Media, 2009.
[19] G. von Groll, D.J. Ewins, The harmonic balance method with arc-length continuation in rotor/stator contact problems, J. Sound Vib. 241 (2) (2001) 223–233.
[20] S. Stoykov, S. Margenov, Numerical computation of periodic responses of nonlinear large-scale systems by shooting method, Comput. Math. Appl. 67 (12) (2014) 2257–2267.
[21] S.B. Cooper, D. Di Maio, D.J. Ewins, Integration of system identification and finite element modelling of nonlinear vibrating structures, Mech. Syst. Sig. Process. 102 (2018) 401–430.
[22] J.V. Ferreira, A.L. Serpa, A.P. Prado, Experimental nonlinear frequency response determination using the arc-length method, IMAC-XXI: Conference & Exposition on Structural Dynamics, 2003.
[23] T. Karaağaçlı, H. Özgüven, Experimental modal analysis of nonlinear systems by using response-controlled stepped-sine testing, Mechanical Systems and Signal Processing. 146 (2021), 107023, https://doi.org/10.1016/j.ymssp.2020.107023.
[24] S. Peter, R.I. Leine, Excitation power quantities in phase resonance testing of nonlinear systems with phase-locked-loop excitation, Mechanical Systems and Signal Processing 96 (2017) 139–158, https://doi.org/10.1016/j.ymssp.2017.04.011. ISSN 0888–3270,.
[25] Fey, Rob & Winter, Berend & Wijker, Jaap. (1999). Sine Sweep and Steady-State Response of a Simplified Solar Array Model with Nonlinear Support.
[26] A.H. Nayfeh, D.T. Mook, Nonlinear Oscillations, John Wiley and Sons, New York, 1979.
[27] Mayes, R., Ankers, L., Daborn, P. *et al.* Optimization of Shaker Locations for Multiple Shaker Environmental Testing. *Exp Tech* 44, 283–297 (2020).https://doi.org/10.1007/s40799-019- 00347-7.
[28] M. Magnevall, A. Josefsson, K. Ahlin, Experimental verification of a control algorithm for nonlinear systems, Society for Experimental Mechanics, International modal analysis conference XXIV, 2006.
[29] A. Josefsson, M. Magnevall, K. Ahlin, Control algorithm for sine excitation on nonlinear systems, International Modal Analysis Conference XXIV (2006).
[30] T.M. Cameron, J.H. Griffin, An Alternating Frequency/Time Domain Method for calculating the Steady-State Response of Nonlinear Dynamic Systems, Journal of Applied Mechanics 56 (1) (1989) 149–154, https://doi.org/10.1115/1.3176036.
[31] Y. Colaïtis, A. Batailly, The harmonic balance method with arc-length continuation in blade-tip/casing contact problems, Journal of Sound and Vibration 502 (2021/06/23/ 2021,), 116070, https://doi.org/10.1016/j.jsv.2021.116070.
[32] T. Detroux, L. Renson, L. Masset, G. Kerschen, The harmonic balance method for bifurcation analysis of large-scale nonlinear mechanical systems, Computer Methods in Applied Mechanics and Engineering vol. 296 (2015/11/01/ 2015,) 18–38, https://doi.org/10.1016/j.cma.2015.07.017.
[33] M. Krack, Extension of the single-nonlinear-mode theory by linear attachments and application to exciter-structure interaction, Journal of Sound and Vibration 505 (2021) 116120.
[34] G. Gatti, An adjustable device to adaptively realise diverse nonlinear force-displacement characteristics, Mechanical Systems and Signal Processing, Volume 180,, 109379, ISSN 0888–3270 (2022), https://doi.org/10.1016/j.ymssp.2022.109379.

[35] A. Marcelo Tusset, V. Piccirillo, A.M. Bueno, et al., Chaos control and sensitivity analysis of a double pendulum arm excited by an RLC circuit based nonlinear shaker, Journal of Vibration and Control. 22 (17) (2016) 3621–3637, https://doi.org/10.1177/107754631456478.
[36] Oliveira, L., Varoto, P., Peres, M., (2011). Shaker structure interaction: Overview and updated results. 18th International Congress on Sound and Vibration 2011, ICSV 2011. 3. 2516-2523.
[37] P.S. Varoto, L.P.R. de Oliveira, On the Force Drop Off Phenomenon in Shaker Testing in Experimental Modal Analysis, Shock and Vibration 9 (4-5) (2002) 165–175.
[38] G. Tomlinson, A simple theoretical and experimental study of the force characteristics from electrodynamic exciters on linear and nonlinear systems, in: Proceedings of the 5th International Modal Analysis Conference, Society for Experimental Mechanics (SEM), London, England, 1987, pp. 1479-1486.
[39] L. Renson, A. Gonzalez-Buelga, D.A.W. Barton, S.A. Neild, Robust identification of backbone curves using control-based continuation, Journal of Sound and Vibration 367 (2016) 145–158.
[40] E. Bureau, F. Schilder, I. Ferreira Santos, J. Juel Thomsen, J. Starke, Experimental bifurcation analysis of an impact oscillator—Tuning a non-invasive control scheme, Journal of Sound and Vibration 332 (22) (2013) 5883–5897.
[41] X. Jing, X.u. Yuyang Chai, J.B. Chao, In-situ adjustable nonlinear passive stiffness using X-shaped mechanisms, Mechanical Systems and Signal Processing, Volume 170,, 108267, ISSN 0888–3270 (2022), https://doi.org/10.1016/j.ymssp.2021.108267.
[42] D. de Klerk, D.J. Rixen, S.N. Voormeeren, General Framework for Dynamic Substructuring: History, Review and Classification of Techniques, AIAA Journal 46 (5) (2008) 1169–1181.
[43] K. Malte, J. Gross, Harmonic balance for nonlinear vibration problems, Vol. 1, Springer International Publishing, Cham, 2019.

PROFESSIONAL REFERENCES

B. F. Spencer, Jr., Ph.D., PE
Nathan M. & Anne M. Newmark Endowed Chair in Civil Engineering
Director, Newmark Structural Engineering Laboratory
Director, Multi-Axial Full-Scale Sub-Structured Testing & Simulation Facility (NEES@UIUC)
Director, Smart Structures Technology Laboratory
Department of Civil & Environmental Engineering
University of Illinois at Urbana-Champaign
2113 Newmark Laboratory, MC-250
205 N. Mathews Ave. Urbana, IL 61801
Email: bfs@illinois.edu ; Website: http://sstl.cee.illinois.edu/
Phone: (217) 419-4780

Michael D. Todd, Ph.D., SE
Professor and Chair
Structural Engineering Department
Director, Structural Health Monitoring Laboratory
Jacobs School of Engineering
University of California, San Diego
9500 Gilman Drive Mail Code 0085
La Jolla, CA 92093
Email: mdtodd@ucsd.edu; Website: http://shm.ucsd.edu/Site/Home.html
Phone: (858) 534-5951

Jerome P. Lynch, Ph.D., F. EMI
Professor in the Department of Civil and Environmental Engineering
Vinik Dean of Engineering
Professor in the Department of Electrical & Computer Engineering
Pratt School of Engineering
Duke University
305 Nello L. Teer Engineering Building
Box 90271
Durham, NC 27708-0271
Email: jerome.lynch@duke.edu; Website: http://www-personal.umich.edu/~jerlynch// (former)
Phone: (734) 276-6148

Dan M. Frangopol, Ph.D.
The Fazlur R. Khan Endowed Chair of Structural Engineering and Architecture
Department of Civil and Environmental Engineering
Engineering Research Center for Advanced Technology for Large Structural Systems
(ATLSS Center)
Lehigh University
117 ATLSS Drive, Imbt Labs
Bethlehem, PA 18015-4729
Email: dan.frangopol@lehigh.edu; Website: http://www.lehigh.edu/~dmf206/
Phone: (610) 758-6103 or (610) 758-6123

Branko Glišić, Ph.D., F. ISHMII
Professor and Chair
Department of Civil and Environmental Engineering
Princeton University
E205 EQuad
Princeton, NJ 08544
Email: bglisic@princeton.edu
Website http://glisic-structuralhealthmonitoring.princeton.edu
Phone: (609) 258-4600

My development as an educator goes together with my experience as an engineer and scholar. I want to collaborate with the Lyles School of Civil Engineering at Purdue University to educate and train engineers. My experience working in industry and my Professional Engineering license in the state of Indiana qualifies me to inspire students to learn the skills that will make them competent in their profession, while advocating for values that promote ethical behavior. During my eight years as faculty in the Department of Civil, Construction and Environmental Engineering (CCEE) at the University of New Mexico (UNM) I have adapted my teaching style for my students' needs and their backgrounds and the scores have grown through the years. I firmly believe effective teaching needs to be motivational, creative, goal-oriented, and based on students' needs. Motivational teaching engages and reinforces students' learning paths. For example, when I teach structural dynamics to graduate students, I introduce sensors that the students build and attach themselves to small structures, so they can see and measure responses from their own loading events, which motivate the interest of the students by hands-on experience. Creative instruction provides students with new tools to overcome problems they perceived to be unsolvable. For example, in all my courses (both graduate and undergraduate) I expose the students in their final project to smart sensing technology, which the majority has not used before or never thought would use. Applied education help students understand that the materials they study will assist them in solving important problems. When I teach structural design, I ask the students to conduct and present projects on structures that they chose to design, generally a new bridge or building design. The goal of learning about structural engineering becomes real. Student-oriented mentoring reaches students of diverse backgrounds, races, orientations, and nationalities to impact and catalyze their experience at Purdue University.

My interest will be to motivate students to eventually develop their own learning and their own research path while at Purdue University. Teaching both undergraduate and graduate level courses, I have learned that when students are motivated with specific goals, they choose to direct their learning autonomously and independently. My teaching method at Purdue University will also be creative. Creative teaching allows students to develop their own methods of learning new concepts of unexplored territories. For example, when collecting data in structural dynamics for their final project, I permitted that students could add a new/unique section to their final reports. Their class work became their own, self-directed research interest because they could individually grow in their own learning. I learned that students learn new materials more effectively if they understand how they can use them in their careers. At the laboratory I help students master (who did not have any previous experience) digital signal processing, data acquisition, experimental modal analysis, shaking table operation, and sensor calibration. I have gained extensive experience mentoring undergraduate and graduate students, post-doctorate associates, visiting faculty from other countries, and even high school interns. My teaching experiences have provided me with an awareness that effective teaching needs to be student oriented. I promote diversity of backgrounds and cultures in my research group, and everybody seems to enjoy learning from different countries, traditions, and nationalities. My teaching interests include undergraduate courses related to fundamental principles of engineering (structural analysis, statics), design (steel, concrete, structures), and graduate courses (structural dynamics, advanced experimental dynamics, signal processing). I am interested to develop multi-disciplinary courses covering signal processing, augmented reality, unmanned aerial systems, field monitoring and remote sensing.

My research plan is to contribute to engineering with the discovery, development, and dissemination of innovative solutions towards sustainable and resilient infrastructure. Advancing original research helps addressing today's urgent worldwide challenges and equipping the future leaders in structural engineering. My research advances the new generation of civil infrastructure with cutting-edge sensing algorithms applied to structural dynamics and controls in smart structures; novel Human-Infrastructure Interfaces (HII) with human-in-the-loop new theories and experiments; and new methodologies towards trusted performance-based monitoring, management, and disaster prevention and recovery of infrastructure. I want to enhance efficient, sustainable, and resilient structures and systems design with a combination of innovative, out-of-the-box approaches to satisfy the needs of stakeholders of today and the future. My research approaches are motivated to assist private and public owners to prioritize design, management and protection of infrastructure systems and networks with informed decisions.

My research focus at the University of New Mexico (UNM) to date has been related to structural dynamics, complex systems, and HII. My research group explores new research questions about the monitoring, control, inspection, and management of structural systems, as well as design and assessment of structures under extreme demands. Infrastructure owners (railroads, highways, and public entities such as the city of Albuquerque, the County of Los Alamos, National Laboratories, or the Tribal Government of Ohkay Owingeh) inform my research priorities. I designed a new bridge protection crash beam against truck impacts with support of Sandia National Laboratories (SNL) and the private industry which was designed and built and is currently under service. I have developed new performance-based management of railroad bridges integrating Unmanned Aerial Systems (UAS), lasers, and computer vision, which is funded both by the rail industry and governmental offices: National Academy of Sciences (NAS), and the Transportation Research Board (TRB) Rail SAFETY IDEA program (twice). It also resulted in a US patent granted in 2020. My research in multiple-input multiple-output (MIMO) investigation and the control of non-linear systems is funded by two different research units in SNL. I currently investigate advancing the stabilization of nonlinear vibrations with experimental work supported by simulations, annually funded by SNL. I developed a new comprehensive inspection method that uses Machine Learning (ML) to automatically classify data sounds generated by robotic arms tapping on critical structures aided by UAS and ground robots. This research was funded by Los Alamos National Laboratory (LANL) to inform the management of nuclear storage facilities. I am developing a new inspector-data interface with a new project funded by the Department of Energy to enable safe, sustainable, and resilient nuclear storage inspections, design, and maintenance.

The second focus of my research is on the domain of HII, acknowledging the need for including human in the loop to advance engineering new frontiers both in the laboratory and in the field. My research emphasis is inspections and human control of structural dynamics responses with augmented human intervention and robot mediation. In 2017 I published the first paper on Augmented Reality (AR) of structural inspections which was presented at the International Workshop of Structural Health Monitoring (IWSHM), funded initially by the Engineering Institute of LANL. This year I won the SHM in Action competition at IWSHM. This research is now funded by the Air Force Research Laboratory (AFRL), the Office of Naval Research (ONR), the Federal Railroad Administration (FRA), NAS, the National Cooperative Highway Research Program (NCHRP), the National Science Foundation (NSF), and the New Mexico Space Grant Consortium (NMSGC). Research outcomes include the quantification and enhancement of human control of shakers and robots with a new closed loop that enables human input of vibrations into shakers by visualizing responses with AR on real time, enabling a new paradigm for real-time visualization

of structural testing both in the laboratory and eventually in the field. My goal is to accelerate the engineering assessment of structures from cradle to grave (construction to failure/demolition) both under normal loads and extreme events. My professional experience in industry equips my transformative, fundamental research to contribute to practical implementation in the field. I will continue to advance my research in construction inspection at Purdue University using AR, and will grow collaborations with the Division of Construction Engineering and Management.

The third research area is directed towards the development of Low-cost Efficient Wireless Intelligent Sensors (LEWIS) systems for Smart and Connected Communities. My research team involves participation from students with different backgrounds (Civil Engineering, Electrical and Computer Engineering, Mechanical Engineering, Computer Science). Supported by the first NSF CIVIC National Competition in 2021, this research co-designs Structural Health Monitoring (SHM) solutions informed by the community, the Native-American Pueblo of Ohkay Owingeh in New Mexico. The main objective of my research is equipping Ohkay Owingeh for resilient and sustainable responses to post wildfire flooding on real-time. Adaptive and resilient solutions include adaptable hardware and software, scalable systems co-fabricated with the stakeholder, and recognition of owner sovereignty, critical in SHM. To enable cybersecurity of SHM, in 2020 I founded the brand-new ROTC cybersecurity program for undergraduates at UNM. I am leading the development of cybersecurity of SHM for critical infrastructure with ROTC/civilian students and plan to propose a roadmap for the cybersecurity of SHM for public and private stakeholders.

I will develop a research program at the Lyles School of Civil Engineering at Purdue University that is funded both by industry and government agencies (national and international). I want to collaborate with Purdue Engineering and contribute to the Pinnacle of Excellence at Scale. Collaborating across the different areas of engineering and with other disciplines across the Purdue University the solutions will be able to transform our society through new and innovative research that includes diverse and forward approaches. I will advance research on HII in collaboration with the existing initiatives at Purdue, including but not limited to Autonomous and Connected Systems (ACS), Cislunar and the partnership between IU Medicine and Purdue Engineering. I am interested to collaborate and build research alliances with faculty members of Purdue University and the Lyles School of Civil Engineering and Bowen Laboratory in particular. I also want to collaborate with research at the steel bridge research, inspection, training, and engineering (S-BRITE) Center and the Centre for High Performance Buildings (CHPB). I will train students from different departments which will attract our own civil engineering students to other fields of research and learning. The collaborations with other leading Universities across the world will enable my students to become worldwide leaders in civil engineering for the next decades. I want to be recognized in Purdue University for my research productivity and my scholar career, by my research peers in the disciplines I work, and by the other departments in campus. My research objectives as a faculty member at Purdue University are to:

- Continue to advance structural engineering systems by working with engineers and owners to design, assess, inform, and manage infrastructure from cradle to grave
- Lead HII new theories that advance engineering frontiers in smart cities and communities
- Utilize my experiences, resources, and potential to identify and develop new research that provides technical service to society, with human-centered approaches to engineering
- Establish a high-quality research that will advance the state-of-the-art of human in the loop adaptive and resilient infrastructure research using data, AR, and ML in the laboratory
- Lead national, international, and interdisciplinary collaborations that are externally funded and have an impact in engineering, society, recommended practices and engineering codes.